(NASA-CP-2284) ELEVENTH NASTRAN USER'S N84-15590
COLLOQUIUM (Computer Software Management and THRU
Information) 310 p HC A14/MF A01 CSCL 20K N84-15608
Unclas
G3/39 18069

NASA Conference Publication 2284

Eleventh NASTRAN® Users' Colloquium

Proceedings of a colloquium held at
San Francisco, California
May 2-6, 1983

NASA
National Aeronautics
and Space Administration

Scientific and Technical
Information Branch

1983

FOREWORD

NASTRAN® (NASA STRUCTURAL ANALYSIS) is a large, comprehensive, nonproprietary, general purpose finite element computer code for structural analysis which was developed under NASA sponsorship and became available to the public in late 1970. It can be obtained through COSMIC (Computer Software Management and Information Center), Athens, Georgia, and is widely used by NASA, other government agencies, and industry.

NASA currently provides continuing maintenance of NASTRAN® through COSMIC. Because of the widespread interest in NASTRAN®, and finite element methods in general, the Eleventh NASTRAN® Users' Colloquium was organized and held at the Holiday Inn-Fisherman's Wharf, San Francisco, May 2-6, 1983. (Papers from previous colloquia held in 1971, 1972, 1973, 1975, 1977, 1978, 1979, 1980 and 1982, are published in NASA Technical Memorandums X-2378, X-2637, X-2378, X-2893, X-3278, X-3428, and NASA Conference Publications 2018, 2062, 2131, 2151 and 2249.) The Eleventh Colloquium provides some comprehensive general papers on the application of finite element methods in engineering, comparisons with other approaches, unique applications, pre- and post-processing or auxiliary programs, and new methods of analysis with NASTRAN®.

Individuals actively engaged in the use of finite elements or NASTRAN® were invited to prepare papers for presentation at the Colloquium. These papers are included in this volume. No editorial review was provided by NASA or COSMIC, however, detailed instructions were provided each author to achieve reasonably consistent paper format and content. The opinions and data presented are the sole responsibility of the authors and their respective organizations.

PRECEDING PAGE BLANK NOT FILMED

PAGE ii INTENTIONALLY BLANK

CONTENTS

Page

FOREWORD iii

1. BANDIT IN NASTRAN 1
by Gordon C. Chan (Sperry Corporation)

2. NASA/MSFC NASTRAN AUXILIARY I/O ROUTINES 6
by Malcolm Tagg (McDonnell Douglas Technical Services Company) and Bob Thornton (Boeing Computer Support Services)

3. USING PAFEC AS A PREPROCESSOR FOR COSMIC/NASTRAN 21
by W. H. Gray (Oak Ridge National Laboratory) and T. V. Baudry (PAFEC Engineering Consultants)

4. THE GPRIME APPROACH TO FINITE ELEMENT MODELING 33
by Dolores R. Wallace, James M. McKee and Myles M. Hurwitz (David W. Taylor Naval Ship Research and Development Center)

5. ORTHOTROPIC HOLE ELEMENT 46
by J. W. Markham (Lockheed-Georgia Company) and C. V. Smith (Georgia Institute of Technology)

6. GENERALIZING THE TRAPRG AND TRAPAX FINITE ELEMENTS . . . 76
by Myles M. Hurwitz (David W. Taylor Naval Research and Development Center)

7. ACOUSTICAL MODES OF ARBITRARY VOLUMES USING NASTRAN TRANSIENT HEAT TRANSFER RF9 82
by V. Elchuri, G. C. C. Smith and A. Michael Gallo (Bell Aerospace Textron)

8. AN ALTERNATIVE METHOD OF ANALYSIS FOR BASE ACCELERATED DYNAMIC RESPONSE IN NASTRAN 89
by V. Elchuri, A. Michael Gallo and G. C. C. Smith (Bell Aerospace Textron)

9. A NASTRAN DMAP PROCEDURE FOR CALCULATION OF BASE EXCITATION MODAL PARTICIPATION FACTORS 113
by William R. Case (NASA Goddard Space Flight Center)

10. FINITE ELEMENT ANALYSIS OF FLUID-FILLED ELASTIC PIPING SYSTEMS 141
by G. C. Everstine, M. S. Marcus and A. J. Quezon (David W. Taylor Naval Ship Research and Development Center)

11. PROPAGATING PLANE HARMONIC WAVES THROUGH FINITE LENGTH PLATES OF VARIABLE THICKNESS USING FINITE ELEMENT TECHNIQUES 161
by J. H. Clark, A. J. Kalinowski and C. A. Wagner (Naval Underwater Systems Center)

PAGE iv INTENTIONALLY BLANK

PRECEDING PAGE BLANK NOT FILMED

12. PROPAGATION OF FLEXURAL AND MEMBRANE WAVES WITH FLUID LOADED NASTRAN PLATE AND SHELL ELEMENTS 178
by A. J. Kalinowski and C. A. Wagner
(Naval Underwater Systems Center)

13. DYNAMIC CERTIFICATION OF A THRUST-MEASURING SYSTEM FOR LARGE SOLID ROCKET MOTORS 207
by R. A. LeMaster and R. B. Runyan
(Sverdrup Technology, Inc.)

14. DETERMINATION OF ELEVATOR AND RUDDER HINGE FORCES ON THE LEARJET MODEL 55 AIRCRAFT 226
by Robert R. Boroughs and Viswa Padmanabhan
(Gates Learjet Corporation)

15. A NEW METHOD FOR GENERATING AND MAINTAINING RIGID FORMATS IN NASTRAN 249
by P. R. Pamidi and W. Keith Brown (RPK Corporation)

16. IMPLEMENTATION OF ELASTIC-PLASTIC STRUCTURAL ANALYSIS INTO NASTRAN 255
by Alvin Levy, A. B. Pifko and P. L. Ogilvie
(Grumman Aerospace Corporation)

17. ELASTIC-PLASTIC ANALYSIS OF ANNULAR PLATE PROBLEMS USING NASTRAN 281
by P. C. T. Chen (Benet Weapons Laboratory)

18. BOLT IN BORE BOUNDARIES 293
by T. G. Butler (Butler Analyses)

N84
15591

UNCLAS

D1

N84 15591

BANDIT in NASTRAN

Gordon C. Chan
Sperry Corporation

SUMMARY

BANDIT (ref. 1 and 2) has been implemented into the NASTRAN April '83 release. It is now a permanent feature in NASTRAN and will be included in all future releases for all four computing machines (IBM, CDC, UNIVAC, and VAX).

INTRODUCTION

Originally BANDIT operated as a preprocessor of NASTRAN. It read the NASTRAN input cards and produced a set of resequencing (SEQGP) cards that would greatly reduce the computational time required by the matrix decomposition module of NASTRAN for a large structure. In the past, many computer centers had installed BANDIT in their systems together with the NASTRAN program. The user would run the BANDIT program and NASTRAN as if they were one program (or two separated programs depending on how the two programs were actually tied together in the computer systems). In some cases, the user was required to pass the input cards and the output SEQGP cards between the two programs, and in others, the data was manipulated through the use of cataloged disc files. Although there is nothing wrong with this BANDIT-NASTRAN arrangement, there are, however, several shortcomings:

1. Each installation requires patching the BANDIT-NASTRAN operation for each new NASTRAN release.

2. The complete NASTRAN input deck is read and decoded twice, once by BANDIT and once by NASTRAN, which is inefficient and redundant. In addition, BANDIT requires that all continuation cards must follow immediately their parent input cards.

3. BANDIT uses Fortran files which may become dead files for NASTRAN which uses its own GINO files. These dead files are carried along throughout the entire duration of NASTRAN execution.

4. When source code is added to NASTRAN for a new connection element, the element table in BANDIT needs to be updated and re-compiled, and the BANDIT executable program re-generated, or the $-APPEND option must be used.

5. There are four versions of BANDIT for IBM, CDC, UNIVAC, and VAX computers.

The BANDIT in the NASTRAN April '83 release has removed all the above deficiencies, and it comes in one version applicable to the four computing machines.

To reduce redundancy and other input limitations, all the input card handling subroutines of the original program were not used. Only thirty-two of the original seventy-two source codings were installed in LINK 1 of NASTRAN. The overlay segment for BANDIT routines is therefore greatly simplified. BANDIT is executed now only when the user's input deck is read in by NASTRAN, decoded, and free of error.

BANDIT IMPLEMENTATION

The implementation of BANDIT in NASTRAN follows two simple guidelines: a NASTRAN user needs no prior knowledge of BANDIT, its theory, and input requirement; and BANDIT should not prematurely terminate the NASTRAN job due to user input error. In addition, most of the useful features and program flexibility of the original BANDIT version are retained in this implementation. Eight options are available to the user to utilize some special features that the program offers. The original BANDIT program uses the $-sign input cards for these options, whereas in NASTRAN, NASTRAN card input (see NASTRAN User's Manual, p. 2.1-2) is used. The following table compares the two methods (with default values underlined):

Original BANDIT	BANDIT in NASTRAN	OPTION USEAGE
$GRID=n	(not used)	To inform BANDIT no. of grid points
$MPC=NO,YES	BANDTMPC=0,1,2	To include MPC's and rigid elements in resequencing (1), rigid elements only (2), or none of these (0)
(none)	BANDTDEP=0,1	To include (0) or to exclude (1) dependent grids if BANDTMPC-1, or 2
$METHOD=CM, =GPS, =both	BANDTMTH=1,2,3,	To use Cuthill-Mckee method (1), Gibb-Poole-stockmeyer method (3), or both (2)
$CRIT=2,1,3, 4	BANDTCRI=1,2,3 4	To set criterion for evaluation: rms-wavefront (1), bandwidth (2), profile (3), or max-wavefront (4)
$PUNCH=NO,YES	BANDTPCH=0,1	To punch (1) out SEQGP cards and terminate NASTRAN job
$NASTRAN=NO, =YES	(not used)	To execute NASTRAN after BANDIT (IBM only)
(none)	BANDTRUN=0,1	To generate SEQGP cards unconditionally (1)

Original BANDIT	BANDIT in NASTRAN	OPTION USEAGE
$DIMENSION=n	BANDTDIM=m	To redefine scratch array dimensions to n (or 100x[m], default=150)
(none)	BANDIT=-1,0	To skip BANDIT in NASTRAN (-1)

BANDIT OPTIONS

Currently NASTRAN provides two methods to skip over BANDIT operation. First, the NASTRAN BANDIT=-1 option can be used. The second method is to include one or more SEQGP cards in the bulk data deck. In this second method, BANDIT would terminate since the user has already stated his choice of SEQGP resequencing cards. However, the NASTRAN BANDTRUN=1 option can be used to force BANDIT to generate new SEQGP cards to replace the old SEQGP set already in the input bulk data deck. In all instances when BANDIT is executed, NASTRAN will issue a page of summary to keep the user informed of the basic resequencing computations. The user may refer to reference (1) for definition of the technical terms used.

The NASTRAN HICORE card can be used in the UNIVAC machine to increase the open core for BANDIT operation. In all machines, BANDIT automatically counts the number of grid points used in a NASTRAN job, and it is able to set up the exact array dimensions needed for its internal computation. However, if the user's structure model uses more grid points in the connecting elements than the total number of grid points as defined in the GRID cards, BANDIT will issue a fatal message and stop. In the case where non-active grid points (defined in the GRID cards but nowhere used in the model) do exist, BANDIT will add them to the end of the SEQGP cards, and their presence will not cause fatal crashing in a NASTRAN job.

Rigid elements and MPC's are included in the BANDIT computation only when the BANDMPC=1 (or 2) option is requested, and their depending grid points can be controlled by the BANDTDEP option. The rigid elements are treated as a set of MPC cards (ref. 3). Reference (1) states: "It should be emphasized here that only in rare cases would it make sense to let BANDIT process MPC's. The main reasons for this are that BANDIT does not consider individual degrees of freedom and, in addition, cannot distinguish one MPC set from another."

CONSIDERATION OF SOME SPECIAL ELEMENTS

The axisymmetic elements produce two grid numbers for each grid point (RINGAX) defined in the bulk data deck. Therefore, BANDIT in NASTRAN will use twice the number of grid points in its computation and produce the 1000000 and

2000000 series of grid numbers in the generated SEQGP cards. Other pseudo elements (such as the surface elements used in heat or fluid problems) which are not present in the element definition table (GPTABD data block) of the NASTRAN program are therefore excluded in BANDIT computation. On the contrary, any new element (developed by user), whose specification is defined in the GPTABD data block, is automatically brought into grid point resequencing.

NASTRAN RESTART

A few comments about NASTRAN restart jobs and BANDIT are needed to clarify BANDIT operational procedure:

1. BANDIT is automatically skipped if it is an unmodified restart job. However, the previously generated SEQGP cards are already absorbed into the NASTRAN data base, such as the EQEXIN, SIL, BGPDT, etc. A message is printed to inform the user that BANDIT is not needed.

2. BANDIT is always executed if it is a modified restart job.

3. BANDIT can always be executed if the restart job contains one or more of the NASTRAN-BANDIT options (e.g., NASTRAN BANDTMTH=2). A NASTRAN BANDIT=-1 option can be used to stop BANDIT execution unconditionally.

At the beginning of a NASTRAN job, the Input File Processor modules (IFP1 and IFP) in LINK 1 read the executive and case control cards and process the complete bulk data deck. The SEQGP cards generated by BANDIT are added directly to the NASTRAN data base (GEOM1 file) at a much later stage. In other words, since these SEQGP cards are not part of the original bulk data deck, they are simply not available for the restart/alter feature of NASTRAN.

NASTRAN BULKDATA OPTION

A new option (key work BULKDATA) is also added to the NASTRAN card in the April '83 release. It allows NASTRAN just to examine the input data deck and echo any user error detected. Since this new option (NASTRAN BULKDATA=1) and any of the BANDIT options share a common switch in NASTRAN internal programming, they cannot be used simultaneously. The BANDTPCH option acts almost like the BULKDATA option, but in addition, the SEQGP cards are punched out.

CONCLUSION

The author wishes to thank Dr. G. C. Everstine for his permission to use his program (BANDIT, release 9.0) for this project.

REFERENCES

1. Everstine, G. C.: BANDIT USER'S GUIDE, COSMIC Program No. DOD-00033, May 1978.

2. Everstine, G. C.: "Reduction of Matrix Wavefront for NASTRAN", 7th NASTRAN Users' Colloquium, NASA Conference Publication 2062, October 1978, pp. 111-122.

3. Pamidi, P. R.: "Addition of Rigid Elements to NASTRAN", 6th NASTRAN Users' Colloquium, NASA Conference Publication 2018, October 1977, pp. 449-468.

N84
15592

UNCLAS

D2 N84 15592

NASA/MSFC NASTRAN AUXILIARY I/O ROUTINES

Malcolm Tagg
McDonnell Douglas Technical Services Company
and
Bob Thornton
Boeing Computer Support Services

ABSTRACT

Since the initial installation of NASTRAN on the UNIVAC 1100/82 computer at the Marshall Space Flight Center (MSFC), a number of "local" codes have been incorporated as "user routines." This paper describes four of these codes and how interested users may obtain additional information.

INTRODUCTION

The MAP elements supplied by COSMIC/NASTRAN contain the user subroutine names OUTPT4, DUMOD3, etc., along with corresponding dummy subroutines. Locally generated "user routines" are compiled and the relocatable elements are copied over the dummy relocatables for mapping into the COSMIC/NASTRAN system. Several local codes have been generated for the MSFC computer installations by BCSS and its predecessors and incorporated into NASTRAN in this manner.

The routines were written in the FORTRAN V language as used with standard COSMIC/NASTRAN. All of the appropriate links were mapped using the MAP elements supplied with the COSMIC/NASTRAN package.

The "user routines" are described in the following format: 1) purpose of routine or function, 2) installation of routine into standard COSMIC/NASTRAN, 3) example showing use of the routine. Note that the routine names used in the text differ from the DMAP "calling" names.

BACKGROUND/REQUIREMENTS

OUTPT4 -	This module was written to create FORTRAN-written, unformatted user tapes containing banded matrix data recovered from NASTRAN matrix data blocks as requested by the user via the OUTPUT4 DMAP instruction. The data is in a simple compact, convenient form and contains no special labeling codes.
INPTT4 -	Companion module to OUPT4, reads matrix data blocks from OUTPT4 tapes.
DUMOD3 -	This module was created to convert NASTRAN tabular data blocks into matrix data block format for convenience in manipulation and output, especially by OUTPT4. The element or gridpoint identification data is also recovered and output separately.

INPTT3 - This routine uses coding supplied by Rockwell International (RI) for reading matrix data in that company's customary format into NASTRAN matrix data blocks. The RI data is in a compact Fortran-formatted coded form, which appears to have quite widespread acceptance in the aerospace field.

PFDR - Print File Data Retrieval post processor originally written to extract OUTPT4 data from the NASTRAN print file, it is particularly useful when data output is required from more than one link execution as occurs frequently during substructure recovery procedures. In such cases, the normal output files are rewound after each link has been executed, thus ensuring that subsequent executions of the output modules will overwrite earlier ones. The print file is, of course, rewind inhibited. The program has now been generalized to extract all types of data. The user is required to provide header information to enable the program to find the data on the NASTRAN print file.

IMPLEMENTATION

1. OUTPT4 - Outputs selected matrices to binary file INP1.

   A. Entry Point - OUTPT4; SUBROUTINE: WRTAPE

   B. NASTRAN Link: LINK14

   C. DMAP Calling Sequence: OUTPUT4 I1,I2,I3,I4,I5//V,N,P1/V,N,P2 $

   D. Input Data Blocks: Ii - Any matrix data block which the user desires to be written on NASTRAN file INP1. Purged data blocks are ignored. Up to five data blocks may be output.

   E. Output Data Blocks: None.

   F. Method: The OUTPT4 routine checks to determine whether the matrix data block is purged. If it is not, a call is made to subroutine WRTAPE, which writes each column of the matrix onto the user tape INP1. Parameters P1 and P2 provide controls corresponding to those in the standard OUTPT2 module (q.v.).

   G. Example: A comprehensive example of OUTPT4 and INPTT4 usage is provided as part of the description for the latter routine.

2. INPTT4 - reads matrix data from an OUTPT4 file assigned to INP2 into a specified matrix data block.

   A. Entry Point: INPTT4.

   B. NASTRAN Link: LINK2.

   C. DMAP Calling Sequence:

      INPUTT4 /MDB,,,,/V,N,P1/V,N,P2/V,N,P3 $

   D. Input Data Blocks: None.

   E. Output Data Blocks:

      MDB - Matrix data block to be loaded with data from user file INP2.

   F. Method: Retrieves one matrix from user file INP2 for each call to the routine. This file may be the INP1 file generated by the OUTPT4 routine or a similar user-written FORTRAN file. The required format for this file and usage of parameters P1, P2 and P3 are described in the OUTPUT4 documentation.

   G. Examples: The use of both INPTT4 and OUTPT4 is illustrated in the DMAP ALTER sequence of Figure 1. Two matrices are read from a file previously created by OUTPT4 and subsequently printed using the MATPRN module (Figure 2). The OUTPT4 listing is shown in Figure 3.

   H. Notes:

      1. The primary use of this routine is to enable the user to obtain NASTRAN generated matrices in a FORTRAN binary format for subsequent use in user-written Fortran programs. Similarly formatted matrices created by NASTRAN OUTPT4 or by user-written Fortran programs can be read into NASTRAN data blocks by using the companion INPTT4 module.

      2. The order of retrieval of matrix data blocks must be in the order which they were written.

      3. Matrices output by OUTPT4 will be written on file INP1. This tape must be assigned as INP2 in subsequent NASTRAN runs when using INPTT4 to recover the matrices. Parameter usage is discussed in the user documentation.

**ORIGINAL PAGE IS
OF POOR QUALITY**

DMAP ALTER SEQUENCE FOR INPTT4 AND OUTPT4

```
ID RI ORBITER
APP       DISPLACEMENT
SOL   1,0
DIAG 8
TIME 150
$
$       INPUTS KG,MO INTO KORB,MORB
ALTER 36
INPUTT4/KORB,,,,/C,N,193/C,N,193/C,N,2 $
CHKPNT KORB $
MATPRN KORB,,,,//  $
OUTPUT4 KORB,,,,//C,N,1/C,N,1 $
EXIT
ENDALTER
CEND
```

FIGURE 1

ORIGINAL PAGE IS
OF POOR QUALITY

MATRIX AFTER INPTT4 EXECUTION

```
     MATRIX KOHE      (GINO NAME 101 ) IS A REAL        193 COLUMN X    193 ROW RECTANG  MATRIX.
COLUMN       1        ROWS       1 THRU     193    -----------------------------------------------------------------

   1.79086+05  -1.07880+05  -1.53271+03  -6.38503+02   8.54546+03   6.40303+04  -2.67360+03   8.04492+03  -6.21306+04   2.73919+04
  -1.54760+06  -4.70712+04   6.09942+04   1.53621+04  -3.93061+04  -1.17151+04  -5.08813+02   1.47939+04   9.36227+03  -4.04306+03
   6.15556+03   2.60374+03   3.49066+03  -1.63617+04   6.73577+03   1.33630+03   3.31632+04   2.17690+03  -1.00340+03   3.26114+03
  -3.42620+03  -2.19477+03  -3.61942+03  -5.61740+03  -2.08431+02   9.47095+02  -9.34969+01   2.66353+01   1.12700+02  -2.29765+03
  -7.60416+01  -5.16667+02   7.57949+02   2.66266+01  -1.72016+07  -1.03655+03  -7.54797+01   3.02732+02   7.39621+02  -3.20177+01
  -1.57521+02  -2.14741+03  -1.23374+03  -1.35438+02   9.99146+02  -4.34526+00  -5.69904+00  -1.04996+03   3.69242+02  -3.20291+02
   1.15503+03   3.42164+02   5.19550+02   1.05538+03  -5.76560+02  -6.72740+02  -1.96999+03  -2.32856+02   1.57910+07  -1.07910+03
   2.15553+01  -1.19422+02   1.16490+03   2.92930+01   1.90114+07   9.30117+02  -6.01263+01  -3.15512+02  -1.60142+03  -3.24193+01
   1.41490+02  -1.03484+03   2.48042+01  -9.36665+01   1.04907+03   1.03796+01   8.69191+01   7.54985+02  -4.44715+01  -1.96645+02
  -1.10709+03  -2.04461+01   1.12624+02  -8.79758+02   3.72626+01  -1.02561+02   8.50141+02   1.00713+01   4.56671+01   6.50030+02
  -3.90209+01  -2.03712+02  -6.93611+02  -3.46946+01   1.70353+02  -6.05045+02   3.10612+02  -5.57702+02   5.46569+02   1.01666+02
   5.69183+02   6.43029+02  -2.02404+02  -5.66990+02  -7.06079+02  -2.51645+02   5.30664+02  -4.04049+02   1.30917+01   2.60741+02
   2.19636+02   4.63965+00   1.44420+01   2.77059+01  -4.56488-01  -6.25733+01   1.36373+02  -6.30554+01  -4.11779+02  -4.41472+02
  -6.52806+00  -2.66957+01  -1.17255+02   7.17144-01  -4.74618+00   7.43808+01   4.71110+01  -2.71173+02   4.20144+02   4.79257-02
  -5.69695+01   5.72646+01   7.65008+00   6.06184+01  -2.08660+07   2.26952-01   1.95195+00  -5.90909-01   2.10491+00   1.60561+01
   4.76750+01  -5.07263-02  -2.04308+00   4.26695+01  -9.02156+00   5.32595+01   2.61094+01  -4.23244-01   1.41305+01   6.24920+01
  -5.19581-01   6.76566-01   1.68200+01  -1.03797+00   7.23572+00   6.22935+00   8.00607-01  -4.18914+00   1.73934+00   1.06025+00
   1.37092+00   1.34269+01   2.49711+00   5.64631+00   6.24980+00   1.17707+00  -8.20952-01   1.37650+00  -2.37244-01  -2.08880+00
   2.96312+00  -2.64142-01  -4.91156+00  -7.96025-01   3.13635+01   1.63129-01   2.70938+00  -1.01071+02   1.52410+02  -2.40704+02
  -9.06665-01   1.15397+01  -3.46547+00

COLUMN       2        ROWS       1 THRU     193    -----------------------------------------------------------------

  -1.07680+05   7.80277+04   3.70717+02   4.84021+01  -2.72050+03  -7.29513+04   4.10120+02  -7.47900+03   5.99746+04  -1.93296+04
   1.25611+06   4.59847+04  -7.19089+04  -1.46343+04   3.32303+04   1.24812+04   5.92197+02  -1.33631+04  -8.51639+03   1.46401+03
  -2.19433+03  -8.60012+02  -3.31926+03   1.43461+04  -6.19309+03  -4.63664+02  -1.12717+04  -1.12324+03   3.11155+02  -1.17374+03
   1.13243+03   1.96333+03   3.45384+03   4.90311+03   2.11648+02  -7.16707+02   4.04461+00  -2.91020+01  -8.73917+01   2.10733+03
   1.27005+01   2.45799+02  -1.54507+02  -4.74296+00   6.00539+01   2.70197+02   6.90104+01  -3.21252+02  -8.21505+02   2.05750+01
   1.44660+02   1.99067+03   3.45443+00   5.31798+01  -1.90102+07  -2.94960-01  -7.22724+00   2.60983+02  -3.00061+02   2.15175+02
  -1.19361+03  -7.54566+01  -2.32562+02  -2.17128+02   5.34791+07   6.00126+02   1.02614+03   5.05032+01  -9.79045+01   3.02524+02
  -2.77598+01   7.64857+01  -1.16145+03  -4.15565+00  -9.02279+01  -2.03676+02   6.40158+01   2.00505+02   1.47075+03   6.51373+00
  -6.63792+01   3.20210+02  -2.62652+01   7.14960+01  -1.01601+03  -2.47024+00  -4.46580+01  -1.75672+02   4.16296+01   1.74506+02
   1.69045+03   7.44772+00  -4.74200+01   2.89200+02  -3.63576+01   1.53209+02  -8.15345+02  -7.00534-01  -2.74319+01  -1.61077+02
   3.64905+01   1.80437+02   8.16692+02   1.04523+01  -6.90073+01   2.33094+02  -2.07133+02   4.79420+02  -5.21930+02  -2.43399+01
  -2.61672+02  -1.65164+02   2.56402+02   5.12662+02   6.39723+02   4.73120+01  -1.94494+02   1.43266+02  -3.93256+00  -1.11022+02
  -6.37532+01  -1.31266+00  -6.55650+00  -7.51408+00   5.44258-01   5.01775+01  -1.19143+02   5.60603+01   3.76013+02   3.92645+02
   5.46702+00   3.10629+01   9.73273+01  -1.03693-01   1.74390+00  -6.19400+00  -4.00566+01   2.46100+02  -3.99636+02  -2.09630-02
   5.42260+01  -5.16205+01  -1.99243+00  -1.01472+01   1.14181+02  -7.37161-02  -2.55942-01   7.36607-01  -1.99016+00  -1.65157+01
  -2.02206+01   2.16011-02  -5.29304-01  -1.44526+01   3.51927+00  -1.93752+01  -7.10170+00   8.03655-02  -5.01926+00  -1.94290+01
   2.67359-01  -4.73375-02  -5.11472+00   4.35691-01  -3.70056+00   1.29257+00  -5.46232-01   2.47012+00   1.40973-01  -2.01505-01
  -5.64612-02  -4.67473+00  -7.45290-01  -1.99082+00  -1.87545+00  -1.00701+00   1.04796+00  -9.73227-01   4.25375-01   1.17011+00
   1.74965+00   3.97540-01   2.15040+00   4.04710-01  -1.31223+01  -6.94961-01  -3.43634-01   4.78766+00   3.03699+01   6.42061+01
```

FIGURE 2

OUTPT4 MATRIX LISTING

```
MATRIX KGPB     UNPACKED AND WRITTEN ON TAPE.

GINO FILE NAME=  101
NO. COLS. = 193
NO. ROWS = 193
TYPE= 2
FORM= 2

OPEN CORE LENGTH=  36594
GINO SYSTEM BUFFER= 1795
USABLE OPEN CORE=36799

COLUMN    1

 II=  1   N= 193
 .1790857600039+006  -.1070602100991+006  -.1532708640968+004  -.6765026951153+003   .8545464843010+004   .6403030360934+005
-.2673600845623+004   .0844920017724+004  -.6213861779810+005   .2739180383247+005  -.1547679524046+007  -.4707124617770+005
 .6599420679363+005   .1536206164633+005  -.3930612643212+005  -.1171509024528+005  -.5088128766001+003   .1479387061415+005
 .9362272126090+004  -.4843659214373+004   .6155562610045+004   .2663737834851+004   .3490677110229+004  -.1636165989186+005
 .6735770449507+004   .1336301318293+004   .3316316335123+005   .2176982854405+004  -.1003483916202+004   .3281135544203+004
-.3626002142587+004  -.2199766360603+004  -.3619421717613+004  -.5617481757276+004  -.2084305349123+003   .9470951848585+003
-.9349605550314+002   .2663534391763+002   .1127796933001+003  -.2297650245831+004  -.7602159498467+002  -.5166065282803+003
 .7574491185106+003   .2682656532985+002  -.1720181949317+003  -.1036549079198+004  -.7597960209903+002   .3027311757376+003
 .7396217176657+003  -.3201774781904+002  -.1575210120383+003  -.2147413179671+004  -.1233742098644+002  -.1354378013309+003
 .9991463672001+003  -.9345257456505+001  -.5699040370869+001  -.1049955249227+004   .3692623206508+003  -.3202911956276+003
 .1155033701661+004   .3421642870815+003   .5195578603496+003   .1055376044595+004  -.5765676611441+003  -.6727475970099+003
-.1969993662252+004  -.2328556979063+003   .1579162593593+003  -.1079104905216+004   .2155525231198+002  -.1194217003372+003
 .1164979601846+004   .2929297363163+002   .1901142676756+003   .9361173821657+003  -.6812629763895+002  -.3155117926546+003
-.1601417434624+004  -.3241932022641+002   .1914896985516+003  -.1034835752678+004   .7480421662040+002  -.6366651849072+002
 .1049066672165+004   .1037960574217+002   .0691912739453+002   .7549850252905+003  -.4447150924321+002  -.1966447772531+003
-.1187088729060+004  -.2044809614265+002   .1126235648311+003  -.8797578736642+003   .3772625027526+002  -.1025613965927+003
 .8501491094305+003   .1607127637355+002   .4566714262409+002   .6506377595386+003  -.3902093471358+002  -.2037119876633+003
-.8936100448005+003  -.3469464183194+002   .1783526738817+003  -.6850445867194+003   .3106118129679+003  -.5577620424492+003
 .5465690946355+003   .1016658121785+003   .5941033169289+003   .6430286811313+003  -.2824036723346+003  -.5609900583475+003
-.7660785959702+003  -.2516449911394+003   .5306630631900+003  -.4049493300542+003   .1369160729965+002   .2607409538874+003
 .2190380410756+003   .4639846643713+001   .1444196155122+002   .2770589848948+002  -.4564862070858+000  -.6257320791626+002
 .1363726056791+003  -.6305538010736+002  -.9117792304944+003  -.4419720702665+003  -.6528063642309+001  -.2669566232166+002
-.1172551697132+003   .7171436963086+000  -.4746179520887+001   .2438878525460+002   .4711177366701+002  -.2711172708616+003
 .4201440597444+003   .4792569061435-001  -.5896946457473+002   .5726457006872+002   .7850061135559+001   .6061842060605+002
-.2680595624057+003   .2269520454896+000   .1951950659934+001  -.5969092969711+000   .2104906544339+001   .1605611459048+002
 .4767560151427+002  -.5072626679920-001  -.2043089751106+001   .4786956657478+002  -.9821556306136+001   .5325953648383+002
 .2616939430697+002  -.4232443730466+000   .1913840393641+002   .6249197936927+002  -.5145811078370+000   .6765662240254+000
 .1681995507548+002  -.1037971864893+001   .7235715943354+001   .6722934610247+001   .8086865262964+000  -.4189139696497+001
 .1739339341986+001   .1060246369173+001   .1370916371773+001   .1342893882165+002   .2497107900626+001   .5646307378245+001
 .6249797704870+001   .1177865923164+001  -.8209519510192+000   .1376577604860+001  -.2372430215088+000  -.2086790443471+001
 .2463121222749+001  -.2641419130353+000  -.4911555050387+001  -.7960248661158+000   .3136351948590+002   .1631290323414+000
 .2709375489809+001  -.1010712529194+001   .1524097930662+003  -.2487084336703+003  -.9060551229222+000   .1153969372898+002
-.3465473142709+001

COLUMN    2

 II=  1   N= 193
-.1076802106991+006   .7402773625755+005   .3707167220733+003   .4848213354613+002  -.2728499669663+004  -.2295130713037+005
 .4101276314431+003  -.7478996330606+004   .5997463476713+005  -.1932950855025+005   .1250108212040+007   .4598469445369+005
-.7196865483632+005  -.1463439406105+005   .3323032622675+005   .1248110227817+005   .5921970300954+003  -.1336305170872+005
```

FIGURE 3

ORIGINAL PAGE IS
OF POOR QUALITY

3. DUMOD3

A. Entry Point: DUMOD3

B. NASTRAN Link: LINK7

C. DMAP Calling Sequence:

```
DUMMOD3  TDB,,,,,,,/MDB,,,,,,,/C,N,P1/C,N,O $
```

D. Input Data Blocks:

TDB NASTRAN Table Data Block.

E. Output Data Blocks:

MDB NASTRAN Matrix Data Blocks.

F. Method: Converts tabular data blocks into matrix data block format. Up to eight data blocks may be converted. The tables are mapped into a P1 x 8 matrix and the grid point/element ID's into array LTLID which is listed and punched on cards.

G. Examples: The example illustrates how the SPCFORCE (OQG table) can be reformatted using the DMAP sequence shown in Figure 4. The LTLID array of gridpoint ID numbers is shown in Figure 5. Figure 6 shows the NASTRAN SPCFORCE output and Figure 7 shows the corresponding DUMOD3 matrix, IFLOAD, as output using OUTPT4.

DUMOD3 AND OUTPT4 DMAP INSTRUCTIONS

```
120  DUMMOD3  006,,,,,,,,/IFLOAD,,,,,,,/C,N,100/C,N,0  $
121  CHKPNT   IFLOAD  $
122  OUTPUT4  IFLOAD,,,,//C,N,0/C,N,1  $
```

FIGURE 4

LTLID (ELEMENT/GRIDPOINT ID) ARRAY PRINTED AND PUNCHED BY DUMOD3

```
@XQT   *NASTRAN.LINK7

*** DIAG  8 MESSAGE -- TRAILER FOR DATA BLOCK IFLOAD    =        6      800        2        1      237     2962
      201          6          600          2          1
LUCKY YOU - MISSION ACCOMPLISHED

 LTLID ARRAY FOLLOWS
    50100     50200     50300     50400    200300    200700    201000    201300    201700    202100    205300    206000    206400

   207500    207600    207700    208000    208500    208800    209200    210500    211200    211300    211800    211900    213400

   213700    214100    214800    215900    217500    218200    219700    220100    220200    220500    220700    220800    220900

   221000    221200    221600    221700    222000    222200    222500    227900    228300    228700    229300    229400    230000

   260100    260200    260300    260400    260500    260600    260700    260800    260900    261000    262100    262200    300100

   300200    300300    300400    300500    300600    300700    300800    300900    301000    301100    301200    301300    301400

   301500
```

FIGURE 5

```
                            F O R C E S   O F   S I N G L E - P O I N T   C O N S T R A I N T

POINT ID.   TYPE        T1              T2              T3          R1          R2          R3
   501       G     -1.206804-05     1.199143-04     1.613958-04     .0          .0          .0
   502       G      4.743631-06    -2.396741-04    -1.591604-04     .0          .0          .0
   503       G      1.039475-05     1.796075-04     1.850083-04     .0          .0          .0
   504       G     -4.584176-06    -4.991144-05     1.962856-05     .0          .0          .0
  2003       G      6.776796-04    -4.590919-03    -2.676502-05     .0          .0          .0
  2007       G      8.541583-03    -4.224124-03     3.366251-05     .0          .0          .0
  2010       G     -2.066444-03    -1.081322-02    -3.450337-05     .0          .0          .0
  2013       G     -8.890361-04    -1.502390-02    -7.701640-05     .0          .0          .0
  2017       G      3.489469-03     2.208480-02     3.170490-04     .0          .0          .0
  2021       G      1.604919-03    -1.295724-03    -6.565984-06     .0          .0          .0
  2053       G      4.066217-03    -6.056302-03    -3.244750-05     .0          .0          .0
  2060       G     -2.663704-03     2.597022-02    -1.893663-04     .0          .0          .0
  2064       G     -5.511136-03     3.506613-02    -6.132162-05     .0          .0          .0
  2075       G     -2.132388-04    -1.438704-02     1.652850-05     .0          .0          .0
  2076       G      6.916324-03     5.005876-03     3.090334-06     .0          .0          .0
  2077       G     -1.588821-02    -1.470724-02    -1.176732-05     .0          .0          .0
  2080       G      1.702856-02    -2.640372-03     2.055277-06     .0          .0          .0
  2085       G     -7.705988-04     5.992521-03     4.369031-05     .0          .0          .0
  2088       G     -6.792754-03    -1.247024-02     6.748242-05     .0          .0          .0
  2092       G     -5.295667-03    -1.091623-02    -1.549079-04     .0          .0          .0
  2105       G      3.217898-03     2.227146-03     3.284419-05     .0          .0          .0
  2112       G      2.620365-04    -2.599823-02     8.186604-05     .0          .0          .0
  2113       G      3.677660-03     1.458527-02     4.641478-05     .0          .0          .0
  2118       G     -4.814373-03    -1.145327-02     1.504774-05     .0          .0          .0
  2119       G      3.294960-03     9.743377-03    -4.582586-05     .0          .0          .0
  2134       G     -6.445710-03     2.721332-02    -3.786112-05     .0          .0          .0
  2137       G      5.345116-03     1.546585-02    -5.719251-06     .0          .0          .0
  2141       G      5.601869-03     8.156471-03    -1.156974-04     .0          .0          .0
  2148       G     -4.004943-03    -5.853392-03    -3.789817-05     .0          .0          .0
  2159       G     -1.881301-03    -2.715342-02    -4.199450-05     .0          .0          .0
  2175       G     -4.314905-03     1.696265-02    -3.387852-05     .0          .0          .0
  2182       G     -1.063962-02    -1.892261-02     1.339583-06     .0          .0          .0
  2197       G      6.898105-03    -4.473658-03     5.992265-06     .0          .0          .0
  2201       G     -1.200352-03    -1.297658-02    -6.877478-05     .0          .0          .0
  2202       G     -1.789929-03    -2.374511-03     5.776048-05     .0          .0          .0
  2205       G      1.422885-03     2.387991-03    -3.556397-06     .0          .0          .0
  2207       G      4.545874-03    -1.132318-02     3.139352-05     .0          .0          .0
  2208       G      4.005946-03     1.341997-02     3.141458-05     .0          .0          .0
  2209       G     -3.969116-03     1.414541-02    -6.278013-05     .0          .0          .0
  2210       G      5.832229-04     1.905805-02    -2.440898-05     .0          .0          .0
  2212       G     -1.365599-03    -3.370620-02    -1.837631-06     .0          .0          .0
  2216       G      4.266109-04    -1.273158-02     1.448176-05     .0          .0          .0
  2217       G     -6.719694-04    -6.144261-03    -2.363826-05     .0          .0          .0
  2220       G      3.261826-05     9.935439-03     2.497232-05     .0          .0          .0
  2222       G     -2.091690-03     8.261646-03    -2.354926-05     .0          .0          .0
```

NASTRAN SFCFORCE OUTPUT LISTING
FIGURE 6

```
MATRIX IFLOAD   UNPACKED AND WRITTEN ON TAPE.

GINO FILL NAME=  101
NO. COLS. =    6
NO. ROWS = 800
TYPE= 1
FORM= 2


OPEN CORE LENGTH= 113066
GINO SYSTEM BUFFER= 1795
USABLE OPEN CORE=*****


COLUMN     1

II=    2    N= 628
-.12068036-04    .11991427-03    .16139576-03    .00000000    .00000000    .00000000    .00000000    .00000000
 .47436311-05   -.23967405-03   -.15916036-03    .00000000    .00000000    .00000000    .00000000    .00000000
 .16394751-04    .17960747-03    .16540830-03    .00000000    .00000000    .00000000    .00000000    .00000000
-.45841763-05   -.44911439-04    .19628555-04    .00000000    .00000000    .00000000    .00000000    .00000000
 .87767962-03   -.45979189-02   -.26765019-04    .00000000    .00000000    .00000000    .00000000    .00000000
 .95415825-02   -.42241237-02    .33662506-04    .00000000    .00000000    .00000000    .00000000    .00000000
-.20664438-02   -.10813224-01   -.34503365-04    .00000000    .00000000    .00000000    .00000000    .00000000
-.86903608-03   -.15023900-01   -.77016397-04    .00000000    .00000000    .00000000    .00000000    .00000000
 .34894688-02    .22094805-01    .31764897-03    .00000000    .00000000    .00000000    .00000000    .00000000
 .16049189-02   -.12457244-02   -.65659436-05    .00000000    .00000000    .00000000    .00000000    .00000000
 .40662169-02   -.60563016-02   -.32447500-04    .00000000    .00000000    .00000000    .00000000    .00000000
-.26637043-02    .25970218-01   -.18936626-03    .00000000    .00000000    .00000000    .00000000    .00000000
-.55111363-02    .35066124-01   -.61321623-04    .00000000    .00000000    .00000000    .00000000    .00000000
-.21323483-03   -.14357036-01    .16528504-04    .00000000    .00000000    .00000000    .00000000    .00000000
 .61163244-02    .50058757-02    .30963344-05    .00000000    .00000000    .00000000    .00000000    .00000000
-.15889205-01   -.14707240-01   -.11757316-04    .00000000    .00000000    .00000000    .00000000    .00000000
 .17028559-01   -.26403725-02    .20552766-05    .00000000    .00000000    .00000000    .00000000    .00000000
-.77059880-03    .59925707-02    .43690311-04    .00000000    .00000000    .00000000    .00000000    .00000000
-.67927536-02   -.12473242-01    .67462422-04    .00000000    .00000000    .00000000    .00000000    .00000000
-.52956668-02   -.10916229-01   -.15440786-03    .00000000    .00000000    .00000000    .00000000    .00000000
 .32178978-02    .22271459-02    .12844188-04    .00000000    .00000000    .00000000    .00000000    .00000000
 .26263655-03   -.25998233-01    .81866044-04    .00000000    .00000000    .00000000    .00000000    .00000000
 .38776596-02    .14595273-01    .46419777-04    .00000000    .00000000    .00000000    .00000000    .00000000
-.46143731-02   -.11453275-01    .15047738-04    .00000000    .00000000    .00000000    .00000000    .00000000
 .32948604-02    .97433770-02   -.45845860-04    .00000000    .00000000    .00000000    .00000000    .00000000
-.66457099-02    .27213320-01   -.37861124-04    .00000000    .00000000    .00000000    .00000000    .00000000
 .53451161-02    .15465854-01   -.57192513-05    .00000000    .00000000    .00000000    .00000000    .00000000
 .56018686-02    .81564706-02   -.11569742-03    .00000000    .00000000    .00000000    .00000000    .00000000
-.46049429-02   -.58533918-02   -.37898167-04    .00000000    .00000000    .00000000    .00000000    .00000000
-.18013013-02   -.27153418-01   -.41994500-04    .00000000    .00000000    .00000000    .00000000    .00000000
-.43149046-02    .16862650-01   -.33878517-04    .00000000    .00000000    .00000000    .00000000    .00000000
-.10639619-01   -.18922612-01    .13395834-05    .00000000    .00000000    .00000000    .00000000    .00000000
 .68981051-02   -.44736578-02    .59922645-05    .00000000    .00000000    .00000000    .00000000    .00000000
-.12003521-02   -.12976578-01   -.68774775-04    .00000000    .00000000    .00000000    .00000000    .00000000
-.17899293-02   -.23745111-02    .57760480-04    .00000000    .00000000    .00000000    .00000000    .00000000
 .14228448-02    .23679906-02   -.35563966-05    .00000000    .00000000    .00000000    .00000000    .00000000
 .45458743-02   -.11323180-01    .31393525-04    .00000000    .00000000    .00000000    .00000000    .00000000
 .40059464-02    .13419974-01    .31414580-04    .00000000    .00000000    .00000000    .00000000    .00000000
-.39691163-02    .19195413-01   -.62760133-04    .00000000    .00000000    .00000000    .00000000    .00000000
 .56322291-03    .19058050-01   -.24408977-04    .00000000    .00000000    .00000000    .00000000    .00000000
```

FIGURE 7

OUTPT4 LISTING OF DUMOD3 MATRIX FORMATTED SPCFORCE TABLE

ORIGINAL PAGE IS
OF POOR QUALITY

4. INPTT3 - Reads matrix data from an RI-formatted file assigned to INPT into specified matrix data blocks.

   A. Entry Point: INPTT3.

   B. NASTRAN Link: LINK2

   C. DMAP Calling Sequence:

      INPUTT3   KO,MO,,,/KX,MX,,,/C,N,-1/C,N,0/C,N,0 $

   D. Input Data Blocks: RI formatted matrices from file INPT.

   E. Output Data Blocks: All NASTRAN matrix data blocks.

   F. Method: Reads the matrices from an RI-formatted data file into NASTRAN matrix data blocks. Up to five matrices may be read.

   G. Examples: Figure 8 shows the DMAP ALTER sequence required for loading two matrices into the Normal Modes Analysis Rigid Format and adding them into the mass and stiffness matrices. The diagnostic messages printed by NASTRAN to indicate successful completion of the INPUTT3 instruction are shown in Figure 9.

   H. Notes: The file INPT must be assigned containing the RI-formatted data.

ORIGINAL PAGE IS
OF POOR QUALITY

INPUTT3 DMAP ALTER SEQUENCE

```
ID  RI ORBITER
APP       DISPLACEMENT
SOL     3,0
TIME 150
$
$           INPUTS KO, MO INTO KORB, MORB
ALTER 36
INPUTT3  KO,MO,,,/KORB,MORB,,,/C,N,-1/C,N,0/C,N,0  $
CHKPNT   KORB,MORB  $
$
$          FORMS KF1, MF1 AND ADDS KORB, MORB FORMING KFF, MFF
ALTER 71,72
EQUIV    KNN,KF1/SINGLE/MNN,MF1/SINGLE  $
CHKPNT   KF1,MF1  $
ALTER 74,75
SCE1     USET,KNN,MNN,,/KF1,KFS,,MF1,,  $
CHKPNT   KFS,KF1,MF1  $
ALTER 76
ADD5     KF1,KORB,,,/KFF  $
CHKPNT   KFF  $
ADD5     MF1,MORB,,,/MFF  $
CHKPNT   MFF  $
ENDALTER
CEND
```

FIGURE 8

NASTRAN MESSAGE TO DENOTE INPUTT3 MATRIX ENTRY

```
@XQT NASTRAN*NASTRAN.LINK2
 DATA BLOCK KO          FOUND WHILE SEARCHING FOR KORB
 MATRIX BLOCK KORB        IS OF SIZE  797 BY  797 AND TYPE     6

 *** DIAG  8 MESSAGE -- TRAILER FOR DATA BLOCK KORB        =        797       797
 DATA BLOCK MO          FOUND WHILE SEARCHING FOR MORB
 MATRIX BLOCK MORB        IS OF SIZE  797 BY  797 AND TYPE     6

 *** DIAG  8 MESSAGE -- TRAILER FOR DATA BLOCK MORB        =        797       797
```

FIGURE 9

5. PFDR - Print File Data Retrieval post processor

A. Method:

Repeated executions of OUTPUT4 and other output modules within a single NASTRAN run (especially in DMAP Looping) will cause previously written matrix data blocks on INP1 to be overwritten by subsequent calls to the output module. This being a system characteristic, the problem could not be resolved internally. The matrices were preserved in their entirety, however, when written by OUTPUT4 onto the NASTRAN print file. Hence, the print file is saved for subsequent input to a post-processor which extracts the matrices and writes them to a single file, which may be copied to tape for later processing. This approach enables the user to obtain the results of a number of output requests in a single run.

B. Input to PFDR:

The input to the post-processor is simply the NASTRAN printout file itself. This file can be obtained by the instruction @BRKPT PRINT$/FILENAME on the UNIVAC computer. This instruction simply diverts the symbolic print data to the previously assigned file FILENAME, which can then be read by PFDR.

C. The PFDR Post-Processor:

The NASTRAN print file is converted to ASCII code to enable it to be read by the post-processor. The data "key phrase" is input to the post-processor. If no "key" is given, the processor automatically defaults to OUTPUT4 data.

D. Output Data:

The output data will contain the OUTPT4 matrices or the particular data identified by the key phrase. This data is usually copied to tape for subsequent use. The data formats are described in the user documentation.

E. Implementation:

PFDR is currently not available on the MSFC IBM system.

F. Example: A sample runstream is shown in Figure 10.

E. Examples

PFDR SAMPLE RUNSTREAM

```
$
$          PRINT FILE DATA RETRIEVAL
$
@DELETE,C PRXXXX.
@DELETE,C OPXXXX.
@CAT,P PRXXXX,F/I/POS/200
@ASG,A PRXXXX.
@BRKPT PRINTS/PRXXXX
@XQT *NASTRAN.LINK1

(NASTRAN RUN)

@BRKPT PRINTS
@USE 31,OPXXXX.
@ED,UQ PRXXXX.
EXIT
@ASG,A C*NASTRAN.
@PRT,TC C*NASTRAN.
@XQT C*NASTRAN.X
@ED,UP OPXXXX.
EXIT
@ASG,TJ OP4TP,U9S,SAVE04 . PALIIF
@COPY,GMC OPXXXX.,OP4TP.
@COPY,GMC OPXXXX.,OP4TP.
@FREE OP4TP.
@FREE PRXXXX.
@FREE OPXXXX.
@SYM PRXXXX.,,MHSP
@SYM OPXXXX.,,MHSP
```

KEY:

PRXXXX - FILE TO WHICH PRINTOUT IS DIVERTED

OPXXXX - FILE TO WHICH EXTRACTED DATA IS WRITTEN

31 - ALTERNATE PRINT FILE DYNAMICALLY ATTACHED TO OPXXXX

C*NASTRAN.X - EXECUTABLE ELEMENT OF PFDR

OP4TP - TAPE TO WHICH OPXXXX IS COPIED

MHSP - DENOTES PHYSICAL UNIT FOR PRINTER

FIGURE 10

SUMMARY

The MSFC COSMIC/NASTRAN Auxiliary I/O routines provide useful, additional capabilities for input and output of various matrices and tables between external files and NASTRAN. The PFDR print file post-processor allows the user to extract any type of data that is available from the NASTRAN print file. These routines are in frequent use on the MSFC UNIVAC 1100 and IBM systems.

In conclusion, the authors would like to acknowledge the work of Messrs. J. Moorman, P. Halford and D. Harper, who contributed various enhancements under the aegis of the MSFC Engineering Systems Branch of the Huntsville Computer Complex.

Prospective users may obtain further information from
AH33/W. E. Galloway, NASA, MSFC, AL, Telephone: 205-453-2294.

N84
15593

UNCLAS

N84 15593 D3

USING PAFEC AS A PREPROCESSOR FOR COSMIC/NASTRAN*

W. H. Gray
Fusion Energy Division
Oak Ridge National Laboratory
Oak Ridge, Tennessee

T. V. Baudry
PAFEC Engineering Consultants
Knoxville, Tennessee

SUMMARY

Programs for Automatic Finite Element Calculations (PAFEC) is a general purpose, three-dimensional linear and nonlinear finite element program (ref. 1). PAFEC's features include free-format input utilizing engineering keywords, powerful mesh generating facilities, sophisticated database management procedures, and extensive data validation checks. Presented here is a description of a software interface that permits PAFEC to be used as a preprocessor for COSMIC/NASTRAN. This user-friendly software, called PAFCOS, frees the stress analyst from the laborious and error prone procedure of creating and debugging a rigid-format COSMIC/NASTRAN bulk data deck. By interactively creating and debugging a finite element model with PAFEC, thus taking full advantage of the free-format engineering-keyword-oriented data structure of PAFEC, the amount of time spent during model generation can be drastically reduced. The PAFCOS software will automatically convert a PAFEC data structure into a COSMIC/NASTRAN bulk data deck. The capabilities and limitations of the PAFCOS software are fully discussed in the following report.

INTRODUCTION

Numerous general purpose programs are currently available to assist engineers during the data preparation phase of a NASTRAN finite element method problem. The goal of these preprocessors is to accept a minimum amount of user data and create the rigid-format input data structure required by the COSMIC/NASTRAN Bulk Data (NBD), since the NBD is devoid of any sophisticated automatic data generation schemes. Two such sets of software (ref. 2 and 3) based upon other programs were presented at last year's COSMIC/NASTRAN conference. Many others have been presented in previous years. Properly designed preprocessing aids, like these, can greatly reduce the time spent by an engineer in creating the rigid-format required by the NBD. If these aids are interactively executed, much correcting and debugging of a finite element model can be accomplished prior to submission of even the first COSMIC/NASTRAN execution for a new problem. Although most of the available preprocessing aids for COSMIC/NASTRAN meet their design goals, the authors of this paper prefer to use the free-format data preparation and automatic mesh generation capabilities of the PAFEC suite of finite element computer programs. This paper describes software developed for utilizing PAFEC as a preprocessor for COSMIC/NASTRAN.

---

*Research sponsored by the Office of Fusion Energy, U.S. Department of Energy, under contract W-7405-eng-26 with the Union Carbide Corporation.

At the Oak Ridge National Laboratory (ORNL) COSMIC/NASTRAN is leased upon IBM computer equipment. It is generally executed in a batch processing mode. Serving as an interactive front-end to the IBM machines are several DECsystem-10 computers. Within ORNL's computer environment, users generally prefer to interactively create data and IBM Job Control Language (JCL) on the user-friendly DECsystem-10s and then to route these jobs to the IBM mainframe batch queues for number crunching. Because PAFEC can best be utilized in an interactive environment, the DECsystem-10s were chosen as the computers upon which to execute PAFEC.

The PAFEC suite of program modules is executed as a collection of ten separate phases that create and operate upon a database called the Backing Store (BS) file. Among other capabilities, PAFEC has extensive mesh generation facilities; a free-format, engineering-keyword-oriented, modular data preparation scheme; extremely simple methods to represent repetitive data values; automatic load generation facilities; and a complete graphics software package to display the created finite element data. An optionally available interactive program, the PAFEC Interactive Graphics Suite (PIGS), can be obtained to enhance all the above mentioned capabilities. PAFEC is not simply a preprocessor. Solution sequences exist for linear static and dynamic structural mechanics problems as well as for treating certain classes of nonlinear structural mechanics and heat transfer problems.

On the ORNL DECsystem-10s an additional facility has been implemented in the PAFEC control scheme that will automatically invoke the PAFEC to COSMIC/NASTRAN preprocessor for a stress analyst. Mnemonically designated PAFCOS (ref. 4), this software contains several subroutines. The main subroutine, called PAFNBD, serves as a controller for the other subroutines. The other subroutines convert the PAFEC BS internal format for the axis systems, nodal points, material properties, element topologies, element properties, and single- or multipoint constraints into the rigid-format of the COSMIC/NASTRAN NBD. Unique rigid-format continuation card mnemonics are generated as necessary. Upon successful completion of PAFEC PHASE 4, the user's job will have created a disk file, <name>04.NBD, that contains the COSMIC/NASTRAN NBD (<name> symbolically represents the user's PAFEC finite element model job name and 04 is appended to the job name to indicate the file was created in PHASE 4). Thus, the stress analyst can interactively generate, debug, and display a finite element model with PAFEC; convert a model to COSMIC/NASTRAN rigid-format bulk data using user-friendly software; and then solve the model using COSMIC/NASTRAN upon one of the larger mainframe computers at ORNL.

ORGANIZATION

First, a discussion of the most salient features of the model generating capabilities of PAFEC is presented. (Although PAFEC has complete solution capability, it will not be discussed here as it is not germane to the subject of this report.) Secondly, in the remainder of this report, we describe the details of subprogram PAFCOS, its supporting software, and the modifications to the PAFEC executive control. Finally, an example using this software is presented.

MODEL GENERATION WITH PAFEC

The PAFEC modular data system has many advantages. From the user's standpoint, the finite element data are very easy to input and are intelligible without additional documentation. Additionally, data prepared for other finite element programs can be used as input data by PAFEC with less text-editing manipulation. From the system's standpoint, the data modules are easily scanned to determine the solution sequence and the software required to perform the user's specific finite element task (ref. 5).

A PAFEC data module consists of three parts: (1) the module header card, (2) the module contents card, and (3) the free-format numerical data. The module header card and the numerical data are required for every module that the user inputs for a particular finite element problem. (Only those data modules that are needed are entered as data.) The contents card is optional and is used to alter the default definition of certain parts of the data or to change the order of the numerical data located in the third part of the data module. An example of the NODES data module, a fundamental data module, is presented to demonstrate the three parts of the PAFEC modular data:

```
NODES
Z=0.0
NODE          X       Y
   1         0.0     0.0
   2         0.0     1.0
   3         1.0     1.0
   4         1.0     0.0
```

The first card represents the module header card, the second card is a constant contents data card, the third card is a contents data card, and the last four cards present the free-format nodal numerical data.

Other data modules can be used to define nodal coordinates; among these are:

NODES	The NODES module can be used to define nodal coordinates in any axis set.
AXES	The AXES module can be used to define different axis sets.
SIMILAR.NODES	Once any number of nodes have been defined, the SIMILAR.NODES module can be used to define other nodes that are similar but perhaps more conveniently located in another axis system.
LINE.NODES	The LINE.NODES module can be used to define any number of nodes to lie upon the same straight line.
ARC.NODES	Similar to the LINE.NODES module, the ARC.NODES module can be used to define any number of nodes to lie upon the same circular arc.

PAFBLOCKS	When used in conjunction with the MESH module, the PAFBLOCKS module will cause two- and three-dimensional blocks of nodes and elements to be generated.

Several data modules are used in the description of finite element topology, types, material properties, and thicknesses. These modules include:

ELEMENTS	The ELEMENTS module describes the element type, properties, group number, and topology for individual elements.
PAFBLOCKS	When used in conjunction with the MESH module, the PAFBLOCKS module will cause two- and three-dimensional blocks of nodes and elements to be generated.
REFERENCE.IN.PAFBLOCKS	The REFERENCE.IN.PAFBLOCKS module permits modification of generated elements within a PAFBLOCK.
PLATES.AND.SHELLS	The PLATES.AND.SHELLS module describes element thicknesses, material number, and other information for membrane, bending, and axisymmetric finite element analysis.
BEAMS	The BEAMS module describes pertinent information for beam elements.
MASSES	The MASSES module is used in dynamic finite element analyses to add mass at nodes.
SPRINGS	The SPRINGS module is used to input simple axial and torsional springs into a finite element analysis.
GROUP.OF.SIMILAR.ELEMENTS	The GROUP.OF.SIMILAR.ELEMENTS module copies selected elements into new elements by simply incrementing element topology. This facility can be used to conveniently describe finite element geometries that contain repetitious sections.

PAFEC examines the data modules describing a structure and the user's control module to determine how many degrees of freedom to permit at each nodal coordinate. To apply constraints at individual or groups of nodes, the following data modules can be used:

RESTRAINTS	The RESTRAINTS module is the most generally used module for describing the degrees of freedon to be constrained. Each row in the data module can be used to describe the constraints at one node, or, by using the PLANE and possibly AXIS entry, all the nodes that lie on a line or on a plane can be constrained at once.
ENCASTRE	The ENCASTRE module can be used to constrain all the degrees of freedom for a set of nodes.

SIMPLE.SUPPORTS	The SIMPLE.SUPPORTS module can be used to constrain all the translational degrees of freedom for a set of nodes while leaving the rotational degrees of freedom unchanged.
DISPLACEMENTS.PRESCRIBED	The DISPLACEMENTS.PRESCRIBED module can be used to apply nonzero displacements at certain nodes.
REPEATED.FREEDOMS	The REPEATED.FREEDOMS module is used to constrain two or more nodes to move by an identical amount in a particular direction. This module is useful when there is slippage possible at some joint in a structure. By arranging two nodes to be coincident and therefore to have separate and unrelated degrees of freedom, the REPEATED.FREEDOMS module can be used to define those degrees of freedom that are to be continuous across the joint.
HINGES.AND.SLIDES	The HINGES.AND.SLIDES module is the complement of the REPEATED.FREEDOMS module. Instead of specifing constrained degrees of freedom, this module is used to specify unconstrained degrees of freedom.
LOCAL.DIRECTIONS	The LOCAL.DIRECTIONS module does not describe constraints directly. However, this module can be used to force PAFEC to resolve degrees of freedom in different directions other than the global coordinate axes directions.
GENERALIZED.CONSTRAINTS	The GENERALIZED.CONSTRAINTS module permits writing arbitrary linear functions relating displacements among any number of nodes. Rigid links may be specified with this module.

THE PAFCOS SOFTWARE INTERFACE

The PAFCOS software developed at ORNL permits the user to define a finite element model, using the previously discussed modular data dictionary, and then to automatically create a rigid-format, COSMIC/NASTRAN bulk data deck. Subroutine PAFNBD serves as a controller for several other subroutines, individually discussed below, that are collectively located in the PAFCOS subroutine library. When the user includes the COSMIC/NASTRAN control directive in a PAFEC control module, then a call to subroutine PAFNBD will be inserted in the PHASE 4 FORTRAN generated for the job. Execution of the PAFNBD subroutine will cause the axis systems, nodal coordinates, material properties, element topologies, element properties, and constrained degrees of freedom to be successively converted from internal PAFEC BS format to COSMIC/NASTRAN bulk data rigid format. Upon successful completion of the constraint conversion, subroutine PAFNBD returns to the PHASE 4 FORTRAN and normal PAFEC execution.

The PAFCOS software is written in FORTRAN-66 and uses the PAFEC series R09800 subroutines exclusively for accessing the data modules contained in the user's BS file. Therefore, this software is easily implemented in any system where PAFEC has been installed. (A FORTRAN-77 version of the software is being created.) The next several sections discuss the functions of the individual subprograms contained within the PAFCOS software library.

Subroutine PNCOOR

Subroutine PNCOOR performs the processing of axis definitions from PAFEC BS to COSMIC/NASTRAN format. This subprogram processes each entry of BS module 68 (the internal storage number given to PAFEC axis sets) and writes the appropriate COSMIC/NASTRAN CORD2R, CORD2C, or CORD2S data cards, depending upon whether the PAFEC coordinate system is rectangular, cylindrical, or spherical, respectively. Unique continuation card mnemonics are generated as necessary.

Subroutine PNNOD

Subroutine PNNOD generates COSMIC/NASTRAN GRID cards from the PAFEC BS module 1 (the internal storage number given to PAFEC global, cartesian nodal coordinates). All GRID cards are specified in global coordinates. If PAFEC BS module 4 is not empty, then the GRID card will also contain the appropriate output coordinate system designation. Otherwise, the output coordinate system will be the global rectangular coordinate system.

Subroutine PNMAT

Subroutine PNMAT creates COSMIC/NASTRAN MAT1 data cards from the PAFEC BS module 31 (the internal storage number given to the PAFEC materials data). Only isotropic elastic materials are converted, a subprogram PNMAT limitation. Each material in the data module is reformatted and written onto the output file with unique continuation card mnemonics.

Subroutine PNETOP

Subroutine PNETOP processes the element data stored in PAFEC BS modules 17 and 18. Each element definition is processed individually with mappings from PAFEC element types and topologies to COSMIC/NASTRAN element types and their corresponding topologies. The following element mappings are currently supported.

PAFEC element mnemonic	COSMIC/NASTRAN element card	Element type
30100	CELAS2	Spring element
30200	CMASS2	Mass element
34000	CBAR	Simple beam element
34200	CBAR	Offset beam element
34400	CROD	Simple rod element
36100	CTRMEM	Triangular membrane element
36200	CQDMEM1	Quadralateral membrane element
37100	CIHEX1	8-node brick element

37120	CIHEX2	20-node brick element
37130	CIHEX3	32-node brick element
37200	CWEDGE	6-node wedge element
41320	CTRIA2	Triangular plate element
43110	CTRSHL	6-node triangular plate element
44100	CTRIA2	Triangular plate element
44200	CQUAD2	4-node quadralateral plate element

Unique continuation card mnemonics are generated for each element type requiring a multicard element topology. Also, special processing is required for each PAFEC spring element (number 30100) and mass element (number 30200) since each of these elements may yield as many as six COSMIC/NASTRAN CELAS2 or CMASS2 element data cards. (Unique element numbers are generated for any newly created elements.)

Subroutine PNPROP

Subroutine PNPROP performs generation of COSMIC/NASTRAN element property cards. Several PAFEC BS modules are examined and the following mapping is used to create the appropriate COSMIC/NASTRAN property cards.

PAFEC element mnemonic	COSMIC/NASTRAN property card
30100	PELAS
34000	PBAR
34200	PBAR
34400	PROD
36100	PTRMEM
36200	PQDMEM
37100	PIHEX
37120	PIHEX
37130	PIHEX
37200	PWEDGE
41320	PTRIA2
43110	PTRSHL
44100	PTRIA2
44200	PQUAD2

Subroutine PNDOF

Subroutine PNDOF processes constraint data stored in PAFEC BS module 2. Each degree of freedom is examined for constraint codes. Any constrained degree of freedom generates an appropriate COSMIC/NASTRAN SPC data card. PAFEC REPEATED.FREEDOMS are output as COSMIC/NASTRAN MPC data cards for the repeated degrees of freedom.

Subroutine PGCMPC

If GENERALIZED.CONSTRAINTS are defined via PAFEC BS module 143, then subroutine PGCMPC generates appropriate COSMIC/NASTRAN data cards for each generalized constraint. An arbitrary limitation of three independent nodes for any dependent node has been set in subroutine PGCMPC. Unique continuation card mnemonics are generated as necessary.

INTEGRATION OF THE PAFCOS SOFTWARE INTERFACE INTO THE PAFEC MACRO DICTIONARY

Minor additions to the PAFEC MACRO dictionary were all that was necessary to completely implement the PAFCOS software into the PAFEC PHASE execution scheme. The PAFEC MACRO dictionary is used by the PAFEC driving program to create FORTRAN and job control information for a particular PAFEC PHASE. Within each PAFEC user data file there exists a control module and possibly several sets of data modules. (The PAFEC control module is analogous to the executive and case control cards of a COSMIC/NASTRAN data deck.) Based upon the user-specified PAFEC control directives, the PAFEC driver program determines which PHASE and what subroutine within the PHASE should be executed. In order to permit a user-friendly interface between the PAFEC system and the PAFCOS software, a single new control directive, appropriately named COSMIC/NASTRAN, was added to the PAFEC MACRO dictionary.

PHASE 4 was chosen as the appropriate PHASE to create a COSMIC/NASTRAN NBD, due to finite element model generation completeness. The MACRO dictionary was modified to conditionally include a call to subroutine PAFNBD (the driver for the PAFCOS software) in the PHASE 4 FORTRAN, based upon the presence or absence of the COSMIC/NASTRAN control directive. Similarly, an instruction was inserted to conditionally include the precompiled PAFCOS relocatable object module in the linkage edit step of the PHASE 4 job control. Therefore, to access the PAFCOS software all the user must do is to simply insert the phrase COSMIC/NASTRAN following the PHASE=4 PAFEC control directive somewhere within his control module. For example, the following few lines represent a valid PAFEC control module that would invoke the PAFCOS software:

```
CONTROL
NAME.ABCD
PHASE=4
COSMIC/NASTRAN
STOP
CONTROL.END
```

AN ILLUSTRATIVE EXAMPLE

This rather academic example demonstrates most of the capabilities of the PAFCOS software. It is intentionally brief so that a very small COSMIC/NASTRAN bulk data deck is created. The following listing is a copy of the PAFEC data deck that generates the small three-dimensional plate finite element model shown in figure 1.

```
TITLE PAFCOS TEST
CONTROL
SAVE.RESULTS
```

```
CONCATENATE.OUTPUT
SAVE.PLOTS
NAME.T
PHASE=4
COSMIC/NASTRAN
STOP
CONTROL.END
NODES
NODE.NO X.IN    Y.IN    Z.IN
1
2       1.5     0       0.8
3       3.0
4       0       5.0
5       0.75    5       0.4
6       1.5     5.0
PAFBLOCKS
ELEMENT=44200
N1      N2      TOPOLOGY.OF.BLOCK
1       2       1 3 4 6 2 0 0 5
MESH
REFER   SPACING
1       2
2       2 1.5 1
PLATES.AND.SHELLS
MATERIAL        THICKNESS.IN
1               0.81
MATERIALS
MATERIAL        E       NU      RO
1               27E6    .27     7.7
RESTRAINTS
NODE    PLANE   DIRECTION
1       2       0
MODES.AND.FREQ
AUTOMATIC.MASTERS       MODES
10                      4
END.OF.DATA
```

After successful execution of PHASE 4 on an ORNL DECsystem-10 computer using the above PAFEC data, a file, T04.NBD, is created containing the COSMIC/NASTRAN bulk data deck. For completeness this data deck is listed below:

```
GRID           1           0.000   0.000   0.000       0
GRID           2           1.500   0.000   0.800       0
GRID           3           3.000   0.000   0.000       0
GRID           4           0.000   5.000   0.000       0
GRID           5           0.750   5.000   0.400       0
GRID           6           1.500   5.000   0.000       0
GRID           7           0.000   2.222  -0.000       0
GRID           8           1.167   2.222   0.622       0
GRID           9           2.333   2.222   0.000       0
GRID          10          -0.000   3.889  -0.000       0
GRID          11           0.917   3.889   0.489       0
GRID          12           1.833   3.889   0.000       0
MAT1          12.70E+071.06E+07   2.707.70E+000.00E+00               +MAT001
+MAT001
```

```
SPC      10000     1  123456
SPC      10000     2  123456
SPC      10000     3  123456
SPC      10000     4       6
SPC      10000     6       6
SPC      10000     7       6
SPC      10000     9       6
SPC      10000    10       6
SPC      10000    12       6
CORD2R       1     0     0.0     0.0     0.0     0.0     0.0    1.0+C2R001
+C2R001    1.0   0.0     0.0
CORD2C       2     0     0.0     0.0     0.0     0.0     0.0    1.0+C2C002
+C2C002    1.0   0.0     0.0
CORD2S       3     0     0.0     0.0     0.0     0.0     0.0    1.0+C2S003
+C2S003    1.0   0.0     0.0
CQUAD2       1     1       1       2       8       7
CQUAD2       2     1       2       3       9       8
CQUAD2       3     1       7       8      11      10
CQUAD2       4     1       8       9      12      11
CQUAD2       5     1      10      11       5       4
CQUAD2       6     1      11      12       6       5
PQUAD2       1     1    0.81
```

All that remains for the user to do is to merge the above file with the IBM JCL procedure for executing COSMIC/NASTRAN at ORNL, add an executive and case control deck, and then submit the job.

CONCLUDING REMARKS

For production problems, using PAFEC and the PAFCOS software as a preprocessor for COSMIC/NASTRAN eliminates a large majority of the cards necessary for a finite element analysis. This software has been used to preprocess several large magnet structural analysis problems at ORNL and has demonstrated an over 95% reduction in the total number of cards typed for these problems. Future improvements are planned to convert and/or create even more of the data.

REFERENCES

1. PAFEC 75 Systems Reference Manual. PAFEC LD., Nottingham, England, November 1978.

2. Durocher, L. L. and Gasper, A. F.: An Interactive Review System for NASTRAN. Tenth NASTRAN Users' Colloquium, NASA CP-2249, May 1982, pp. 45-64.

3. Hirt, E. F. and Fox, G. L.: Recent Developments of NASTRAN Pre- and Post-processors: Response Spectrum Analysis (RESPAN) and Interactive Graphics (GIFTS). Tenth NASTRAN Users' Colloquium, NASA CP-2249, May 1982, pp. 18-44.

4. The first implementation of this software was called PAFNAS and was documented in the following reference: Baudry, T. V. and Gray, W. H.: PAFNAS, A PAFEC to COSMIC/NASTRAN Conversion. First U. S. A. PAFEC Users' Conference, June 1981.

5. PAFEC For the Engineer. PAFEC LD., Nottingham, England, Feburary 1981.

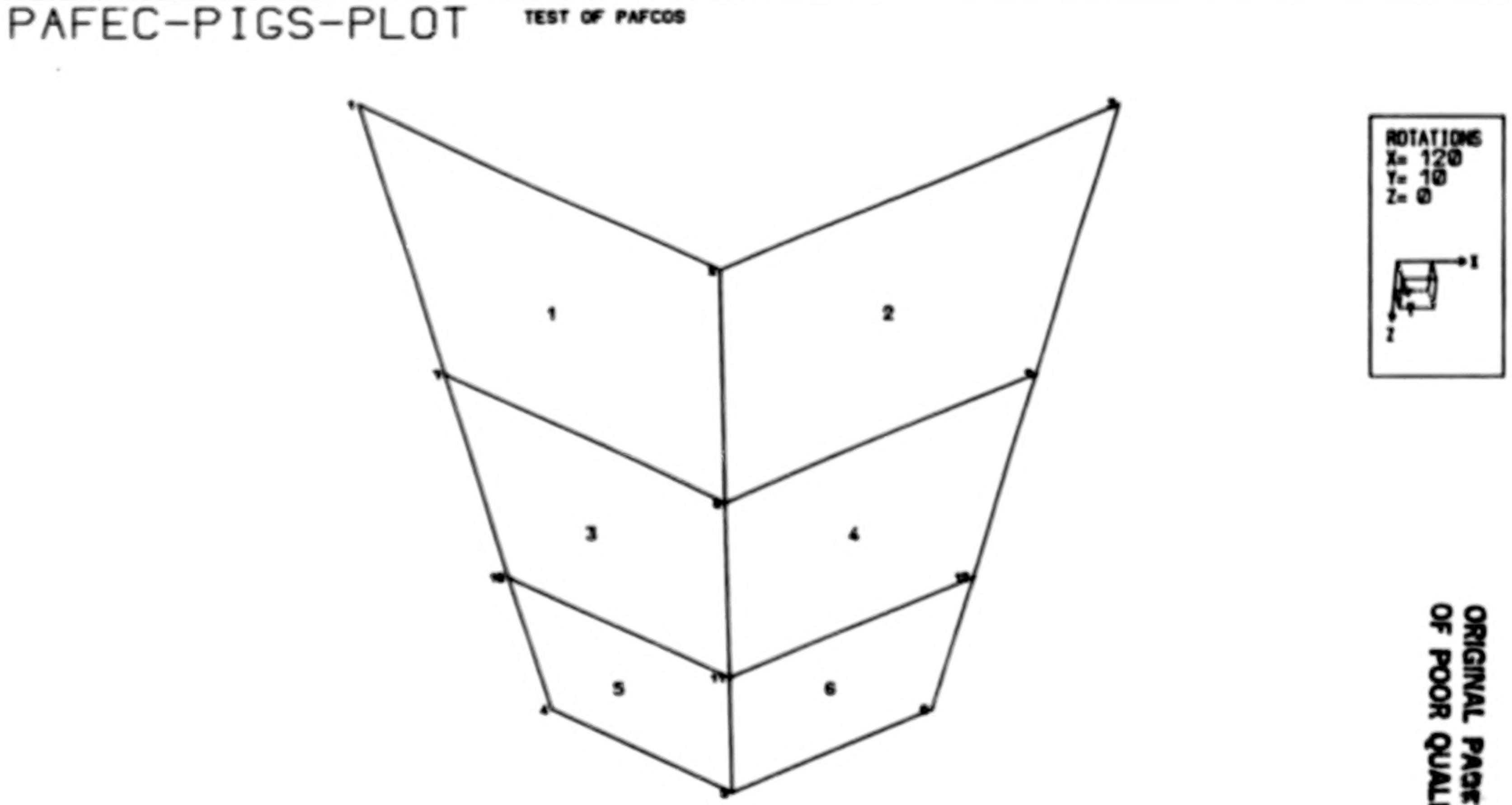
PAFEC-PIGS-PLOT
TEST OF PAFCOS
1
2
3
4
5
6
ROTATIONS
X= 120
Y= 10
Z= 0
X
Z

Figure 1. The finite element mesh for the example problem showing the element and nodal numbers.

N84
15594

UNCLAS

D4

THE GPRIME APPROACH TO FINITE ELEMENT MODELING

N84 15594

Dolores R. Wallace, James M. McKee and Myles M. Hurwitz

David W. Taylor Naval Ship R&D Center
Bethesda, Maryland 20084

SUMMARY

GPRIME, an interactive modeling system, runs on the CDC 6000 computers and the DEC VAX 11/780 minicomputer. This system includes three components: 1) GPRIME, a user-friendly geometric language and a processor to translate that language into geometric entities, 2) GGEN, an interactive data generator for 2-D models; and 3) SOLIDGEN, a 3-D solid modeling program. Each component has a computer-user interface of an extensive command set. All of these programs make use of a comprehensive B-spline mathematics subroutine library, which can be used for a wide variety of interpolation problems and other geometric calculations. Many other user aids, such as automatic saving of the geometric and finite element data bases and hidden line removal, are available. This interactive finite element modeling capability can produce a complete finite element model, producing an output file of grid and element data.

INTRODUCTION

Finite element analysis has become the predominant method for performing structural analysis on digital computers of all types. Almost any conceivable structure, from a small valve to an entire ship, may be analyzed by the finite element method.

However, the creation of a finite element model of the structure to be analyzed by this method is a major task. Even a small problem can require large amounts of geometric data, with many details to be considered. An engineer can spend a vast amount of time defining the numerical model of a structure and verifying the correctness of this data. The extreme generality of this engineering method has frustrated attempts to create an effective automatic finite element data generator with comparable generality. Finite element models frequently need refinements which require a return to the geometry for more information and details to complete the modeling. Hence, complete geometric data, and efficient management of that data, are essential to make these modifications simple.

The term "geometric modeling" appears frequently in current computer graphics and computer-aided design literature. Many scientists and engineers maintain (correctly) that they have been "modeling geometry" in traditional ways for a great many years. Most recent geometric modeling in the computer-based science has been evolving for more than a decade, but the distinctions between the old technique and the new are significant, even if they sometimes appear to be rather subtle. Although the older geometric techniques could be said to permit the modeling of any required shape, there was little consistency in the representation of different types of objects (ref. 1). Today, good mathematical tools, such as B-spline functions, are making possible the reality of representing all objects by sets of continuous, well-behaved functions. This development makes possible not only better finite element modeling but also solutions for a wide range of problems in several disciplines of physics.

With GPRIME (ref. 2) the finite element modeling process is automated by providing a geometric representation of the structure while retaining the broad generality of the finite element method. With this complete geometric data base of the structure, both the general data generator GGEN (ref. 3) and the 3-D data generator SOLIDGEN (ref. 4) may be used to produce the finite element model necessary for structural analysis. The basic assumption of the GPRIME approach is that, if a systematic and accurate mathematical model of the geometry of a structure could be stored in the computer, the task of creating general finite element data generators would be greatly simplified. The advent of low cost, interactive computer graphics makes the GPRIME approach even more attractive, since problem areas in an automatically generated model can be easily resolved by interactive methods at the graphics screen.

The Navy and DTNSRDC have long been interested in geometric modeling techniques. Since 1976, the Numerical Structural Mechanics Branch of the Computation, Mathematics and Logistics Department has been developing a geometric modeling system consisting of the B-spline mathematical tools to define geometric representations, a geometric language to access this modeler, and the interface needed for implementing it interactively on a computer. This language, called GPRIME, was originally formulated to support finite element data generation for structural analysis. As indicated earlier, two data generation programs are now available for use with the GPRIME geometry: GGEN, for general interactive modeling including the two-dimensional shell-type element and SOLIDGEN, for generating three-dimensional solid models. GPRIME, GGEN, and SOLIDGEN were first developed for use on the CDC 6000 and CYBER computers under the NOS and NOS/BE operating systems, and are now also operating on the DEC VAX 11/780 minicomputer. The graphics capabilities assume that Tektronix storage-tube type graphics terminals will be used. The programs may be used in batch or interactive-graphics modes, or mixed modes. The programs use the RATFOR pre-processor for structured FORTRAN.

GPRIME COMPUTER GRAPHICS: A GEOMETRIC MODELING SYSTEM

Geometric Constructions

- Classical primitives of geometry
- B-spline mathematical functions, in 1, 2, and 3 dimensions
- Parametric representations independent of analysis model
- Rotations, translations, scaling of geometry
- Geometry generation from digitized data, keyboard or cursor definition, or combination

Graphic Display and Viewing Options

- Hidden line removal
- Rotating, translating, scaling display of geometry
- Selection of geometry items to be displayed
- Status of all viewing, plot, axes parameters

- Program-to-user messages
- Annotation of geometries, definitions, names, at screen

Generation of Finite Element Models

- Data generation for 2-D plate/shell elements, general elements
- 3-D solid element generator
- Output formatter

Processing Controls

- Interactive and batch operating modes
- Restart capability
- HELP messages on definitions, commands, as requested by user

Applications

- Hydromechanics modeling, structural finite element analysis, ship magnetostatic signatures, thermal analysis
- Potential application in ship vulnerability, infrared detection, cost and weight estimation, CAD/CAM, composite studies.

EVOLUTION OF GEOMETRIC MODELING: THE PATH TO GPRIME

During its evolution, geometric modeling has taken many forms. Its "correct" description is discussed in many forums today. Designer's sketches and engineering drawings have long been thought of as geometric models. The fact that this type of representation is heavily laced with graphic shorthand and engineering insight becomes obvious when we begin to ask computers to translate these drawings into instructions for manufacturing the parts described on these drawings. Achieving this automation requires that a computer be provided with all the details of the draftsman's shorthand, so that it can "understand" the old drawings, or that it be provided with sufficient geometric information rather than engineering terms such as "fillet" in model descriptions. Both developments are taking place, i.e., direct reading from blue prints and more complete numerical input data, but the complete geometric representation appears to be the key to large-scale automation.

Discrete finite element models are now routinely used for structural analysis. These models are usually thought of as rather elegant geometric models, but are of no use in defining a machine cutter path, and really of little use to a finite element analyst who requires models with a more detailed mesh. Coordinate information for constructing finite element models is defined at a discrete number of points-period. Some sort of interpolation may be used on this data to find intermediate points, but because the finite element data points were created to meet the requirements for one specific analysis, those points may not represent the basic detailed geometric shape of the structure.

From work with early computers and primitive computer graphics techniques, automatic drafting programs emerged. These programs "spoke" in the language familiar to draftsmen. Soon designers wanted to connect this type of program to programs that guided numerically controlled tools. These marriages have become or are now evolving into computer-aided design and computer-aided manufacturing (CAD/CAM) systems. To accommodate these new demands, the designer's language has evolved from the draftsman's, with the addition of a vocabulary of geometric shapes and geometric operations. Intersections of classical cylinders with complex "sculptured surfaces," (ref. 5) as in Figure 1, make the definition of true three-dimensional geometric representations considerably easier than drawing with the draftsman's two-dimensional notation.

We have used the term "old geometry" to collectively refer to the many different computer methods used to describe geometric shapes, which, by their nature, are limited to certain special applications. Some of these methods are the closed form polygonal approximations of spheroids and ellipsoids, the ellipsoidal modeling of airplanes and submarines, and point by point finite element descriptions. Similarly, we have used "new geometry" to refer to evolving methods of geometric description. These descriptions attempt to be mathematically complete for any application and to permit manipulation of all geometric forms without having to resort to special processing for different combinations of valid representations. For example, the B-spline mathematical functions afford good data representations of a structure. The new geometry has obvious roots in the old; however, the new approach represents attempts to develop a general solution to the geometric modeling problem, whereas the older geometries were developed to solve particular problems.

The new geometry has not come into the world without its share of growing pains. As new capability is added to older techniques, program developers have attempted to maintain compatibility between the old forms and the new forms of geometry. As more of the properties of the new geometry are exploited, it becomes more difficult to maintain compatibility. Either the old forms will have to be abandoned, or translators will have to be created to produce an equivalent new form for the old definitions. Similarly, once we have a very convenient way to represent geometry and to combine forms easily, the modeler's creativity can quickly outstrip the available mathematics. For example, volume intersections computed using "old" techniques may yield only edges of boundary which can be drawn; this is insufficient to completely define a new volume because there is not information on how the function varies through the volume. These problems are evident in the technique known as "combinatorial geometry," (ref. 5) which permits boolean operations on three-dimensional solids. If simple unions and intersections are permitted without restriction, it is easy to imagine how a few simple shapes could mushroom into a computationally-intractable situation. Often, these problems can be avoided by limiting the number of combinations or by deferring the boolean operations until they can be handled by later applications programs in which a knowledge of the final product can simplify the choice of functional representation.

The need for complete geometric description has also been evolving in other areas of computer simulation. Finite element and finite difference modeling can be easily automated if an adequate geometric description is available. Numerical solutions, which require that new meshes be generated at various points in the computation, demand such a representation, once the models advance from simple classical shapes to the complexities of the real world. The rest of this report briefly describes: GPRIME for providing geometric representations and GGEN and SOLIDGEN which use this geometry for finite element modeling.

GEOMETRIC LANGUAGE PROCESSOR: GPRIME

Overview

As the finite element method gained popularity with structural engineers, the need for an accurate finite element model that could be developed in a reasonable time at reasonable cost became obvious. The computer program GPRIME, a geometric modeling system, provides the geometry for these finite element methods. GPRIME addresses the requirements for a practical geometric modeling system-mathematical representation, man-machine interface, data base management, and implementation (ref. 6). The geometry is defined in GPRIME via a geometric language of definitions and commands that simplifies the creation of complex models. Classical shapes are defined using straight-forward expressions, and more general curves and surfaces can be defined using digitized coordinate data. By using the B-spline mathematical functions, GPRIME can provide the engineer with a complete geometric model, constructed with well-behaved continuous functions, independent of the discrete model used in the analysis.

The GPRIME processor itself uses interactive computer graphics to define geometric entities and to aid in visualizing the model being created. The processor creates a geometric data base (referred to as UMF - user master file) which may be used for restarting the definition process at later sessions and for communication with user's programs. The implementation of GPRIME allows the user various controls over the entire system.

The Geometry Modeler

From construction drawings, tool cutter data, digitized data, measurements, or other forms of model description, the engineer may begin to define a geometric model with a combination of either general curves and surfaces, or with classical forms of geometry. These classical forms include points, lines, arcs, circles, cylinders, cones, spheres, and surfaces of revolution. These entities are represented internally by B-spline functions, which are also useful in smoothing and fitting applications, as shown in Figure 2. The parametric representations of these entities make it easy to locate points and curves of intersection in complex geometric configurations. In fact, the intersection capability provides a very useful tool for data-checking of models of complex structures.

Rotations, translations, and scaling of the geometry are available through the GPRIME language. GPRIME was designed for use in creating finite element structural analysis models, but it can be applied wherever a geometric description of an object is required. A set of user-callable subroutines is available for user access to the internal B-spline definitions stored on a UMF (user master file from GPRIME) data base. These subroutines are referred to as the GPRIME Data Base Access Capability (GDBAC).

Design Aids

Special GPRIME commands provide the capabilities of controlling model changes, viewing options and other user aids. The user may delete or change any part of a constructed geometrical model, and the GPRIME processor will automatically change any of the components dependent on or affected by the geometrical changes.

Viewing options allow the user to control the viewpoint, as well as to effect translations, hidden line removal, and rotations. The hidden lines have been removed in the propeller shown in Figure 3. Plotting options permit plots of all or some of the curves, surfaces, points or user-defined groups of data. An optional status table shows the current status of plotting, viewing, printing, and axes options. The printing options are provided for annotation of various tables on the screen. A command also permits the user to obtain an output file containing the definitions and commands used in a session. An interactive call for HELP gives the user instructions as needed in using these commands and definitions. Executive control permits the initial session to begin with an input file of definitions and to restart later sessions from the saved geometric data base. GPRIME also provides a macro facility which contains a user-defined set of GPRIME commands. For frequently used procedures, such as defining two surfaces and their curve of intersection, or frequently used viewing options, the user can, via the macro command, execute in one line several previously defined statements.

In summary, GPRIME provides powerful generation algorithms for developing a geometrical model from which finite element models may be generated. The geometry may be used in a variety of applications, such as smoothing functions, data-checking, ship vulnerability studies, or wherever geometry is required. Additional GPRIME capabilities include viewing, plotting, editing, and file options enabling the engineer to significantly reduce the time required for model generation. Finally, the GPRIME data base is available for use by user programs.

INTERACTIVE DATA GENERATOR: GGEN

Overview

With the availability of a general geometric language processor, such as GPRIME, which provides a data base of a representative geometric model, finite element modeling becomes easier and more complete. GGEN is a computer program for creating finite element models from an interactive computer terminal. GGEN is different from most other finite element data generators in that it references geometric information that has been defined using the GPRIME geometric language. One advantage of the GPRIME-GGEN approach includes the ability to define interactively a three-dimensional model from a two-dimensional terminal screen or digitizing board.

GGEN Procedures

The GGEN generator has been implemented as a module of the GPRIME language processor. This implementation permits GGEN to use many of the graphics and data management features of GPRIME. These features include GPRIME processing of changes, print options, HELP messages, new geometry, and access to existing geometry. All these processes may be performed interactively, one at a time, with program control remaining in GGEN. However, if the user wishes to return to GPRIME, GGEN will automatically save GGEN data.

Any GPRIME geometry, such as points, curves, surfaces, or groups of these, may be referenced by GGEN at any time during an interactive session. The first curve or surface activated is the default, that is, the curve or surface from which new elements are created, unless another curve or surface is referenced by a given command. The number of curves, surfaces, and groups which may be active at one time is limited by user specified parameters. Commands are provided to remove unneeded items, including points, from the list of active geometries.

Data Generation and Display

Node points and elements can be created in a bulk mode by using one command with various options. These options include generating points, elements, or both. Such bulk generation will produce a "uniform" mesh on the specified reference curve or surface. Prior to the bulk generation, the user may enter another command to cause broad variations in the mesh.

Although GGEN automatically numbers nodes and elements, an option exists to assign numbers to the nodes and elements. Points and elements may also be defined individually or in small groups. In one command, both passive (type-in) and interactive (cross-hairs, tracking cross) methods are used. In the other, the user selects from a user-menu, that is, a set of instructions printed on the screen, to perform the various creation functions interactively.

Deletion of nodes and elements is similar to the creation process, either by using a type-in command or by making a menu selection. Note: GGEN assumes the usage of a storage tube type terminal, meaning that any item drawn remains until the entire screen is erased. Deleted items will be marked deleted with an "X" until the picture is redrawn. Any item so marked can be restored later, if the item was deleted by mistake.

By entering the EDIT command, the user may perform most GGEN functions under interactive control. In this mode the user selects a function to be performed from a list, called the menu, displayed on the right side of the screen. (see Figure 4.) The user indicates the desired function by moving the terminal's crosshair cursor inside the box enclosing the function name on the menu. Alternatively, the function may be selected using the keyboard by entering the character displayed at the left of the name of that function. GGEN acknowledges the user's selection by highlighting the box that encloses the name of that function.

The menu functions permit the user to delete and create nodes and elements by selecting node points and elements on the screen with the cross hair cursor.

The user can selectively display GGEN points, curves, surfaces, and elements as in GPRIME. Items may also be identified with labels as the user chooses. One command allows the redisplay of all currently defined items under the control of the current plot parameters. The piping tee in Figure 5 uses the option to shrink element representation away from associated node points. Any new items included in the parameter list of this command will also be plotted.

Output

All generated finite element data may be passed to a local file, "FEDATA," using a punch command. Point data, element data, or both can be put on this file. All current data can be entered or, optionally, only those items that have changed since the last usage of the command. This output file is available to the user for direct input to finite element programs or for later editing.

GENERATING THREE-DIMENSIONAL SOLID STRUCTURES: SOLIDGEN

Overview

The first proposed application of the GPRIME geometric modeling approach was for the generation of three-dimensional solid finite element models. The proposed concept consisted of two parts. First, GPRIME surfaces would be defined to bound the structural model. Then, a data generation program would generate brick-like solid elements on the interior of a defined volume.

The SOLIDGEN program was developed to implement the data generation concept. There was no restriction on the GPRIME surface used to bound a SOLIDGEN model and those boundary surfaces may either define a face of the model or extend beyond the region being defined, whichever the user finds more convenient. The shape of the generated elements is governed by the bounding surfaces and additional reference surfaces provided by the user.

SOLIDGEN Technique

To generate a satisfactory finite element model with SOLIDGEN, the user must first visualize the general shape of the generalized model. For example, will the elements lie in more or less concentric rings about a cylindrical recess or will they make up a rectangular brick-work? This type of information is conveyed to SOLIDGEN by selecting and ordering the reference surfaces in such a way that they form a mesh of six-sided super elements, called zones. The generated elements will follow the general pattern defined by these zones.

The three diagrams of Figure 6 demonstrate the procedure from sketch through the geometry to the solid element model of a globe valve. The designer has marked an octant of the symmetric valve with reference surfaces shown in Figure 6a. Together, these six-sided super elements define the boundary of the solid model. The geometry required by SOLIDGEN here is not an exact detailed structure but rather the general bounding surfaces or surfaces of revolution seen in Figure 6b. SOLIDGEN builds the brick elements of Figure 6c from these surfaces. The output file contains all the grid point and element data.

CONCLUSION

Although GPRIME's biases are toward the solution of research and development problems, obviously there are many other areas of potential application. From early in its development it was clear that GPRIME would provide a powerful geometric capability useful for many scientific applications. Thus, it comes as no surprise that GPRIME is being used for hydromechanics modeling, for ship vulnerability studies, and for infrared modeling as well as for generating finite element data. It offers potential use in simulation, in finite element modeling of composites, and in cost and weight estimation problems. In the manufacturing area, its possible applications to computer-aided design and computer-aided manufacturing procedures seem obvious.

A library of B-spline subroutines makes it a simple task for program developers to include GPRIME geometry in their programs. The data generators GGEN and SOLIDGEN were the first example of using these internal routines for specialized applications, in this case, to address the needs of finite element analyses.

GPRIME and its data generators have been providing a strong geometric capability, at the forefront of geometry modeling. In their present form, they do require continual maintenance on several computer systems in order to ensure their usefulness. However, many extensions can be made that would enhance their usefulness to Navy programs. For example, the mathematics routines can be expanded to include multiple intersection points. Better display characteristics and improved user-computer interface methods would help the user. Other enhancements could permit graphical changes in the geometry, a more general output format, and the addition of more elements. Improved data-handling techniques could make the data base access even more efficient. As these mathematical and computer science ideas become realities in GPRIME, it will become easier to solve larger and more complex problems.

REFERENCES

1. McKee, J.M.; and R.J. Kazden: GPRIME B-Spline Manipulation Package--Basic Mathematical Subroutines. DTNSRDC Report 77-0036 April 1977.

2. McKee, J.M. et al.: GPRIME: A Geometric Language for Finite Element Modeling Program Manual. DTNSRDC Report 82/062 Sep 1982.

3. Wallace, D.R. and J.M. McKee: GPRIME/GGEN Interactive Finite Element Data Generator. DTNSRDC Report (in publication).

4. Kazden, R.J.: The GPRIME-SOLIDGEN Finite Element Modeling Capability. Second Chautauqua on Productivity in Engineering and Design, the CAD Revolution, Nov. 15-17, 1982.

5. Requicha, A.A.G.; and H.B. Voecker: Solid Modeling: A Historical Summary and Contemporary Assessment, IEEE Computer Graphics and Applications, pp. 9-24, March 1982.

6. Requicha, A.A.G.: Representations for Rigid Solids: Theory, Methods, and Systems, ACM Computing Surveys, Vol. 12, No 6, pp. 437-464, December 1980.

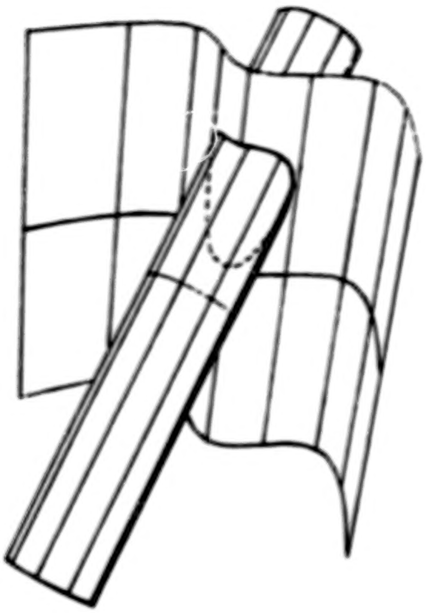

Figure 1 - Two-Surface Intersection

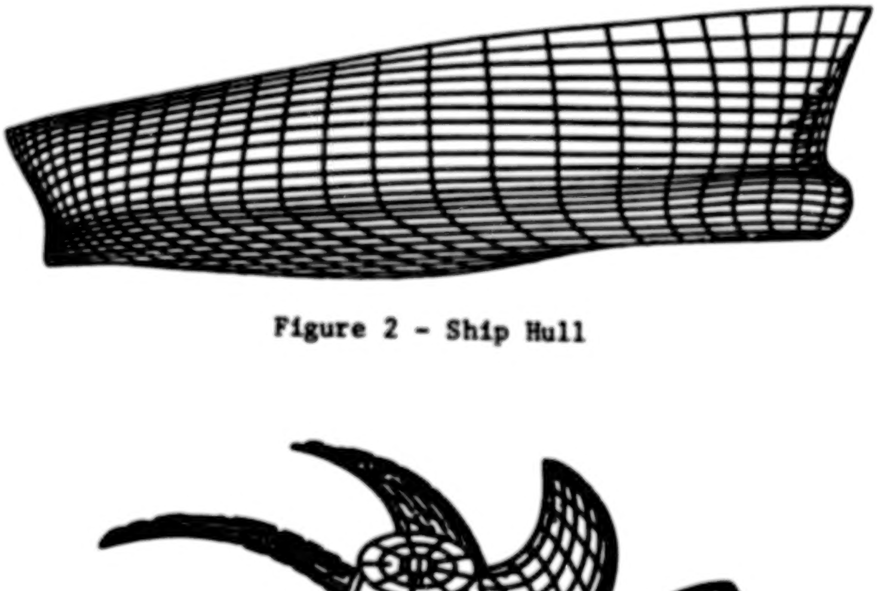

Figure 2 - Ship Hull

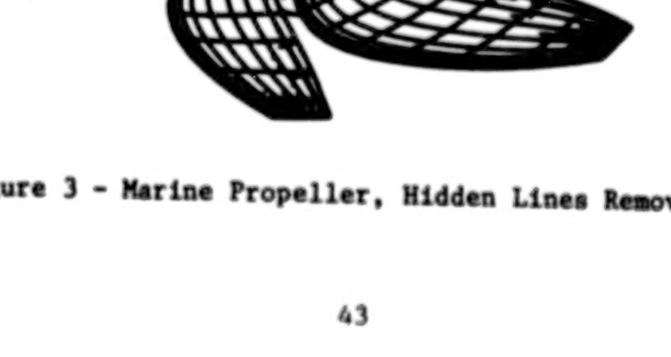

Figure 3 - Marine Propeller, Hidden Lines Removed

A.	REDRAW WORKSPACE
B.	SWITCH TABLET/CROSS
C.	ALIGN MENU (UL,LR)
D.	ALIGN ORTH (PT1,PT2,PT3)
E.	E N D (INPUT/EDIT)

G.	DELETE NODES
H.	(CHANGE)
I.	(LAST)
J.	DELETE ELEMENTS
K.	(CHANGE)
L.	(LAST)
M.	CREATE NODES
N.	CREATE ELEMENTS
O.	ELEMENTS + NODES
P.	2 NODES/ELEM.
Q.	3 NODES/ELEM.
R.	4 NODES/ELEM.

Z.	REPEAT MESSAGE
	* TASK COMPLETED
	** IMPROPER OPTION
	*** MISSED BOX
	**** POINT NOT ON C/S
	***** OTHER

0	ZVAL
*1	S1
2	S2
3	C2

Figure 4 - GGEN/EDIT Menu

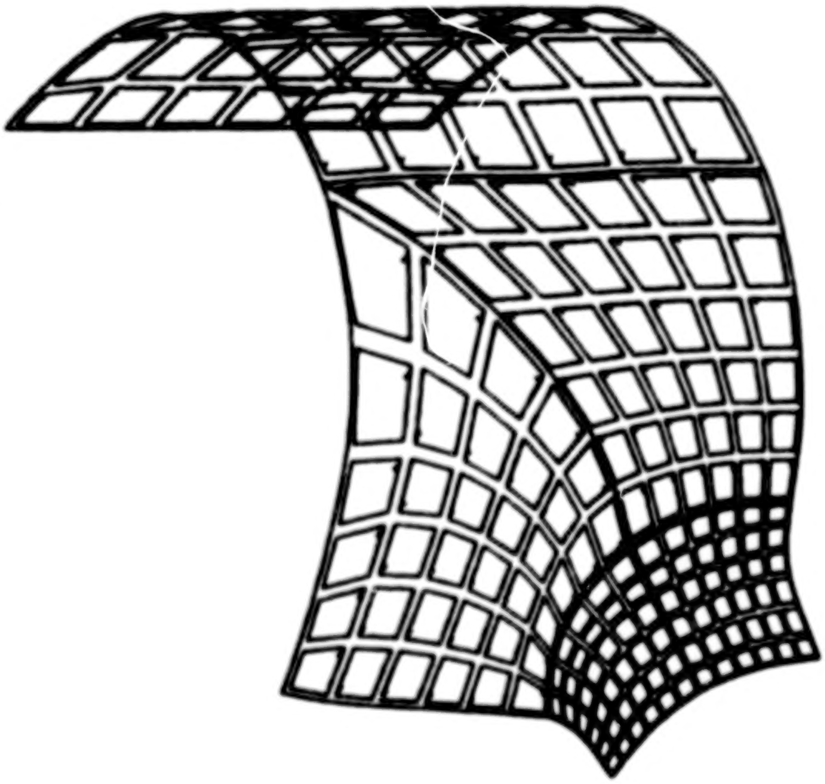

Figure 5 - Piping Tee, Element Shrink

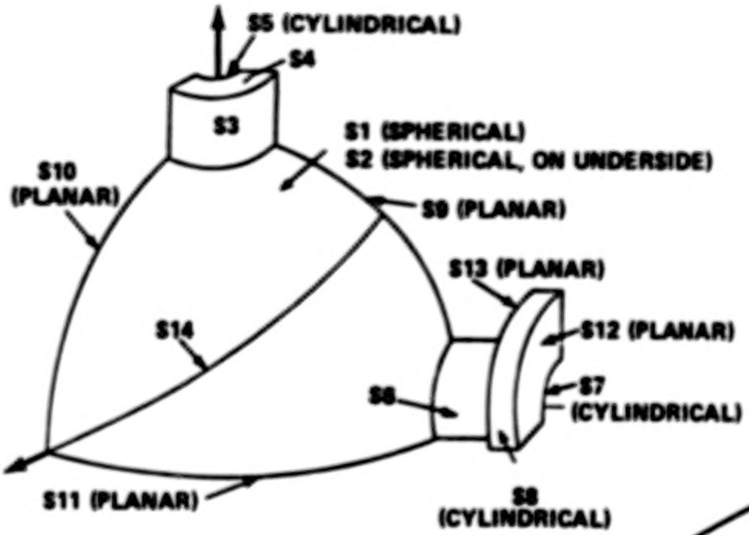
S5 (CYLINDRICAL)
S4
S3
S1 (SPHERICAL)
S2 (SPHERICAL, ON UNDERSIDE)
S10 (PLANAR)
S9 (PLANAR)
S13 (PLANAR)
S14
S12 (PLANAR)
S6
S7 (CYLINDRICAL)
S11 (PLANAR)
S8 (CYLINDRICAL)

Figure 6a - Engineer's Sketch

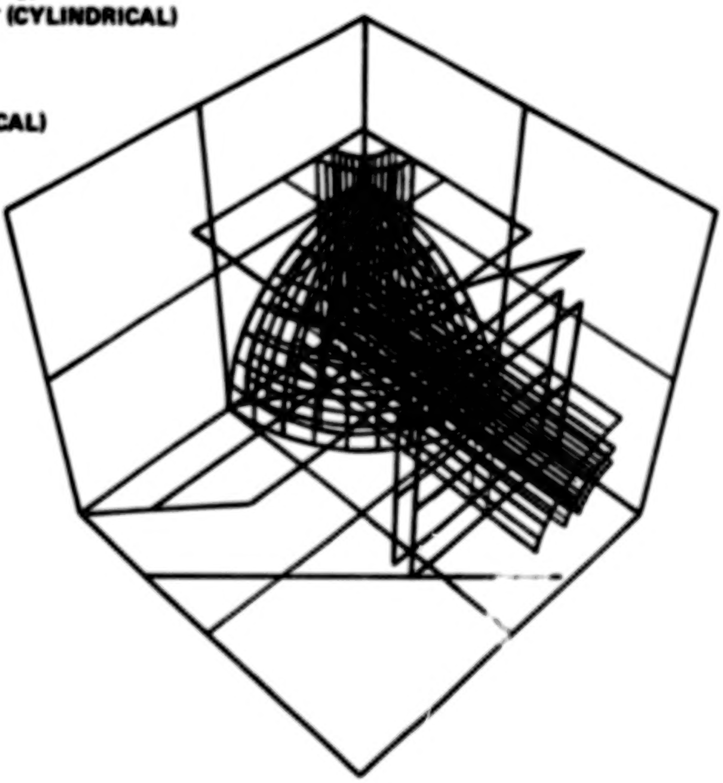

Figure 6b - Geometry

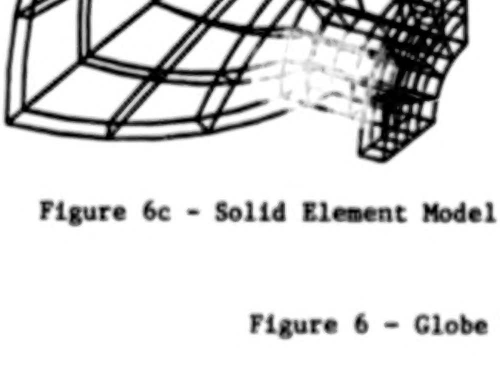

Figure 6c - Solid Element Model

Figure 6 - Globe Valve, from Sketch to Solid Elements

N84
15595

UNCLAS

D5

N84 15595

ORTHOTROPIC HOLE ELEMENT

J. W. Markham
Lockheed-Georgia Company

C. V. Smith
Consultant
Georgia Institute of Technology

SUMMARY

A finite element was developed to adequately represent the state of stress in the region around a circular hole in orthotropic material experiencing reasonably general loading. This has been achieved through a complementary virtual work formulation of the stiffness and stress matrices for a square element with a center circular hole. The element has been incorporated into COSMIC-NASTRAN as a "dummy" element. Sample problems have been solved and these results are presented.

INTRODUCTION

Mechanical fastening is the most used joining method in present flight vehicle structures. This results in connection details that contain many circular holes. These connections are subjected to very general loading with the additional complications of load transfer through fasteners and the use of nonisotropic materials in the connection. Because of the high stresses in these areas, it is important that an accurate evaluation of the local stresses around each hole be obtained to evaluate the performance of the joint.

The finite element method is an effective way to treat problems with complex geometry, material, and loading. However, because of the complexity of the stress state around fastener holes, a large number of conventional elements would be required to provide an adequate representation of the hole neighborhood. This means the cost of the analysis, both in computer costs and manhours, will be high.

A solution to this problem would be an efficient special purpose finite element which provides an accurate representation of the state of stress around a hole without the need for many conventional elements. This has been done previously for isotropic materials. In 1981, under a contract with NASA-Langley, Lockheed-Georgia Co. developed an orthotropic hole element (Ref. 1).

ELEMENT GEOMETRY

The orthotropic hole element is considered to be a thin plate in a state of plane stress with displacements on the external boundary specified so as to insure displacement continuity with adjacent elements. The element is a variable-noded total element and is defined via ADUM7, CDUM7, and PDUM7 input cards into NASTRAN. The user may specify the number of nodes on each of the three boundaries as shown in Figure 1. The nodes on the exterior of the element have two cartesian degrees of freedom whereas the nodes on the hole wall have only a single radial degree of freedom. The ratio of element width to hole diameter is determined from grid point locations and is thus a user choice; however, a ratio of four is recommended. The material properties may be isotropic or orthotropic and are defined by MAT1 or MAT2 cards. Characteristics which are not defined for this element include mass properties, thermal loading, material nonlinearity, and differential stiffness.

ELEMENT INPUT

A great deal of user flexibility has been retained in the input for this element. Defaults have been provided and therefore the input can be quite simple. The following input is required for the element:

- Total number of nodes
- Element and property identification
- Grid point connection
- Material identification
- Thickness

The following input is optional:

- Number of segments on each of the three boundaries
- Number of integration intervals per segment for each of the boundaries
- Number of Gaussian integration points per interval for boundary integration
- Number of integration intervals per volume octant
- Number of stress terms with powers of $r > -2$. Input for each of the four symmetry conditions.
- Number of stress terms with powers of $r < -2$. Input for each symmetry condition.
- Definition of stress output locations.

ELEMENT ADVANTAGES

Use of the orthotropic hole element can result in a substantial savings in computer costs and manhours. Savings in computer costs can be obtained particularly with models containing multiple holes because the congruency feature of NASTRAN can be used conveniently. This means that several hole elements of similar geometry can be included in the model and the stiffness matrix is only generated once. For complex geometries involving conventional elements, the congruency feature is impractical.

Use of the hole element can also result in substantial savings in manhours. A single hole element can replace dozens or even hundreds of conventional elements, therefore reducing the time required for modeling. Typically, an orthotropic hole element can be defined with eight input cards, thus no data generators or preprocessors are required for these areas of the model. Another advantage that results in manhour savings is the stress output generated by the hole element. The user can obtain stress components at any location within the element. With a conventional model, obtaining stresses at desired locations can be a laborious task because of the need to manipulate data and because of the large number of elements involved.

EXAMPLE PROBLEMS

The example problems which follow were solved with the COSMIC-NASTRAN program at Lockheed-Georgia Company with the orthotropic hole element implemented. They are intended to demonstrate the performance of the element in a variety of applications.

Isotropic Plate with Uniaxial Tension

The orthotropic hole element can be used in isotropic applications by simply specifying isotropic elastic coefficients. This is demonstrated by presenting the solution for an infinite isotropic plate with unit uniaxial tension at infinity (see Figure 2). The finite element model is shown in Figure 3. The plate width is 20 times the hole diameter, which represents an essentially infinite plate. Poisson's ratio is set at 0.3205.

Table 1 presents results for the three stress components at four values of radius and four values of θ. The hole element stiffness and stress matrices were based on a geometry of 8 exterior nodes and 12 interior nodes (on the hole boundary). The hole boundary is given by $r = 1$. Note the excellent satisfaction of the zero radial stress boundary condition; the results were typically 10^{-6} times the magnitude of external loading. The circumferential stress results are also very good, with an error of only 0.2% on the maximum tension stress concentration factor and 1.5% on the maximum compression stress. The zero shear stress condition is perfectly satisfied since it was included in the original stress assumptions.

The stresses away from the hole boundary are also very well represented by the hole element results.

Isotropic Plate with Half Cosine Loaded Hole

A load transfer problem for which a comparison solution is available (Ref. 3) is that of an infinite isotropic plate with Poisson's ratio equal to 0.25, loaded with uniform traction on one end and a cosine variation of radial tractions on the hole boundary (see Figure 4). The total load on the end is equal to 2P, and the radial tractions on the loaded hole boundary are given by

$$T_r = \frac{4P}{\pi} \cos\phi, \quad -\frac{\pi}{2} \lessapprox \phi \lessapprox \frac{\pi}{2}$$

The finite element model is shown in Figure 3. Table II presents results for the region around the hole, based on a geometry of 8 exterior nodes and 16 interior nodes. The value of P is set equal to 1.0.

Stresses at the hole boundary are very well represented by the finite element results. The radial stresses follow the cosine curve over the loaded region and are of the order of 10^{-2} on the unloaded portion of the boundary. The variation of circumferential stress is reasonably accurate, with an error of 3% on the maximum stress concentration.

In the region around the hole, the results from the hole element solution continue to give a good description of the stress state.

$\pm 45^o$ Laminated Plate

The example problems with isotropic material serve to confirm the basic theoretical approach and to partially validate the computer solution. There remains to demonstrate satisfactory performance in applications with orthotropic materials. The first material selected has material properties as follows:

$$E_x = E_y = E, \quad G_{xy} = 1.697528E, \quad \nu_{yx} = \nu_{xy} = 0.735$$

Note that even though $E_x = E_y$, this material is rather "far" from isotropic, with some unspecified measure, due to the large value of Poisson's ratio and the fact that E, G, and ν do not satisfy the isotropic relationship. These properties describe the $\pm 45^o$ graphite/epoxy laminate considered in Reference 4.

The first loading is unit tensile tractions in the y-direction, applied as shown in Figure 2 with the finite element model given in Figure 3. The computed radial stresses at the hole boundary were of the order 10^{-6} times the exterior loading thus satisfying traction boundary conditions. Figure 5 shows the variation of circumferential stress around the hole boundary for a hole element geometry consisting of 8 exterior nodes and 12 interior nodes. Also shown is the exact solution for an infinite plate, given by

$$\tau_\theta = \frac{3.05786 \cos^2 \theta - 1}{2.8809072(\cos^4 \theta - \cos^2 \theta) + 1}$$

which can be deduced from Reference 5, p. 175. The orthotropic hole element results contain the essential feature that the maximum stress concentration does not occur at the familiar location of $\theta = 0^\circ$. The error in maximum stress is only 0.7%.

The hole loaded with half-cosine distributed tractions has also been solved; see Figure 4. The resulting radial stresses on the boundary are essentially identical to the results achieved in the case of isotropic material. The maximum circumferential stress on the hole boundary is $\tau_\theta = 0.79$ at $\phi = 125^\circ$, which can be compared with the hole element results for isotropic material of $\tau_\theta = 0.84$ at $\phi = 85^\circ$. Again, it is seen that the location of maximum stress has shifted around the circle from the familiar location.

Plywood

The next material selected has properties as follows:

$$E_y = E, \quad E_x = 2E, \quad G_{xy} = 0.11667E, \quad \nu_{xy} = 0.036$$

These properties describe a plywood material for which Reference 5 contains many results for an infinite plate. Note that the plywood properties are quite different from the $\pm 45^\circ$ lamination properties, both in magnitudes and relationships. This provides further checks on the ability of the hole element to handle different types of orthotropic material.

The types of loading considered are unit tensile tractions in the y-direction (Figure 2), unit compressive tractions in the x-direction with constraint in the y-direction (Figure 6a), and uniform unit internal pressure on the hole boundary (Figure 6b). For all cases, the finite element model is shown in Figure 3; and the element geometry contains 8 exterior nodes and 24 interior nodes.

For the uniaxial tension, there is the usual excellent satisfaction of traction boundary condition, with τ_r of the order 10^{-6}. Circumferential stresses around the hole boundary are shown in Figure 7. Also shown are the exact results for an infinite plate, given by

$$\tau_\theta = \frac{4.8557 \cos^2 \theta - 0.7071}{-6.9994 \cos^4 \theta + 7.4994 \cos^2 \theta + 0.5}$$

which can be deduced from Reference 5 p. 175. The general features of the variation of stress are demonstrated by the hole element results.

The constrained compression results satisfy the hole boundary conditions, with τ_r of the order 10^{-5}. Circumferential stresses around the boundary are shown in Figure 8. The exact results for infinite plate are given by

$$\tau_\theta = \frac{1.1155 - 6.5174 \sin^2\theta}{-13.9989 \sin^4 \theta + 12.9989 \sin^2 \theta + 2}$$

deduced from Reference 5 p. 179.

The internal pressure results provided boundary radial stresses of the magnitude -1.00002, which is again excellent satisfaction of boundary conditions. Circumferential stresses around the boundary are shown in Figure 9, compared to infinite plate exact results given by Reference 5 p. 173.

$$\tau_\theta = \frac{4.8829 - 15.8432 \sin^2 \theta + 13.9989 \sin^4\theta}{2 + 12.9989 \sin^2\theta - 13.9989 \sin^4\theta}$$

Orthotropic Laminates with Pin-Loaded Holes

A class of problems which is of particular interest to the aircraft industry is that of pin-loaded holes in orthotropic laminates. Finite element solutions for a variety of graphite epoxy laminates were presented by Crews (Ref. 6). The finite element model used for these analyses was quite detailed, as shown in Figure 10. These results are used here as a basis of comparison to results obtained using the orthotropic hole element.

A NASTRAN model was constructed as shown in Figure 11. The particular case presented here is for $W/d = 20$. The load is applied at the center of the fastener and is reacted on both edges of the model in order to more closely approximate an infinite sheet. A feature of Lockheed-Georgia's version of COSMIC-NASTRAN was invoked to properly account for the contact area of the fastener. The hole element geometry consisted of 16 exterior nodes and 20 interior nodes. Six different laminates were considered. These were (1) quasi-isotropic (2) 0° (3) 90° (4) $[0^\circ/90^\circ]_s$ (5) $[\pm45^\circ]_s$ and (6) $[0^\circ/\pm45^\circ]_s$. Figures 12-17 present plots of the tangential and radial stress components obtained by the hole element for these respective materials in comparison to the results obtained by Crews using a detailed classical model.

These plots indicate that a reasonable correlation was obtained for the tangential stress distribution at the hole boundary. Peak tangential stress differed by no more than 12%. Excellent correlation of radial stress distribution was obtained for all cases.

Multiple Holes

Figure 18 shows a finite element model of a plate containing five holes. For economy in modeling, it is desirable to develop the hole element stiffness matrix only once and then transform this matrix as necessary to represent all the hole elements. This is possible in NASTRAN by using the congruency feature, and this feature has been checked by determining the solution to Figure 18 with tension applied parallel to the row of holes. The material is isotropic with Poisson's ratio of 0.3205.

The maximum stress concentration factor is given in Reference 7, p. 194 for an intermediate hole in an infinite row of holes. In order to simulate the infinite row, the displacements of each loaded end of the model were constrained to be uniform across the width of the plate. The finite element result for stress concentration is 2.78, based on a hole element geometry containing 8 exterior nodes and 12 interior nodes. Reference 7 gives 2.65; there is a 5% difference in results.

Concluding Remarks

The performance of the orthotropic hole element in solving a variety of problems has demonstrated that it can produce acceptable results with significant advantages in computer costs, model preparation time, and post-processing of data. Even though the emphasis in this paper has been on problems concerning fastener holes, the use of this element is applicable to any isotropic or orthotropic plate containing circular holes.

TABLE 1

STRESSES FOR AN ISOTROPIC PLATE SUBJECTED TO UNIAXIAL TENSION

	θ deg	τ_r^*	τ_r^{**}	τ_θ^*	τ_θ^{**}	$\tau_{r\theta}^*$	$\tau_{r\theta}^{**}$
r = 1	0	0	0	3.006	3.000	0	0
	30	0	0	2.005	2.000	0	0
	60	0	0	-0.006	0	0	0
	90	0	0	-1.015	-1.000	0	0
r = 2	0	0.279	0.281	1.221	1.219	0	0
	30	0.327	0.328	0.923	0.922	0.572	0.568
	60	0.422	0.422	0.325	0.328	0.571	0.568
	90	0.467	0.469	0.028	0.031	0	0
r = 3	0	0.143	0.148	1.076	1.074	0	0
	30	0.295	0.296	0.815	0.815	0.516	0.513
	60	0.594	0.593	0.296	0.296	0.516	0.513
	90	0.739	0.741	0.031	0.037	0	0
r = 4	0	0.083	0.088	1.036	1.037	0	0
	30	0.278	0.278	0.784	0.784	0.482	0.482
	60	0.659	0.659	0.284	0.278	0.488	0.482
	90	0.851	0.850	0.010	0.025	0	0

* Hole Element Results
** Reference 2

TABLE II

STRESSES FOR AN ISOTROPIC PLATE WITH LOAD TRANSFER

	ϕ deg	$\tau_r{}^*$	$\tau_r{}^{**}$	$\tau_\theta{}^*$	$\tau_\theta{}^{**}$	$\tau_{r\theta}{}^*$	$\tau_{r\theta}{}^{**}$
r = 1	0	-1.271	-1.273	0.372	0.412	0	0
	30	-1.099	-1.103	0.467	0.470	0	0
	60	-0.649	-0.637	0.649	0.612	0	0
	90	-0.041	0	0.834	0.810	0	0
	120	-0.012	0	0.415	0.373	0	0
	150	0.003	0	0.056	0.053	0	0
	180	0.003	0	-0.094	-0.065	0	0
r = 1.2	0	-0.995	-0.977	0.314	0.348	0	0
	30	-0.844	-0.829	0.358	0.381	0.035	0.021
	60	-0.445	-0.429	0.460	0.443	0.046	0.029
	90	0.038	0.034	0.477	0.415	-0.032	-0.031
	120	0.055	0.078	0.289	0.274	-0.097	-0.081
	150	0.023	0.038	0.070	0.088	-0.064	-0.051
	180	0.006	0.024	-0.015	-0.011	0	0
r = 1.5	0	-0.726	-0.726	0.232	0.241	0	0
	30	-0.604	-0.609	0.256	0.253	0.042	0.026
	60	-0.288	-0.293	0.295	0.266	0.046	0.028
	90	0.045	0.037	0.266	0.231	-0.047	-0.045
	120	0.094	0.086	0.179	0.152	-0.119	-0.105
	150	0.055	0.049	0.062	0.055	-0.083	-0.070
	180	0.035	0.033	0.010	0.012	0	0

* Hole Element Results

** Reference 3

ORIGINAL PAGE IS
OF POOR QUALITY

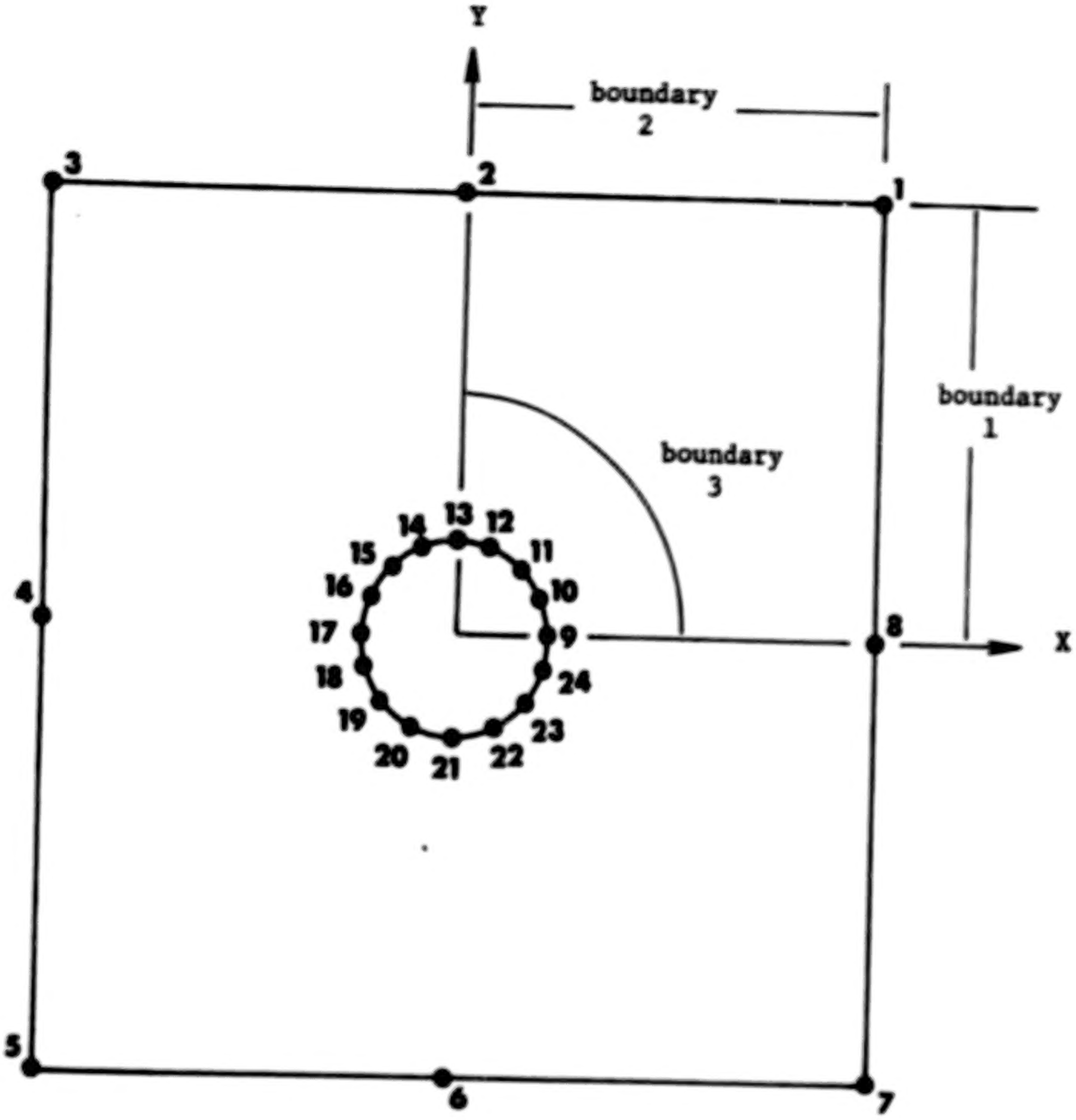
Y
boundary
2
3
2
1
boundary
1
boundary
3
13
12
14
11
15
10
16
4
17
9
8
X
18
24
19
23
20
21
22
5
6
7

Figure 1. Orthotropic Hole Element Geometry

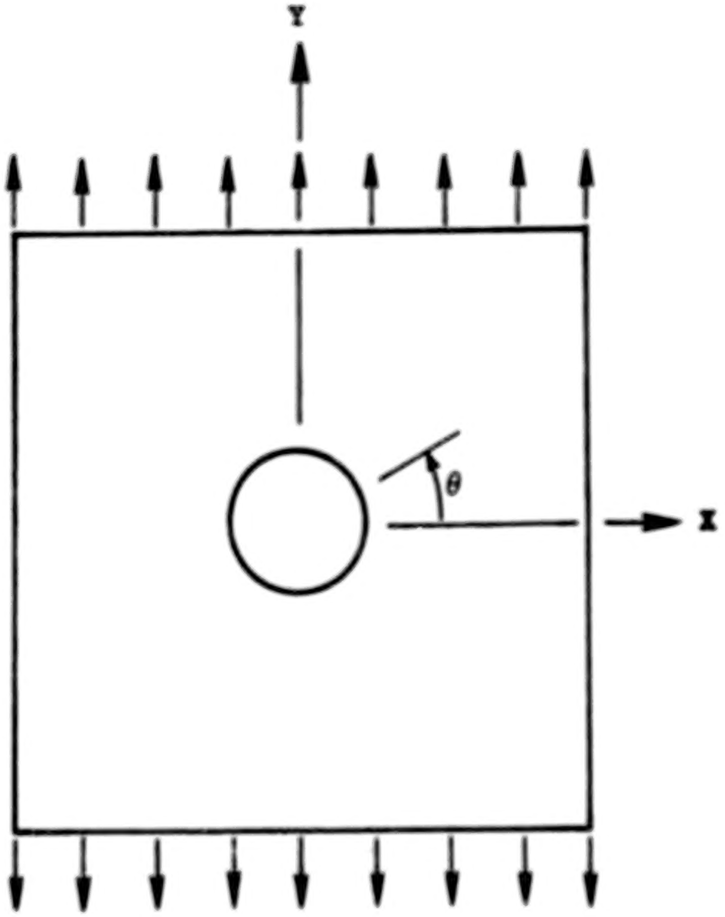

Figure 2. Unit Tensile Traction in the Y-Direction

ORIGINAL PAGE IS
OF POOR QUALITY

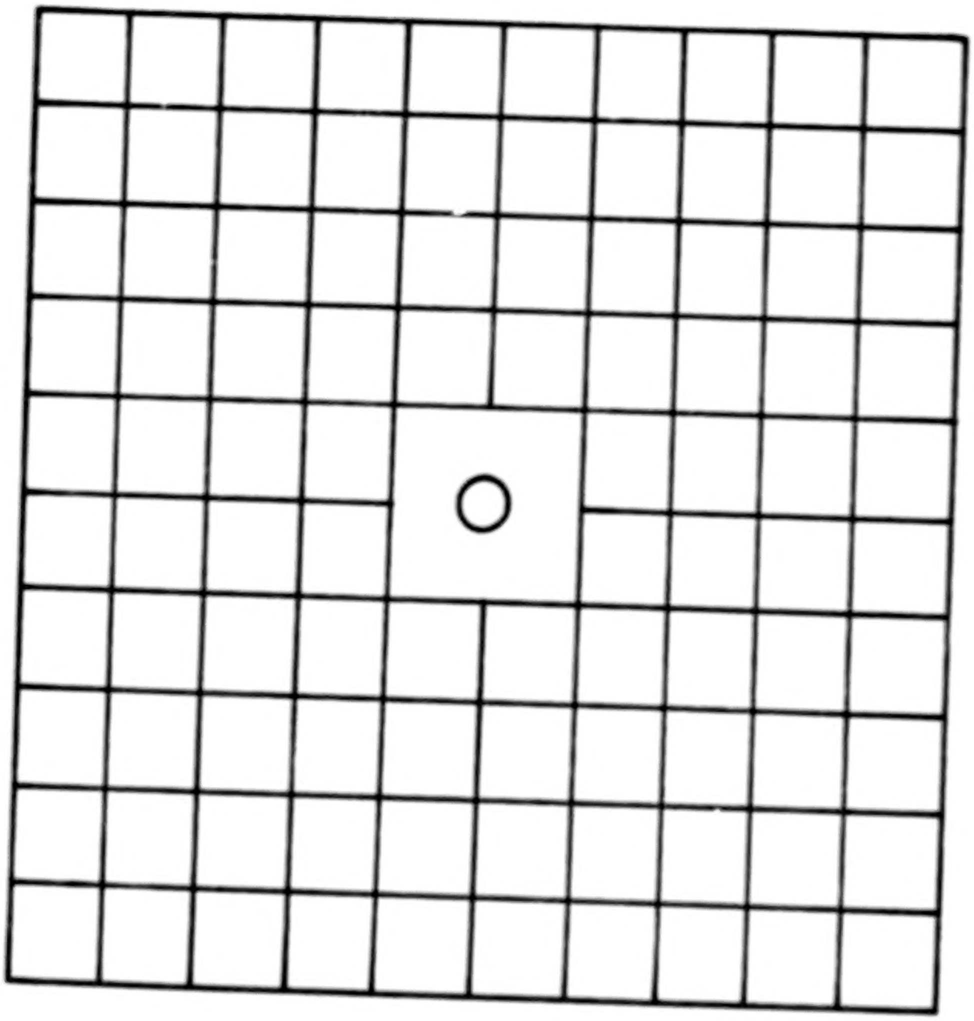

Figure 3. Finite Element Model

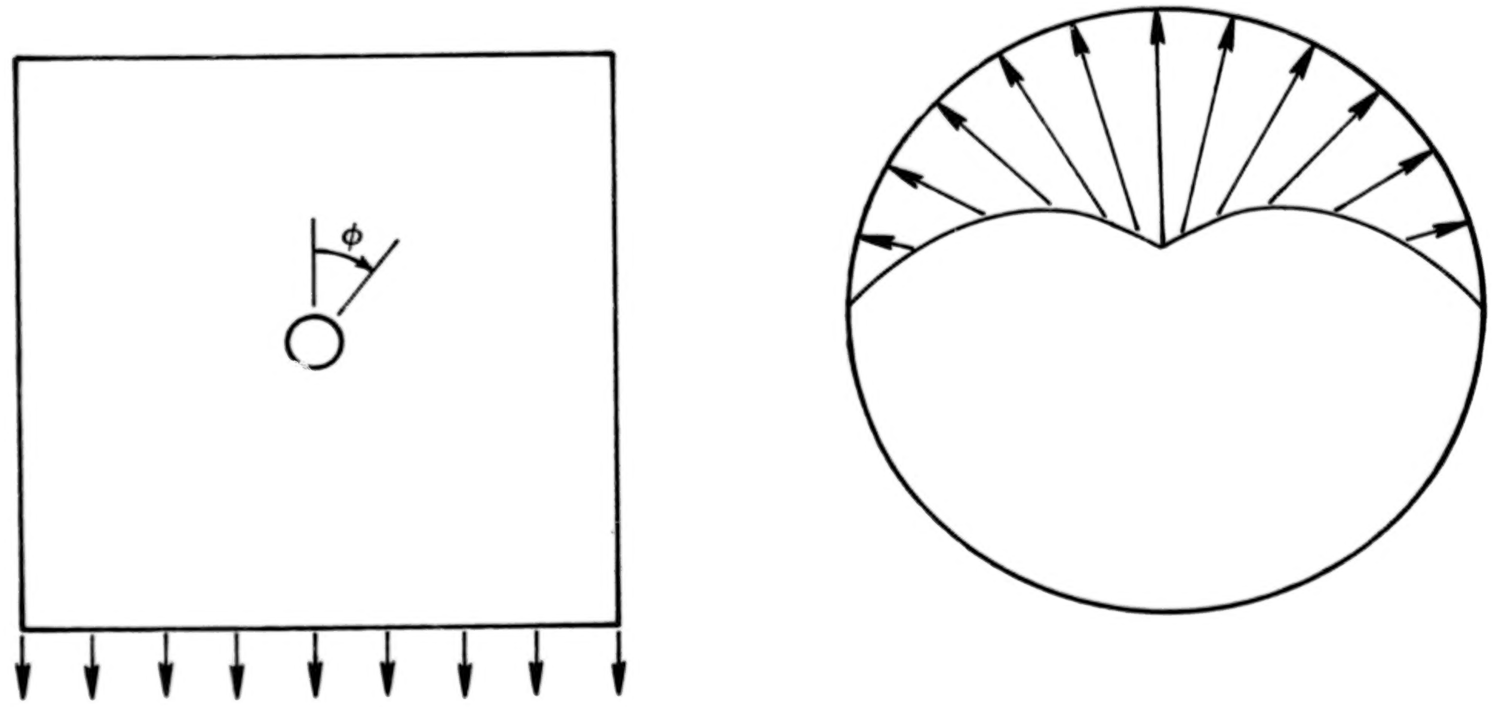

(a) External Loading

(b) Half Cosine Distribution of Traction on the Hole Boundary

Figure 4. Load Transfer Problem

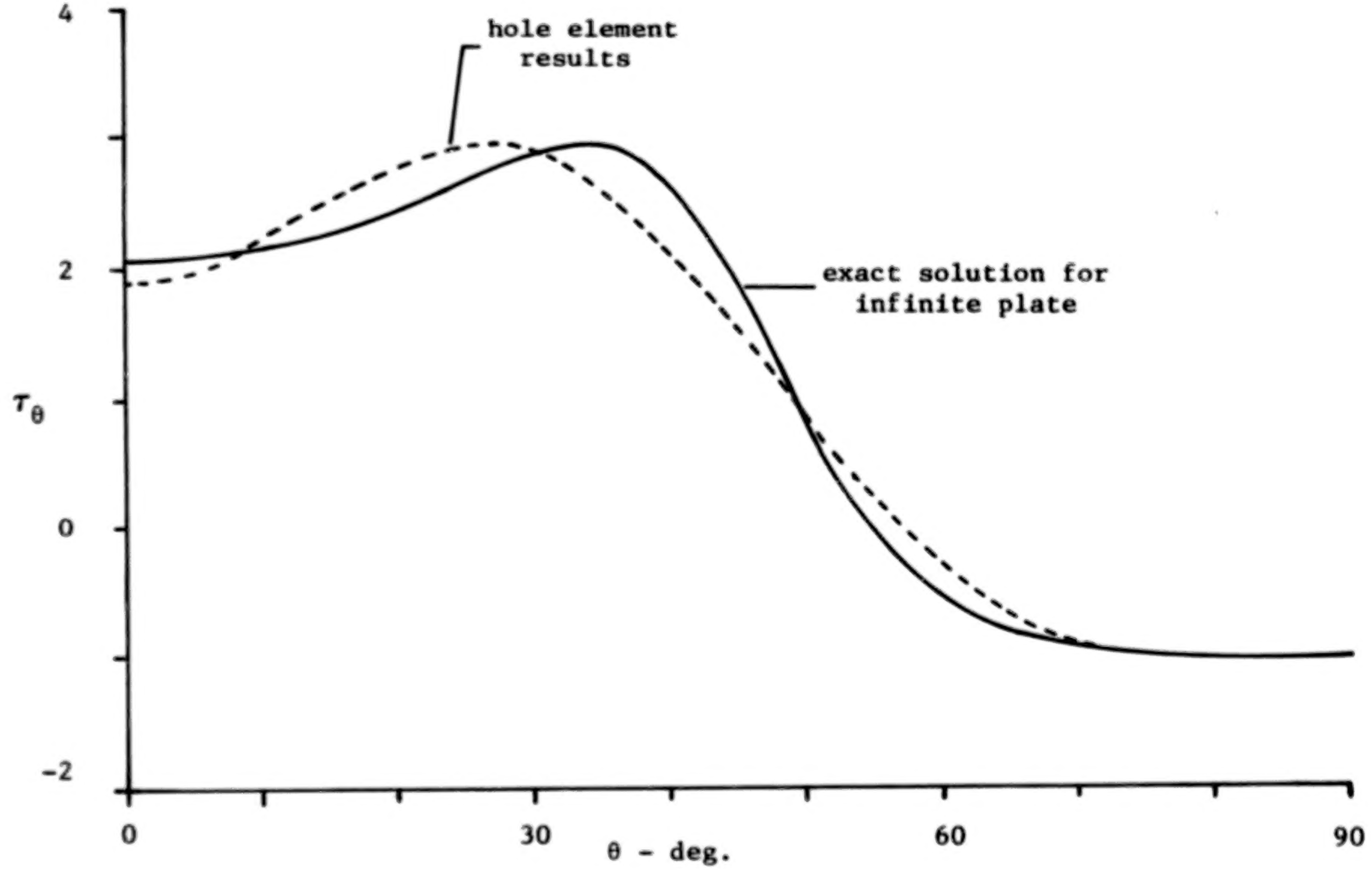

Figure 5. Circumferential Stress at the Open Hole Boundary for a $\pm 45^o$ Laminate with Unit Uniaxial Tensile Traction

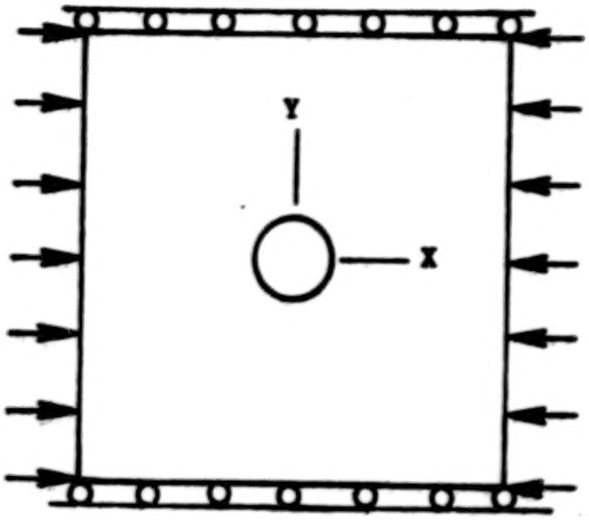

(a) Constrained Compression

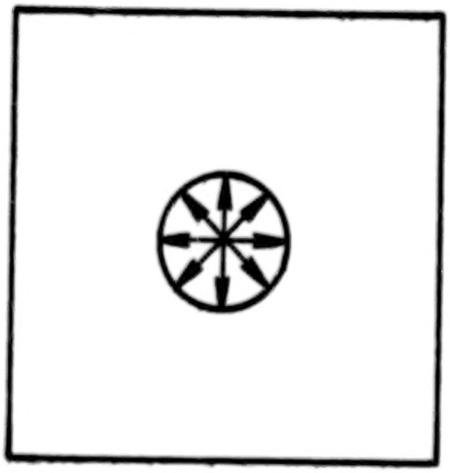

(b) Internal Pressure

Figure 6. External Loadings

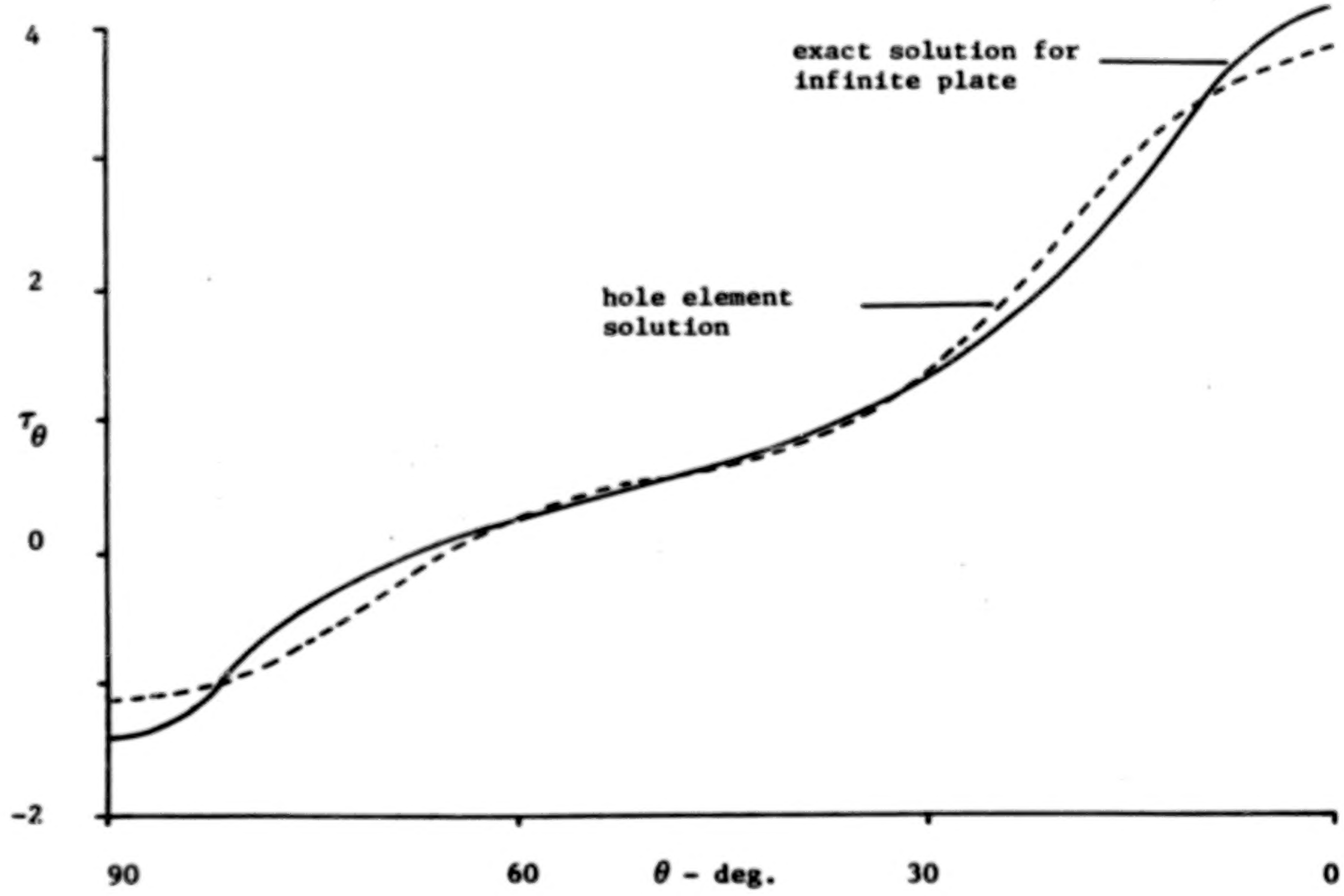

Figure 7. Circumferential Stress at the Open Hole Boundary for Plywood with Unit Uniaxial Tensile Traction

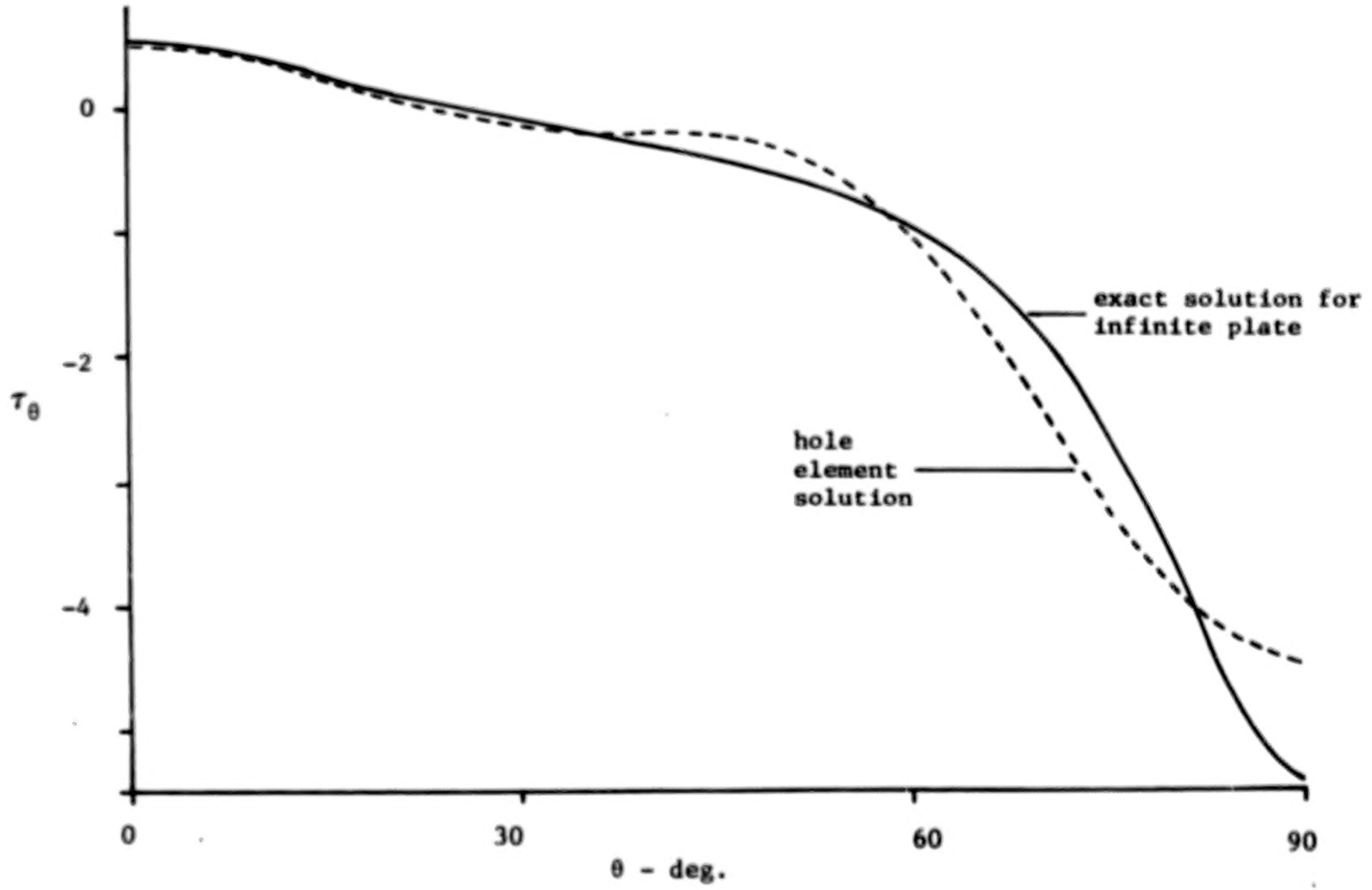

Figure 8. Circumferential Stress at the Open Hole Boundary for Plywood with Unit Constrained Compression

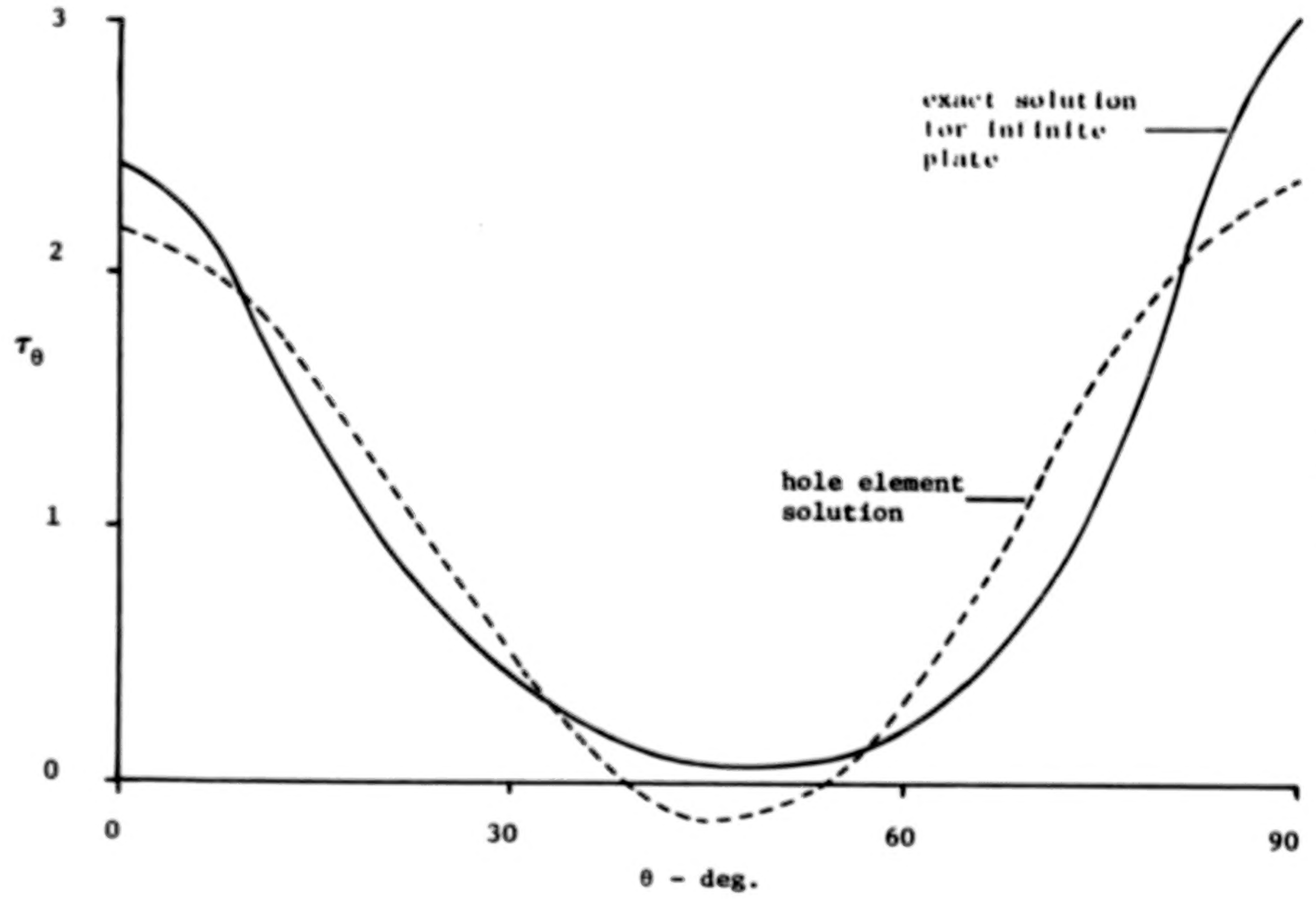

Figure 9. Circumferential Stress at the Hole Boundary for Plywood with Unit Internal Pressure on the Boundary

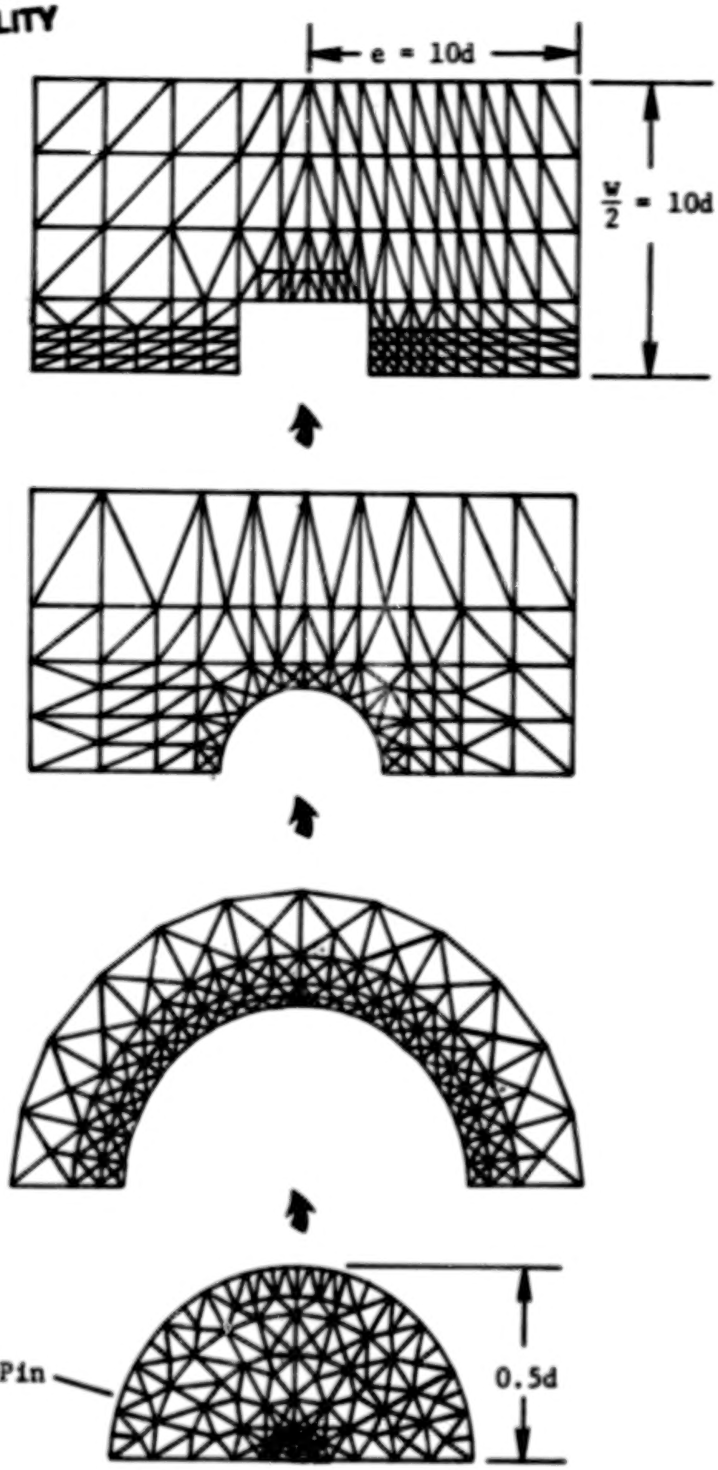
e = 10d
$\frac{w}{2}$ = 10d
Pin
0.5d

Figure 10. Detailed Finite Element Model for Analysis of Orthotropic Laminates with Pin-Loaded Holes

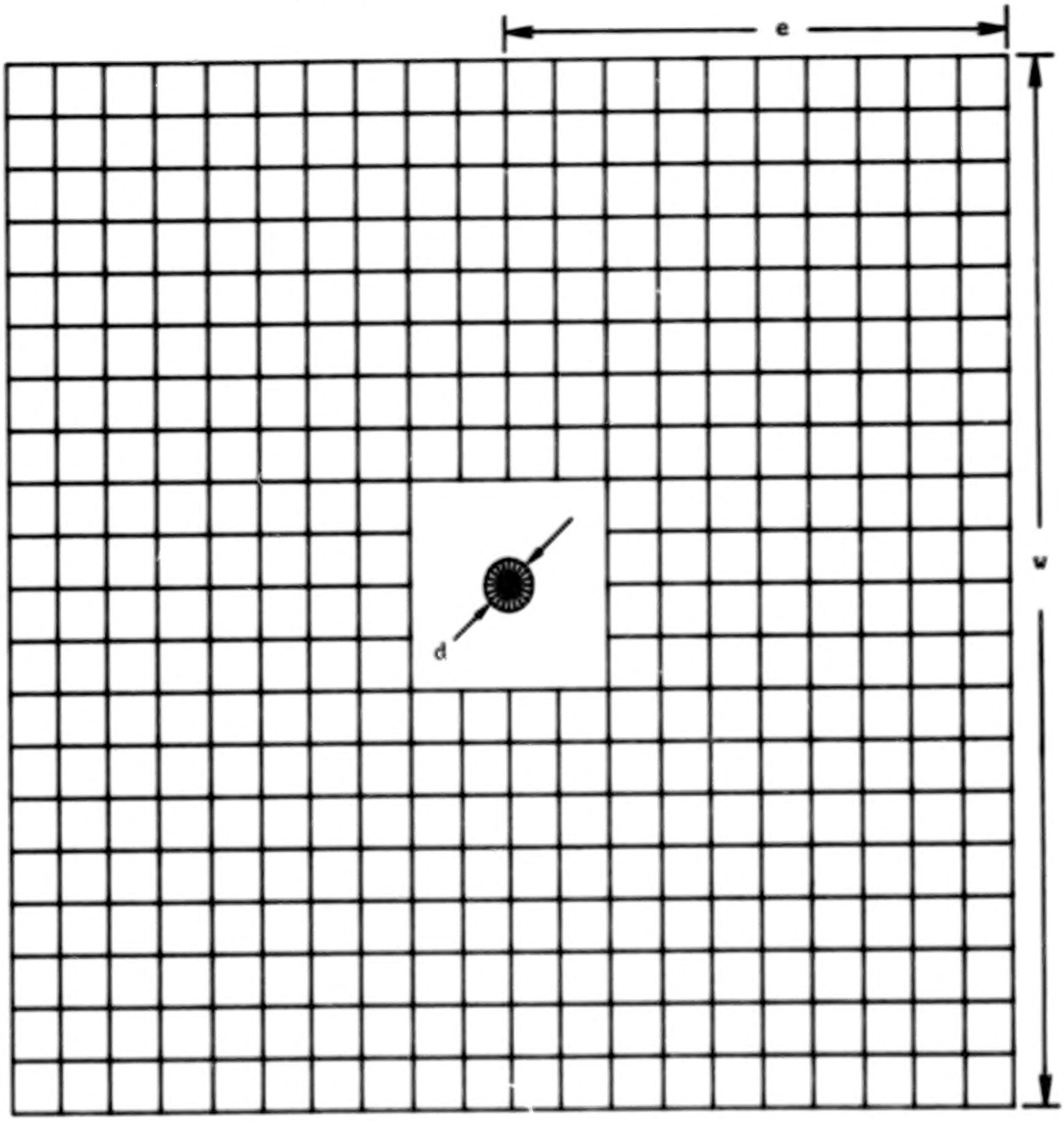

Figure 11. Finite Element Model with Hole Element

ORIGINAL PAGE IS OF POOR QUALITY

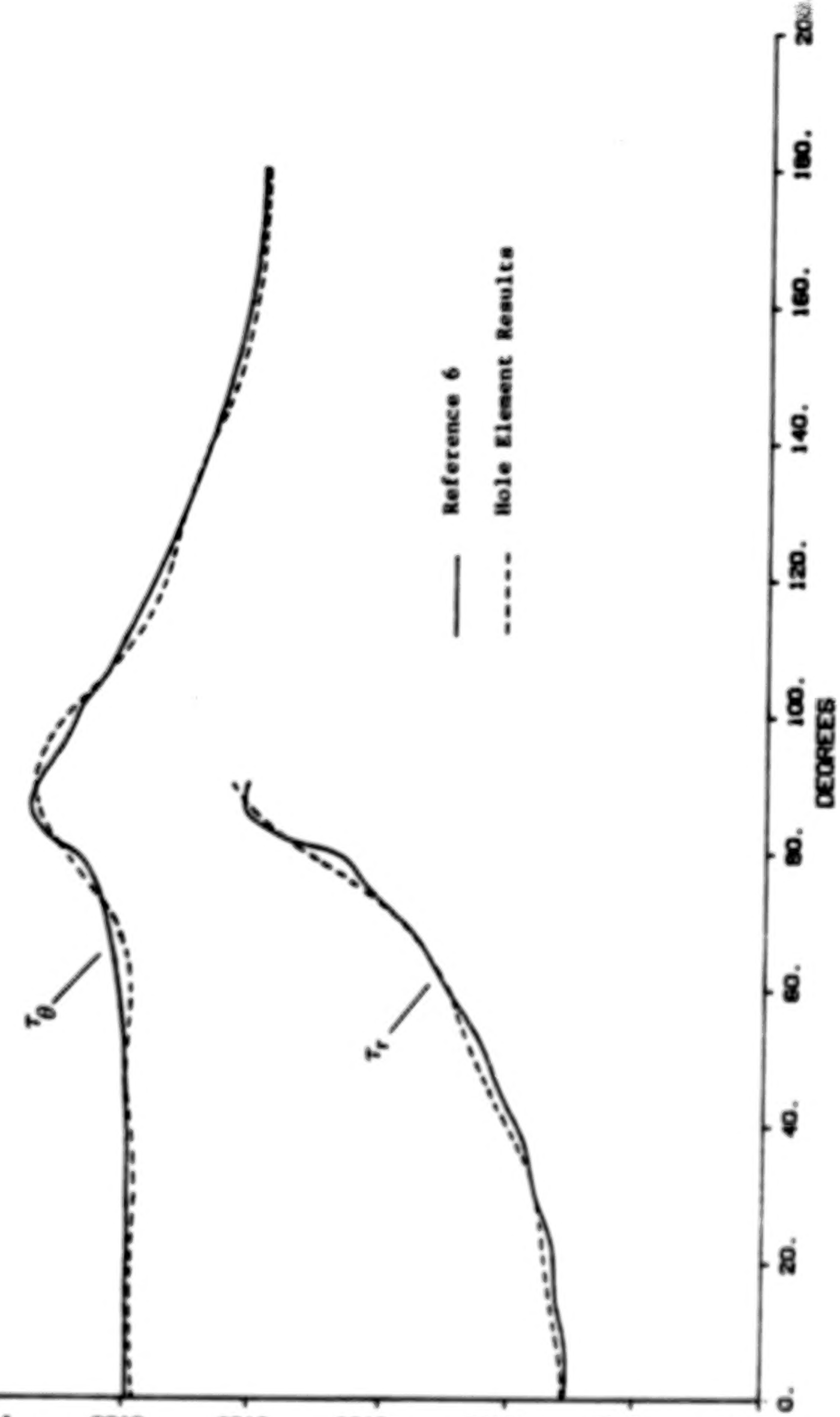

Figure 12. Stresses in the Quasi-Isotropic Laminate

ORIGINAL PAGE IS OF POOR QUALITY

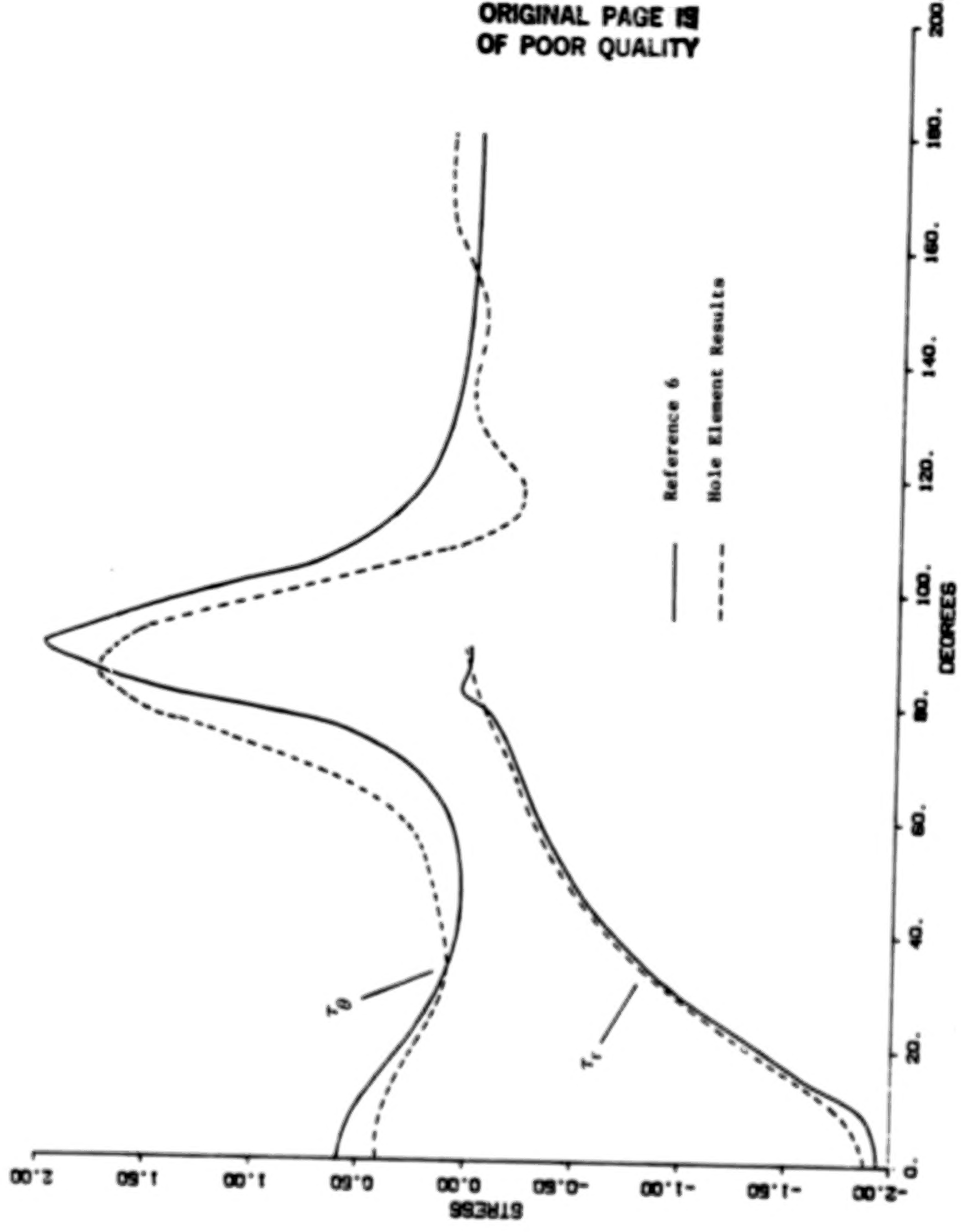

Figure 13. Stresses in the 0^0 Laminate

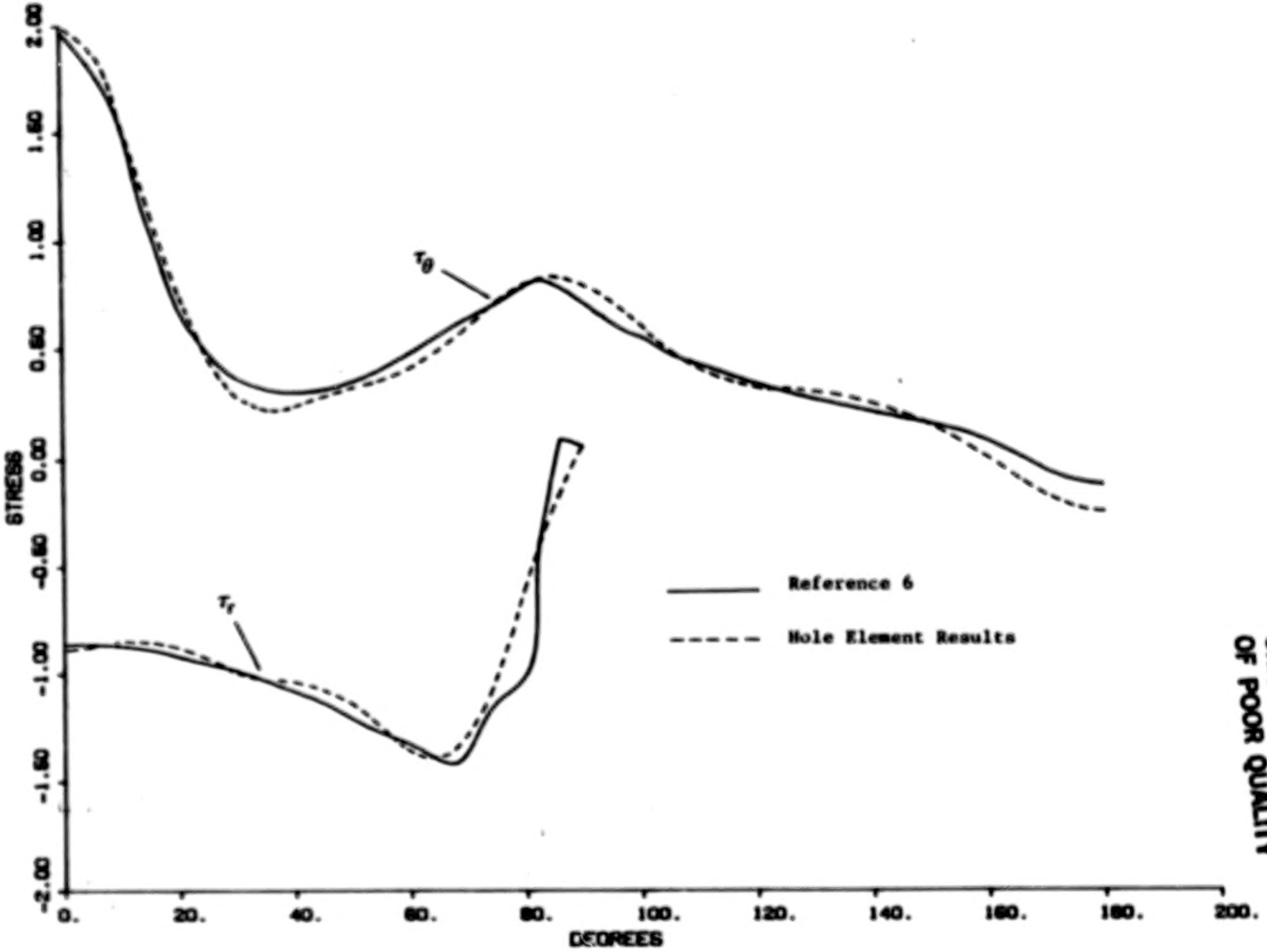

Figure 14. Stresses in the 90° Laminate

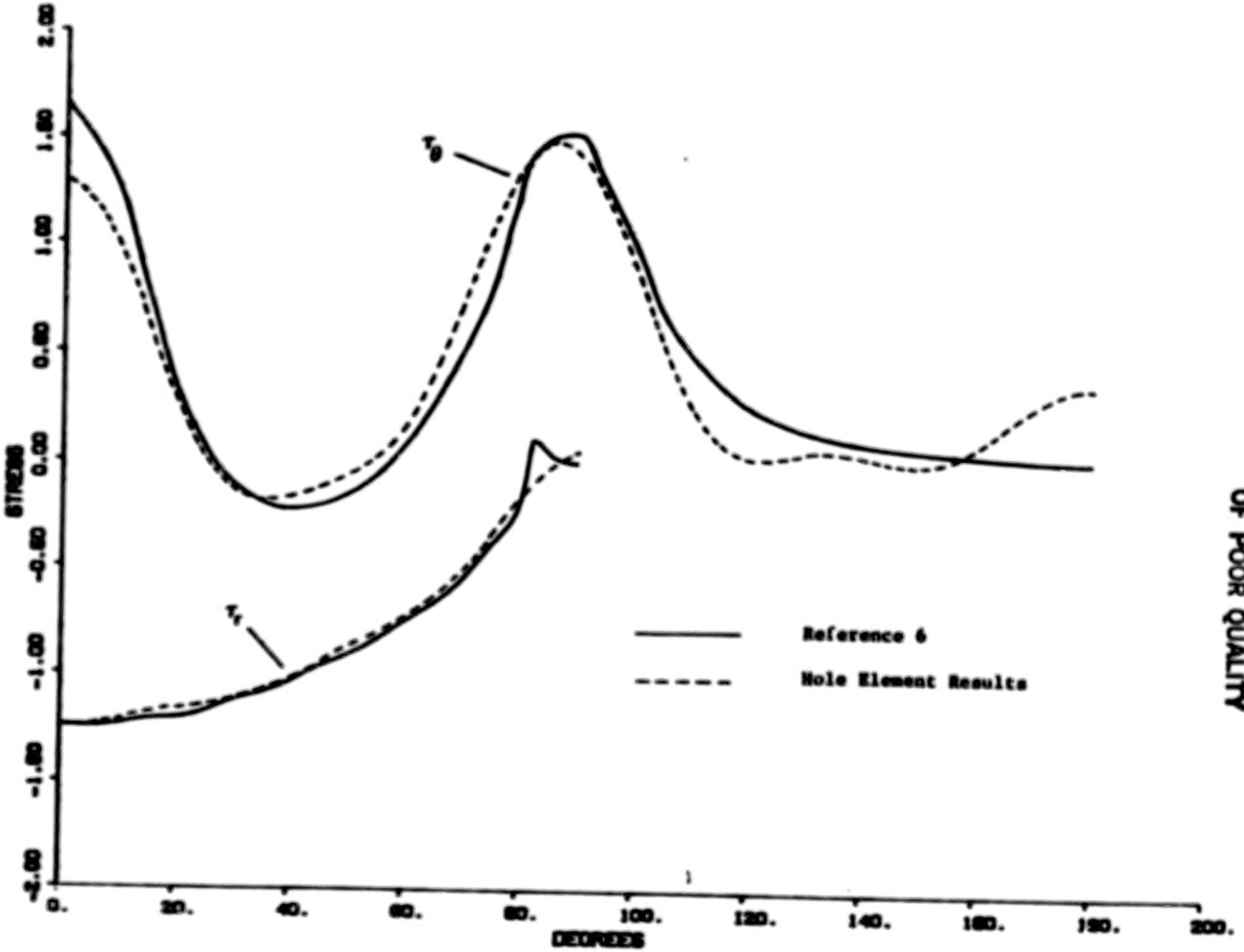

Figure 15. Stresses in the $[0°, 90°]_s$ Laminate

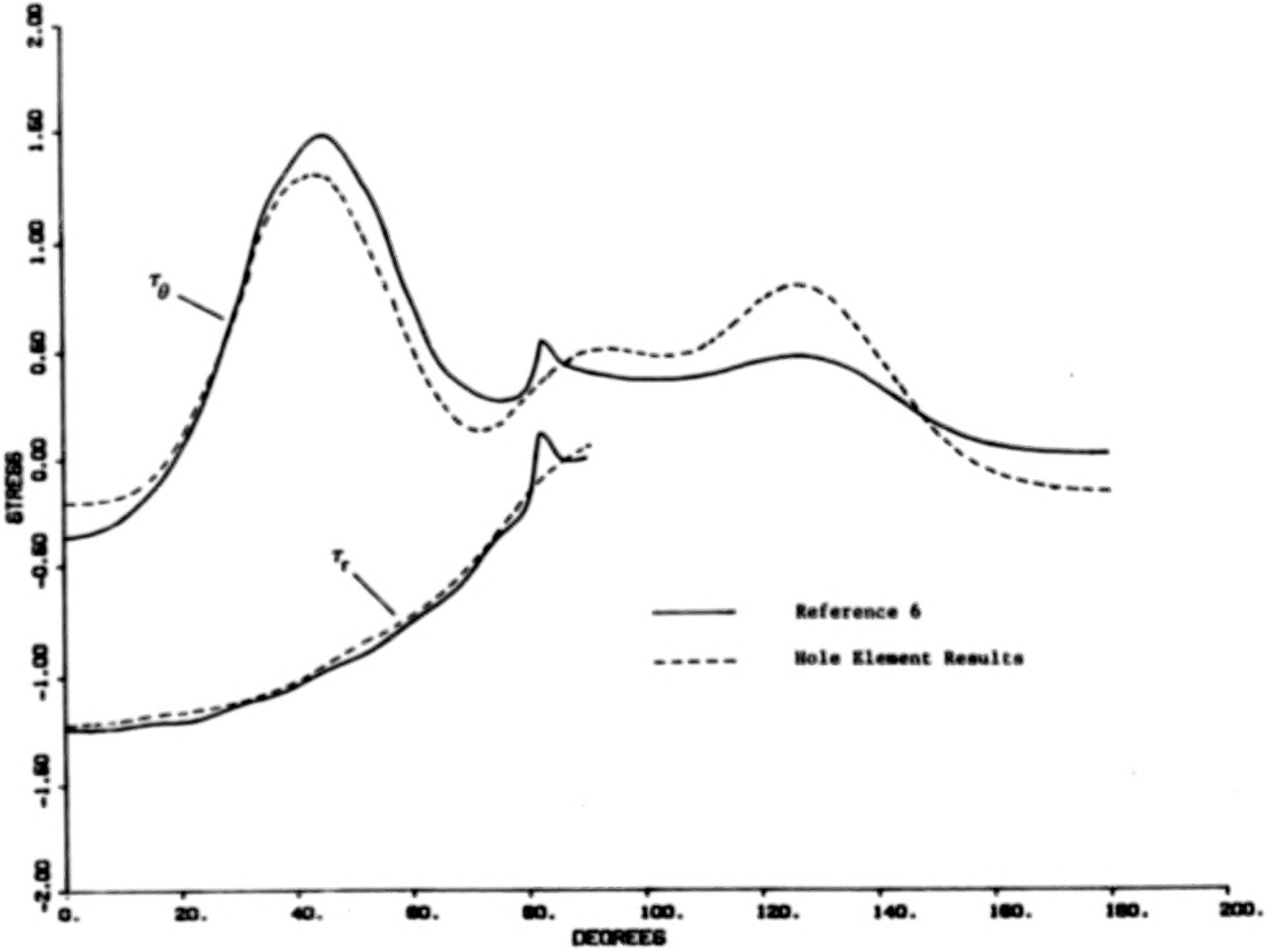

Figure 16. Stresses in the $[\pm 45^\circ]_s$ Laminate

ORIGINAL PAGE IS
OF POOR QUALITY

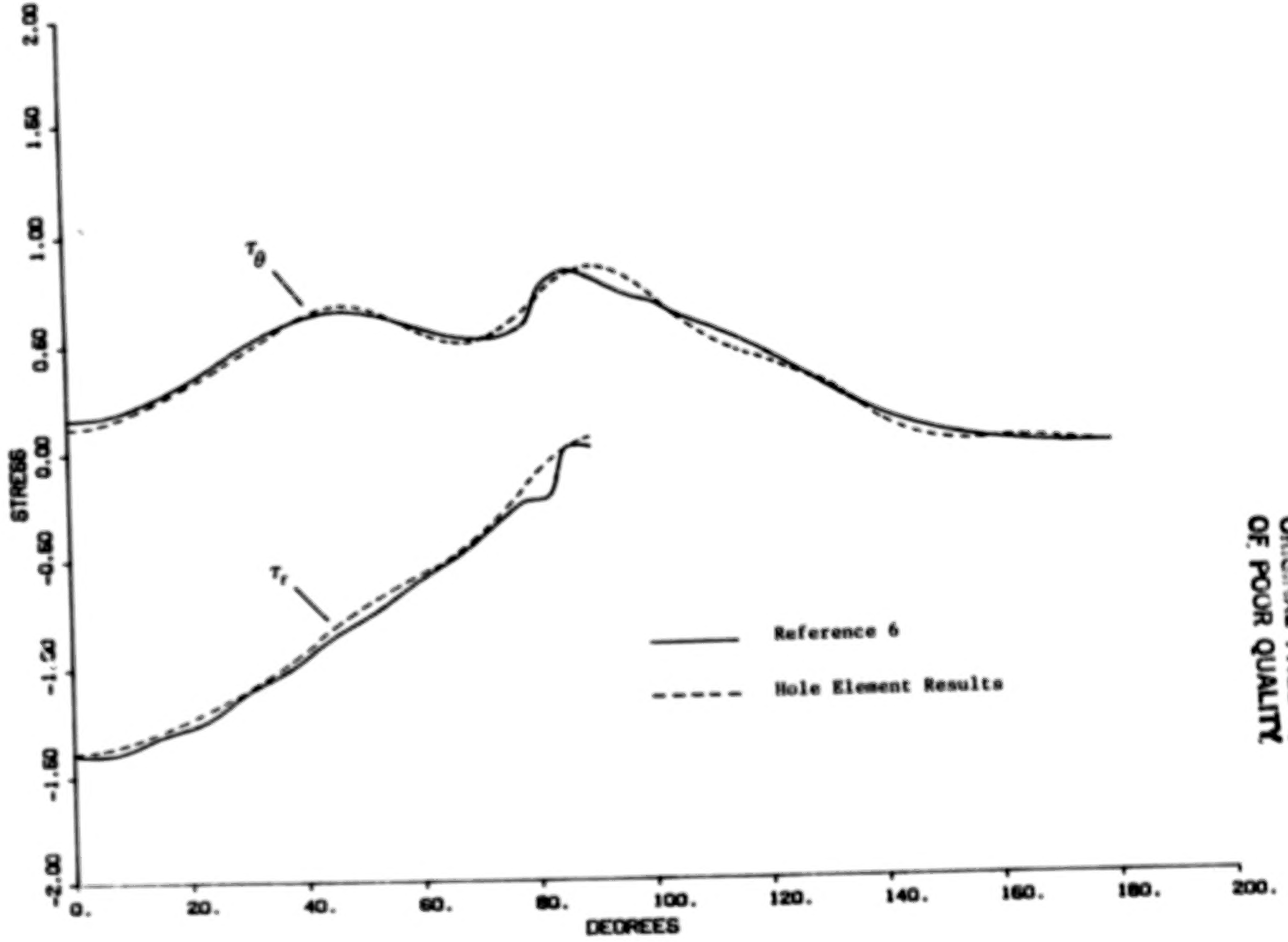

Figure 17. Stresses in the $[0^o/\pm45^o]_s$ Laminate

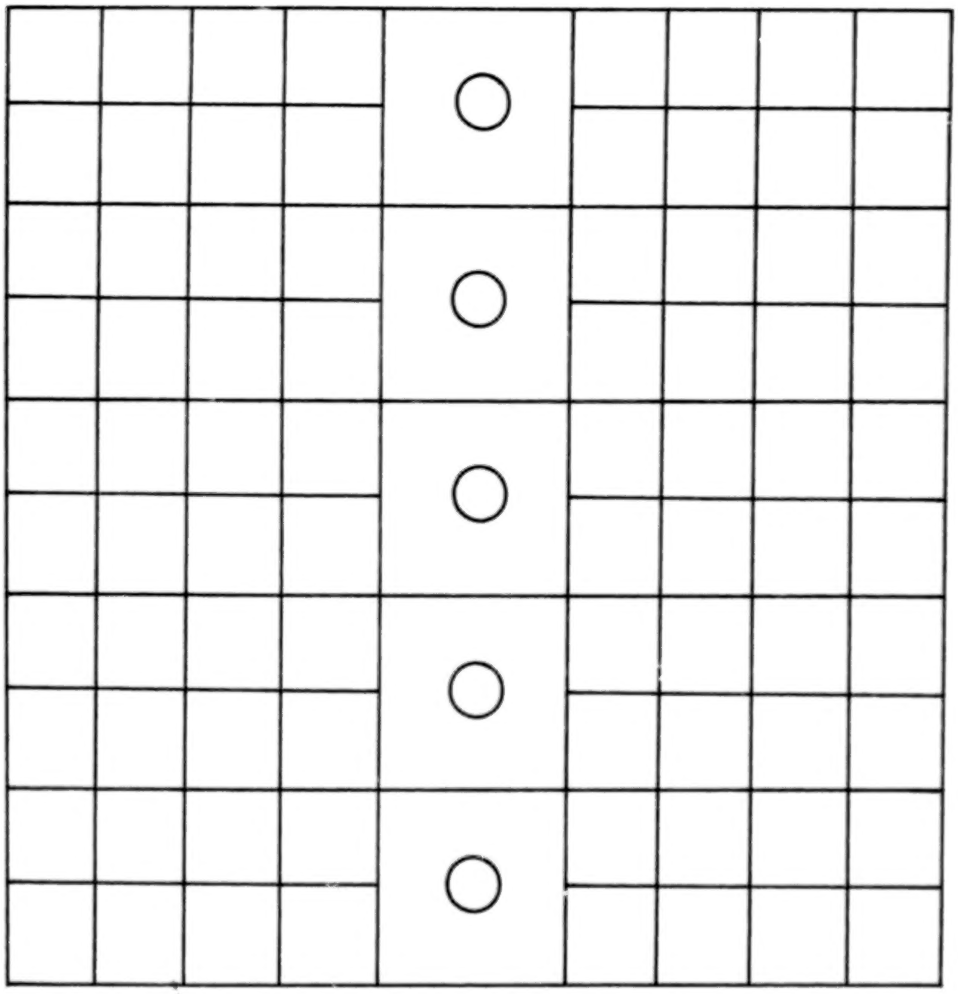

Figure 18. Finite Element Model for a Plate with Multiple Holes

REFERENCES

1. Smith, C. V.; Markham, J. W.; Kelley, J. W.; and Kathiresan, K.: Development of an Orthotropic Hole Element. NASA CR165759, August, 1981.

2. Timoshenko, S. P.; and Goodier, J. N.: Theory of Elasticity. Third Edition, McGraw-Hill Book Company, New York, 1970.

3. Bickley, W. G.: The Distribution of Stress Round a Circular Hole in a Plate. Philosophical Transactions of the Royal Society of London, Series A , Vol. 227, 1928, pp. 383-415.

4. Hong, C. S.; and Crews, J. H.: Stress Concentration Factors for Finite Orthotropic Laminates with a Circular Hole and Uniaxial Loading. NASA TP1469, May, 1979.

5. Lekhnitskii, S. G.: Anisotropic Plates. Second Edition, Gordon and Breach, New York, 1968.

6. Crews, J. H.; Hong, C. S.; and Raju, I. S.: Stress-Concentration Factors for Finite Orthotropic Laminates with a Pin-Loaded Hole. NASA TP1862, May, 1981.

7. Peterson, R. E.: Stress Concentration Design Factors. John Wiley and Sons, New York, 1953.

N84
15596

UNCLAS

D6 **N84 15596**

ORIGINAL PAGE IS
OF POOR QUALITY

GENERALIZING THE TRAPRG AND TRAPAX FINITE ELEMENTS

Myles M. Hurwitz

David W. Taylor Naval Ship R&D Center
Bethesda, Maryland 20084

SUMMARY

The NASTRAN TRAPRG and TRAPAX finite elements are very restrictive as to shape and grid point numbering. The elements must be trapezoidal with two sides parallel to the radial axis. In addition, the ordering of the grid points on the element connection card must follow strict rules. The paper describes the generalization of these elements so that these restrictions no longer apply.

INTRODUCTION

Since NASTRAN's inception in the early 1970's, the axisymmetric trapezoidal ring element TRAPRG has been an accurate, efficient element used in solid axisymmetric problems. More recently, the TRAPAX element was introduced to handle non-axisymmetric loading for such structures. While these two elements usually perform very well, the restrictions imposed upon the user in the specification of the elements can be considered, at best, difficult, at worst, unreasonable, in light of today's automatic data generators. The restrictions require that the elements be trapezoidal, rather then generally quadrilateral, with the top and bottom edges parallel to the radial axis. Also, the specification of the grid points on the connection card must be given counterclockwise starting with the grid point with smaller radial coordinate of the two grid points with the smaller axial coordinate. This paper presents the reasons for these restrictions, how the restrictions have been removed, the imposition of a new, but less stringent restriction, and an example problem.

THEORY

The stiffness matrix for a finite element is usually represented as

$$[K] = \int_V [B]^T [D] [B] dv \tag{1}$$

where [B] is the matrix of strain-displacement relations and [D] is the materials matrix describing the constitutive relations. The NASTRAN Theoretical Manual (ref. 1) defines [B] for TRAPRG and TRAPAX elements. The manual shows that, in order to evaluate the integral of Equation (1), the integrals

$$\int_A r^p z^q dr dz, \quad p = -1,\ 0,\ 1,\ 2,\ 3 \text{ and } q = 0,\ 1,\ 2 \tag{2}$$

must be evaluated over the cross-sectional area of the element. The NASTRAN Programmer's Manual (ref. 2) describes how the integrals (2) are computed analytically. It is because of the nature of the expressions involved in the exact representation of these integrals that the original restrictions on the elements were imposed. The restrictions have been removed by replacing the exact integration with Gauss quadrature, as follows.

The three-point quadrature is given as

$$\int_A r^p z^q dr dz = \sum_{l=1}^{3} \sum_{m=1}^{3} r^p z^q(\xi_l, \eta_m)\, H_l H_m \, |J(\xi_l, \eta_m)| \tag{3}$$

where

$$r = \sum_{i=1}^{4} N_i r_i$$

$$z = \sum_{i=1}^{4} N_i z_i$$

N_i = $1/4(1 + \xi\xi_i)(1 + \eta\eta_i)$, the linear isoparametric shape function over the square $\xi = -1$ to $+1$ and $\eta = -1$ to $+1$

r_i, z_i = r,z coordinates of the grid points at the four corners of the element

ξ_l, η_m = isoparametric coordinates at which $r^p z^q$ is evaluated in a three-point Gauss quadrature

H_l, H_m = quadrature weights corresponding to ξ_l, η_m

$|J(\xi_l, \eta_m)|$ = determinant of the Jacobian, $\begin{vmatrix} \frac{\partial r}{\partial \xi} & \frac{\partial z}{\partial \xi} \\ \frac{\partial r}{\partial \eta} & \frac{\partial z}{\partial \eta} \end{vmatrix}$, evaluated at (ξ_l, η_m)

With this formulation, the restrictions on the trapezoidal shape and grid point numbering can be removed.

There is, however, one situation which can cause numerical problems. Note that, in integrals (2), if $p = -1$ and $r \rightarrow 0$, then the integral $\rightarrow \infty$. Two cases can be examined. The first is the core element, a TRAPRG element with exactly two grid points with zero radius. (NASTRAN does not allow the TRAPAX element to be a core element since it does not allow a RINGAX ring to have a zero radius.) At these two points, the radial displacement must be zero. This condition can be assured as follows. If u and w are the radial and axial displacements, respectively, at some point within an element, then the assumed displacement functions are (ref. 1)

$$u = B_1 + B_2 r + B_3 z + B_4 rz \tag{4}$$

$$w = B_5 + B_6 r + B_7 z + B_8 rz \tag{5}$$

where the B_i are unknown coefficients. Then,

$$\begin{Bmatrix} u_1 \\ w_1 \\ \vdots \\ u_4 \\ w_4 \end{Bmatrix} = \begin{bmatrix} \\ H_{Bu} \\ \\ \end{bmatrix}^{-1} \begin{Bmatrix} B_1 \\ \vdots \\ B_8 \end{Bmatrix}$$

where u_i, w_i are the displacements of the ith grid point. If $r_i = 0$, then u_i must be 0, which means that the (2_i-1)th column of H_{Bu} can be zeroed. In addition, from Equation (4), $0 = u = B_1 + B_3 z$ for all z. Therefore, $0 = B_1 = B_3$, which can be assured by zeroing the first and third columns of H_{Bu}. However, the only terms of H_{Bu} which contain a form of (2) with $p = -1$ are in the first and third columns. Therefore, for a TRAPRG core element with $r_i = 0$, no numerical problems exist.

Now consider a second case - one where some r_i is small compared with some other r_i in the element. Comparisons between the analytical integration and the Gauss quadrature show that if

$$\frac{r_{max}}{r_{min}} > 10 \tag{7}$$

then the Gauss quadrature results begin to significantly degrade ($r_{max} = \max r_i$, $i = 1, \ldots, 4$). Therefore, inequality (7) is not allowed. This restriction should impose a hardship mainly when a TRAPAX core element is desired. This hardship however should require only an extra element or two to transition to larger radii.

SAMPLE PROBLEM

The sample problem for this work was a normal modes analysis of a thick-walled cylinder of inner radius 5.0 inches, outer radius 6.25 inches, and length 3.5 inches. The finite element model for the unmodified version of NASTRAN is shown in Figure 1a and, for the version which removes the restriction, in Figure 1b. Both models used the TRAPAX element. The results are shown in Table 1. The comparison of the results shows a degradation at the highest mode computed. However, this can be expected because of the severity of the non-uniform mesh.

REFERENCES

1. The NASTRAN Theoretical Manual (Level 17.5), NASA SP-221 (05), Dec. 1978.

2. The NASTRAN Programmer's Manual (Level 17.5), NASA SP-223 (05), Dec. 1978.

TABLE 1. COMPARATIVE RESULTS

MODE	NATURAL FREQUENCIES (CPS)	
	RESTRICTIVE ELEMENTS	GENERAL ELEMENTS
1	1090.003	1090.000
2	1660.250	1660.864
3	1760.034	1760.101
4	1988.622	1989.121
5	2071.862	2071.920
6	5407.311	5209.751

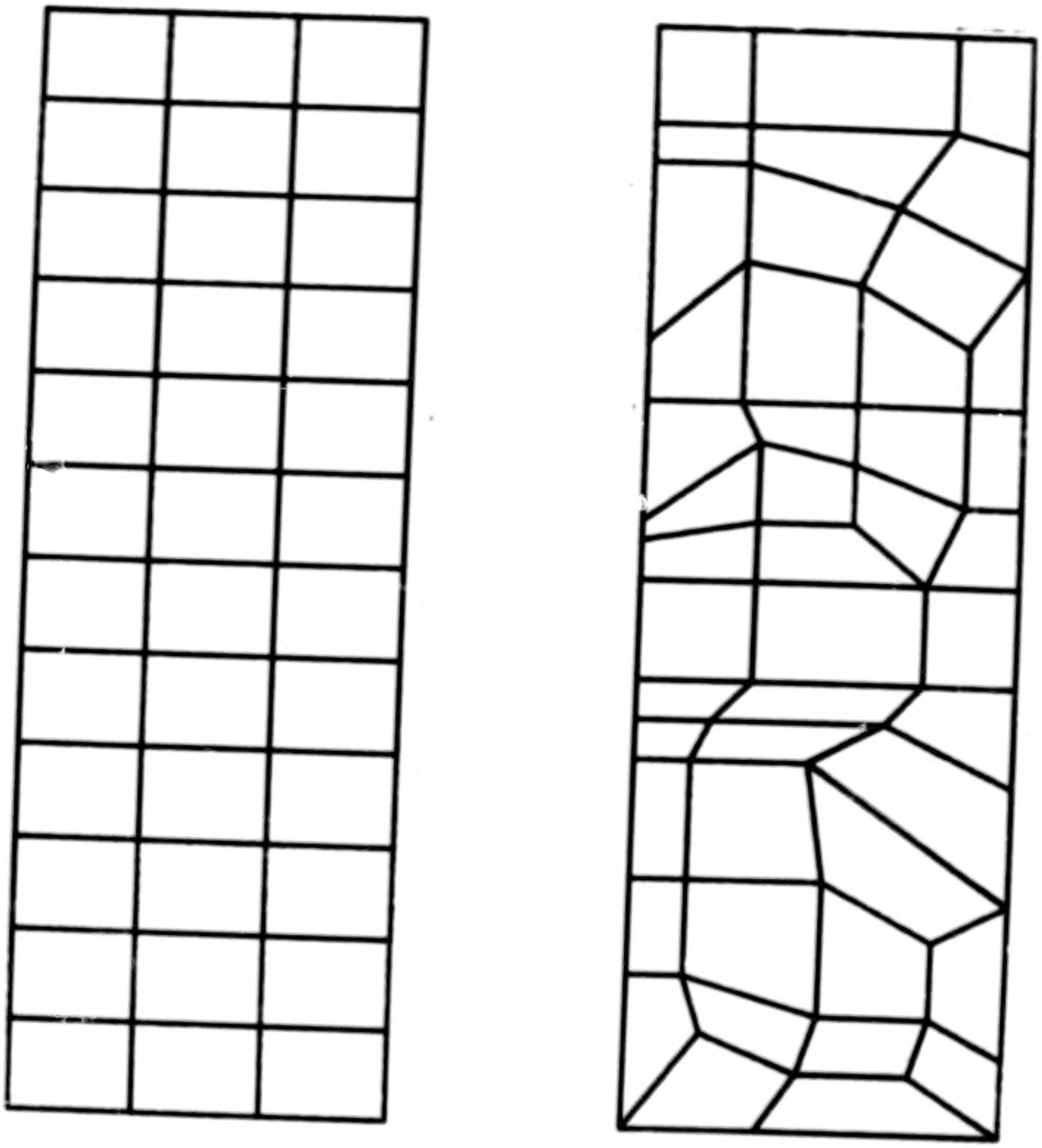

Figure 1a

Figure 1b

Figure 1. Finite Element Models

N84
15597

UNCLAS

D7

N84 15597

ACOUSTICAL MODES OF ARBITRARY VOLUMES USING NASTRAN TRANSIENT HEAT TRANSFER RF9

V. Elchuri, G. C. C. Smith, A. Michael Gallo
Bell Aerospace Textron, Buffalo, New York

SUMMARY

An equivalence between temperature and pressure, heat conduction and 'stiffness', and heat capacity and 'mass' is defined, enabling acoustical modal analysis of arbitrary three-dimensional volumes. The transient heat transfer analysis rigid format in NASTRAN, RF9, has been ALTERed providing the acoustical analysis capability. Examples and ALTERs are included.

INTRODUCTION

A twenty-node isoparametric acoustic finite element model was developed in Reference 1 for analyzing the acoustic modes of irregular shaped cavities. In the present paper,

1. the existence of an identical element in NASTRAN (IHEX2) and,
2. the recognition of the similarity between the acoustical matrices of Reference 1 and the thermal matrices of NASTRAN

have enabled the posing and solution of the acoustics eigenvalue problem for arbitrary three-dimensional cavities bounded by 'hard' acoustic surfaces. A simple modification of the transient heat transfer rigid format RF9 provides the acoustics analysis formulation in NASTRAN.

SIMILARITY OF ACOUSTICAL AND THERMAL MATRICES

Summarizing the finite element formulation of Reference 1, the pressure p in a volume V bounded by a surface S satisfies the three-dimensional wave equation and boundary conditions:

$$\nabla^2 p + (\omega^2/a_0^2)p = 0 \text{ in V, and} \tag{1}$$

$$\nabla p \cdot \hat{n} = 0 \text{ on S,} \tag{2}$$

where ω is the frequency of vibration of the acoustical mode, a_0 is the speed of sound, and $\hat{n}$ is the outward normal to S. Representing the volume V by an assemblage of three-dimensional finite elements, the corresponding eigenvalue problem becomes

$$[K - \omega^2 M]\{p\} = 0 \quad , \tag{3}$$

where for the ith element

$$[k]_i = \int_{V_i} [B]_i^T [B]_i dV \quad , \tag{4}$$

$$[m]_i = \int_{V_i} \frac{1}{a_0^2} \lfloor N \rfloor_i^T \lfloor N \rfloor_i \, dV \, , \quad \text{and} \tag{5}$$

$$[B]_i = \begin{bmatrix} \frac{\partial}{\partial x} \\ \frac{\partial}{\partial y} \\ \frac{\partial}{\partial z} \end{bmatrix} \lfloor N \rfloor_i \, . \tag{6}$$

The shape function $\lfloor N \rfloor_i$ approximates the pressure within the ith element in terms of the nodal pressures $\{p\}_i$ as

$$p = \lfloor N \rfloor_i \, \{p\}_i \quad . \tag{7}$$

A comparison with the NASTRAN heat transfer analysis capability (Ref. 2) indicates that,

1. equation (4) is identical to the heat conduction matrix, if the thermal conductivity is unity, and
2. equation (5) is identical to the heat capacity matrix, if the thermal capacity per unit volume is $1/a_0^2$.

The temperature degrees of freedom in the thermal analysis are taken to correspond to the pressure degrees of freedom in the acoustics analysis.

The above correspondence together with the real eigenvalue analysis module (READ) permit the determination of the acoustical modes and frequencies. An ALTER package to be used in HEAT APPROACH RF9 is included in the Appendix.

EXAMPLES

The two examples of Reference 1, shown in Figures 1 and 2, were analyzed using the modified RF9. The results, generally in agreement, are presented in Tables 1 and 2, and Figure 3. It is noted that the missing geometric dimensions in Figure 2 were scaled from the figure of Reference 1.

CONCLUDING REMARKS

With a simple modification, and a 'redefinition' of thermal conductivity and capacity, the transient heat transfer rigid format in NASTRAN has been used to determine the acoustical modes and frequencies of arbitrary volumes. The volume can be modelled by any of the solid elements permitted by RF9. Although only acoustically hard surfaces have been considered in this paper, simple extensions to other boundary conditions are considered to be possible.

ORIGINAL PAGE IS
OF POOR QUALITY

REFERENCES

1. Petyt, M., Lea, J., and Koopmann, G. H., "A Finite Element Method for Determining the Acoustic Modes of Irregular Shaped Cavities," Journal of Sound and Vibration (1976), 45 (4), pp 495-502.

2. NASTRAN Theoretical Manual, NASA SP-221(05), December 1978.

APPENDIX

```
$ ALTER HEAT RF 9 (NASTRAN RELEASE APRIL 1982)
$
ALTER    26,26 $ SET NOMGG=1 BECAUSE OF ERROR IN IHEX2 LOGIC.
EMG      HEST,CSTM,MPT,DIT,GEOM2,/HKELM,HKDICT,DUM1,DUM2,HBELM,HBDICT/
         S,N,NOKGGX/ 1/ S,N,NOBGG $
ALTER    67,67 $ COMPUTE AND PRINT MODES
DPD      DYNAMICS,GPL,HSIL,HUSET/GPLD,HSILD,HUSETD,TFPOOL,HDLT,,,
         HNLFT,HTRL,EED,HEQDYN/HLUSET/S,N,HLUSETD/123/S,N,NODLT/
         123/123/S,N,NONLFT/S,N,NOTRL/S,N,NOEED//S,N,NOUE $
PARAM    //*MPY*/NEIGV/1/-1 $
READ     HKAA,HBAA,,,EED,HUSET,CASECC/LAMA,PHIA,,OEIGS/
         *MODES*/S,N,NEIGV $
OFP      OEIGS,LAMA,,,, // $
SDR1     HUSET,,PHIA,,,HGO,GM,,,,/PHIG,,/1/*REIG* $
SDR2     CASECC,CSTM,MPT,DIT,HEQDYN,HSIL,,,BGPDP,LAMA,,PHIG,
         HEST,,/,,OPHIG,,,PPHIG/*REIG* $
OFP      OPHIG,,,,, // $
PLOT     FLTPAR,GPSETS,ELSETS,CASECC,BGPDT,HEQEXIN,HSIP,,PPHIG,HGPECT,
         /PLOTX3/HNSIL/HLUSEP/JUMPPLOT/PLTFLG/PFILE $
PRTMSG   PLOTX3// $
ENDALTER
```

TABLE 1. ACOUSTIC FREQUENCIES OF A RIGHT-ANGLED PARALLELOPIPED (cyc/T)

(a) Symmetric Modes

Mode	Exact Frequency*	Ref. 1	This Paper
1, 0, 0	699	702	680
2, 0, 0	1398	1542	1495
0, 0, 1	1500	1506	1460
1, 0, 1	1655	1664	1613
2, 0, 1	2057	2155	2090
3, 0, 0	2097	2525	2448
3, 0, 1	2579	--	2925

TABLE 1. ACOUSTIC FREQUENCIES OF A RIGHT-ANGLED PARALLELOPIPED (cyc/T) (Contd.)

(b) Antisymmetric Modes

Mode	Exact Frequency*	Ref. 1	This Paper
0, 1, 0	1250	1255	1255
1, 1, 0	1432	1440	1430
2, 1, 0	1876	1988	1952
0, 1, 1	1953	1963	1928
1, 1, 1	2074	2089	2048
2, 1, 1	2401	2499	2440
3, 1, 0	2442	2875	2808
3, 1, 1	2866	3346	3233

$$* \; f_{\ell,\, m,\, n} = \frac{a_s}{2} \left[\left(\frac{\ell}{\ell}\right)^2 + \left(\frac{m}{\ell_y}\right)^2 + \left(\frac{n}{\ell_z}\right)^2 \right]^{1/2} , \text{ (Ref. 1)}$$

ℓ_x, ℓ_y, ℓ_z sides of the parallelopiped

TABLE 2. ACOUSTIC FREQUENCIES OF MODEL VAN (cyc/T)

(a) Symmetric Modes

	Ref. 1		
Mode	Experimental	Calculated	This Paper
1	606	593	562
2	1174	1150	1104
3	1549	1556	1524
4	1613	1605	1580
5	1817	1829	1751
6	1992	2026	1993

(b) Antisymmetric Modes

	Ref. 1		
Mode	Experimental	Calculated	This Paper
1	1220	1168	1118
2	1352	1317	1245
3	1675	1634	1568
4	1996	1956	1940
5	2021	1997	1968
6	2176	2187	2109

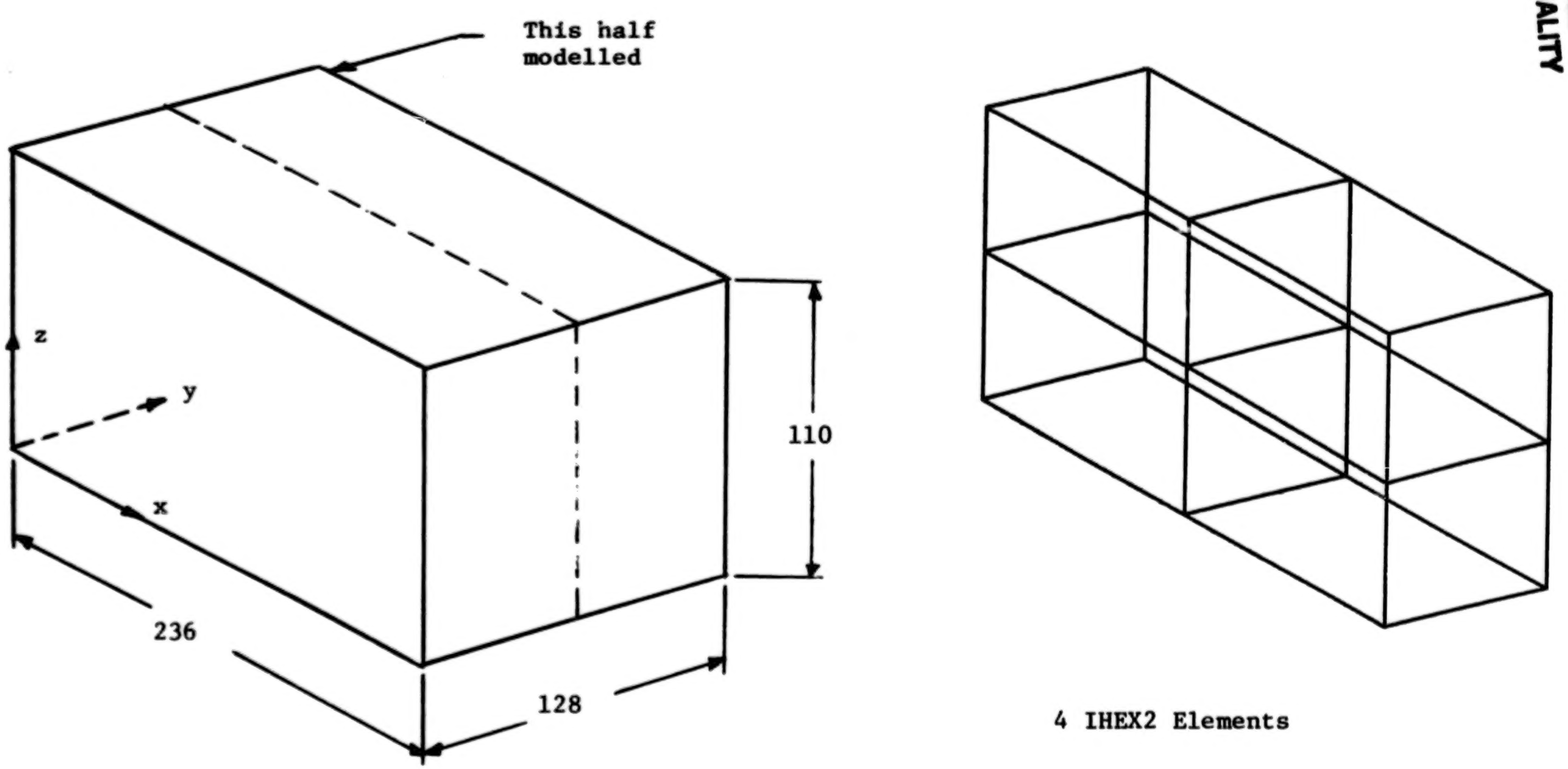
This half modelled
z
y
x
110
236
128

4 IHEX2 Elements

FIGURE 1. DETAILS OF RIGHT-ANGLED PARALLELOPIPED

C-2

ORIGINAL PAGE IS
OF POOR QUALITY

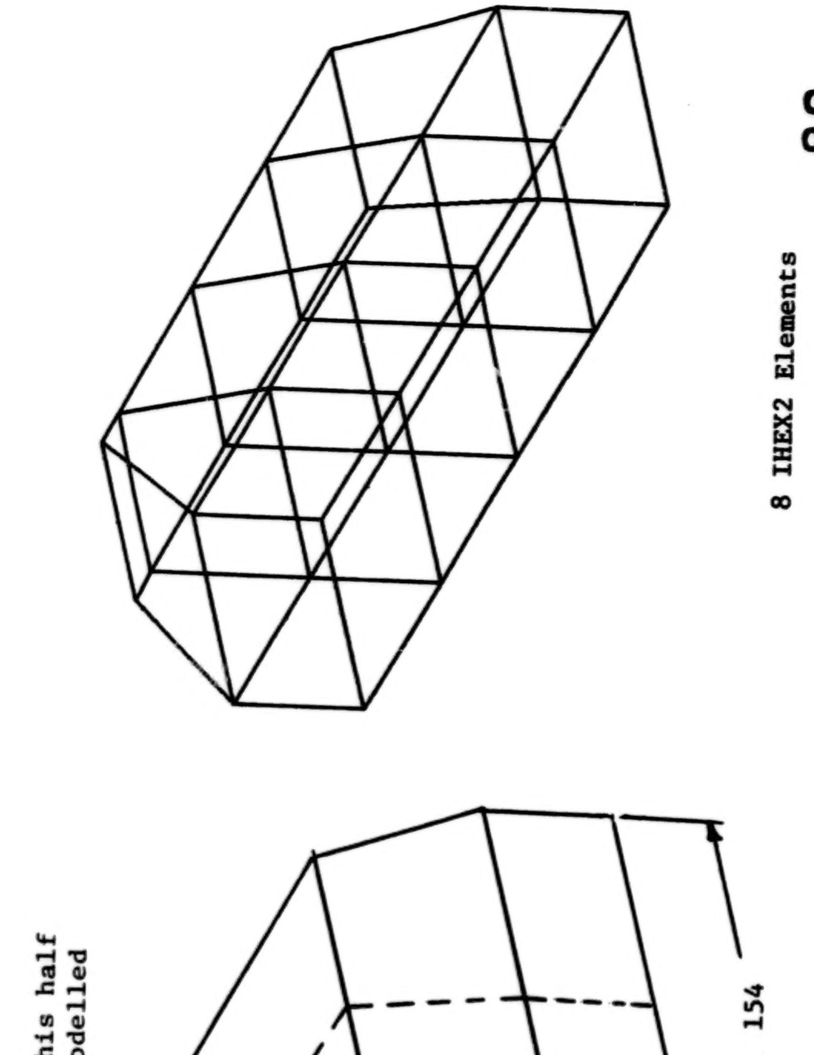
8 IHEX2 Elements
This half modelled
128
112
310
154

FIGURE 2. DETAILS OF MODEL VAN

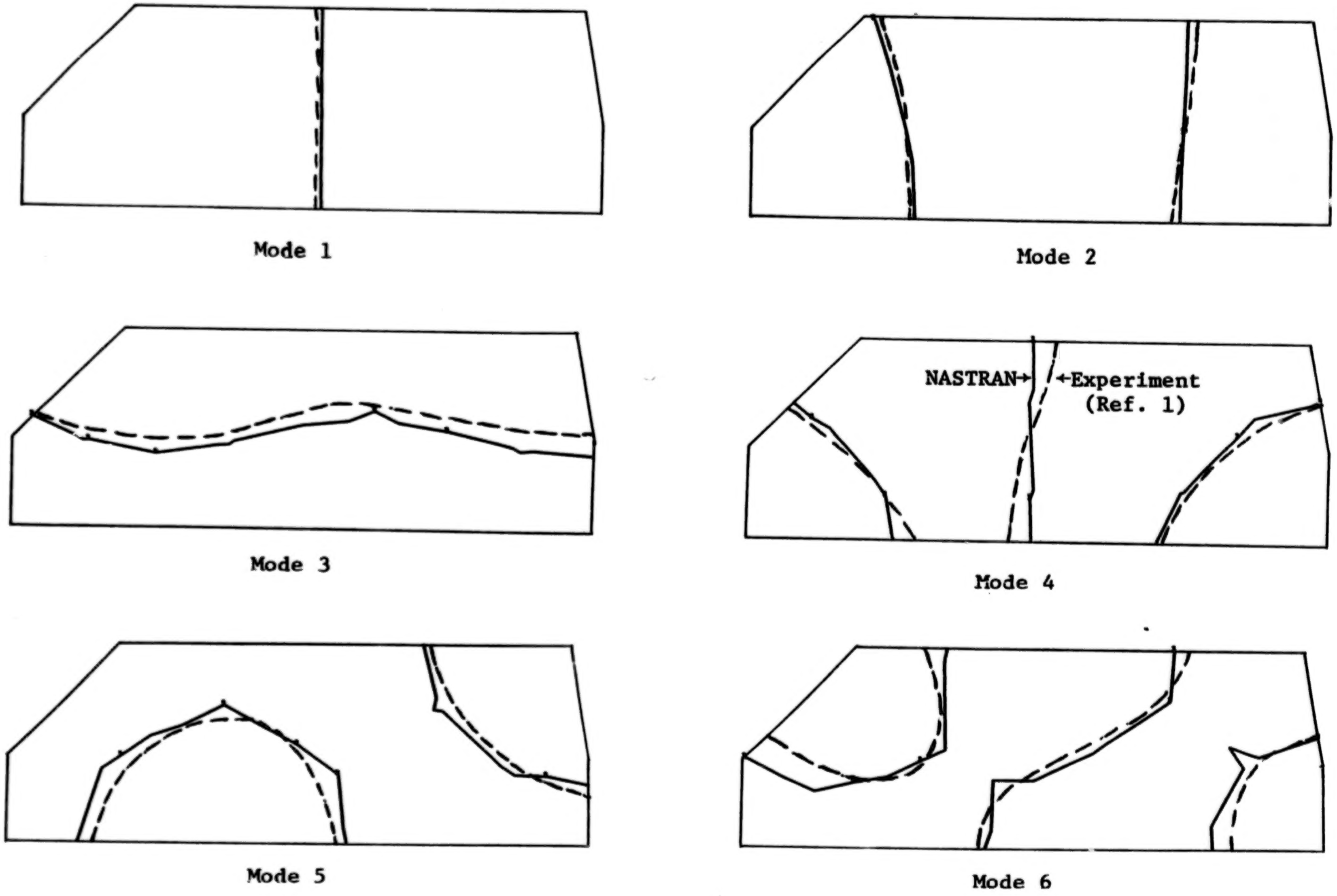
Mode 1
Mode 2
Mode 3
NASTRAN→
←Experiment (Ref. 1)
Mode 4
Mode 5
Mode 6

FIGURE 3. SYMMETRIC ACOUSTIC MODES OF MODEL VAN (Figure 2)

N84
15598

UNCLAS

ORIGINAL PAGE IS
OF POOR QUALITY

N84 15598 D8

AN ALTERNATIVE METHOD OF ANALYSIS FOR BASE ACCELERATED DYNAMIC RESPONSE IN NASTRAN

V. Elchuri, A. Michael Gallo, G. C. C. Smith
Bell Aerospace Textron, Buffalo, New York

SUMMARY

An alternative method of analysis to determine the dynamic response of structures subjected to base accelerations is presented. The method is exact as opposed to the approximate technique of using unusually large masses and loads to enforce desired base accelerations. This paper presents the relevant equations of motion, ALTERs for direct and modal frequency-, random- and transient-response rigid formats, and illustrative examples.

INTRODUCTION

Dynamic environments of industrial structures and structural components are frequently specified in terms of base accelerations. The dynamics analysis capabilities of NASTRAN, however, provide for the specification of loads rather than accelerations. An approximate technique is therefore, generally practiced wherein the structural degrees of freedom with known (base) accelerations are assigned very large masses (or mass moments of inertias, of the order of 10^6 to 10^{12} times the total structural mass) and subjected to correspondingly large loads to enforce the desired base accelerations (ref. 1). This method can, in some instances, lead to erroneous results as shown by the frequency response function in Figure 1. The function represents $\sigma_{xx,1}$ in element 2 when the cantilevered plate, shown in Figure 2, is subjected to a unit base acceleration $\ddot{z}$ (f) = 1. A concentrated mass of 10^8 units was used in the z (translation) degree of freedom at grid point 1. The solution was obtained using the direct frequency and random-response rigid format DISP RF 8. A viscous damping matrix proportional to the structural stiffness matrix, BDD = 2.0 E-6 KDD, was used enabling a direct comparison of the results with those from the alternative method.

The method discussed in the following sections avoids the use of fictitious large masses thereby eliminating any associated conditioning problems. For a modal formulation of the problem, the modal basis currently available in NASTRAN rigid formats is used. These modes are the base-relaxed modes including rigid body modes, and constitute a plausible basis for base excited dynamic response calculations. The prevailing boundary conditions are satisfied by all modes. The user directly specifies base accelerations on existing NASTRAN bulk data cards.

NOMENCLATURE

Note: A consistent set of FLT units has been used throughout this paper.

	Damping matrix, $FL^{-1}T$
	Viscous damping, $FL^{-1}T$
f	Frequency, T^{-1}
g	Modal damping coefficient
i	$\sqrt{-1}$
K	Stiffness matrix FL^{-1}
k	Stiffness, FL^{-1}
M	Mass matrix, $FL^{-1}T^2$
m	Mass, $FL^{-1}T^2$
P	Load vector, F
p	Derivative operator $\frac{d}{dt}$, T^{-1}
t	Time, T
u	Displacement vector, L
$\ddot{y},\ddot{z}$	Translational accelerations, LT^{-2}
ω	Circular frequency = $2\pi f$, T^{-1}
ω_n^i	Circular frequency of ith natural mode, T^{-1}
ϕ	Modal matrix
$\sigma_{xx,1}$	Normal stress component in basic × direction, z- fiber, FL^{-2}

Subscripts:

a, d, h, ℓ, p, r	NASTRAN displacement sets

$D \equiv d\text{-}r$ set

METHOD OF ANALYSIS

Direct Formulation

After the application of constraints and partitioning to both structural and direct input matrices, the equation of forced motion is

$$\left[[M_{dd}]p^2 + [B_{dd}]p + [K_{dd}]\right]\{u_d\} = \{P_d\ (t \text{ or } \omega)\}\ . \tag{1}$$

The displacement vector u_d is partitioned as

$$\{u_d\} = \left\{\begin{array}{c} u_D \\ \hline u_r \end{array}\right\}\ , \tag{2}$$

with u_r representing the base accelerated degrees of freedom. Equation (1) can now be rearranged into the following two equations:

$$\left[\left[\begin{array}{c|c} M_{DD} & 0 \\ \hline 0 & M_{rr} \end{array}\right] p^2 + \left[\begin{array}{c|c} B_{DD} & B_{Dr} \\ \hline 0 & 0 \end{array}\right] p + \left[\begin{array}{c|c} K_{DD} & K_{Dr} \\ \hline 0 & 0 \end{array}\right]\right]\left\{\begin{array}{c} u_D \\ \hline u_r \end{array}\right\}$$

$$= \left\{\begin{array}{c} P_D - [M_{Dr}]p^2\ \{u_r\} \\ \hline [M_{rr}]p^2\ \{u_r\} \end{array}\right\}\ , \text{ and} \tag{3}$$

$$\left[[M_{rD} \mid M_{rr}]p^2 + [B_{rD} \mid B_{rr}]p + [K_{rD} \mid K_{rr}]\right]\left\{\begin{array}{c} u_D \\ \hline u_r \end{array}\right\} = \{P_r\}\ . \tag{4}$$

Given the base accelerations p^2u_r, equation (3) is solved for u_d, pu_d and p^2u_d. Equation (4), in turn, can be solved for P_r— the loads required on the base degrees of freedom to cause the desired base accelerations.

Modal Formulation

The displacement vector u_d is written as

$$\{u_d\} = \left\{\begin{array}{c} u_D \\ \hline u_r \end{array}\right\} = \left[\begin{array}{c} \phi_{Dh} \\ \hline \phi_{rh} \end{array}\right]\{u_h\} = [\phi_{dh}]\{u_h\}\ , \tag{5}$$

where the modal matrix ϕ_{dh} has been appropriately expanded to include any extra points (ref. 2). Substituting equation (5) in equation (3), and premultiplying both sides by ϕ_{dh}^T, the resulting equation of motion is

$$\left[[M_{hh}]p^2 + [B_{hh}]p + [K_{hh}]\right]\{u_h\} = \{P_h\}\ , \tag{6}$$

where

$$\left.\begin{array}{l} [M_{hh}] = [\phi_{dh}]^T \left[\begin{array}{c|c} M_{DD} & 0 \\ \hline 0 & M_{rr} \end{array}\right][\phi_{dh}]\ , \\ \\ [B_{hh}] = [B^1_{hh}] + [\phi_{dh}]^T \left[\begin{array}{c|c} B_{DD} & B_{Dr} \\ \hline 0 & 0 \end{array}\right][\phi_{dh}]\ , \\ \\ [K_{hh}] = [\phi_{dh}]^T \left[\begin{array}{c|c} K_{DD} & K_{Dr} \\ \hline 0 & 0 \end{array}\right][\phi_{dh}]\ , \text{ and} \end{array}\right\} \tag{7}$$

(continued)

(continued)

$$\{P_h\} = [\phi_{dh}]^T \left\{ \begin{array}{c} P_D - [M_{Dr}]p^2\{u_r\} \\ \hline [M_{rr}]p^2\{u_r\} \end{array} \right\} \quad . \qquad (7)$$

Consistent with the existing capabilities of NASTRAN rigid formats for modal frequency- and random-, and transient-response analyses (DISP RFs 11 and 12), the modal damping matrix B_{hh} consists of contributions due to,

1. the damping matrix B^1_{hh} proportional to the mass matrix as

$$[B^1_{hh}] = [\, \omega^h_n \, g(\omega^h_n) \,] \, [\phi_{dh}]^T \left[\begin{array}{c|c} M_{DD} & M_{Dr} \\ \hline 0 & 0 \end{array} \right] [\phi_{dh}] \quad , \qquad (8)$$

with the elements of the diagonal matrix corresponding to all extra points set to zero, and

2. the direct input matrix.

Given the base accelerations p^2u_r, equation (6) is solved for u_h, pu_h and p^2u_h. Equation (5) is used to recover the displacement vector u_d and its rates pu_d and p^2u_d. Equation (4) can be used to recover the loads P_r. The damping terms B_{rD} and B_{rr} are partitions of the directly specified damping matrix B2PP.

IMPLEMENTATION IN NASTRAN

The method of analysis discussed in the previous section has been implemented in NASTRAN April 1982 release in the form of DMAP ALTERs. The ALTER packages for the displacement approach rigid formats 8, 9, 11 and 12 are given in the Appendix. Existing NASTRAN utility modules have been used to partition and merge various matrices for the rearranged equation of motion. The functional module FRRD2 for the frequency response rigid formats has been modified to solve coupled equations of motion. These modifications are also included in the Appendix.

In using these ALTER packages, the following points are to be considered.

1. The base accelerated degrees of freedom are specified on the SUPORT bulk data card.

2. The base accelerations are specified on RLOADi or TLOADi bulk data cards akin to specifying loads.

3. The base accelerated degrees of freedom must have non-zero mass (or mass moment of inertia). No fictitious large masses are required.

4. In rigid formats 8 and 11, external loads can be applied to all (p-r) set degrees of freedom.

5. In rigid formats 9 and 12, external loads can be applied to all (d-r) set degrees of freedom.

6. An OLOAD request for the base accelerated (r set) degrees of freedom in RFs 8 and 11 results in the loads on these degrees of freedom necessary to cause the

specified base accelerations. Such a request in RFs 9 and 12 will output the specified base accelerations. This is due to the non-availability of pu_d and p^2u_d in distinct data blocks.

7. If OLOADs are requested for the base accelerated degrees of freedom in RF8 and 11, a real diagonal matrix named FREQ must be input on DMI bulk data cards with entries sorted in an ascending order from the FREQ or FREQi bulk data card. The order of the FREQ matrix must be equal to the entries on the FREQ or FREQi bulk data card.

8. Mode acceleration method of data recovery is available both in RF11 and RF12.

9. The data recovery procedures in all the four rigid formats remain unchanged, with the exception of stress recovery. The stresses are computed using displacements (or modal displacements) relative to the base. This is due to the fact that in problems with specified base accelerations, the absolute displacements can become extremely large. The subsequent stress calculations, as a result, are based on small differences of large numbers, and can be in error as shown by the stress response at very low frequencies in Figure 1. It is to be noted that any limitations imposed by these ALTER packages are as a direct result of utilizing existing functional and utility modules, with the necessary exception of FRRD2. These limitations can easily be overcome by creating new (dummy) modules.

ILLUSTRATIVE EXAMPLES

Two problems (Figures 2 and 3) are considered to illustrate the alternative method of determining base accelerated dynamic response. The problem in Figure 3 is used to illustrate the accuracy of all the four ALTER packages. The problem in Figure 2 is used to compare response calculations with those shown in Figure 1.

Figure 3 shows a 2-degree of freedom system subjected to a known base acceleration at mass m_1. The problem is to determine the acceleration response of mass m_2. The following steps are followed in obtaining and cross-checking the solution by various ways:

1. RF8 with ALTERs is used to determine $\ddot{y}_2(f)$ and $P_1(f)$, given $\ddot{y}_1(f)$.

2. RF8 without ALTERs is used to determine $\ddot{y}_1(f)$ and $\ddot{y}_2(f)$, given $P_1(f)$.

3. Steps 1 and 2 are repeated with RF11.

4. RF9 with ALTERs is used to determine $\ddot{y}_2(t)$, given $\ddot{y}_1(t)$.

5. Step 4 is repeated with RF12.

Figures 4 and 5 show the results of steps 1 through 3 which compare well with the theoretical results given by

$$\ddot{y}_2(\omega) = \left[\frac{k + i\omega c}{k + i\omega c - \omega^2 m_2}\right] \ddot{y}_1(\omega) \quad ,\text{and} \quad P_1(\omega) = m_1\ddot{y}_1(\omega) + m_2\ddot{y}_2(\omega) \ . \qquad (9)$$

ORIGINAL PAGE IS OF POOR QUALITY

Figure 6 presents the comparison of results of steps 4 and 5 with theory. The [illegible]

$$\left.\begin{aligned}
&\ddot{y}_2(t) = 1 - \frac{e^{-\zeta\omega_n t}}{\sqrt{1-\zeta^2}} \cos\left(\sqrt{1-\zeta^2}\,\omega_n t + \gamma_o'\right) , \\
\text{where} \quad &\zeta = c \,/\, (2\sqrt{km_2}) , \\
&\omega_n = \sqrt{k/m_2} \quad , \text{ and} \\
&\gamma_o' = \tan^{-1}\left(\frac{\zeta}{\sqrt{1-\zeta^2}}\right) , \\
\text{for} \quad &\ddot{y}_1(t) = 0 \; , \; t < 0 \\
&\phantom{\ddot{y}_1(t)} = 1 \; , \; t > 0 \; .
\end{aligned}\right\} \qquad (10)$$

Figure 7 presents the frequency response function of Figure 1, using RF8 with base acceleration ALTERs. For comparison, a damping matrix proportional to the structural stiffness matrix was used in both solutions (BDD = 2.0 E-6 KDD). The response does not rely on the selection of any fictitious large masses. The error in the stress response at low frequencies is also eliminated.

CONCLUDING REMARKS

1. An alternative method of determining base accelerated dynamic response in NASTRAN has been presented and demonstrated, avoiding the use of fictitious large masses.

2. Although this paper discusses the problem and its solution in terms of absolute degrees of freedom, a number of variations can be simply achieved to suit particular problems. As an example, the introduction of the degrees of freedom relative to the base degrees of freedom, at least in the absence of extra points, can be easily accomplished by the transformation

$$\left.\begin{aligned}
&\{u_d\} \equiv \{u_a\} = \left\{\begin{matrix} u_\ell \\ \hline u_r \end{matrix}\right\} = \left[\begin{array}{c|c} I & D \\ \hline 0 & I \end{array}\right] \left\{\begin{matrix} u_{\ell,\text{rel.}} \\ \hline u_r \end{matrix}\right\} \quad , \quad \text{(set e null)} \\
\text{with} \quad &[D] = -[K_{\ell\ell}]^{-1}\,[K_{\ell r}] \; .
\end{aligned}\right\} \qquad (11)$$

This is useful in addressing shock spectrum response problems, and can lead to symmetric coefficient matrices and uncoupled (modal) equations of motion.

4. The method can form the basis for considering displacement and velocity base excitation problems in NASTRAN.

REFERENCES

1. MSC/NASTRAN Application Manual, Vol. I, January 1981.

2. NASTRAN Theoretical Manual, NASA SP-221(05), December 1978.

3. Myklestad, N. O., Fundamentals of Vibration Analysis, McGraw-Hill Book Company, Inc., 1956.

ORIGINAL PAGE IS
OF POOR QUALITY

APPENDIX

```
$$
$$ ALTERS TO SOL 8 (NASTRAN APRIL 1982) FOR BASE ACCELERATION.
$$
ALTER 87 $
RBMG1     USET,KAA, / KLL,KLR,KRR,,, $
RBMG2     KLL / LLL $
RBMG3     LLL,KLR,KRR / DM $
ALTER 121,122 $
FRLG      CASEXX,USETD,DLT,FRL,GMD,GOD,DIT,/PPF,PSF,PDF,FOL,PHF/
          *DIRECT*/FREQY/*FREQ* $
EQUIV     PPF,PDF/NOSET $
VEC       USETD/VP/*P*/*COMP*/*R* $
VEC       USETD/VD/*D*/*COMP*/*R* $
PARTN     PPF,,VP/PPF1,PPF2,,/1 $
PARTN     PDF,,VD/PDF1,PDF2,,/1 $
PARTN     MDD,VD,/MDD11,MDD21,MDD12,MDD22 $
PARTN     BDD,VD,/BDD11,BDD21,BDD12,BDD22 $
PARTN     KDD,VD,/KDD11,KDD21,KDD12,KDD22 $
MERGE     MDD11,,,MDD22,VD,/ MDD1 /-1/0/1 $
MERGE     BDD11,,BDD12,,VD,/ BDD1 /-1/0/1 $
MERGE     KDD11,,KDD12,,VD,/ KDD1 /-1/0/1 $
MPYAD     MDD12,PPF2,PDF1/ PDFF1 /0/-1 $
MPYAD     MDD22,PPF2,     / PDFF2 /0 $
MERGE     PDFF1,PDFF2,,,,VD/ PDFF /1/0/2 $
FRRD2     KDD1,BDD1,MDD1,,PDFF,FOL/UDVF/0.0/0.0/-1.0 $
ADD       FREQ,/OMEGAI/(0.0,6.283185) $
ADD       FREQ,/OMEGA1/(6.283185,0.0) $
DIAGONAL OMEGA1/OMEGA2/*SQUARE*/2.0 $
MERGE     MDD21,,MDD22,,VD, / MDD2 /1/0/2 $
MERGE     BDD21,,BDD22,,VD, / BDD2 /1/0/2 $
MERGE     KDD21,,KDD22,,VD, / KDD2 /1/0/2 $
SMPYAD    MDD2,UDVF,OMEGA2,,, / TEMP1 / 3/-1 $
SMPYAD    BDD2,UDVF,OMEGAI,,, / TEMP2 / 3 $
ADD       TEMP1,TEMP2 / TEMP3 $
MPYAD     KDD2,UDVF,TEMP3 / PPF2/ 0 $
MERGE     PPF1,PPF2,,,,VP / PPF / 1/0/2 $
EQUIV     PPF,PNEF/MPCF1 $
COND      LBL18A,MPCF1 $
VEC       USETD/VECNEM/*P*/*NE*/*M* $
PARTN     PPF,,VECNEM/PBNEF,PMF,, / 1 $
MPYAD     GMD,PMF,PBNEF/ PNEF / 1 $
LABEL     LBL18A $
EQUIV     PNEF,PFEF/SINGLE $
COND      LBL18B,SINGLE $
VEC       USETD/VECFES/*NE*/*FE*/*S* $
```

```
PARTN    PNEF,,VECFES/PFEF,PSF,, / 1 $
LABEL    LBL18B $
EQUIV    PFEF,PDF/OMIT $
COND     LBL18C,OMIT $
VEC      USETD/VECDO/*FE*/*D*/*O* $
PARTN    PFEF,,VECDO/PBDF,POF,, / 1 $
MPYAD    GOD,POF,PBDF/ PDF/ 1 $
LABEL    LBL18C $
ALTER 123,123 $ USE FOL INSTEAD OF PPF
VDR      CASEXX,EQDYN,USETD,UDVF,FOL,XYCDB,/OUDVC1,/*FREQRESP*/
         *DIRECT*/S,N,NOSORT2/S,N,NOD/S,N,NOP/0 $
ALTER 139,139 $ USE FOL INSTEAD OF PPF
SDR2     CASEXX,CSTM,MPT,DIT,EQDYN,SILD,,,BGPDP,FOL,QPC,UPVC,EST,XYCDB,
         PPF/OPPC1,OQPC1,OUPVC1,,OEFC1,PUPVC1/*FREQRESP*/
         S,N,NOSORT2 $
VEC      USETD / VD2 / *D*/*A*/*E* $
VEC      USETD / VA2 / *A*/*L*/*R* $
PARTN    UDVF,,VD2 / UAVF,UEVF,, / 1 $
PARTN    UAVF,,VA2 / ULVF,URVF,, / 1 $
MPYAD    DM,URVF,ULVF / ULVFP / 0 / -1 $
UMERGE   USETD,ULVFP, / UAVFP / *A*/*L*/*R* $
UMERGE   USETD,UAVFP,UEVF / UDVFP / *D*/*A*/*E* $
EQUIV    UDVFP,UPVCP/NOA $
COND     LBL19A,NOA $
SDR1     USETD,,UDVFP,,,GOD,GMD,,,, / UPVCP,, / 1/*DYNAMICS* $
LABEL    LBL19A $
SDR2     CASEXX,CSTM,MPT,DIT,EQDYN,SILD,,,BGPDP,FOL,,UPVCP,EST,
         XYCDB,/,,,OESC1,, /*FREQRESP*/S,N,NOSORT2 $
ENDALTER
```

ORIGINAL PAGE IS
OF POOR QUALITY

```
$$
$$ ALTERS TO SOL 9 (NASTRAN APRIL 1982) FOR BASE ACCELERATION.
$$
ALTER 87 $
RBMG1    USET,KAA, / KLL,KLR,KRR,,, $
RBMG2    KLL / LLL $
RBMG3    LLL,KLR,KRR / DM $
ALTER 125,125 $
VEC      USETD/VD/*D*/*COMP*/*R* $
PARTN    PD,,VD/PD1,PD2,,/1 $
PARTN    MDD,VD,/MDD11,MDD21,MDD12,MDD22 $
PARTN    BDD,VD,/BDD11,BDD21,BDD12,BDD22 $
PARTN    KDD,VD,/KDD11,KDD21,KDD12,KDD22 $
MERGE    MDD11,,,MDD22,VD,/ MDD1 /-1/0/1 $
MERGE    BDD11,,BDD12,,VD,/ BDD1 /-1/0/1 $
MERGE    KDD11,,KDD12,,VD,/ KDD1 /-1/0/1 $
MPYAD    MDD12,PD2,PD1/ PDD1 /0/-1 $
MPYAD    MDD22,PD2,   / PDD2 /0 $
MERGE    PDD1,PDD2,,,,VD/ PDD /1/0/2 $
TRD      CASEXX,TRL,NLFT,DIT,KDD1,BDD1,MDD1,PDD/
         UDVT,PNLD / *DIRECT*/NOUE/1/S,N,NCOL/C,Y,ISTART $
ALTER 139,139 $
SDR2     CASEXX,CSTM,MPT,DIT,EQDYN,SILD,,,BGPDP,TOL,QP,UPV,EST,
         XYCDB,PPT/OPP1,OQP1,OUPV1,,OEF1,PUGV/*TRANRESP* $
VEC      USETD / VD2 / *D*/*A*/*E* $
VEC      USETD / VA2 / *A*/*L*/*R* $
PARTN    UDVT,,VD2 / UAVT,UEVT,, / 1 $
PARTN    UAVT,,VA2 / ULVT,URVT,, / 1 $
MPYAD    DM,URVT,ULVT / ULVTP / 0 / -1 $
UMERGE   USETD,ULVTP, / UAVTP / *A*/*L*/*R* $
UMERGE   USETD,UAVTP,UEVT / UDVTP / *D*/*A*/*E* $
EQUIV    UDVTP,UPVTP/NOA $
COND     LBL19A,NOA $
SDR1     USETD,,UDVTP,,,GOD,GMD,,,, / UPVTP,, / 1/*DYNAMICS* $
LABEL    LBL19A $
SDR2     CASEXX,CSTM,MPT,DIT,EQDYN,SILD,,,BGPDP,TOL,,UPVTP,EST,
         XYCDB,/,,,OES1,, /*TRANRESP* $
ENDALTER
```

ORIGINAL PAGE IS
OF POOR QUALITY

```
$$
$$ ALTERS TO SOL 11 (NASTRAN APRIL 1982) FOR BASE ACCELERATION.
$$
ALTER 93 $
PARAM    //*ADD*/KDEK2/NOGENL/NOSIMP $
ALTER 95,96 $
PARAM    //*ADD*/NOBGG/-1/0 $
PARAM    //*ADD*/NOK4GG/-1/0 $
GKAD     USETD,GM,GO,KAA,,MAA,,K2PP,M2PP,B2PP/
         KDD,BDD,MDD,GMD,GOD,K2DD,M2DD,B2DD/*FREQRESP*/*DISP*/
         *DIRECT*/0.0/0.0/0.0/NOK2PP/NOM2PP/NOB2PP/MPCF1/SINGLE/
         OMIT/NOUE/NOK4GG/NOBGG/KDEK2/V,Y,MODACC=-1 $
EQUIV    B2DD,BDD/NOBGG/M2DD,MDD/NOSIMP/K2DD,KDD/KDEK2 $
FRLG     CASEXX,USETD,DLT,FRL,GMD,GOD,DIT,/PPF,PSF,PDF,FOL,PHF/
         *DIRECT*/FREQY/*FREQ* $
EQUIV    PPF,PDF/NOSET $
VEC      USETD/VP/*P*/*COMP*/*R* $
VEC      USETD/VD/*D*/*COMP*/*R* $
PARTN    PPF,,VP/PPF1,PPF2,,/1 $
PARTN    PDF,,VD/PDF1,PDF2,,/1 $
PARTN    MDD,VD,/MDD11,MDD21,MDD12,MDD22 $
PARTN    BDD,VD,/BDD11,BDD21,BDD12,BDD22 $
PARTN    KDD,VD,/KDD11,KDD21,KDD12,KDD22 $
MERGE    MDD11,,,MDD22,VD,/ MDD1 /-1/0/1 $
MERGE    BDD11,,BDD12,,VD,/ BDD1 /-1/0/1 $
MERGE    KDD11,,KDD12,,VD,/ KDD1 /-1/0/1 $
MPYAD    MDD12,PPF2,PDF1/ PDFF1 /0/-1 $
MPYAD    MDD22,PPF2,    / PDFF2 /0 $
MERGE    PDFF1,PDFF2,,,,VD/ PDFF /1/0/2 $
GKAM     USETD,PHIA,MI,LAMA,DIT,,,,CASEXX/
         MXHH,BXHH,KXHH,PHIDH/NOUE/C,Y,LMODES=0/
         C,Y,LFREQ=0.0/C,Y,HFREQ=-1.0/-1/-1/-1/
         S,N,NONCUP/S,N,FMODE $
MPYAD    PHIDH,PDFF,/PHF/1/1/0/0 $
SMPYAD   PHIDH,MDD1,PHIDH,,,/MHH/3/1/1/0/1 $
SMPYAD   PHIDH,KDD1,PHIDH,,,/KHH/3/1/1/0/1 $
PURGE    B2HH/NOB2PP $
COND     LBL13A,NOB2PP $
SMPYAD   PHIDH,BDD1,PHIDH,,,/B2HH/3/1/1/0/1 $
LABEL    LBL13A $
EQUIV    MAA,M1DD/NOUE $
COND     LBL13B,NOUE $
VEC      USETD/VD1/*D*/*A*/*E* $
MERGE    MAA,,,,VD1,/ M1DD /-1/0/1 $
LABEL    LBL13B $
PARTN    M1DD,VD,/M1DD11,,M1DD12, $
MERGE    M1DD11,,M1DD12,,VD,/ M1DD2 /-1/0/1 $
SMPYAD   PHIDH,M1DD2,PHIDH,,,/M1HH2/3/1/1/0/1 $
DIAGONAL MXHH/MINV/*SQUARE*/-1.0 $
```

```
SMPYAD   MINV,BXHH,M1HH2,,, / TEMP1 / 3 $
ADD      TEMP1,B2HH / BHH $
PARAM    //*ADD*/NONCUP/1/0 $
ALTER    99,100 $
FRRD2    KHH,BHH,MHH,,PHF,FOL/UHVF/0.0/0.0/-1.0 $
DDR1     UHVF,PHIDH/UDVF $
ADD      FREQ,/OMEGAI/(0.0,6.283185) $
ADD      FREQ,/OMEGA1/(6.283185,0.0) $
DIAGONAL OMEGA1/OMEGA2/*SQUARE*/2.0 $
MERGE    MDD21,,MDD22,,VD, / MDD2 /1/0/2 $
MERGE    BDD21,,BDD22,,VD, / BDD2 /1/0/2 $
MERGE    KDD21,,KDD22,,VD, / KDD2 /1/0/2 $
SMPYAD   MDD2,UDVF,OMEGA2,,, / TEMP2 / 3/-1 $
SMPYAD   BDD2,UDVF,OMEGAI,,, / TEMP3 / 3 $
ADD      TEMP2,TEMP3 / TEMP4 $
MPYAD    KDD2,UDVF,TEMP4 / PPF2 / 0 $
MERGE    PPF1,PPF2,,,,VP / PPF / 1/0/2 $
EQUIV    PPF,PNEF/MPCF1 $
COND     LBL15A,MPCF1 $
VEC      USETD/VECNEM/*P*/*NE*/*M* $
PARTN    PPF,,VECNEM/PBNEF,PMF,, / 1 $
MPYAD    GMD,PMF,PBNEF/ PNEF / 1 $
LABEL    LBL15A $
EQUIV    PNEF,PFEF/SINGLE $
COND     LBL15B,SINGLE $
VEC      USETD/VECFES/*NE*/*FE*/*S* $
PARTN    PNEF,,VECFES/PFEF,PSF,, / 1 $
LABEL    LBL15B $
EQUIV    PFEF,PDF/OMIT $
COND     LBL15C,OMIT $
VEC      USETD/VECDO/*FE*/*D*/*O* $
PARTN    PFEF,,VECDO/PBDF,POF,, / 1 $
MPYAD    GOD,POF,PBDF/ PDF/ 1 $
LABEL    LBL15C $
ALTER 101,101 $ USE FOL INSTEAD OF PPF
VDR      CASEXX,EQDYN,USETD,UHVF,FOL,XYCDB,/OUHVC1,/*FREQRESP*/
         *MODAL*/S,N,NOSORT2/S,N,NOH/S,N,NOP/FMODE $
ALTER 116,116 $ USE FOL INSTEAD OF PPF
DDR2     USETD,UDV1F,PDF,K2DD,B2DD,MDD,FOL,LLL,DM/
         UDV2F,UEVF,PAF/*FREQRESP*/NOUE/REACT/FRQSET $
ALTER 122,122 $ USE FOL INSTEAD OF PPF
SDR2     CASEXX,CSTM,MPT,DIT,EQDYN,SILD,,,BGPDP,FOL,QPC,UPVC,EST,
         XYCDB,PPF/OPPC1,OQPC1,OUPVC1,OESC1,OEFC1,PUGV/*FREQ*/
         S,N,NOSORT2 $
ALTER 128,128 $
SDR2     CASEXX,CSTM,MPT,DIT,EQDYN,SILD,,,,LAMA,QPH,PHIPH,EST,XYCDB,/
         ,IQP1,IPHIP1,,IEF1,/*MMREIG*/S,N,NOSORT2 $
ALTER 129,129 $ USE FOL INSTEAD OF PPF
SDR2     CASEXX,,,,EQDYN,SILD,,,,FOL,,,,XYCDB,PPF/
         OPPCA,,,,,/*FREQ* $
VEC      USETD / VD2 / *D*/*A*/*E* $
VEC      USETD / VA2 / *A*/*L*/*R* $
PARTN    PHIDH,,VD2 / PHAVF,PHEVF,, / 1 $
PARTN    PHAVF,,VA2 / PHLVF,PHRVF,, / 1 $
MPYAD    DM,PHRVF,PHLVF / PHLVFP / 0 / -1 $
UMERGE   USETD,PHLVFP, / PHAVFP / *A*/*L*/*R* $
UMERGE   USETD,PHAVFP,PHEVF / PHDVFP / *D*/*A*/*E* $
SDR1     USETD,,PHDVFP,,,GOD,GMD,,,, / PHIPHP,, / 1/*DYNAMICS* $
SDR2     CASEXX,CSTM,MPT,DIT,EQDYN,SILD,,,,LAMA,,PHIPHP,EST,
         XYCDB,/,,,IES1,, /*MMREIG*/S,N,NOSORT2 $
ALTER 134,134 $ USE FOL INSTEAD OF PPF
DDRMM    CASEXX,UHVF,FOL,IPHIP2,IQP2,IES2,IEF2,XYCDB,EST,MPT,DIT/
         ZUPVC2,ZQPC2,ZESC2,ZEFC2, $
ALTER 138,138 $ USE FOL INSTEAD OF PPF
DDRMM    CASEXX,UHVF,FOL,IPHIP1,IQP1,IES1,IEF1,,EST,MPT,DIT/
         ZUPVC1,ZQPC1,ZESC1,ZEFC1, $
ENDALTER
```

```
$$
$$ ALTERS TO SOL 12 (NASTRAN APRIL 1982) FOR BASE ACCELERATION.
$$
ALTER 88 $
PARAM    //*ADD*/KDEKA/NOUE/NOK2PP $
PARAM    //*ADD*/KDEK2/NOGENL/NOSIMP $
EQUIV    KAA,KDD/KDEKA $
ALTER 90,91 $
PARAM    //*ADD*/NOBGG/-1/0 $
PARAM    //*ADD*/NOK4GG/-1/0 $
GKAD     USETD,GM,GO,KAA,,MAA,,K2PP,M2PP,B2PP/
         KDD,BDD,MDD,GMD,GOD,K2DD,M2DD,B2DD/*TRANRESP*/*DISP*/
         *DIRECT*/C,Y,G=0.0/C,Y,W3=0.0/0.0/NOK2PP/NOM2PP/NOB2PP/
         MPCF1/SINGLE/OMIT/NOUE/NOK4GG/NOBGG/KDEK2/V,Y,MODACC=-1 $
EQUIV    B2DD,BDD/NOGPDT/M2DD,MDD/NOSIMP/K2DD,KDD/KDEK2 $
GKAM     USETD,PHIA,MI,LAMA,DIT,,,,CASECC/
         MXHH,BXHH,KXHH,PHIDH/NOUE/C,Y,LMODES=0/
         C,Y,LFREQ=0.0/C,Y,HFREQ=-1.0/-1/-1/-1/
         S,N,NONCUP/S,N,FMODE $
VEC      USETD/VD/*D*/*COMP*/*R* $
EQUIV    MAA,M1DD/NOUE $
COND     LBL12,NOUE $
VEC      USETD/VD1/*D*/*A*/*E* $
MERGE    MAA,,,,VD1,/ M1DD /-1/0/1 $
LABEL    LBL12 $
PARTN    M1DD,VD,/M1DD11,,M1DD12, $
MERGE    M1DD11,,M1DD12,,VD,/ M1DD2 /-1/0/1 $
SMPYAD   PHIDH,M1DD2,PHIDH,,,/M1HH2/3/1/1/0/1 $
DIAGONAL MXHH/MINV/*SQUARE*/-1.0 $
SMPYAD   MINV,BXHH,M1HH2,,,/B1HH/3 $
ALTER 99,99 $
TRLG     CASEXX,USETD,DLT,SLT,BGPDT,SIL,CSTM,TRL,DIT,GMD,GOD,,EST,
         MGG/PPT,PST,PDT,PD,,TOL / S,N,NOSET/NCOL $
ALTER 101,101 $
PARTN    PD,,VD/PD1,PD2,,/1 $
PARTN    MDD,VD,/MDD11,MDD21,MDD12,MDD22 $
PARTN    BDD,VD,/BDD11,BDD21,BDD12,BDD22 $
PARTN    KDD,VD,/KDD11,KDD21,KDD12,KDD22 $
MERGE    MDD11,,,MDD22,VD,/ MDD1 /-1/0/1 $
MERGE    BDD11,,BDD12,,VD,/ BDD1 /-1/0/1 $
MERGE    KDD11,,KDD12,,VD,/ KDD1 /-1/0/1 $
MPYAD    MDD12,PD2,PD1/ PDD1 /0/-1 $
MPYAD    MDD22,PD2,    / PDD2 /0 $
MERGE    PDD1,PDD2,,,,VD/ PDD /1/0/2 $
MPYAD    PHIDH,PDD,/PH/1/1/0/0 $
SMPYAD   PHIDH,MDD1,PHIDH,,,/MHH/3/1/1/0/1 $
SMPYAD   PHIDH,KDD1,PHIDH,,,/KHH/3/1/1/0/1 $
EQUIV    B1HH,BHH/NOB2PP $
COND     LBL13A,NOB2PP $
SMPYAD   PHIDH,BDD1,PHIDH,,,B1HH/BHH/3/1/1/0/1 $
```

```
LABEL     LBL13A $
PARAM     //*ADD*/NONCUP/1/0 $
TRD       CASEXX,TRL,NLFT,DIT,KHH,BHH,MHH,PH/UHVT,PNLH/
          *MODAL*/NOUE/NONCUP/S,N,NCOL/C,Y,ISTART $
ALTER 128,128 $
SDR2      CASEXX,CSTM,MPT,DIT,EQDYN,SILD,,,,LAMA,QPH,PHIPH,EST,
          XYCDB,/,IQP1,IPHIP1,,IEF1,/*MMREIG* $
ALTER 129 $
VEC       USETD / VD2 / *D*/*A*/*E* $
VEC       USETD / VA2 / *A*/*L*/*R* $
PARTN     PHIDH,,VD2 / PHAVT,PHEVT,, / 1 $
PARTN     PHAVT,,VA2 / PHLVT,PHRVT,, / 1 $
MPYAD     DM,PHRVT,PHLVT / PHLVTP / 0 / -1 $
UMERGE    USETD,PHLVTP, / PHAVTP / *A*/*L*/*R* $
UMERGE    USETD,PHAVTP,PHEVT / PHDVTP / *D*/*A*/*E* $
SDR1      USETD,,PHDVTP,,,GOD,GMD,,,, / PHIPHP,, / 1/*DYNAMICS* $
SDR2      CASEXX,CSTM,MPT,DIT,EQDYN,SILD,,,,LAMA,,PHIPHP,EST,
          XYCDB,/,,,IES1,, /*MMREIG*/S,N,NOSORT2 $
ENDALTER
```

```
./ CHANGE NAME=FRD2B
./ NUMBER SEQ1=70,NEW1=71,INCR=1,INSERT=YES
C
C     COMMON FRD2BC IS INITIALIZED BY ROUTINE FRRD2.
C
      COMMON /FRD2BC/ IH
./ NUMBER SEQ1=410,NEW1=411,INCR=1,INSERT=YES
C
C     IF IH=0, USE COMPLEX DOUBLE PRECISION ARITHMETIC.
C
      IF (IH .EQ. 0) ITY = 4
./ NUMBER SEQ1=500,NEW1=510,INCR=1,INSERT=YES
      CALL MAKMCB(MC,OUT,IROW,IFO,ITY)
./ DELETE SEQ1=510,SEQ2=510
./ CHANGE NAME=FRD2C
./ NUMBER SEQ1=120,NEW1=121,INCR=1,INSERT=YES
C
C     COMMON FRD2BC IS INITIALIZED BY ROUTINE FRRD2.
C
      COMMON /FRD2BC/ IH
./ NUMBER SEQ1=240,NEW1=241,INCR=1,INSERT=YES
C
C     IF IH=0, USE COMPLEX DOUBLE PRECISION ARITHMETIC.
C
      IF (IH .EQ. 0) IOUT = 4
./ NUMBER SEQ1=370,NEW1=371,INCR=1,INSERT=YES
C
C     IF IH=0, THEN DO NOT USE INCORE CAPABILITIES BECAUSE FOR IH=0
C              COMPLEX DOUBLE PRECISION ARITHMETIC WILL BE REQUESTED
C              AND SUBROUTINE INCORE CALLED BY FRD2C IS WRITTEN ONLY
C              FOR COMPLEX SINGLE PRECISION MATRICES.
C
      IF (IH .EQ. 0) GO TO 102
./ NUMBER SEQ1=1070,NEW1=1071,INCR=1,INSERT=YES
C
C     IF IH=0, USE COMPLEX DOUBLE PRECISION ARITHMETIC.
C
      IF (IH .EQ. 0) IOUT = 4
./ CHANGE NAME=FRRD2
./ NUMBER SEQ1=270,NEW1=271,INCR=1,INSERT=YES
C
C     COMMON FRD2BC WILL BE USED BY ROUTINES FRD2B AND FRD2C.
C
      COMMON /FRD2BC/ IH
./ NUMBER SEQ1=440,NEW1=441,INCR=1,INSERT=YES
C
C     IF QHHL IS PURGED AND MACH NUMBER IS NEGATIVE THEN
C     SOLVE THE COUPLED EQUATION = (-W**2.M + IW.B + K)U = P
C     USING COMPLEX DOUBLE PRECISION ARITHMETIC.
C     VARIABLE IH WILL BE USED TO CONTROL SOLUTION LOGIC IN
```

```
C     ROUTINES FRRD2, FRD2B AND FRD2C.
C
      IF (MCB(1).LE.0 .AND. M.LT.0.0) NONCUP = 1
C
./ NUMBER SEQ1=720,NEW1=721,INCR=1,INSERT=YES
C
C     IF IH=0, THEN DO NOT USE INCORE CAPABILITIES BECAUSE FOR IH=0
C              COMPLEX DOUBLE PRECISION ARITHMETIC WILL BE REQUESTED
C              AND SUBROUTINE INCORE CALLED BY FRD2C IS WRITTEN ONLY
C              FOR COMPLEX SINGLE PRECISION MATRICES.
C
      IF (IH .EQ. 0) GO TO 20
./ NUMBER SEQ1=1210,NEW1=1211,INCR=1,INSERT=YES
C
C     IF IH = 0, THEN CREATE NULL TRAILERS FOR SCR2(QHR) AND SCR3(QHI).
C                THESE DATA BLOCKS ARE NORMALLY GENERATED BY FRD2A IF
C                IH IS NOT EQUAL TO ZERO EACH TIME THRU THE LOOP ON
C                NFREQ IN THIS ROUTINE. SINCE FRD2A IS NOT EXECUTED IF
C                IH EQUALS ZERO THEN AFTER THE FIRST PASS THE TRAILERS
C                FOR SCR2 AND SCR3 WOULD BE INCORRECT SINCE SCR2 AND
C                SCR3 ARE ALSO USED BY FRD2C AS SCRATCH DATA SETS.
C
      IF (IH .NE. 0) GO TO 38
      CALL MAKMCB(MCB,SCR2,0,0,0)
      CALL WRTTRL(MCB)
      MCB(1) = SCR3
      CALL WRTTRL(MCB)
   38 CONTINUE
C
./ NUMBER SEQ1=1480,NEW1=1481,INCR=1,INSERT=YES
C
C     CREATE A PSEUDO FRL DATA BLOCK ON SCR1 FROM DATA BLOCK FOL FOR
C     INPUT TO ROUTINE FRD2F. (NO TRAILER IS NECESSARY).
C     THE FREQUENCIES FROM FOL HAVE BEEN READ INTO IZ(1) DURING THE
C     SET-UP AT THE BEGINING OF THIS ROUTINE. THESE FREQUENCIES MUST
C     BE CONVERTED TO RADIAN FREQUENCIES FOR FRL (W = 2PI*F).
C
      CALL GOPEN(SCR1,IZ(IBUF1),1)
      DO 210 I = 1,NFREQ
      Z(I) = Z(I) * TWOPI
  210 CONTINUE
      CALL WRITE(SCR1,Z,NFREQ,1)
      CALL CLOSE(SCR1,1)
      CALL FRD2F(MHH, BHH, KHH, SCR1, 1, NLOAD, NFREQ, PHF, UHVF)
./ DELETE SEQ1=1490,SEQ2=1490
```

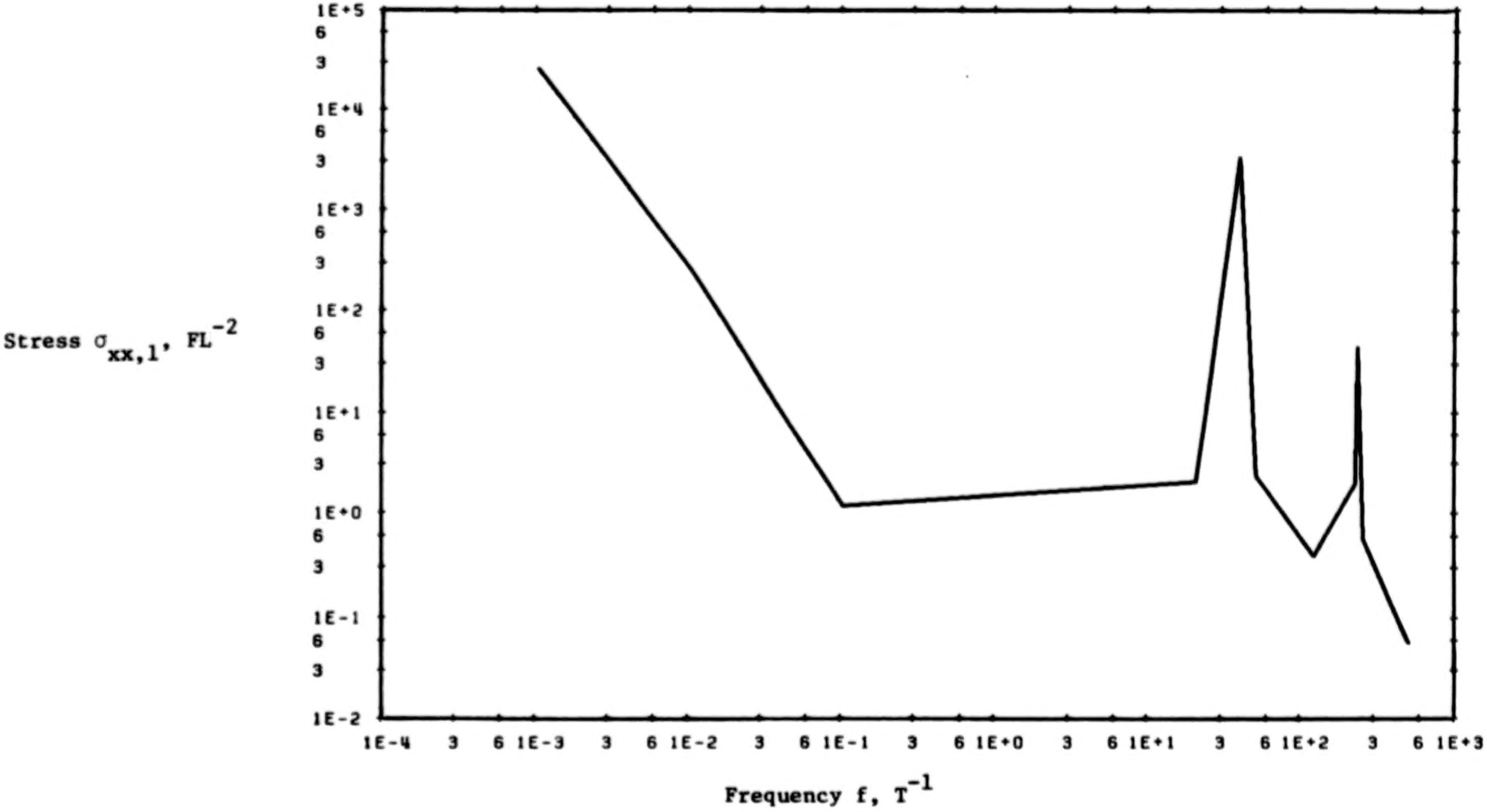

Figure 1. Stress Response $\sigma_{xx,1}$ in Element 2 of Example 1 (Figure 2), RF8 With Large Mass.

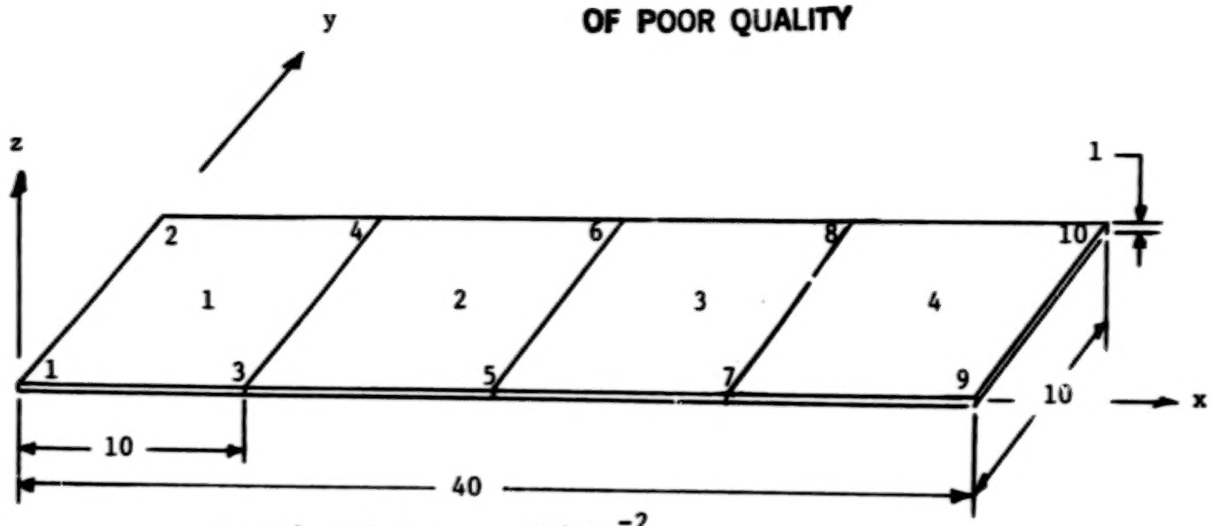
y
z
1
2
4
6
8
10
1
2
3
4
1
3
5
7
9
10
x
10
40

Young's Modulus = 1E8 FL^{-2}

Poisson's Ratio = 0.4

Material Density = 8E-4 $FL^{-4}T^2$

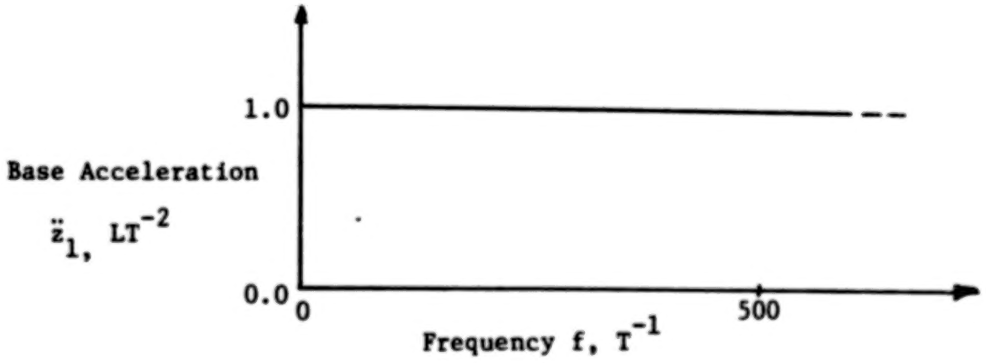

Base Acceleration Input for Figures 1 and 7

Figure 2. Example 1

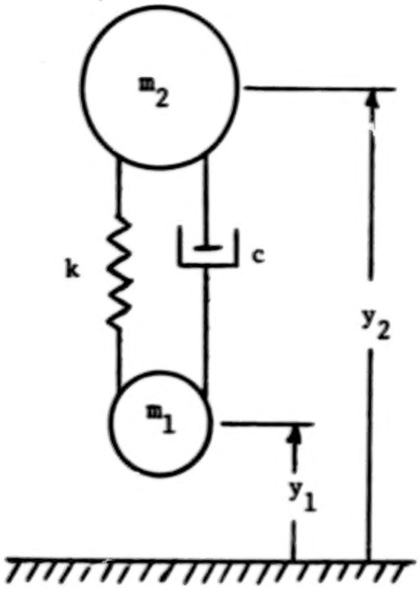

$m_1 = 2 \ FL^{-1}T^2$
$m_2 = 8 \ FL^{-1}T^2$
$k = 4 \ FL^{-1}$
$c = 0.6 \ FL^{-1}T$

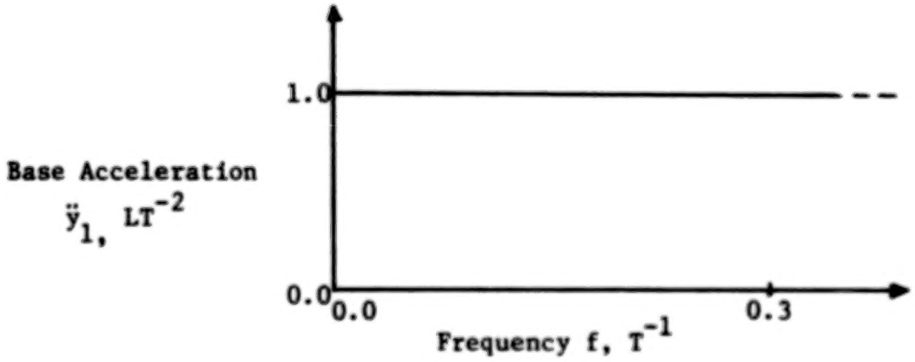

Base Acceleration Input for Figures 4 and 5

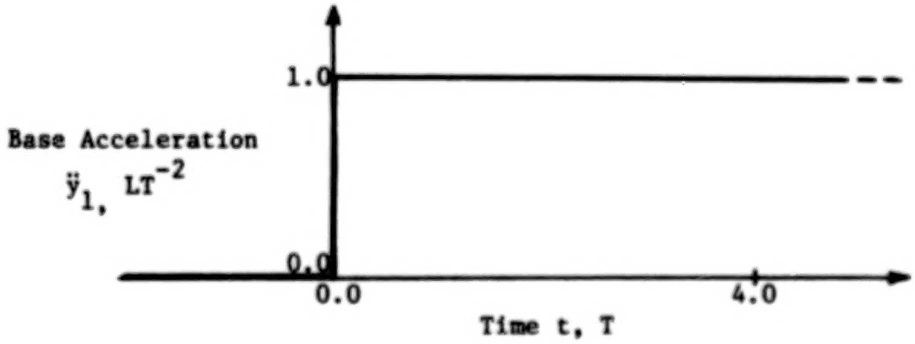

Base Acceleration Input for Figure 6

Figure 3. Example 2

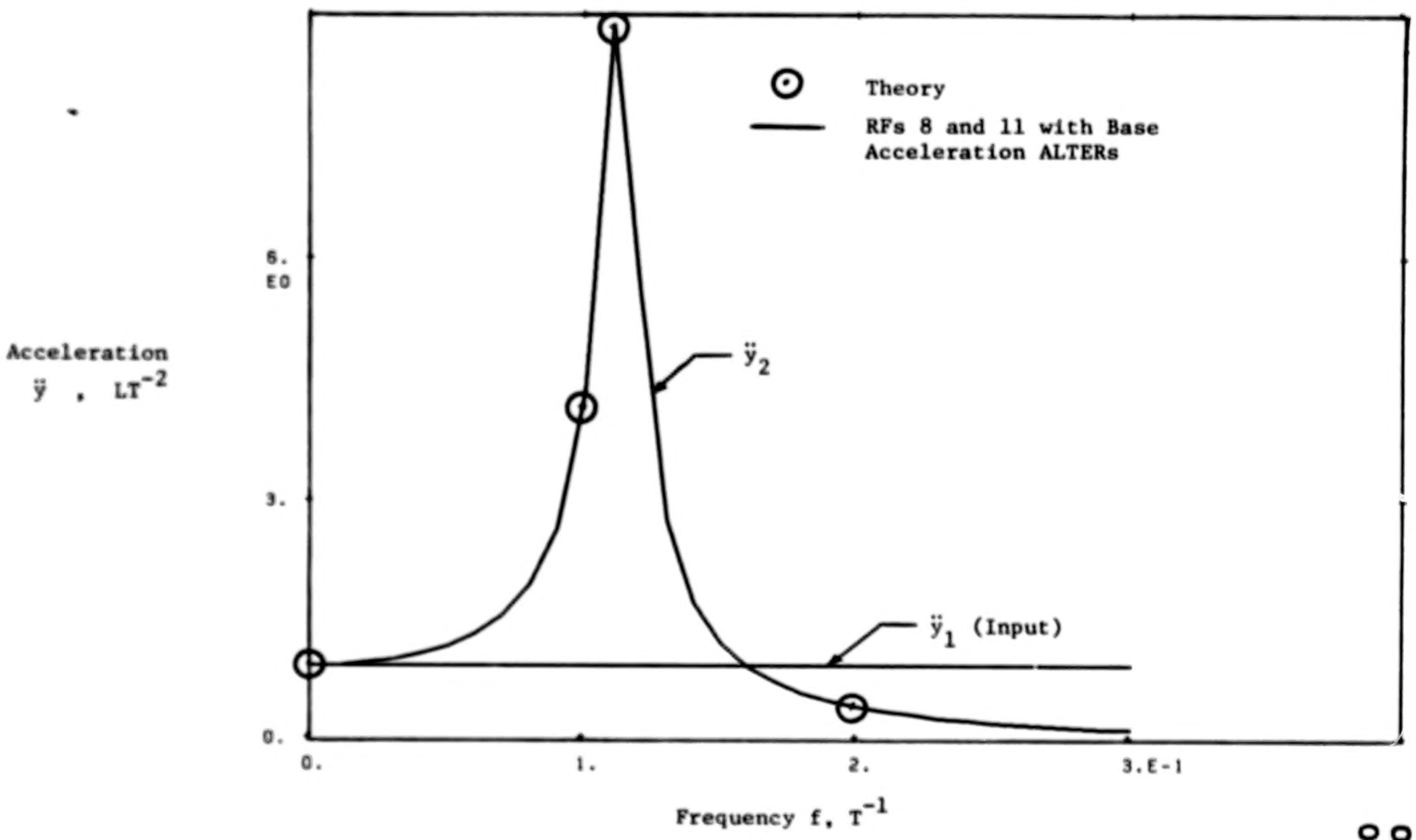

Figure 4. Acceleration Response of Mass m_2 of Example 2 (Figure 3), Frequency Response

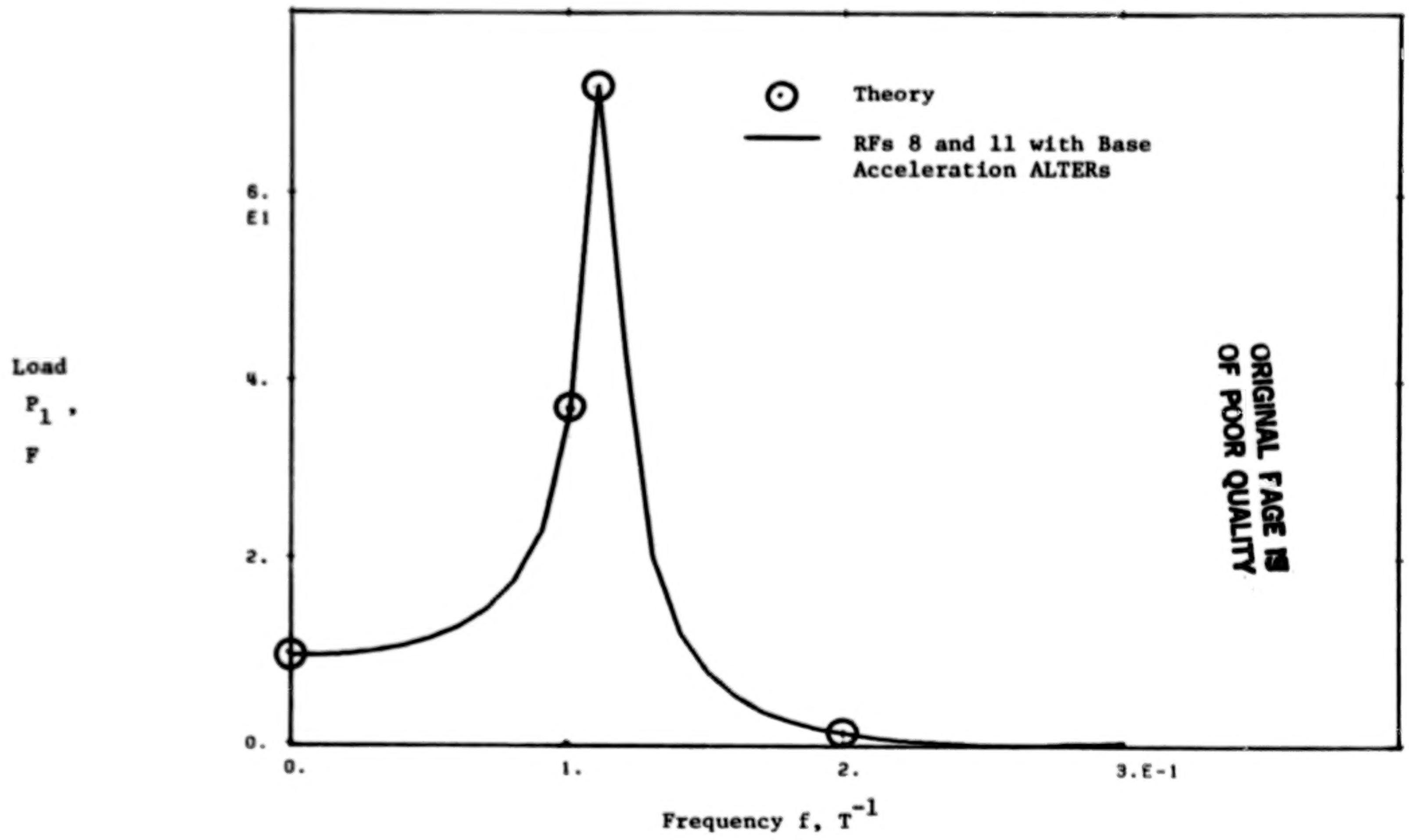

Figure 5. Load Required on Mass m_1 of Example 2 (Figure 3), Frequency Response

ORIGINAL PAGE IS OF POOR QUALITY

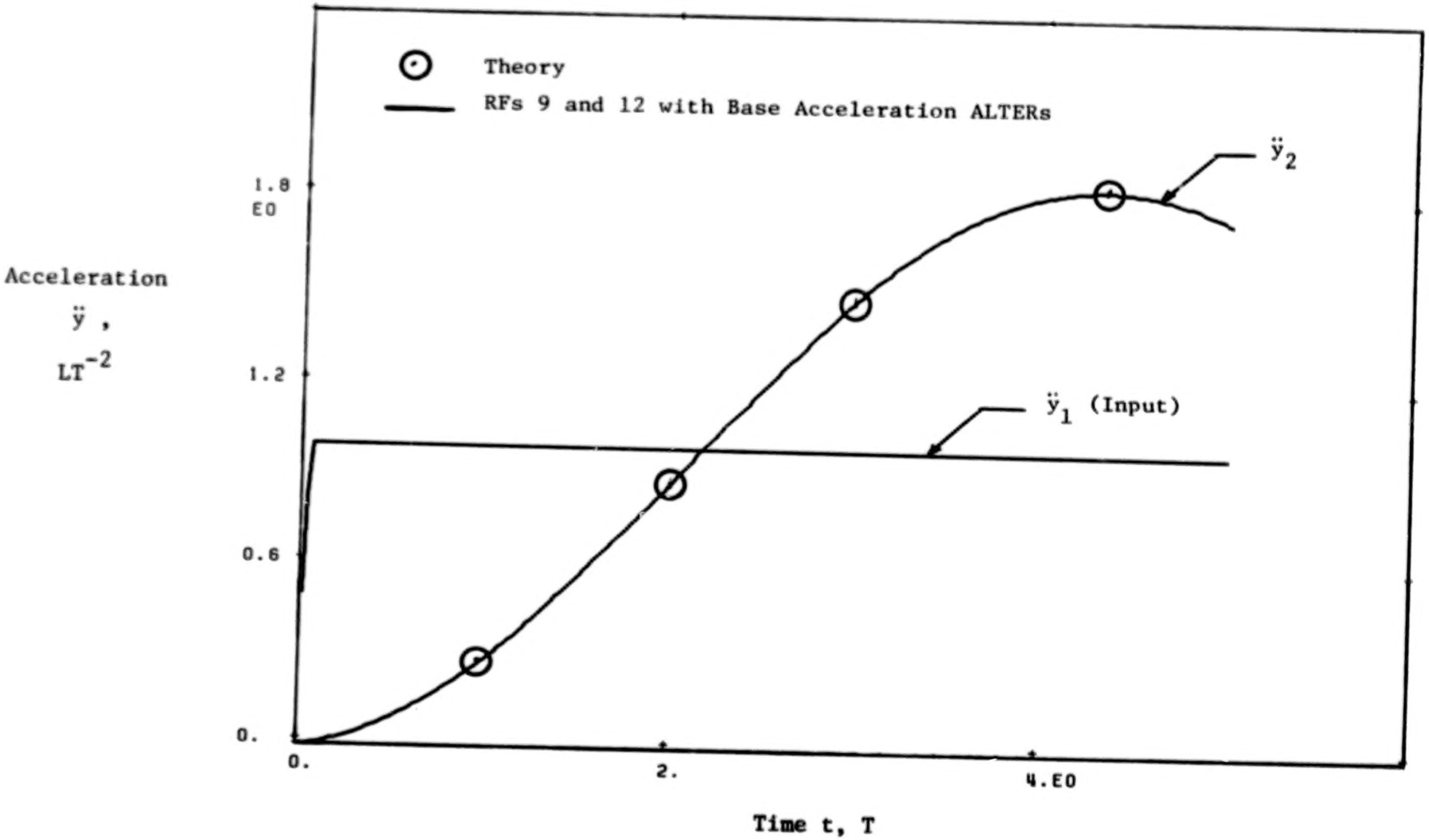

Figure 6. Acceleration Response of Mass m_2 of Example 2 (Figure 3), Transient Response

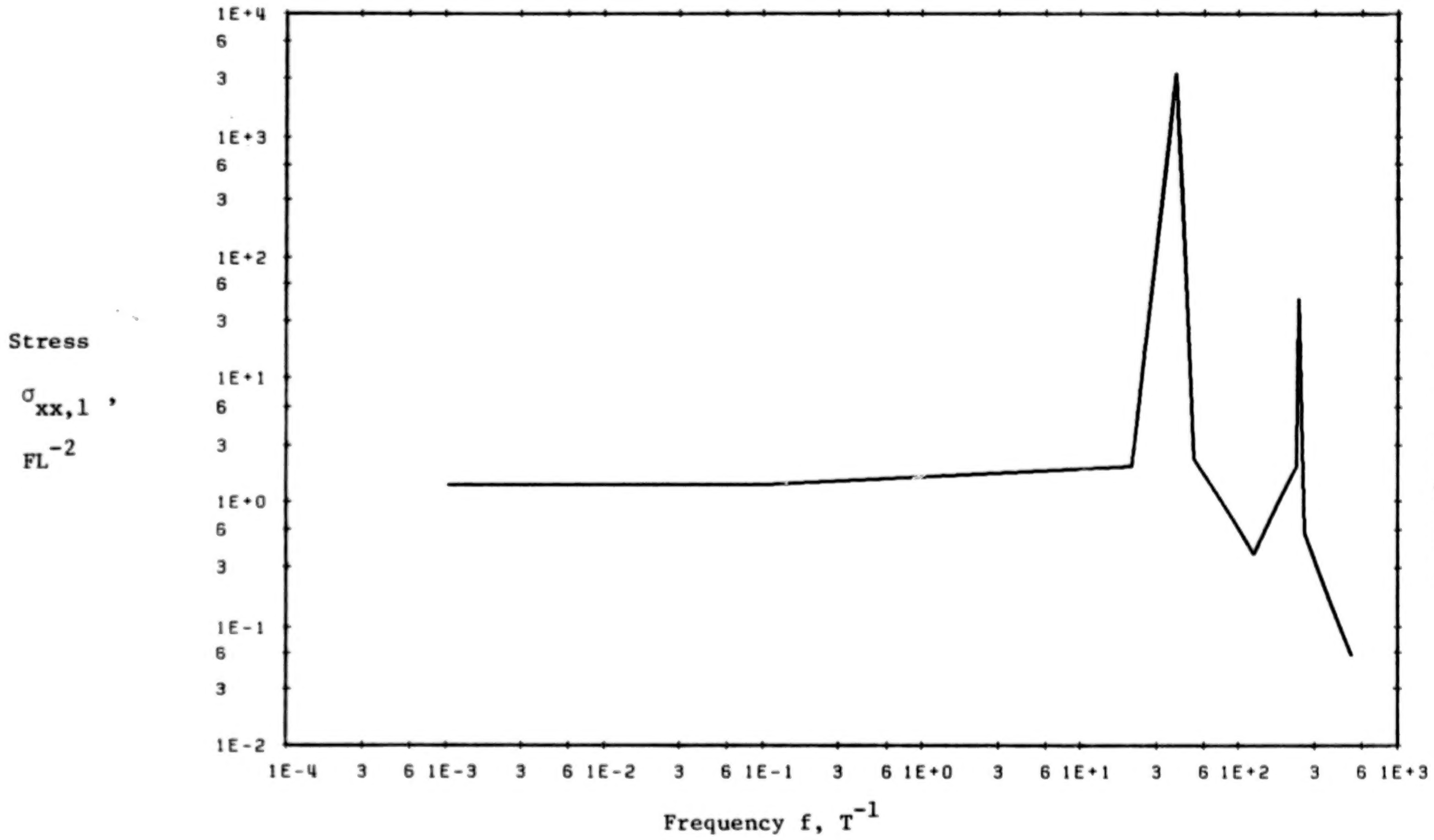

Figure 7. Stress Response $\sigma_{xx,1}$ in Element 2 of Example 1 (Figure 2), RF8 with Base Acceleration ALTERs and no Large Mass.

N84
15599

UNCLAS

N84 15599 D9

A NASTRAN DMAP PROCEDURE FOR CALCULATION OF BASE EXCITATION MODAL PARTICIPATION FACTORS

by

William R. Case
Instrument Systems Branch
Instrument Division
Goddard Space Flight Center
Greenbelt, Maryland

SUMMARY

A common analysis procedure at the Goddard Space Flight Center is to analyze a structure to predict responses that will occur during a sinusoidal or random vibration test in which a predetermined motion is input by the shaker at the shaker/structure interface. Often the loads produced in these tests are a controlling factor in the design of the structure. The response analyses are generally performed in two stages: a modal analysis to determine the undamped eigenvalues and eigenvectors of the structure "cantilevered" at the interface where the structure will attach to the shaker, followed by a subsequent steady state frequency response analysis using the modal information. The output of the modal analysis, while giving information that is useful in comparing with the eigenvalues and eigenvectors obtained in the test, does not give a sufficiently clear indication of which eigenvectors will be important contributors in the subsequent frequency response analysis. The reason for this is that the vibration test loading is really a distributed inertial loading on the whole structure known in terms of the input acceleration as opposed to some known force at a given location in other forced response analyses.

By using the eigenvector data obtained in the normal mode analyses, a modal participation factor can be calculated which gives a clear indication of the relative importance of each calculated mode in terms of its response to any base acceleration input. This factor, like the generalized mass or generalized stiffness already calculated in NASTRAN, is a property of the structure. In addition, however, it is also a property of the base excitation.

This paper presents a technique for calculating the modal participation factors for base excitation problems using a DMAP alter to the NASTRAN real eigenvalue analysis Rigid Format. The DMAP program automates the generation of the "seismic" mass to add to the degrees of freedom representing the shaker input directions and calculates the modal participation factors. These are shown in the paper to be a good measure of the maximum acceleration expected at any point on the structure when the subsequent frequency response analysis is run.

INTRODUCTION

Structures that are analyzed to predict what their responses will be in a vibration test quite often have one feature in common; namely that they are rigidly attached to a vibration shaker at a number of interface degrees of freedom. Such situation, therefore, can be analyzed by multi-point constraining all of the interface degrees of freedom to any convenient single interface grid point with specification of the shaker motion at this grid point. The shaker motion, or base excitation, as it were, is then specified for a nonredundant set of degrees of freedom (DOF) that can easily be identified on a NASTRAN SUPORT bulk data card. In the following derivation of the base excitation modal participation factors, it is assumed that the structure to be analyzed is to have a base motion at a nonredundant set of DOF and that the interface DOF have been constrained to this set of nonredundant DOF. In addition, the derivation is restricted to systems with real eigenvectors.

DERIVATION OF MODAL PARTICIPATION FACTORS

To derive an equation for the modal participation factors due to base excitation consider a general structural model, as shown in Figure 1. Presumably this structure would be rigidly connected to the shaker at several points, denoted in this example as 1 through 4. This situation can be simulated by creating some central point, r, and connecting 1 through 4 to r via rigid elements. Then r is a set of nonredundant DOF at which the shaker motion can be specified. The equations of motion of this structure, using the displacement set notation of NASTRAN, and ignoring damping for the moment, are *

$$\mathbf{M}_{gg}\ddot{\mathbf{u}}_g + \mathbf{K}_{gg}\mathbf{u}_g = \mathbf{P}_g \tag{1}$$

Where $\mathbf{P}_r$ contains the loads necessary to drive the r DOF by the specified base motions imparted by the shaker.

Following elimination of multi-point constraints (via MPC or rigid element cards), single point constraints (SPC's) and DOF omitted via Guyan reduction (OMIT's), $\mathbf{u}_g$ in equation (1) is reduced to $\mathbf{u}_a$ and the equations are

$$\mathbf{M}_{aa}\ddot{\mathbf{u}}_a + \mathbf{K}_{aa}\mathbf{u}_a = \mathbf{P}_a \tag{2}$$

where

$$\mathbf{u}_a = \begin{Bmatrix} \mathbf{u}_l \\ \mathbf{u}_r \end{Bmatrix} \tag{3}$$

---

*Bold face letters will be used to designate matrices, including row and column vectors.

The u_r DOF are identified on SUPORT bulk data cards and u_ℓ are all remaining DOF in u_a. Partitioning equation (2):

$$\begin{bmatrix} M_{\ell\ell} & M_{\ell r} \\ M_{\ell r}^T & M_{rr} \end{bmatrix} \begin{Bmatrix} \ddot{u}_\ell \\ \ddot{u}_r \end{Bmatrix} + \begin{bmatrix} K_{\ell\ell} & K_{\ell r} \\ K_{\ell r}^T & K_{rr} \end{bmatrix} \begin{Bmatrix} u_\ell \\ u_r \end{Bmatrix} = \begin{Bmatrix} 0 \\ P_r \end{Bmatrix} \tag{4}$$

where P_r are the forces exerted by the shaker on the structure and result in the base motions u_r. The forces P_r are not known, a priori; rather the motions (accelerations, velocities or displacements) at the r DOF are known. In this context the forces in P_r are really forces of constraint which are necessary to produce the desired base motion. Notice in equation (4) that there are no applied loads for the ℓ DOF. The situation being simulated here is one in which the only excitation comes about due to the shaker driving the structure at the r DOF.

The DOF u_ℓ can be considered to be made up to two terms:

$$u_\ell = u_\ell^e + u_\ell^r \tag{5}$$

where

u_ℓ^e = displacements of the ℓ DOF when the r DOF are fixed

u_ℓ^r = rigid body displacements of the ℓ DOF due to the r DOF

Thus u_ℓ^e would be the displacement DOF for a structure that was "cantilevered" or fixed at the r DOF. The displacements, u_ℓ^r at the ℓ DOF due to the r DOF not being fixed can be determined simply from geometric considerations and is

$$u_\ell^r = D_{\ell r} u_r \tag{6}$$

where matrix $D_{\ell r}$ is data block DM generated by module RBMG3 in NASTRAN whenever SUPORT bulk data cards defining the existence of r DOF is present. The columns of $D_{\ell r}$ are rigid body displacements at the ℓ DOF due to a unit motion at one of the r DOF. They are rigid body displacements due to the fact that the r DOF are a nonredundant set. Substituting (5) and (6) into (4) the two matrix equations for the unknowns u_ℓ^e and P_r (since u_r is known) are

$$M_{\ell\ell} \ddot{u}_\ell^e + K_{\ell\ell} u_\ell^e = -(M_{\ell\ell} D_{\ell r} + M_{\ell r}) \ddot{u}_r \tag{7}$$

$$P_r = M_{\ell r}^T \ddot{u}_\ell^e + K_{\ell r}^T u_\ell^e + (M_{\ell r}^T D_{\ell r} + M_{rr}) \ddot{u}_r \tag{8}$$

where use of the fact that

$$K_{rr} = K_{lr}^{T} K_{ll}^{-1} K_{lr} \quad ,$$

$$D_{lr} = -K_{ll}^{-1} K_{lr}$$

and thus

$$K_{ll} D_{lr} + K_{lr} = \theta \tag{9}$$

has been made. This is discussed in the NASTRAN Theoretical Manual, Reference 1. Equation (7) is the well known form for base acceleration input where the problem is solved for the motions u_l^c as if the base were fixed but with an equivalent inertia loading on each of the DOF that is the rigid body inertia force due to the base moving. Equation (8) merely solves for the forces required to drive the base at the specified motion. A better form for P_r results if equations (9) and (7) are used to eliminate the stiffness term in (8). The result is

$$P_r = \left(M_{ll} D_{lr} + M_{lr} \right)^{T} \ddot{u}_l^c + \bar{M}_{rr} \ddot{u}_r \tag{10}$$

where

$$\bar{M}_{rr} = D_{lr}^{T} M_{ll} D_{lr} + D_{lr}^{T} M_{lr} + M_{lr}^{T} D_{lr} + M_{rr} \tag{11}$$

is the rigid body mass matrix of the structure relative to the SUPORT DOF and is data block MR generated by NASTRAN in module RBMG4 when SUPORT bulk data cards are used. Equation (7) can be diagonalized with a modal transformation using the "cantilevered" modes of the structure (that is, the modes of the structure when constrained at the r DOF). Define

ϕ_l^j = j^{th} eigenvector of structure when constrained at r DOF.

$\Phi_{ln} = \lfloor \phi_l^1 \;\; \phi_l^2 \; \cdots \; \phi_l^n \rfloor$ = matrix whose columns are eigenvectors,

Then the modal transformation is

$$u_l^c = \Phi_{ln} \xi_n = \lfloor \phi_l^1 \;\; \phi_l^2 \cdots\cdots \phi_l^n \rfloor \begin{Bmatrix} \xi_1 \\ \xi_2 \\ \vdots \\ \xi_n \end{Bmatrix} = \sum_{j=1}^{n} \phi_l^j \xi_j \tag{12}$$

ORIGINAL PAGE IS
OF POOR QUALITY

where ξ_n is a vector of modal DOF ξ_i (i =1, 2,... n) with n being the number of modes used in the dynamic analysis. Substituting (12) into (7) and premultiplying by $\Phi_{\ell n}^T$ the result is

$$m_{nn}\ddot{\xi}_n + k_{nn}\xi_n = -\Phi_{\ell n}^T\left(M_{\ell\ell}D_{\ell r} + M_{\ell r}\right)\ddot{u}_r \qquad (13)$$

where

$$m_{nn} = \Phi_{\ell n}^T M_{\ell\ell}\Phi_{\ell n} \qquad (14)$$

and

$$k_{nn} = \Phi_{\ell n}^T K_{\ell\ell}\Phi_{\ell n} \qquad (15)$$

are both diagonal matrices with m_{nn} containing the generalized masses (denoted as m_i) and k_{nn} the generalized stiffnesses (denoted as k_i) of the cantilevered modes.

With the addition of damping, each individual modal equation in equation (13) is, after dividing through by the generalized mass:

$$\ddot{\xi}_i + 2\gamma_i\omega_i\dot{\xi}_i + \omega_i^2\xi_i = -\frac{1}{m_i}\phi_\ell^{i^T}\left(M_{\ell\ell}D_{\ell r} + M_{\ell r}\right)\ddot{u}_r \qquad (16)$$

The damping factor, g_i , is specified through use of the TABDMP bulk data card.

Define

$$f_r^i = \frac{1}{m_i}\phi_\ell^{i^T}\left(M_{\ell\ell}D_{\ell r} + M_{\ell r}\right) \qquad (17)$$

The row matrix f_r^i contains as many terms as there are DOF identified on the SUPORT card, that is, those that will be given a known motion from the shaker. Each term in f_r^i is identified as being a modal participation factor since the solution to equation (16) for some specified base motion at one DOF will be proportional to the corresponding term in f_r^i .

As an example of this consider the situation when the base motion is a steady state sinusoidal input at some resonant frequency ω_j with an acceleration (complex) magnitude $\bar{\ddot{u}}$. In this case:

$$\ddot{u}_r = \bar{\ddot{u}}_r e^{i\omega_j t}$$

The solution to equation (16) for the modal acceleration $\ddot{\xi}_j$ is

$$\ddot{\xi}_j = \bar{\ddot{\xi}}_j e^{i\omega_j t}$$

where

$$\bar{\ddot{\xi}}_j = -i\left(\mathbf{f}^j_r Q_j \bar{\ddot{\mathbf{u}}}_r\right) \tag{18}$$

and

$$Q_j = 1/2\zeta_j$$

is the modal amplification in mode j. Equation (18) indicates the modal acceleration is, of course, lagging the base acceleration input by 90 degrees.

The significance of the modal participation factors in $\mathbf{f}^j_r$ is evident from equation (18). At resonance, the modal acceleration magnitude is equal to the product of the modal amplification, the participation factor and the magnitude of the input shaker acceleration. For systems with relatively small damping, the magnitude of the accelerations at grid points throughout the structure can be approximated by a single mode response (the resonating mode) so that, for example, using only one mode in equation (12)

$$\begin{aligned}\bar{\ddot{\mathbf{u}}}^e_\ell(\omega_j) &\approx \boldsymbol{\phi}^j_\ell \bar{\ddot{\xi}}_j \\ &= -i\,\boldsymbol{\phi}^j_\ell \mathbf{f}^j_r Q_j \bar{\ddot{\mathbf{u}}}_r\end{aligned} \tag{19}$$

The modal participation factors, together with the eigenvectors calculated in a real eigenvalue analysis can therefore be used to obtain estimates of what the magnitude of the grid point accelerations will be in a subsequent forced base response analysis. The modal participation factors can be easily calculated during the real eigenvalue analysis run (in Rigid Format 3, for example). A matrix of all participation factors for all modes is:

$$\mathbf{F}_{nr} = \{\mathbf{f}^j_r\} = \mathbf{m}^{-1}_{nn} \boldsymbol{\Phi}^T_{\ell n}\left(\mathbf{M}_{\ell\ell}\mathbf{D}_{\ell r} + \mathbf{M}_{\ell r}\right) \tag{20}$$

That is, each row of $\mathbf{F}_{nr}$ is an $\mathbf{f}^j_r$ (the participation factors for one mode). Each column of $\mathbf{F}_{nr}$ gives the participation factors for all modes for one DOF of base acceleration. For example, column 1 of $\mathbf{F}_{nr}$ contains the participation factors for base acceleration in the first DOF entered on the SUPORT card.

ORIGINAL PAGE IS
OF POOR QUALITY

The modal participation factors can be used to easily calculate what is commonly referred to as modal mass. Consider equation (10) for the base loads (the shaker forces required to produce $\ddot{u}_r$). Using the modal transformation in equation (12) the loads P_r in equation (10) can be written as

$$P_r = \sum_{j=1}^{n} P_r^j + \bar{M}_{rr}\ddot{u}_r \tag{21}$$

where

$$P_r^j = (M_{\ell\ell} D_{\ell r} + M_{\ell r})^T \phi_\ell^j \ddot{\xi}_j$$

Using equation (18), the complex amplitude of P_r^j is $\bar{P}_r^j$ where

$$P_r^j = \bar{P}_r^j e^{i\omega t}$$

$$P_r^j(\omega_j) = -i\,(M_{\ell\ell} D_{\ell r} + M_{\ell r})^T \phi_\ell^j f_r^j Q_j \ddot{u}_r$$

Using equation (17):

$$P_r^j(\omega_j) = -i\,(M_{\ell\ell} D_{\ell r} + M_{\ell r})^T \phi_\ell^j \frac{1}{m_j} \phi_\ell^{j^T} (M_{\ell\ell} D_{\ell r} + M_{\ell r}) Q_j \bar{\ddot{u}}_r$$

$$= -i\,\mathfrak{m}_{rr}^j Q_j \bar{\ddot{u}}_r \tag{22}$$

where

$$\mathfrak{m}_{rr}^j = (M_{\ell\ell} D_{\ell r} + M_{\ell r})^T \phi_\ell^j \frac{1}{m_j} \phi_\ell^{j^T} (M_{\ell\ell} D_{\ell r} + M_{\ell r}) \tag{23}$$

is the j^{th} mode modal mass matrix. It is a square matrix of size r and from equations (21) and (22) it is seen that its use is in determining the j^{th} mode contribution to the base forces (required shaker forces). For systems with small damping the forces P_r at a resonance ω_j would be approximately P_r^j so that equation (22) would give an approximation to the total forces. It is interesting to note that if the sum of all modal mass matrices is denoted as

$$\sum_{j=1}^{n} \mathfrak{m}_{rr}^j = \mathfrak{m}_{rr} \tag{24}$$

and if all of the eigenvectors are used ($n=\ell$) then:

$$\mathcal{M}_{rr} = \left(M_{\ell\ell} D_{\ell r} + M_{\ell r}\right)^T M_{\ell\ell}^{-1} \left(M_{\ell\ell} D_{\ell r} + M_{\ell r}\right) \tag{25}$$

If there are no masses at any of the r set of D.O.F then

$$\mathcal{M}_{rr} = \bar{M}_{rr} \tag{26}$$

That is, the sum of the modal masses is the rigid body mass matrix (data block MR from module RBMG4) when all masses are at the r set of DOF. Thus, modal masses can be calculated in a real eigenvalue analysis and can be used to estimate how many modes will have to be used in the subsequent base excitation dynamic analysis to make sure a high percentage of the complete system mass is included (since modal truncation, in effect, truncates mass). This would be useful in transient analysis where the single mode response at resonance is not a valid approximation. The modal mass matrix $\mathcal{M}^j_{rr}$ can easily be determined from the modal participation factors f^j_r. From equations (17) and (23) it is seen that

$$\mathcal{M}^j_{rr} = m_j \, f^{j\,T}_r \, f^j_r \tag{27}$$

DMAP ALTER DESCRIPTION

The DMAP Alter package for calculating the modal participation factors and modal masses is described in detail in Appendix A. The calculations are done, of course, in the real eigenvalue analysis NASTRAN Rigid Format and in particular in either COSMIC Rigid Format 3 or MSC Rigid Formats 3 or 25. The description in Appendix A is an alter package for MSC Rigid Format 25 or COSMIC Rigid Format 3. However, calculation of the modal masses in the COSMIC version is not convenient at this time due to a limitation in the COSMIC version of module DIAGONAL.

As recommended in the MSC documentation, Reference 2, base motion problems are solved by putting all DOF which are to have a specified motion on SUPORT cards and also connecting fictitious large masses to these DOF. If the large masses are very large in comparison to the complete structure mass then, when a force is applied to these DOF, their acceleration will be determined to be very nearly the force divided by the large mass. Making the force equal to the large mass times the desired acceleration at these DOF will then result in the NASTRAN solution for these accelerations to be the desired base accelerations.

Thus, the first portion of the DMAP Alter automates the inclusion of the large (seismic) masses at the DOF identified on SUPORT bulk data cards. The large mass is taken as 10^8 times the diagonal of the rigid body mass matrix (data block MR calculated in module RBMG4). The bulk data deck for the real eigenvalue analysis with the DMAP Alter program should include SUPORT cards for the nonredundant DOF at which base motion is desired. As mentioned previously, the actual base DOF that are connected to the shaker are to be rigidly constrained to some nonredundant set of DOF that are then included on SUPORT cards. (and not single point constrained) to identify them as the base motion DOF.

The second part of the DMAP Alter calculates the matrix $\mathbf{F}_{nr}$ which contains the modal participation factors. These are printed out as matrix data block FNR.

The third part of the DMAP alter calculates the diagonal terms of the modal mass matrix $\mathfrak{m}^{j}_{rr}$. These can only be calculated in the MSC version since they require a feature in the DIAGONAL module (namely raising all elements of a matrix to a power) not available in the COSMIC DIAGONAL module. The matrix which contains the diagonal terms of $\mathfrak{m}^{j}_{rr}$ is data block MJRR and row j of this matrix contains the diagonal terms for mode j. This matrix is also printed out in terms of percent of the corresponding mass in the rigid body mass matrix as matrix data block MJRRP. Addition of each column should give a value of 100 if all modes are used and if there are no masses (other than the fictitious large mass) at the r set of DOF.

SAMPLE PROBLEM

Figure 2 shows a sample problem using the DMAP Alter for a beam which is to be given a base motion at grid point 11. The aluminum beam is 2.54m (100 inches) long with a mass of 9.1kg (beam weight is 20lb). Section properties for the beam are: .0013m^2 (2.0in^2) area and 8.33X10^{-7} m^4 (2.0in^4) moment of inertia. The DOF which are to be given base motion should be the higher numbered DOF in the problem to avoid numerical problems with the large fictitious masses added to these DOF. The fact that the sample problem initially has a nonredundant interface with the shaker (at grid point 11) is of no consequence. As mentioned earlier, if the interface where the structure is to be connected to the shaker is redundant, the interface points can be rigidly connected to some one point that is then called the base motion point.

Appendix B contains selected pages from the NASTRAN run for this sample problem including the bulk data deck listing. The input data is seen to resemble any real eigenvalue run for the beam cantilevered modes except that some of the DOF at the cantilever point (grid point 11) are identified on a SUPORT bulk data card instead of constrained. For the sample problem these were taken to be DOF 1, 3 and 5 signifying that these will be the DOF that would be given a base motion in subsequent dynamic analyses. The remaining DOF at grid point 11 are constrained.

As mentioned previously, the DMAP Alter automates the inclusion of the large fictitious masses at the DOF identified in the r set. The values of these masses are contained in matrix data block MAAB output in the DMAP Alter and included in Appendix B. As seen from MAAB, the large masses are 10^8 times the rigid body masses output from the grid point weight generator (taking into account the latter is in weight units and MAAB is in mass units).

The eigenvalues for the sample problem are included in Appendix B. The first three are rigid body modes due to the three DOF on the SUPORT card. The remaining modes are those that would have been found if the SUPORT DOF had been constrained instead. This is due to the fact that large masses are connected to the SUPORT DOF in order that the elastic modes will be the same as if these DOF were constrained. Several of the modes are shown on Figure 3.

The modal participation factors are shown in Appendix B as the matrix data block FNR. These are also shown in Table 1. Each column in the table is a column of F_{nr} and there are 3 columns; one each for the SUPORT DOF. Each row in the table shows the terms in F_{nr} (which are the rows f_r^i) which are the participation factors for the mode corresponding to that row of the table.

The second column of Table 1 gives the participation factors for base motion in DOF 3 at grid point 11; namely lateral shaker motion. From Table 1 it is seen that mode 1, with a frequency of 10.9hz, has a participation factor of 1.56 while mode 5 does not contribute at all. This is due to the fact that mode 5, as seen from Figure 3 is an uncoupled longitudinal mode of the beam and could have been so identified by visual inspection of the mode shapes for this simple beam problem. For more complicated structures the participation factors are more helpful in identifying significant modes for various base excitations than the visual inspection of the eigenvector data.

The use of the participation factors in estimating grid point accelerations that would be found in a steady state sinusoidal shaker simulation is demonstrated on Figure 4. The figure shows comparison of data from an actual frequency response run using Rigid Format 8 along with the estimated accelerations based on the modal participation factors in table 1.

The solid line is the acceleration at the beam tip as a function of the shaker frequency, , with an input acceleration in the Z lateral direction of 1.5g's at grid point 11. The simple calculation using the participation factors and a single mode response with equation (19) gives acceleration magnitudes indicated by the data points on Figure 4. The good agreement shows the value of knowing the participation factors when the modal analysis is run rather than waiting to determine the frequency response in a later run. The data point for the 490.6hz mode on Figure 4 is not a mode in resonance since the 490.6 mode is a longitudinal mode and the base response in the example is lateral.

The output in Appendix B also shows the diagonals of the modal mass matrices m_{rr}^j as output matrix MJRR. Expressed as a percent of the corresponding mass term in the complete structure rigid body mass matrix, $\bar{M}_{rr}$, the result is output matrix MJRRP. As mentioned previously, if there are no masses at the DOF (other than the fictitious large mass put there for use calculating the participation factors) and if all modes of the structure are used, the columns of MJRRP should add to 100. Table 2 shows the terms from MJRRP. As with the modal participation factors these also clearly indicate which modes are significant in terms of base motion in certain directions. For general base excitation problems, the data from MJRRP is useful in identifying significant modes to be included in the analysis. The columns of Table 2 do not add up to 100 percent for base motion DOF 1 or 3 since the set did have mass. The beams' mass was distributed to all eleven grid points so that the end grid points (1 and 11) each have 5 percent of the total.

CONCLUSIONS

Knowledge of the modal participation factors for base motion can be useful in determining the significant modes to be used in forced base motion problems. Obtaining the participation factors when the modal analysis is run, allows estimates to be made of the subsequent structure responses to the base motion prior to running the base motion dynamic analysis. The participation factors use for steady state base motion frequency response analyses was demonstrated; however they are equally as valid for transient analysis.

REFERENCES

1. The NASTRAN Theoretical Manual (Level 17.5), NASA SP-221(05), December 1978

2. MSC NASTRAN Applications Manual, MSR-32 (VAX), The MacNeal/Schwendler Corporation, May/June 1981

Table 1

Modal Participation Factors for Beam Problem

Mode No.	Frequency (Hz)	Modal Participation Factors From for Base Acceleration at G.P. 11 In: DOF-1	DOF-3	DOF-5
4	10.94	0.	1.5569	-113.590
5	67.82	0.	-.8446	17.800
6	188.0	0.	.4736	-6.124
7	364.5	0.	-.3137	2.923
8	490.6	1.2706	0.	0.
9	595.9	0.	.2161	-1.590
10	878.2	0.	-.1593	.9801
11	1202.	0.	.1371	-.7370
12	1460.	-.4165	0.	0.
13	1545.	0.	.1154	-.5618
14	1861.	0.	-.0806	.3669
15	2086.	0.	-.0453	.1987
16	2393.	-.2414	0.	0.
17	3267.	-.1632	0.	0.
18	4061.	.1171	0.	0.
19	4755.	-.0854	0.	0.
20	5332.	.0613	0.	0.
21	5777.	-.0414	0.	0.
22	6081.	.0240	0.	0.
23	6234.	-.0079	0.	0.

Table 2

Modal Masses for Beam Problem

Mode No.	Diagonals of Modal Mass Matrices* for Base Acceleration at G.P.11 In: DOF-1	DOF-3	DOF-5
4	0.	61.073	97.030
5	0.	18.854	2.4995
6	0.	6.4685	.3228
7	0.	3.3013	.0856
8	80.724	0.	0.
9	0.	1.9882	.0321
10	0.	1.3149	.0149
11	0.	.9087	.0078
12	8.6749	0.	0.
13	0.	.6166	.0044
14	0.	.3585	.0022
15	0.	.1171	.0007
16	2.9142	0.	0.
17	1.3315	0.	0.
18	.6854	0.	0.
19	.3647	0.	0.
20	.1878	0.	0.
21	.0858	0.	0.
22	.0288	0.	0.
23	.0031	0.	0.
Totals	95.0002	95.0008	100.000

*Expressed as percent of total rigid body mass of structure.

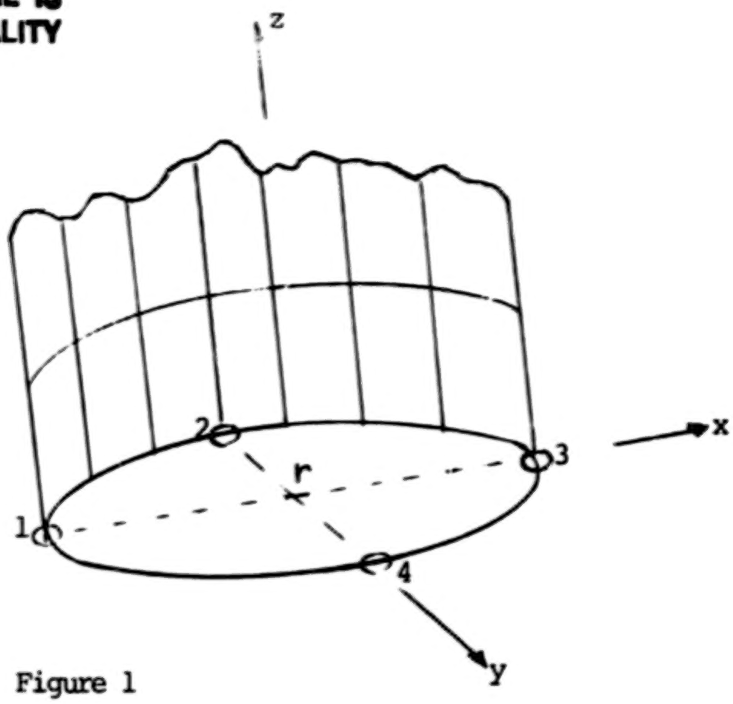

Note: Points 1-4 Are Actual
Structure/Shaker Rigid
Interface Points,
Simulated by Single Point r

Figure 1

General Base Excitation Problem

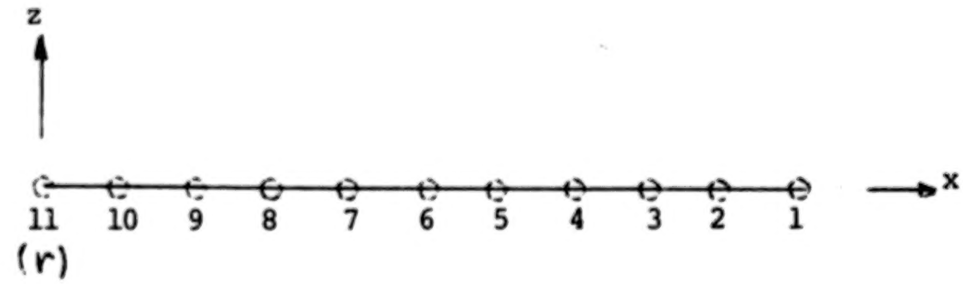
z
x
11
10
9
8
7
6
5
4
3
2
1
(r)

Figure 2

Sample Beam Problem
With Base Excitation At Grid Point 11

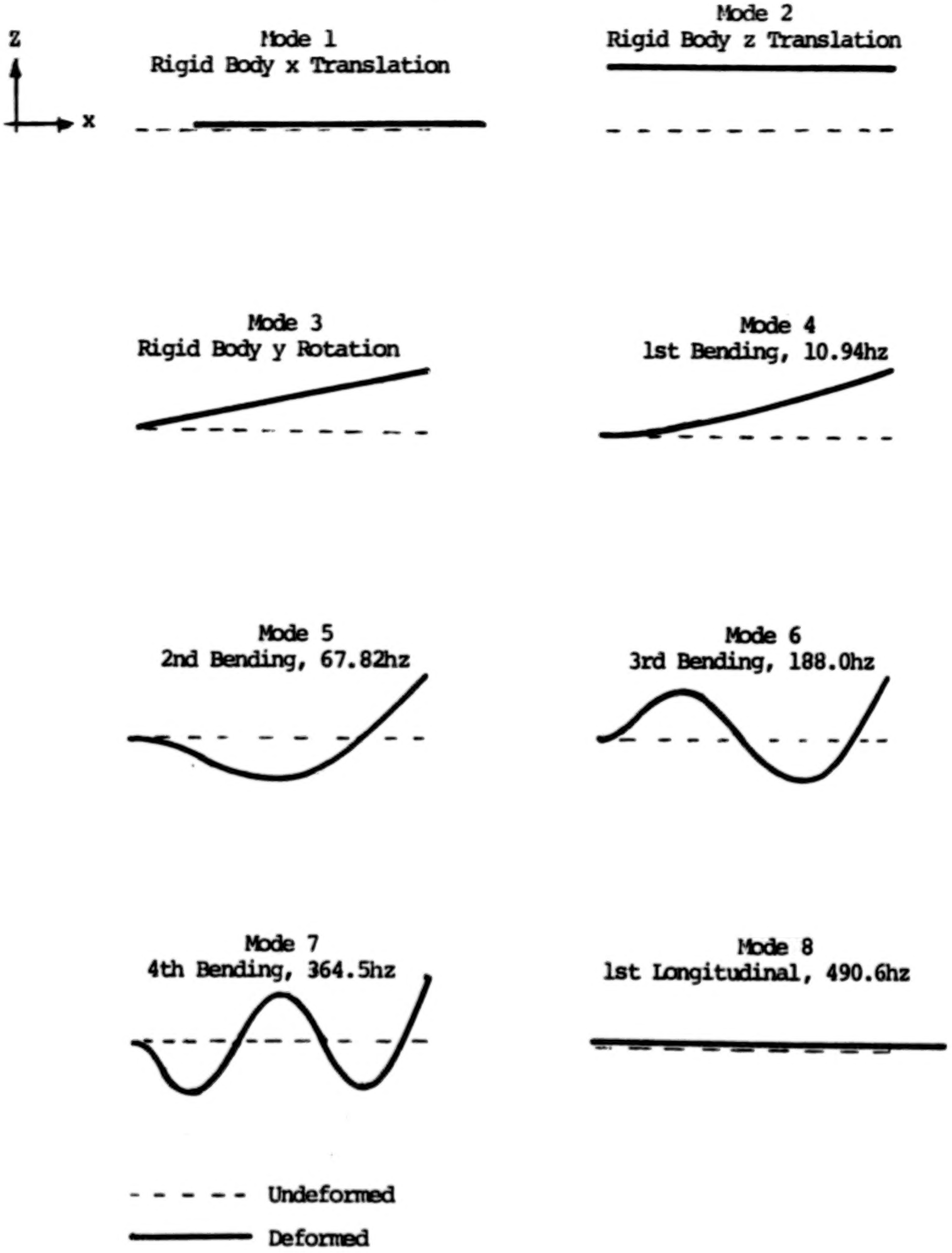
Z
x
Mode 1
Rigid Body x Translation
Mode 2
Rigid Body z Translation
Mode 3
Rigid Body y Rotation
Mode 4
1st Bending, 10.94hz
Mode 5
2nd Bending, 67.82hz
Mode 6
3rd Bending, 188.0hz
Mode 7
4th Bending, 364.5hz
Mode 8
1st Longitudinal, 490.6hz
Undeformed
Deformed

Figure 3

Beam Mode Shapes

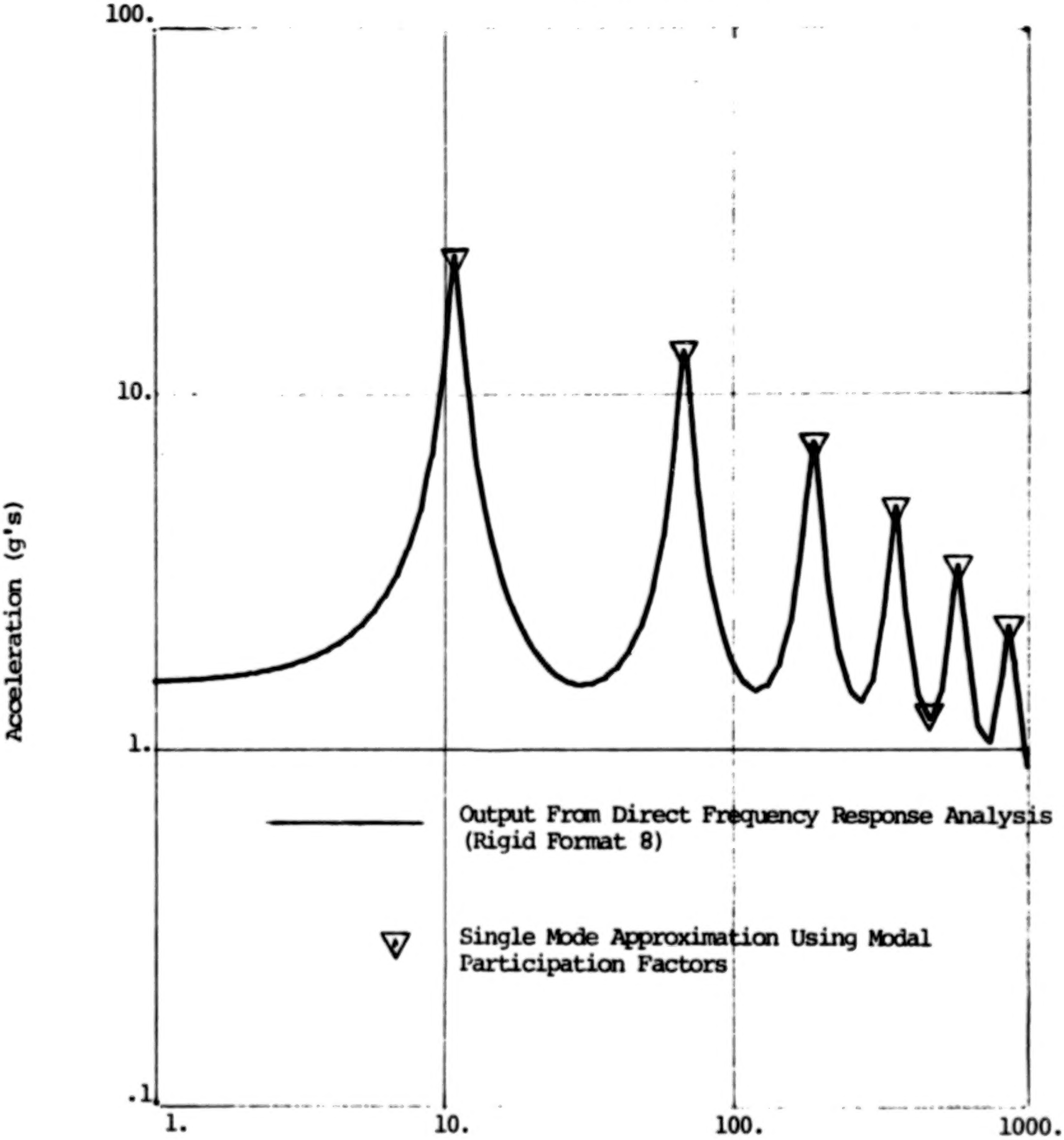

Figure 4

Acceleration at G.P. 1 of Beam due to
1.5g Sinusoidal Base Acceleration at G.P. 11

APPENDIX A

DMAP Alter for Determining Base Excitation Modal Participation Factors
(Real Eigenvalue Analysis Rigid Formats)

```
ALTER a1
PARAM          //C,N,NOP/V,N,T=-1  $
PARAMR         //C,N,DIV/V,N,GRAVO/C,N,1.0/V,Y,WTMASS=-1.0  $
PARAMR         //C,N,COMPLEX/V,N,OUTR/V,N,GRAVO/C,N,0.0/V,N,GRAV  $
DIAGONAL       MR/MRD/C,N,SQUARE  $
ADD            MRD,/WRD/V,N,GRAV  $
ADD            MRD,/MBASE/C,N,(1.E8,0.)  $
VEC            USET/CP/C,N,A/C,N,L/C,N,R  $
MERGE,         ,,,MBASE,CP,/MAAB/C,N,-1  $
MATGPR         GPL,USET,SIL,MAAB//C,N,A/C,N,A  $
ADD            MAAB,MAA/MAAT  $
EQUIV          MAAT,MAA/T  $
ADD            MR,MBASE/NEWMR  $
EQUIV          NEWMR,MR/T  $
ALTER a2
PARTN          PHIA,,CP/PHIL,PHIR,,/C,N,1/C,N,2/C,N,2/C,N,2  $
GKAM,          ,PHIL,MI,LAMA,,,,,CASECC/MGNN,,KGNN,PHILN/C,N,-1/C,N,-0/
               C,Y,LFREQ=.000001/C,Y,HFREQ=1.E20/C,N,-1/C,N,-1/C,N,-1/
               V,N,NOCUP/V,N,FMODE  $
ADD            MGNN,/WGNN/V,N,GRAV  $
MPYAD          MLL,DM,MLR/ML3/C,N,0/C,N,1/C,N,0/C,N,2  $
ADD            ML3,/WL3/V,N,GRAV  $
MPYAD          PHILN,WL3,/FNR0/C,N,1/C,N,1/C,N,0/C,N,2  $
SOLVE          WGNN,FNR0/FNR/C,N,1  $
MATPRN         FNR,,,,//  $
DIAGONAL       FNR/MJRR0/C,N,WHOLE/C,N,2.0  $
MPYAD          WGNN,MJRR0,/MJRR  $
MATPRN         MJRR,,,,  $
TRNSP          MJRR/MJRRT  $
SOLVE          WRD,MJRRT/MJRRDT/C,N,1  $
ADD            MJRRDT,/MJRRPT/C,N,(100.,0.)  $
TRNSP          MJRRPT/MJRRP  $
MATPRN         MJRRP,,,,//  $
ENDALTER
```

Explanation of DMAP Alter Statements

I. Generation of Large Masses for SUPORT Points for Base Motion Analyses

1. DMAP statements 2 through 14 are inserted after module RBMG4 has run. For COSMIC Rigid Format 3 (April 1982 version) the Alter is at a_1= 69 and for MSC Rigid Format 25 (Dec. 1981, version 61B) a_1 is 140.

2-4. PARAM modules set the values of several parameters to be used. Parameter GRAV is the inverse of the regular WTMASS parameter.

5. DIAGONAL extracts the diagonal of the rigid body mass matrix, MR ($\bar{M}_{rr}$ in equation (11)) and calls the result matrix data block MRD.

6. Matrix data block WRD is MRD multiplied by parameter GRAV=1/WTMASS so that WRD is generally in weight units if a PARAM WTMASS card is used in the bulk data.

7. Matrix data block MBASE is 10^8 times MRD. These give the large fictitious masses which are put on the r DOF for base motion problems.

8-9. Module MERGE, using partitioning vector CP generated in module VEC, expands the large fictitious mass matrix, MBASE, up to full "a" set size. Output matrix MAAB has the large fictitious masses for the r DOF but in a matrix of "a" size.

10. The large masses are printed out and can be seen to only exist at the r DOF.

11-12. The large masses are added to the normal mass matrix MAA and the result equivalenced back to MAA so that when MAA is called for in later modules the sum of the normal MAA and the large masses MAAB will be used.

13-14. The real eigenvalue analysis module, READ, uses the rigid body mass matrix, MR, when there are SUPORT DOF. Since the large masses were added at the r DOF, the sum of the MR (from the finite element model) and the large masses (in MBASE) is to be used for MR in module READ.

II. Generation of Modal Participation Factors

15. Following module READ and the output of the eigenvalues and eigenvalue analysis summary, the statements 16 through 23 are inserted for calculation of the modal participation factors. For COSMIC Rigid Format 3 (April 1982) the alter is at a_2=77 and for MSC Rigid Format 25 (Dec. 1981 version 61B) a_2 is 146.

ORIGINAL PAGE IS
OF POOR QUALITY

16-17. Module PARTN extracts the eigenvectors for the ℓ DOF and module GKAM extracts from this the elastic ($\omega > 0$) eigenvectors. The result is called PHILN and is matrix $\Phi_{\ell n}$ used in equation (12). Matrix data block MGNN is the matrix of generalized masses, $\mathcal{M}_{nn}$, in equation (14).

18. Convert MGNN to weight units if a PARAM WTMASS bulk data card is present.

19-20. Calculate $(M_{\ell\ell} D_{\ell r} + M_{\ell r})$ and call the result matrix data block ML3. Note that matrix data block DM is matrix $D_{\ell r}$. Matrix data block WL3 is ML3 in weight units if PARAM WTMASS is present in bulk data.

21-23. Calculate $F_{nr} = \mathcal{M}_{nn}^{-1} \Phi_{\ell n}^{T} (M_{\ell\ell} D_{\ell r} + M_{\ell r})$ and print out F_{nr}, the matrix of modal participation factors.

III. Statements 24 through 31 calculate and print the modal masses. These cannot currently be calculated in COSMIC NASTRAN since the COSMIC version of module DIAGONAL does not have a feature which allows calculation of a matrix which contains the terms of some input matrix raised to some specified power.

24. Module DIAGONAL calculates a matrix, MJRRO, whose terms are the squares of the terms in the modal participation factor matrix, FNR.

25-26. By multiplying MJRRO by the generalized mass (or weight) matrix the diagonal terms of the modal mass matrices are obtained. Matrix MJRR is so arranged that its jth row is the diagonal of the jth modal mass matrix, $\mathcal{M}^{j}_{rr}$, in equation (27). This matrix is printed out.

27-31. The modal mass terms are divided by the corresponding rigid body mass terms for the complete structure and multiplied by 100. The resulting matrix, MJRRP, is printed out and gives the diagonals of the modal masses (in the rows of MJRRP) in percent of the rigid body mass. If there are no masses (other than the large fictitious masses) at the r DOF then the columns of MJRRP should add to 100 if all modes are used.

ORIGINAL PAGE IS
OF POOR QUALITY

Appendix B

Sample Problem Real Eigenvalue Analysis and Modal Participation Factor Calculation

```
                                                              FEBRUARY  15, 1983   NASTRAN 12/ 1/81    PAGE     1

    N A S T R A N   E X E C U T I V E   C O N T R O L   D E C K   E C H O


ID TEST,DMAPBASE
APP DISP
SOL 25,0
TIME 2
DIAG 8,14
ALTER 140
PARAM     //C,N,NOP/V,N,T=-1  $
PARAMR    //C,N,DIV/V,N,GRAVO/C,N,1.0/V,Y,WTMASS=-1.0  $
PARAMR    //C,N,COMPLEX/V,N,OUTR/V,N,GRAVO/C,N,0.0/V,N,GRAV  $
DIAGONAL MR/MRD/C,N,SQUARE  $
ADD       MRD,/WRD/V,N,GRAV  $
ADD       MRD,/MBASE/C,N,(1.E8,0.)  $
VEC       USET/CP/C,N,A/C,N,L/C,N,R  $
MERGE,    ...MBASE,CP,/MAAB/C,N,-1  $
MATGPR    GPL,USET,SIL,MAAB//C,N,R/C,N,R  $
ADD       MAAB,MAA/MAAT  $
EQUIV     MAAT,MAA/T  $
ADD       MR,MBASE/NEWMR  $
EQUIV     NEWMR,MR/T  $
ALTER 146
PARTN     PHIA,,CP/PHIL,PHIR,,/C,N,1/C,N,2/C,N,2/C,N,2  $
GKAM,     ,PHIL,MI,LAMA,....,CASECC/MGNN,,KGNN,PHILN/C,N,-1/C,N,0/
          C,Y,LFREQ=.000001/C,Y,HFREQ=1.E20/C,N,-1/C,N,-1/C,N,-1/
          V,N,NOCUP/V,N,FMODE  $
ADD       MGNN,/WGNN/V,N,GRAV  $
MPYAD     MLL,DM,MLR/ML3/C,N,0/C,N,1/C,N,0/C,N,2  $
ADD       ML3,/WL3/V,N,GRAV  $
MPYAD     PHILN,WL3,/FNRO/C,N,1/C,N,1/C,N,0/C,N,2  $
SOLVE     WGNN,FNRO/FNR/C,N,1  $
MATPRN    FNR,....//  $
DIAGONAL FNR/MJRRO/C,N,WHOLE/C,N,2.0  $
MPYAD     WGNN,MJRRO,/MJRR  $
MATPRN    MJRR,....  $
TRNSP     MJRR/MJRRT  $
SOLVE     WRD,MJRRT/MJRRDT/C,N,1  $
ADD       MJRRDT,/MJRRPT/C,N,(100.,0.)  $
TRNSP     MJRRPT/MJRRP  $
MATPRN    MJRRP,....//  $
ENDALTER
CEND
```

```
TEST OF DMAP PROGRAM TO GEN.MODAL PART.FACTORS FOR BASE ACCEL.        FEBRUARY  15, 1983   NASTRAN 12/ 1/81    PAGE      2
CANTILEVERED BEAM

LONGITUDINAL AND LATERAL MODES

                                   C A S E    C O N T R O L    D E C K    E C H O
        CARD
        COUNT
          1       TITLE = TEST OF DMAP PROGRAM TO GEN.MODAL PART.FACTORS FOR BASE ACCEL.
          2       SUBTITLE = CANTILEVERED BEAM
          3       LABEL = LONGITUDINAL AND LATERAL MODES
          4       ECHO = UNSORT
          5       METHOD = 1
          6       OUTPUT
          7       VECTOR = ALL
          8       SPCF = ALL
          9       BEGIN BULK
```

```
CANTILEVERED BEAM

LONGITUDINAL AND LATERAL MODES

                             I N P U T   B U L K   D A T A   D E C K   E C H O

                  .   1  ..   2  ..   3  ..   4  ..   5  ..   6  ..   7  ..   8  ..   9  ..  10  .
                  GRDSET                                                  246
                  GRID    1               100.    0.      0.
                  GRID    2               90.     0.      0.
                  GRID    3               80.     0.      0.
                  GRID    4               70.     0.      0.
                  GRID    5               60.     0.      0.
                  GRID    6               50.     0.      0.
                  GRID    7               40.     0.      0.
                  GRID    8               30.     0.      0.
                  GRID    9               20.     0.      0.
                  GRID    10              10.     0.      0.
                  GRID    11              0.      0.      0.
                  BAROR                                   0.      0.      1.      1
                  CBAR    1       1       1       2
                  CBAR    2       1       2       3
                  CBAR    3       1       3       4
                  CBAR    4       1       4       5
                  CBAR    5       1       5       6
                  CBAR    6       1       6       7
                  CBAR    7       1       7       8
                  CBAR    8       1       8       9
                  CBAR    9       1       9       10
                  CBAR    10      1       10      11
                  PBAR    1       1       2.0     2.0     2.0
                  MAT1    1       10.+6           0.3     0.1
                  SUPORT     11      135
                  ASET1   13      1       THRU    11
                  EIGR    1       GIV                     23      23              1.-4    +E2
                  +E2     MAX
                  PARAM   GRDPNT  11
                  PARAM   WTMASS  .002591
                  ENDDATA

                  INPUT BULK DATA CARD COUNT =      32

              TOTAL COUNT=    32
```

```
TEST OF DMAP PROGRAM TO GEN.MODAL PART.FACTORS FOR BASE ACCEL.          FEBRUARY  15, 1983   NASTRAN 12/ 1/81    PAGE      8
CANTILEVERED BEAM

LONGITUDINAL AND LATERAL MODES
                 O U T P U T   F R O M   G R I D   P O I N T   W E I G H T   G E N E R A T O R

                                        REFERENCE POINT =       11
                                                  M O
 *  2.000000E+01  0.000000E+00  0.000000E+00  0.000000E+00  0.000000E+00  0.000000E+00 *
 *  0.000000E+00  2.000000E+01  0.000000E+00  0.000000E+00  0.000000E+00  1.000000E+03 *
 *  0.000000E+00  0.000000E+00  2.000000E+01  0.000000E+00 -1.000000E+03  0.000000E+00 *
 *  0.000000E+00  0.000000E+00  0.000000E+00  0.000000E+00  0.000000E+00  0.000000E+00 *
 *  0.000000E+00  0.000000E+00 -1.000000E+03  0.000000E+00  6.700001E+04  0.000000E+00 *
 *  0.000000E+00  1.000000E+03  0.000000E+00  0.000000E+00  0.000000E+00  6.700001E+04 *
                                                  S
                     *  1.000000E+00  0.000000E+00  0.000000E+00 *
                     *  0.000000E+00  1.000000E+00  0.000000E+00 *
                     *  0.000000E+00  0.000000E+00  1.000000E+00 *
          DIRECTION
     MASS AXIS SYSTEM (S)     MASS              X-C.G.        Y-C.G.        Z-C.G.
             X            2.000000E+01      0.000000E+00  0.000000E+00  0.000000E+00
             Y            2.000000E+01      5.000000E+01  0.000000E+00  0.000000E+00
             Z            2.000000E+01      5.000000E+01  0.000000E+00  0.000000E+00
                                                 I(S)
                     *  0.000000E+00  0.000000E+00  0.000000E+00 *
                     *  0.000000E+00  1.700000E+04  0.000000E+00 *
                     *  0.000000E+00  0.000000E+00  1.700000E+04 *
                                                 I(Q)
                     *  0.000000E+00                             *
                     *                1.700000E+04               *
                     *                              1.700000E+04 *
                                                  Q
                     *  1.000000E+00  0.000000E+00  0.000000E+00 *
                     *  0.000000E+00  1.000000E+00  0.000000E+00 *
                     *  0.000000E+00  0.000000E+00  1.000000E+00 *
```

ORIGINAL PAGE IS
OF POOR QUALITY

```
 TEST OF DMAP PROGRAM TO GEN.MODAL PART.FACTORS FOR BASE ACCEL.       FEBRUARY  22, 1983   NASTRAN 12/ 1/81    PAGE     10
 CANTILEVERED BEAM

 LONGITUDINAL AND LATERAL MODES

                MAAB
      POINT             VALUE     POINT          VALUE     POINT          VALUE     POINT          VALUE     POINT          VALUE

COLUMNS       1 (       1-T1) THRU      20 (       10-T3) ARE NULL.

COLUMN       21 (        11-T1).
          11 T1  5.18200E+06

COLUMN       22 (        11-T3).
          11 T3  5.18200E+06

COLUMN       23 (        11-R2).
          11 R2  1.73597E+10
```

ORIGINAL PAGE IS
OF POOR QUALITY

```
TEST OF DMAP PROGRAM TO GEN.MODAL PART.FACTORS FOR BASE ACCEL.       FEBRUARY  15, 1983   NASTRAN 12/ 1/81    PAGE     11
CANTILEVERED BEAM

LONGITUDINAL AND LATERAL MODES

                                               R E A L   E I G E N V A L U E S
  MODE     EXTRACTION        EIGENVALUE            RADIANS              CYCLES               GENERALIZED          GENERALIZED
   NO.       ORDER                                                                              MASS               STIFFNESS
      1        11          0.0                 0.0                  0.0                  5.182000E+06         0.0
      2        22          0.0                 0.0                  0.0                  5.182000E+06         0.0
      3        23          0.0                 0.0                  0.0                  1.735970E+06         0.0
      4        21          4.727787E+03        6.875890E+01         1.094332E+01         1.305586E-02         6.172530E+01
      5        20          1.815695E+05        4.261097E+02         6.781746E+01         1.369489E-02         2.486573E+03
      6        19          1.395168E+06        1.181172E+03         1.879894E+02         1.494427E-02         2.084977E+04
      7        18          5.246433E+06        2.290509E+03         3.645459E+02         1.738694E-02         9.121943E+04
      8   [illegible]      9.503404E+06        3.082759E+03         4.906363E+02         2.591000E-02         2.462332E+05
      9   [illegible]      1.401962E+07        3.744278E+03         5.959203E+02         2.205616E-02         3.092189E+05
     10   [illegible]      3.044624E+07        5.517811E+03         8.781869E+02         2.686599E-02         8.179684E+05
     11   [illegible]      5.704086E+07        7.552540E+03         1.202024E+03         2.504681E-02         1.428692E+06
     12         9          8.413236E+07        9.172369E+03         1.459828E+03         2.591000E-02         2.179870E+06
     13        14          9.420654E+07        9.706006E+03         1.544759E+03         2.398174E-02         2.259237E+06
     14        13          1.367145E+08        1.169250E+04         1.860919E+03         2.858839E-02         3.908448E+06
     15        12          1.717434E+08        1.310509E+04         2.085740E+03         2.950574E-02         5.067415E+06
     16         8          2.260851E+08        1.503613E+04         2.393074E+03         2.591000E-02         5.857865E+06
     17         7          4.214662E+08        2.052964E+04         3.267394E+03         2.591000E-02         1.092019E+07
     18         6          6.511505E+08        2.551765E+04         4.061260E+03         2.591000E-02         1.687131E+07
     19         5          8.926549E+08        2.987733E+04         4.755125E+03         2.591000E-02         2.312869E+07
     20         4          1.122339E+09        3.350133E+04         5.331902E+03         2.591000E-02         2.907981E+07
     21         3          1.317720E+09        3.630042E+04         5.777391E+03         2.591000E-02         3.414214E+07
     22         2          1.459673E+09        3.820567E+04         6.080621E+03         2.591000E-02         3.782013E+07
     23         1          1.534302E+09        3.917017E+04         6.234125E+03         2.591000E-02         3.975376E+07
```

```
TEST OF DMAP PROGRAM TO GEN.MODAL PART.FACTORS FOR BASE ACCEL.        FEBRUARY  15, 1983   NASTRAN 12/ 1/81    PAGE     13
CANTILEVERED BEAM

LONGITUDINAL AND LATERAL MODES

 MATRIX FNR      (GINO NAME 101 ) IS A DB  PREC      3 COLUMN X     20 ROW RECTANG  MATRIX.

COLUMN      1      ROWS      5 THRU     20      --------------------------------------------------
   ROW
    5)    1.2706D+00  0.0000D+00  0.0000D+00  0.0000D+00 -4.1653D-01  0.0000D+00  0.0000D+00  0.0000D+00 -2.4142D-01 -1.6319D-01
   15)    1.1708D-01 -8.5408D-02  6.1280D-02 -4.1421D-02  2.4008D-02 -7.8702D-03

COLUMN      2      ROWS      1 THRU     12      --------------------------------------------------
   ROW
    1)    1.5569D+00 -8.4463D-01  4.7360D-01 -3.1367D-01  0.0000D+00  2.1613D-01 -1.5926D-01  1.3712D-01  0.0000D+00  1.1542D-01
   11)   -8.0610D-02 -4.5339D-02

COLUMN      3      ROWS      1 THRU     12      --------------------------------------------------
   ROW
    1)   -1.1359D+02  1.7800D+01 -6.1238D+00  2.9231D+00  0.0000D+00 -1.5900D+00  9.8005D-01 -7.3703D-01  0.0000D+00 -5.6180D-01
   11)    3.6689D-01  1.9869D-01

THE NUMBER OF NON-ZERO TERMS IN THE DENSEST COLUMN =      10

THE DENSITY OF THIS MATRIX IS  50.00 PERCENT.
```

```
     TEST OF DMAP PROGRAM TO GEN.MODAL PART.FACTORS FOR BASE ACCEL.        FEBRUARY  15, 1983   NASTRAN 12/ 1/81    PAGE     14
     CANTILEVERED BEAM

     LONGITUDINAL AND LATERAL MODES

      MATRIX MJRR     (GINO NAME 101 ) IS A DB  PREC      3 COLUMN X     20 ROW RECTANG  MATRIX.

 COLUMN      1       ROWS       5 THRU     20      ------------------------------------------------
   ROW
    5)     1.6145D+01  0.0000D+00  0.0000D+00  0.0000D+00  1.7350D+00  0.0000D+00  0.0000D+00  0.0000D+00  5.8284D-01  2.6629D-01
   15)     1.3709D-01  7.2945D-02  3.7552D-02  1.7157D-02  5.7638D-03  6.1940D-04

 COLUMN      2       ROWS       1 THRU     12      ------------------------------------------------
   ROW
    1)     1.2215D+01  3.7707D+00  1.2937D+00  6.6026D-01  0.0000D+00  3.9765D-01  2.6298D-01  1.8174D-01  0.0000D+00  1.2331D-01
   11)     7.1697D-02  2.3409D-02

 COLUMN      3       ROWS       1 THRU     12      ------------------------------------------------
   ROW
    1)     6.5010D+04  1.6746D+03  2.1630D+02  5.7338D+01  0.0000D+00  2.1521D+01  9.9593D+00  5.2511D+00  0.0000D+00  2.9213D+00
   11)     1.4852D+00  4.4957D-01

 THE NUMBER OF NON-ZERO TERMS IN THE DENSEST COLUMN =      10

 THE DENSITY OF THIS MATRIX IS  50.00 PERCENT.
```

```
      TEST OF DMAP PROGRAM TO GEN.MODAL PART.FACTORS FOR BASE ACCEL.        FEBRUARY  15, 1983   NASTRAN 12/ 1/81    PAGE     15
      CANTILEVERED BEAM

      LONGITUDINAL AND LATERAL MODES

       MATRIX MJRRP    (GINO NAME 101 ) IS A DB  PREC      3 COLUMN X     20 ROW RECTANG  MATRIX.

 COLUMN      1       ROWS      5 THRU     20      ------------------------------------------------
    ROW
     5)     8.0724D+01  0.0000D+00  0.0000D+00  0.0000D+00  8.6749D+00  0.0000D+00  0.0000D+00  0.0000D+00  2.9142D+00  1.3315D+00
    15)     6.8544D-01  3.6473D-01  1.8776D-01  8.5786D-02  2.8819D-02  3.0970D-03

 COLUMN      2       ROWS      1 THRU     12      ------------------------------------------------
    ROW
     1)     6.1073D+01  1.8854D+01  6.4685D+00  3.3013D+00  0.0000D+00  1.9882D+00  1.3149D+00  9.0871D-01  0.0000D+00  6.1655D-01
    11)     3.5849D-01  1.1705D-01

 COLUMN      3       ROWS      1 THRU     12      ------------------------------------------------
    ROW
     1)     9.7030D+01  2.4995D+00  3.2284D-01  8.5580D-02  0.0000D+00  3.2121D-02  1.4865D-02  7.8375D-03  0.0000D+00  4.3601D-03
    11)     2.2168D-03  6.7100D-04

 THE NUMBER OF NON-ZERO TERMS IN THE DENSEST COLUMN =      10

 THE DENSITY OF THIS MATRIX IS  50.00 PERCENT.
```

ORIGINAL PAGE IS
OF POOR QUALITY

N84
15600

UNCLAS

D/10

FINITE ELEMENT ANALYSIS OF FLUID-FILLED ELASTIC PIPING SYSTEMS

N84 15600

G.C. Everstine, M.S. Marcus, and A.J. Quezon
David W. Taylor Naval Ship R&D Center
Bethesda, Maryland 20084

Dedicated to the Memory of James M. McKee (1942-1983)

SUMMARY

Two finite element procedures are described for predicting the dynamic response of general 3-D fluid-filled elastic piping systems. The first approach, a low frequency procedure, models each straight pipe or elbow as a sequence of beams. The contained fluid is modeled as a separate coincident sequence of axial members (rods) which are tied to the pipe in the lateral direction. The model includes the pipe hoop strain correction to the fluid sound speed and the flexibility factor correction to the elbow flexibility. The second modeling approach, an intermediate frequency procedure, follows generally the original Zienkiewicz-Newton scheme for coupled fluid-structure problems except that the velocity potential is used as the fundamental fluid unknown to symmetrize the coefficient matrices. From comparisons of the beam model predictions to both experimental data and the 3-D model, the beam model is validated for frequencies up to about two-thirds of the lowest fluid-filled lobar pipe mode. Accurate elbow flexibility factors are seen to be crucial for effective beam modeling of piping systems.

INTRODUCTION

The vibrations that occur in fluid-filled piping systems are of interest in a variety of industrial, aircraft, and shipboard applications. The interesting dynamic behavior includes both water hammer (a transient phenomenon) and the steady-state (time-harmonic) vibrations caused by unbalanced rotating machinery such as pumps, for example.

Over 30 years ago, Callaway, Tyzzer, and Hardy (Ref. 1) recognized in their experimental work the importance of the coupling between the vibrations of the liquid and the pipe wall, even for nominally straight pipes. Since then, a number of investigators have proposed various techniques of mathematical modeling for design and analysis purposes.

Most of these techniques have been restricted to straight pipes. Some recent work, for example, was reported by El-Raheb (Ref. 2,3), who analyzed the acoustic propagation in a perfect, finite length, fluid-filled, thin elastic cylindrical shell. El-Raheb obtained eigenfunction expansions for Koiter's consistent shell equations and the Helmholtz equation governing the fluid field.

There have also been some finite element analyses of 2-D fluid cavities of general shape (Ref. 4,5). These approaches, however, avoid the fluid-structure coupling by requiring as input the impedance of the pipe wall.

There has been relatively little fluid-structure interaction work involving general 3-D piping systems containing joints such as elbows and tees. The first such analyses were probably performed by Davidson, Smith, and Samsury (Ref. 6,7). They recognized that a simplified beam model should suffice for the relatively low frequencies which are often of interest. Low frequency dynamic behavior is characterized by pipes which respond only in their beam (rather than lobar) modes and by fluid wavelengths which are large compared to the pipe diameter. Thus, for such situations, the fluid wave propagation through the pipes is essentially planar. This procedure, although fully general in concept, was implemented in a special purpose computer program limited as to the generality and size of problems which could be handled.

The same assumptions formed the basis of a finite element procedure developed by Howlett (Ref. 8) for aircraft hydraulic systems. This procedure modeled the fluid inside the pipe as a beam having zero bending stiffness. Elbows and tees were not modeled explicitly. Instead, compatibility at a joint (elbow or tee) was enforced as an additional constraint requiring the conservation of fluid mass passing through the joint. The Howlett analyses, however, apparently omitted two essential ingredients: (1) the correction to the fluid sound speed to account for the elasticity of the pipe walls, and (2) the flexibility factor correction for the elbows to account for the fact that curved pipes are considerably more flexible than straight pipes of the same cross section (Ref. 9).

More recently, the transfer matrix approach was used by El-Raheb (Ref. 10) to calculate the beam-type dynamic response of 3-D multiplane piping systems consisting of straight sections and elbows. One of El-Raheb's conclusions was that the one-dimensional acoustic assumption is valid for frequencies up to about one-half the frequency of the lowest acoustic mode having two waves around the circumference (n=2).

Schwirian and Karabin (Ref. 11) developed another finite element procedure which was similar to Howlett's (Ref. 8) except that the fluid inside an elbow was apparently modeled with a single straight axial member ("spar" element) with fictitious properties assigned to simulate properly the fluid mass and compressibility. This model also included the pipe hoop strain correction to the fluid sound speed and the flexibility factor correction to the elbow flexibility. No experimental validation of the model was included in the paper.

One additional modeling procedure was formulated by Hatfield and Wiggert (Ref. 12). They used a transfer function approach involving separate analyses of liquid and solid components, followed by synthesis of the component solutions. The scheme was validated for planar piping systems by comparison with experimental data.

In general, beam models of fluid-filled elastic piping systems are very attractive because of their simplicity. Finite element approaches have the added feature of allowing essentially arbitrary specification of geometry, boundary conditions, loadings, and output requests. In addition, finite element models of piping systems can easily be combined with models of the support structure.

In this paper, we will develop further the finite element approach for low frequency prediction by combining ideas from the papers just mentioned. Our model is mathematically equivalent to the Davidson-Smith-Samsury model (Ref. 6,7), a non-finite element approach. Our modeling scheme is similar to those of Howlett (Ref. 8) and Schwirian and Karabin (Ref. 11) except that we model elbows explicitly by a polygonal set of beam elements for the pipe and axial members for the fluid. We will also show the importance of assigning the correct flexibility factors to the elbows. (In general, most classical means of calculating flexibility factors are not adequate for elbows with straight pipe extensions at the ends (Ref. 13, 14)). The modeling approach will be validated in two ways. First, for a simple planar system, comparisons will be made with both experimental data and a general 3-D finite element model which models the pipe as a shell and the contained fluid with 3-D fluid finite elements. Second, for a complex non-planar system, comparisons will be made between a beam solution and a general 3-D finite element solution. Since the latter includes the essential physics of the fully-coupled problem, it provides a good test for the approximate models.

The 3-D finite element solutions to be presented use the generally classical procedures which evolved from the work of Zienkiewicz and Newton (Ref. 15). In our analyses, we make use of the recent improvement (Ref. 16) which shows how to obtain symmetric matrix equations.

LOW FREQUENCY BEAM MODEL

For low frequency dynamic excitation of fluid-filled elastic piping systems, the pipes respond only in their beam (rather than lobar) modes, and the wave propagation in the fluid column is essentially planar. It is assumed either that the fluid is initially at rest, or that the average flow speed is so small compared to the sound speed that the acoustic response is unaffected. The fluid-structure coupling is assumed to occur only at pipe bends and other joints. Thus, the fluid is allowed to slide without friction in straight sections of pipe. The circular pipe cross section is assumed to remain circular. The equation satisfied by either the fluid pressure or the axial component of fluid displacement is the scalar wave equation; thus the fluid can be modeled by an axial structural member (rod).

Finite element models are prepared using the following procedure: Beam elements are used to model both the straight sections and the elbows. If straight beam elements are used, a minimum of three elements is recommended (on the basis of some numerical testing) for 90-degree bends, regardless of the spacing of grid points in adjacent straight sections. In straight sections, the grid point spacing is dictated by the need for accurate normal modes of vibration in the frequency range of interest.

Since a pipe bend is more flexible than an equivalent length of straight pipe, the moments of inertia for the beam elements in each elbow should be divided by the appropriate flexibility factor. For piping systems with straight sections not significantly longer than the arc lengths of the elbows, the elbow stiffness plays an important role in the dynamic response and must be accurately modeled. Thus the flexibility factors assigned to each elbow should apply to the elbow as it is configured in the piping system. In particular, the flexibility factors for 90-degree elbows with straight pipe extensions are sensitive to the length of those extensions (Ref. 13, 14). As shown by Quezon and Everstine (Ref. 14), idealized approaches such as those used in the ELBOW computer program (Ref. 17) are generally not adequate for predicting the flexibility factors of 90-degree elbows with straight pipe extensions.

For the acoustic fluid inside the pipe, a duplicate set of grid points is defined to coincide with the pipe grid points. The fluid is modeled with elastic rod elements (sometimes called spars), which are equivalent to beam elements with zero flexural and torsional stiffness. These elements are assigned the actual mass density ρ for the fluid and a Young's modulus E given by

ORIGINAL PAGE IS OF POOR QUALITY

$$E = \rho c^2 \tag{1}$$

In Equation (1), c, the effective sound speed in a fluid column contained in an elastic circular thin-walled pipe, is obtained from

$$c = \sqrt{B/\rho} \;/\; \sqrt{1 + BD/E_s t} \tag{2}$$

where B is the fluid bulk modulus of elasticity, ρ is the fluid mass density, D is the mean diameter of the pipe, E_s is the Young's modulus of the pipe material, and t is the pipe wall thickness. Since the numerator in Equation (2) is the actual speed of sound in the fluid, the denominator (which is always greater than unity) is the corrective factor which accounts for the elasticity of the pipe. This correction is well known (Ref. 18); according to Krause, Goldsmith, and Sackman (Ref. 19), this relation was first derived by Joukowsky (Ref. 20) over 80 years ago. Equations (1) and (2) can be combined to yield

$$E = B/(1 + BD/E_s t) \tag{3}$$

The fluid, which is modeled with axial members, must have only one independent degree of freedom (DOF) at each grid point. The three rotational DOF are restrained at all fluid points. Both transverse translational DOF at each fluid point are constrained (using multipoint constraints or rigid links) to move with the corresponding structural point. The only remaining DOF, the axial DOF, is free to slide relative to the beam. These constraints are applicable in both the straight sections and the elbows. It is therefore convenient to define for each elbow a separate cylindrical coordinate system whose axis is perpendicular to the plane of the elbow and intersects the center of curvature. For elbows, the independent DOF is thus the azimuthal translation. For each straight section, it is convenient to define a separate Cartesian system with one axis coincident with the pipe axis. It is emphasized that the single independent fluid unknown is the axial displacement, not the pressure. The fluid pressure can be recovered from the finite element program in the usual way by requesting that stresses in the fluid elements be calculated and printed.

The modeling of fluid-filled tees is handled differently from that of elbows. Since fluid entering one leg of a tee can flow out both of the other two branches, the procedure must ensure that the total fluid mass flowing into one branch of the joint equals the total mass flowing out the other two branches (Ref. 8). (This condition is automatically satisfied for an elbow, a two-branch joint.) In the finite element model, we define at the intersection of the tee branches one structural grid point and three fluid grid points, as shown in Figure 1. As with other fluid grid points in the system, each of these three points is permitted to move only in the axial direction for the branch in which it lies. In addition, the three axial DOF

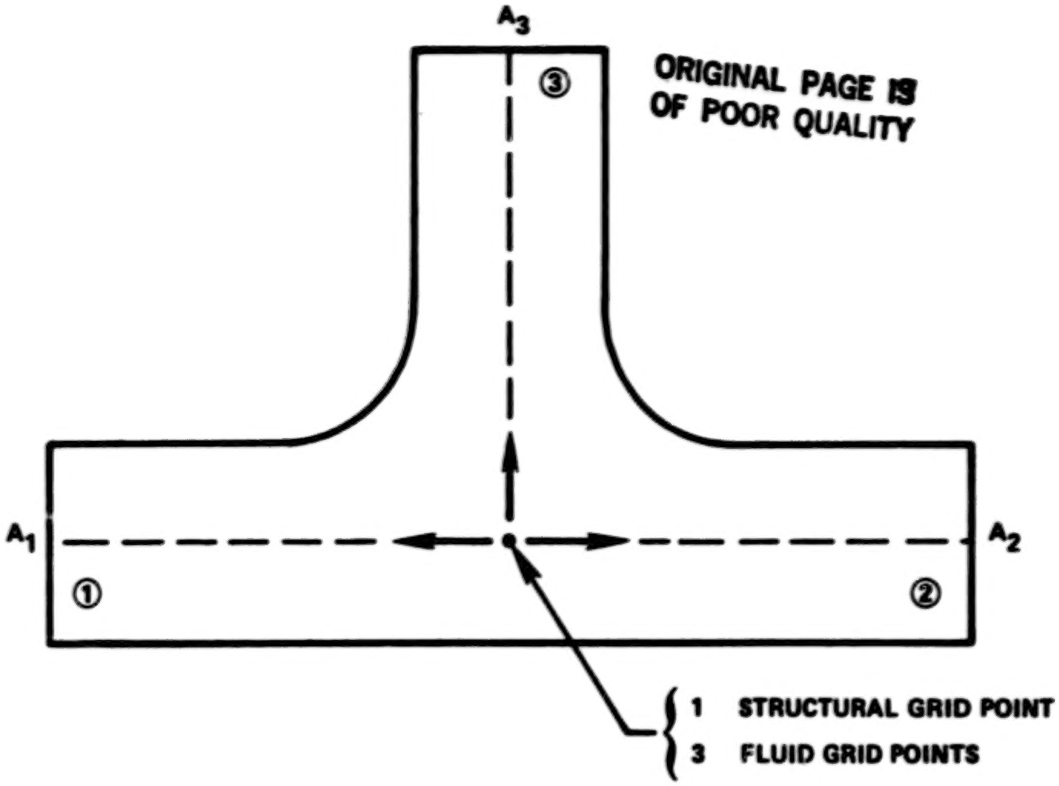

Figure 1 - Low Frequency Model of Piping Tee

are not independent (because of conservation of mass) and must satisfy the relation

$$\sum_{i=1}^{3} A_i (\xi_i - u_i) = 0 \tag{4}$$

where u_i and ξ_i are the axial components of structural and fluid displacements, respectively, and A_i is the fluid cross-sectional area for branch i of the tee. Thus, a tee introduces two independent fluid DOF into the model.

As with elbows, flexibility factors should be used with the beam elements which model the tee. Unfortunately, even less is known about tee flexibilities than about elbow flexibilities. The procedure that we find convenient for computing tee flexibilities is to perform a separate finite element analysis for a tee modeled as a shell. This analysis can be easily made since a tee data generation program (Ref. 21) has been interfaced with NASTRAN by Quezon (Ref. 22) so that, given a few basic parameters, an analysis can be performed within a few hours. No tees are included in the examples in this report.

Damping in the piping system can be directly incorporated in the finite element model by entering the damping loss factor as a material damping constant, which results in complex material moduli.

Because of the versatility of finite element computer codes, various boundary conditions on the fluid column are possible. At a free surface (where the pressure vanishes), the fluid DOF (the axial displacement) is left free, a natural boundary condition. At a fixed boundary, the unknown is restrained. If the pipe modeled is part of a very long system, in which case a non-reflecting fluid boundary is needed, the plane fluid waves can be absorbed by attaching to the fluid DOF a dashpot whose constant (ratio of axial force to velocity) is ρcA, where ρ is the fluid mass density, c is the effective sound speed as given by Equation (2), and A is the cross-sectional area of the fluid column. For a pipe that opens into a large volume of fluid (e.g., the sea), the appropriate boundary condition is that of a piston in an infinite baffle (Ref. 23), in which case the scalar added mass

$$M_a = 8\rho a^3/3 \tag{5}$$

is applied, where ρ is the fluid mass density and 'a' is the radius of the opening. For a pipe with a closed end, the axial fluid displacement at the end is tied to the axial structural displacement using a multipoint constraint equation or rigid link.

The beam model just described can be applied using most general purpose finite element structural analysis codes without modification. The analysis is performed in a single pass with the fluid-structure coupling included in the model. The resulting model has seven independent degrees of freedom at each grid point location, six for the pipe and one for the axial component of fluid displacement. For matrix bandwidth reasons, each fluid grid point should be sequenced adjacent to its corresponding structural point. The major limitation of the model is frequency: this is a low frequency model. More will be said about this limitation later.

INTERMEDIATE FREQUENCY 3-D MODEL

For the dynamic response prediction of piping systems at frequencies for which beam models are not valid, general three-dimensional finite element models are required. In general, this approach models the pipe with shell elements and the contained fluid with 3-D acoustic finite elements. Thus the pipe need not respond only as a beam (for which the cross sections are rigid), and non-planar fluid response is allowed. Such a model generally requires thousands of degrees of freedom, even for simple piping systems. Thus, although 3-D models may find only limited use (given current computing power), it is worthwhile to describe the model's formulation and demonstrate its application. A 3-D model is particularly useful for validating approximate models such as beam models since the limitations of the approximate model can then be determined. The purpose of this section is to describe the general 3-D finite element modeling of non-planar fluid-filled elastic piping systems. We are not aware of any previous finite element analyses of the size to be considered here for the fully-coupled fluid-structure problem.

Most general finite element work involving an elastic structure coupled to an acoustic fluid (for which the fluid pressure satisfies the wave equation) can be traced to the work of Zienkiewicz and Newton (Ref. 15). In their work and in many subsequent papers by others, the fundamental fluid unknown was taken to be the pressure. A few investigators (e.g., Hamdi, Ousset, and Verchery (Ref. 24)) selected the fluid displacement as the unknown.

Everstine (Ref. 25-27) showed how general purpose structural analysis codes could be used, without modification, to solve the common field equations arising in mathematical physics (including the wave and Helmholtz equations of acoustics). He also showed how the codes could be used to solve mixed field problems such as coupled structural-acoustic problems.

More recently, he showed (Ref. 16) that, if the coupled fluid-structure problem were formulated with velocity potential rather than pressure as the fundamental fluid unknown, the nonsymmetric matrices of the pressure formulation would be symmetric. For some situations, including steady-state problems involving damped systems (which are of interest here), significant computational advantages result.

If both fluid and structure are modeled with finite elements, the following matrix equation arises (Ref. 16,28):

$$\begin{bmatrix} M & 0 \\ 0 & Q \end{bmatrix} \begin{Bmatrix} \ddot{u} \\ \ddot{q} \end{Bmatrix} + \begin{bmatrix} B & A \\ A^T & C \end{bmatrix} \begin{Bmatrix} \dot{u} \\ \dot{q} \end{Bmatrix} + \begin{bmatrix} K & 0 \\ 0 & H \end{bmatrix} \begin{Bmatrix} u \\ q \end{Bmatrix} = \begin{Bmatrix} f_1 \\ f_2 \end{Bmatrix} \qquad (6)$$

where q, the fundamental unknown in the fluid, is the time integral of pressure and hence proportional to the velocity potential. The unknown q is a vector with a single unknown at each fluid mesh point. In Equation (6), u is the vector of displacement components in the structure, M and Q are the mass matrices for the structure and fluid, K and H are the stiffness matrices for the structure and fluid, A is the area matrix which converts fluid pressure at interface points to structural loads, B and C are the damping matrices for the structure and fluid, and f_1 and f_2 are the structural and fluid applied loads. If the pressure gradient (or equivalently, fluid motion) is specified at a fluid boundary, f_2 takes the form

$$f_2 = -(A_s \partial q/\partial n)/\rho \qquad (7)$$

where A_s is the area matrix for the boundary surface. In Equation (6), the required "material constants" for the fluid elements are

$$G_e = -1/\rho, \; E_e = 10^{20}\, G_e, \; \rho_e = -1/\rho c^2 \qquad (8)$$

where G_e, E_e, and ρ_e are, respectively, the "shear modulus," "Young's modulus," and "mass density" assigned to the fluid finite elements (Ref. 16,28).

In the fluid-filled piping systems of interest here, damping is introduced by specifying an overall system loss factor. In that case, the matrices K and H in Equation (6) are complex, and B = C = 0. The loss factor η, if uniform, is given by

$$\eta = \mathrm{Im}\,(K) \,/\, \mathrm{Re}\,(K) = \mathrm{Im}\,(H) \,/\, \mathrm{Re}\,(H) \qquad (9)$$

All matrices in Equation (6) except A are automatically formed by the finite element program once the elements are defined. The area matrix A has nonzeros only at rows and columns corresponding to interface degrees of freedom. For piping systems which involve only cylinders and tori, the area contribution at each point is easily calculated analytically, so that A can be generated by an automatic data generation preprocessor.

This finite element scheme can be implemented on any general purpose structural code which allows the user to enter matrix elements directly from the input stream. We used NASTRAN for the analyses described in this paper.

EXAMPLE 1: A PLANAR PIPING SYSTEM

The formulations described in the preceding sections will be illustrated first on a simple planar piping system for which experimental data are available (Ref. 6). This system, shown in Figure 2, consists of two straight sections of standard 4-inch copper-nickel pipe connected by an elbow. The system is filled completely with lubricating oil. Table 1 summarizes the pertinent properties of the system.

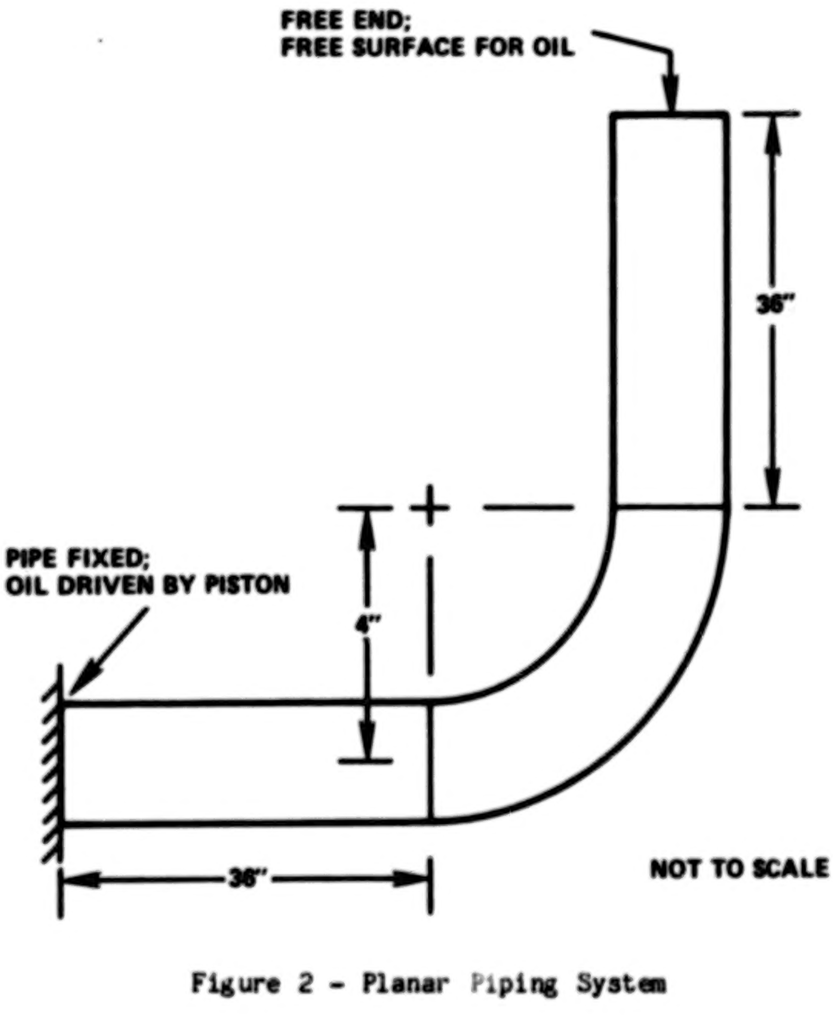

Figure 2 - Planar Piping System

TABLE 1 - CHARACTERISTICS OF PLANAR PIPING SYSTEM

Pipe (4-inch 70-30 Cu-Ni)	
outside diameter (O.D.)	4.5 in
minimum wall thickness	0.203 in
nominal wall thickness	0.232 in
Young's modulus	22,000,000 psi
Poisson's ratio	0.294
weight density	0.323 lb/in^3
Elbow	
bend radius (R)	4 in
bend angle	90 degrees
Fluid (2190 TEP oil)	
actual bulk modulus	282,000 psi
effective bulk modulus in pipe	228,000 psi
weight density	0.0315 lb/in^3

As seen in Figure 2, one end of the pipe was fixed, and the fluid was driven by a piston designed to excite only the fluid. The other end of the system was free. Measurements (Ref. 6) included the fluid pressure at the piston and the inplane components of structural velocity at the free end.

Both beam and 3-D models were prepared for this piping system using the finite element approaches described in the preceding section. The beam model consisted of ten beam elements in each straight section and eight elements in the elbow. For this 2-D problem, each fluid and structural grid point had, respectively, one and three degrees of freedom (DOF). The beam model thus had 112 DOF. The elbow flexibility factor used for the beam analysis was 8.14, which was computed by the ELBOW computer program (Ref. 17). For inplane moment loads on elbows with long straight sections, ELBOW has been shown to be satisfactory, although it does overestimate the flexibility factors slightly (Ref. 14).

The mesh used for the 3-D model is shown in Figure 3. The structural element used is a low-order four-node quadrilateral plate (NASTRAN'S QUAD2). Because of symmetry, only half of the circumference (180 degrees) was modeled. The model had ten elements in the circumferential direction, 19 elements longitudinally in each straight section, and nine elements in the elbow. The dry pipe thus had about 2800 DOF. As shown in Figure 3, the fluid finite element mesh had two elements (a constant strain wedge and an eight-node isoparametric hexahedron) in the radial direction between the center of the pipe and the shell. With the fluid added, the size of the 3-D model increased to about 3900 DOF.

The assumed uniform loss factor used for all calculations for this piping system was 0.0262, independent of frequency. This value was selected on the basis of previous experimental experience with similar systems.

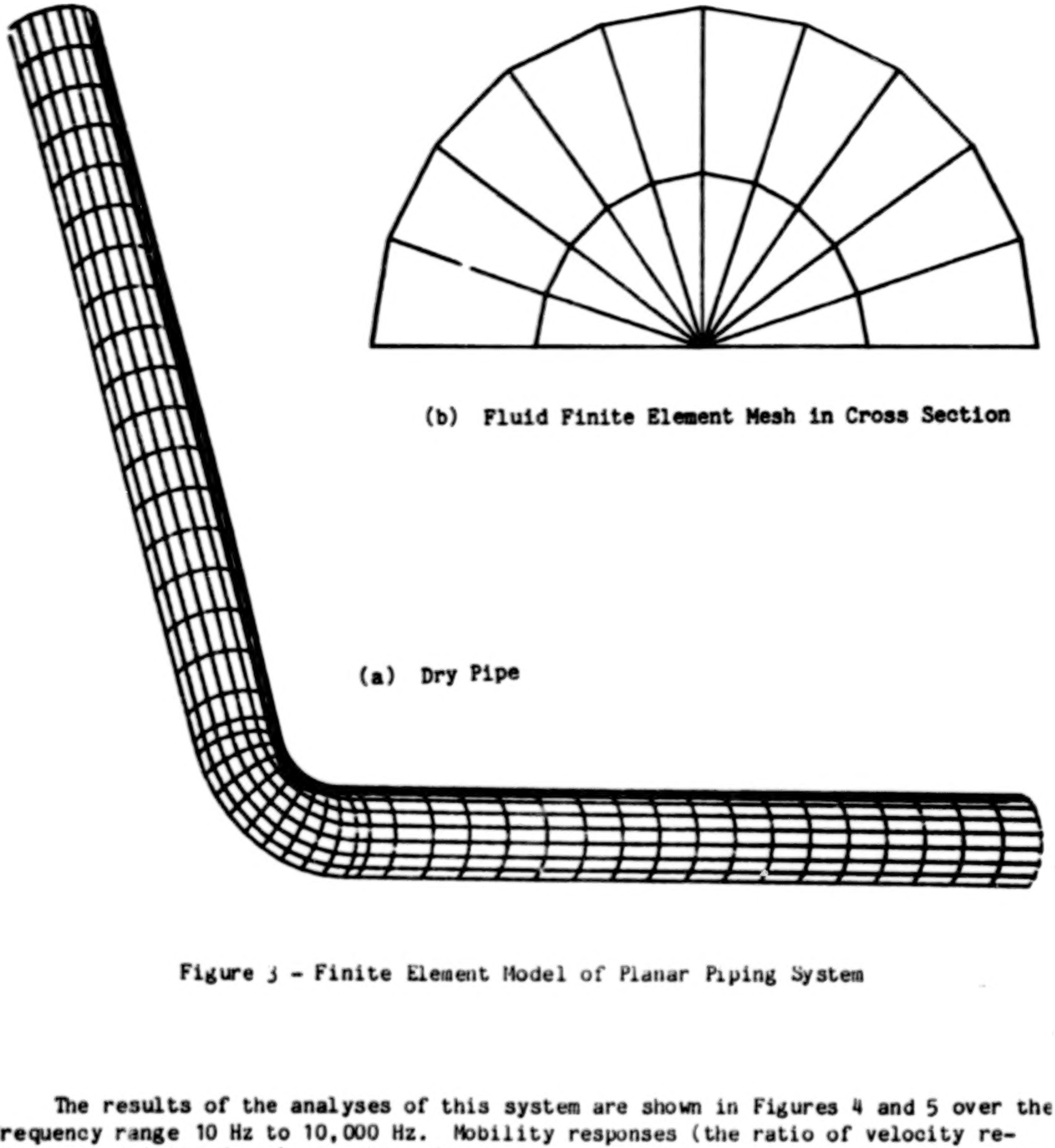

(b) Fluid Finite Element Mesh in Cross Section

(a) Dry Pipe

Figure 3 - Finite Element Model of Planar Piping System

The results of the analyses of this system are shown in Figures 4 and 5 over the frequency range 10 Hz to 10,000 Hz. Mobility responses (the ratio of velocity response to driving force) are shown for both analytical models and the Davidson-Smith experimental data (Ref. 6).

The two analytical solutions shown in Figures 4 and 5 are in reasonably good agreement even for frequencies above the first lobar (n=2) frequency, where the modal density is high. The n=2 lobar frequency for a long pipe can be estimated from the

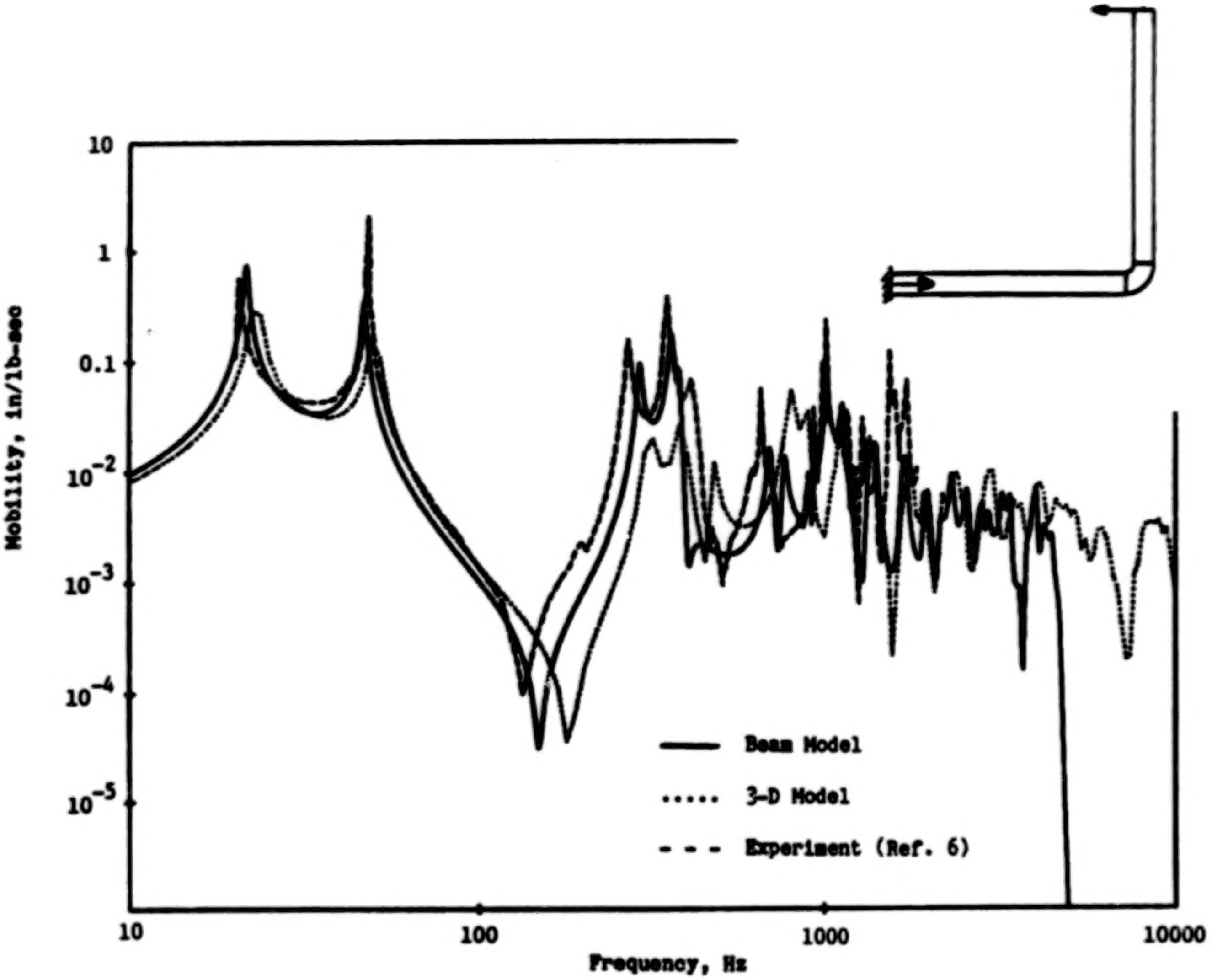

Figure 4 - Mobility of Planar Piping System: Transverse Response at Free End

classical formula (Ref. 29) for the plane strain vibrations of a ring. For a dry ring, the lowest n=2 frequency is

$$f = (1/2\pi)\sqrt{3E_s t^2/5\rho_s r^4(1-\nu^2)} \qquad (10)$$

where E_s, ρ_s, and ν are, respectively, the Young's modulus, mass density, and Poisson's ratio for the pipe material, t is the wall thickness, and r is the mean radius. Thus, from Equation (10), for 4-inch Cu-Ni pipe, the lowest n=2 lobar mode occurs at about 1066 Hz for dry pipe.

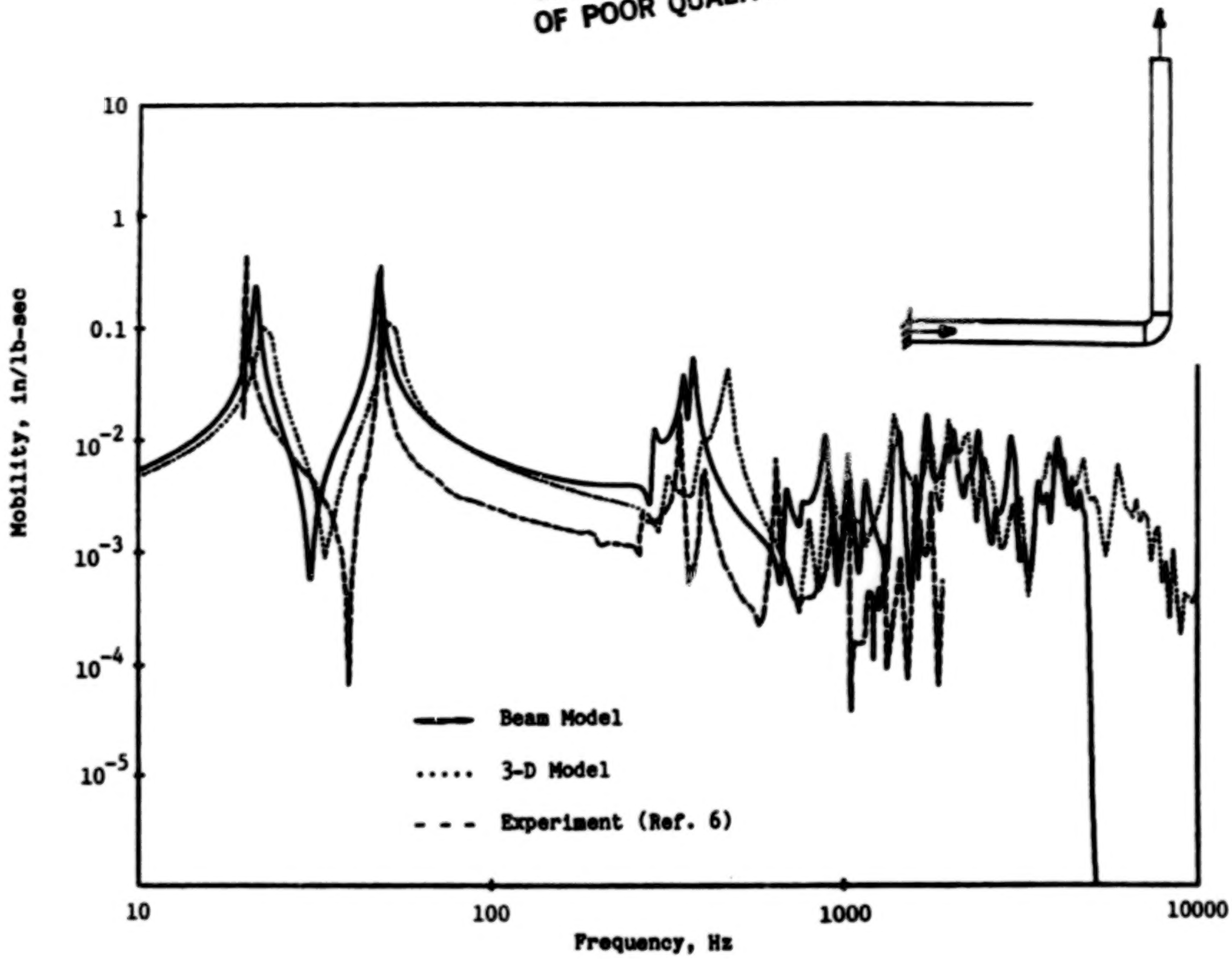

Figure 5 - Mobility of Planar Piping System: Axial Response at Free End

The corresponding fluid-filled frequency can be estimated if ρ_s in Equation (10) is replaced by the effective density ρ_{eff} for the structure-fluid combination:

$$\rho_{eff} = \rho_s + \rho r/2t \tag{11}$$

where ρ is the fluid mass density. With this correction, the lowest n=2 lobar frequency for oil-filled 4-inch Cu-Ni pipe is about 888 Hz.

EXAMPLE 2: A NON-PLANAR PIPING SYSTEM

Although the results for the planar system show good agreement between the beam results and both the 3-D results and the experimental data, this planar system does not provide an adequate test of a beam model. One difficulty which arises with non-planar systems is that the flexibility factor k is hard to calculate. Although idealized approaches for calculating k do not distinguish between inplane and out-of-plane cases, it has been shown (Ref. 14) that, for 90-degree elbows with straight pipe extensions, the out-of-plane flexibility factor differs considerably from the inplane factor. In addition, many piping systems of practical interest have straight sections which are not so long (relative to the elbow arc length) as in the planar system of Example 1. We would expect the elbow flexibilities to become more important to the overall dynamic response for systems with shorter straight sections.

Here we consider a complex 3-D piping system also built with 4-inch Cu-Ni pipe. As shown in Figure 6, the system consists of four straight sections and three elbows (two 90-degree elbows and one 45-degree elbow). The pipe is filled completely with

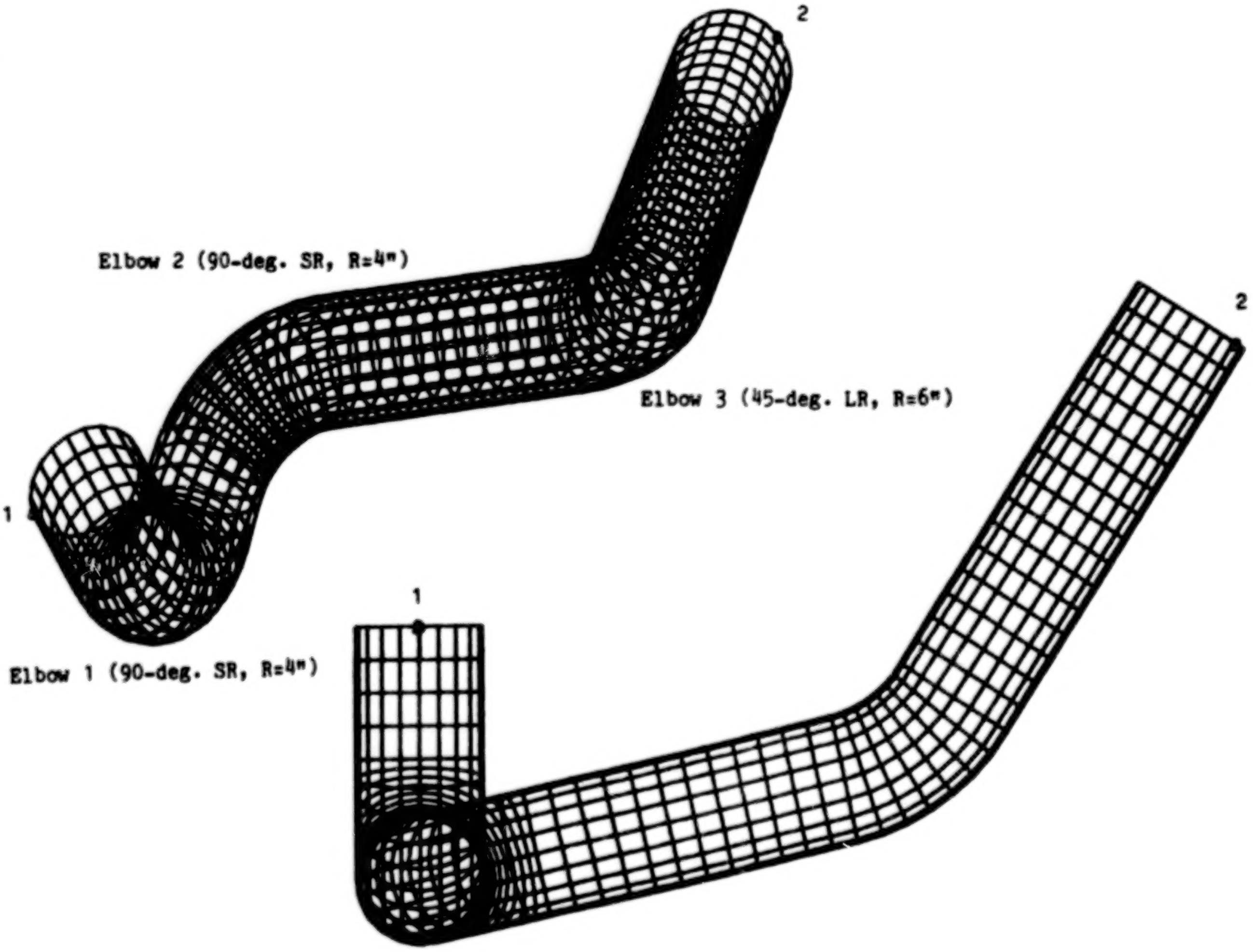
2
Elbow 2 (90-deg. SR, R=4")
2
Elbow 3 (45-deg. LR, R=6")
1
1
Elbow 1 (90-deg. SR, R=4")

Figure 6 - Finite Element Model of Non-Planar Piping System (Two Views)

fresh water. Fluid free surfaces are assumed at both ends of the system. (Experimentally, such conditions could be simulated approximately by capping the ends with flexible rubber membranes.) The loading for this system is a time-harmonic force applied to the structure in the axial direction at point 1. The entire system is assumed to be freely suspended. No experimental data are available for this system.

Both beam and 3-D finite element models were prepared for this piping system. The beam model, which consisted of 21 beam elements, had 154 DOF. The 3-D model (Figure 6) had about 7500 DOF (dry) and 9900 DOF (fluid-filled). The assumed loss factor used for both analyses was 0.02, independent of frequency.

The response predictions for this system are shown in Figures 7 and 8. Since the same pipe size is used as in the planar system, the lowest n=2 dry lobar mode occurs at the same frequency, 1066 Hz. This pipe, however, is filled with water rather than oil, so the lowest fluid-filled n=2 lobar frequency is slightly lower: 867 Hz.

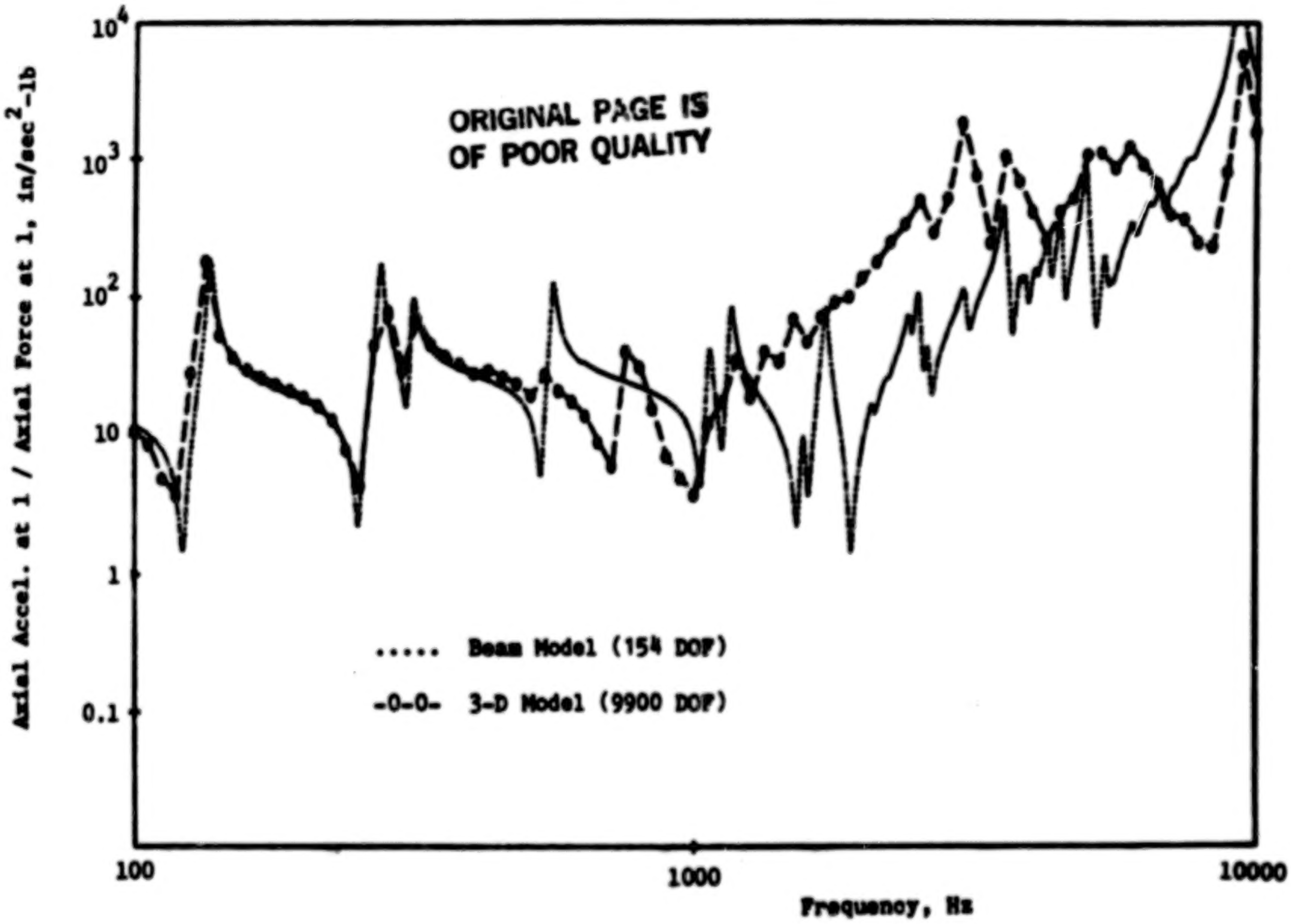

Figure 7 - Acceleration Response of Non-Planar Piping System: Drive Point Accelerance

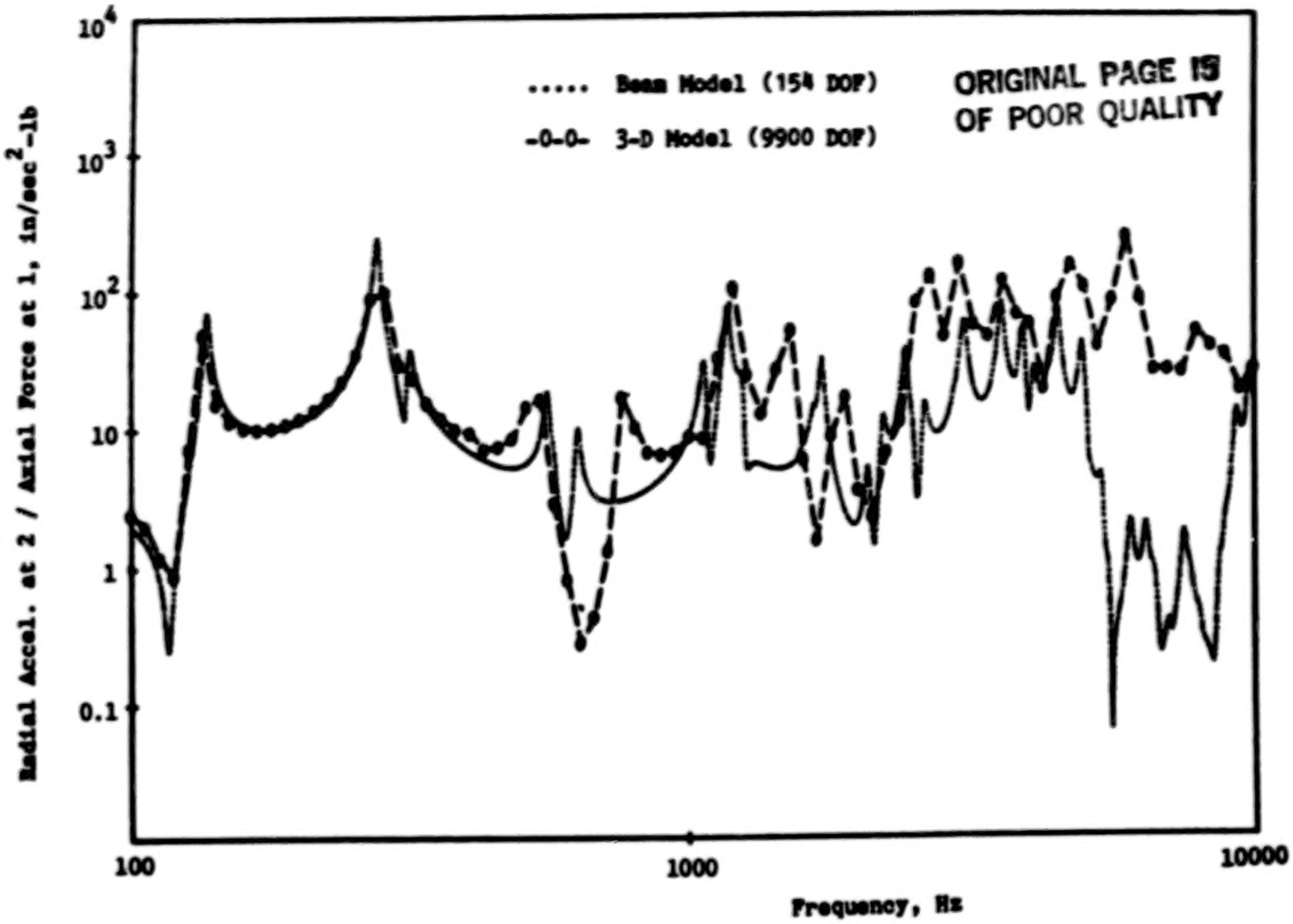

Figure 8 - Acceleration Response of Non-Planar Piping System: Transfer Point Accelerance

The flexibility factors for the 90-degree elbows in the beam model were estimated from the tables published by Quezon and Everstine (Ref. 14) for 90-degree elbows with various lengths of pipe extension. The flexibility factors for the 45-degree elbow in this system were estimated from similar tables now being compiled for 45-degree elbows. (These tables will be published soon.) The flexibility factors used in this beam analysis are listed in the second and third columns of Table 2.

As seen in Figures 7 and 8, the two analyses (beam and 3-D) are in very close agreement up to about 550 Hz, which is about 63% of the lowest n=2 fluid-filled lobar mode (867 Hz) of the pipe. This agreement indicates that the beam model is a valid model for low frequencies.

SENSITIVITY OF RESPONSE TO FLEXIBILITY FACTORS

Here we use the beam model of the non-planar piping system to determine the effects of errors in the flexibility factors used in the analysis. As we indicated

TABLE 2 - FLEXIBILITY FACTORS FOR NON-PLANAR PIPING SYSTEM

ELBOW	FLEXIBILITY FACTORS			
	BASED ON REF. 14		ELBOW PROGRAM [17]	EFFECT IGNORED
	INPLANE	OUT-OF-PLANE		
1 (90-deg. SR)	5.0	2.8	7.8	1.0
2 (90-deg. SR)	5.4	2.8	7.8	1.0
3 (45-deg. LR)	4.2	3.7	5.2	1.0

in the preceding section, the flexibility factors used were based on tables for 90-degree elbows published by Quezon and Everstine (Ref. 14) and other (as yet) unpublished tables for 45-degree elbows with various lengths of straight pipe extensions. Because the low frequency beam results using these factors agree well with the 3-D model results in Figures 7 and 8, these flexibility factors are considered reasonably accurate.

For comparison purposes, analyses were also made using two other sets of flexibility factors. The first set was that calculated by the ELBOW computer program (Ref. 17). ELBOW is probably typical of the idealized approaches used by piping designers. ELBOW's flexibility factors are in close agreement (Ref. 17) with the current ASME code (Ref. 30), which, for zero internal static pressure, uses the relation

ORIGINAL PAGE IS
OF POOR QUALITY

$$k = 1.65\ r^2/tR \tag{12}$$

where k is the flexibility factor, r is the mean radius, t is the wall thickness, and R is the bend radius. The ELBOW program flexibility factors are listed in column 4 of Table 2.

The second additional set of flexibility factors used for an analysis was obtained merely by setting k = 1.0 for all factors. This analysis would show the consequences of ignoring the flexibility factor effect entirely.

The response predictions for all three sets of flexibility factors are shown in Figure 9, in which the drive point accelerances (the ratio of acceleration to force) are plotted over the frequency range 100 Hz to 1000 Hz (the low frequency regime). Figure 9 clearly indicates the importance of using accurate flexibility factors in the analysis.

DISCUSSION AND CONCLUSIONS

We have described two different finite element modeling procedures for predicting the dynamic response of general 3-D fluid-filled elastic piping systems. The beam model, a low frequency procedure, was, for the non-planar system considered,

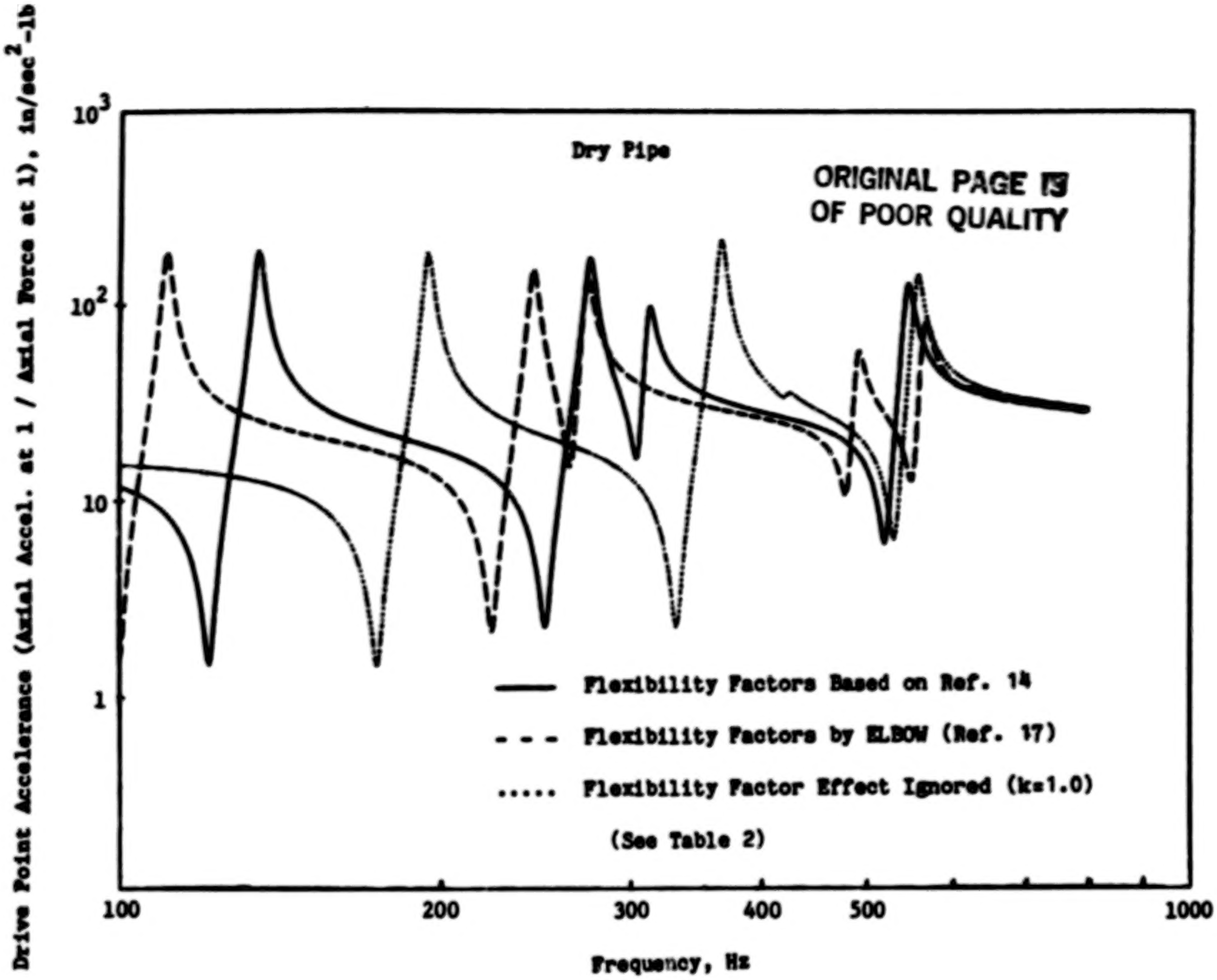

ORIGINAL PAGE IS OF POOR QUALITY

Figure 9 - Sensitivity of Non-Planar Piping System Response to Flexibility Factor

valid for frequencies up to about 63% of the lowest fluid-filled lobar (n=2) pipe mode. For frequencies between that and 100% of the n=2 mode, the general finite element modeling procedure described could be used. For still higher frequencies, where the modal density is high, the finite element approach remains theoretically valid, but the analyst is probably wiser to use statistical energy analysis (S.E.A.) techniques (Ref. 31) instead. The S.E.A. techniques are particularly well suited to the high modal density regime.

It was shown that the accuracy of beam analyses of piping systems depends strongly on the accuracy of the flexibility factors used. Such factors are not required in the 3-D finite element model since they are implicit in a shell model of the pipe.

Finally, the beam analyses presented here used straight beams to model the bends (elbows). It would clearly be preferable to use instead curved beam elements, if available.

REFERENCES

1. Callaway, D.B., F.G. Tyzzer, and H.C. Hardy, "Resonant Vibrations in a Water-Filled Piping System," Journal of the Acoustical Society of America, vol. 23, no. 5, pp. 550-553 (1951).

2. El-Raheb, M., "Acoustic Propagation in Finite Length Elastic Cylinders. Part I: Axisymmetric Excitation," Journal of the Acoustical Society of America, vol. 71, no. 2, pp. 296-306 (1982).

3. El-Raheb, M., "Acoustic Propagation in Finite Length Elastic Cylinders. Part II: Asymmetric Excitation," Journal of the Acoustical Society of America, vol. 71, no. 2, pp. 307-317 (1982).

4. Joppa, P.D., and I.M. Fyfe, "A Finite Element Analysis of the Impedance Properties of Irregular Shaped Cavities with Absorptive Boundaries," Journal of Sound and Vibration, vol. 56, no. 1, pp. 61-69 (1978).

5. Astley, R.J., and W. Eversman, "A Finite Element Method for Transmission in Non-Uniform Ducts Without Flow: Comparison with the Method of Weighted Residuals," Journal of Sound and Vibration, vol. 57, no. 3, pp. 367-388 (1978).

6. Davidson, L.C., and J.E. Smith, "Liquid-Structure Coupling in Curve Pipes," The Shock and Vibration Bulletin, bulletin 40, part 4, pp. 197-207 (1969).

7. Davidson, L.C., and D.R. Samsury, "Liquid-Structure Coupling in Curved Pipes - II," The Shock and Vibration Bulletin, bulletin 42, part 1, pp. 123-136 (1972).

8. Howlett, J.T., "Applications of NASTRAN to Coupled Structural and Hydrodynamic Responses in Aircraft Hydraulic Systems," NASTRAN: Users' Experiences, NASA TM X-2378, National Aeronautics and Space Administration, Washington, DC, pp. 407-419 (1971).

9. The M.W. Kellogg Company, Design of Piping Systems, second edition, John Wiley and Sons, Inc., New York (1964).

10. El-Raheb, M., "Vibrations of Three-Dimensional Pipe Systems with Acoustic Coupling," Journal of Sound and Vibration, vol. 78, no. 1, pp. 39-67 (1981).

11. Schwirian, R.E., and M.E. Karabin, "Use of Spar Elements to Simulate Fluid-Solid Interaction in the Finite Element Analysis of Piping System Dynamics," Fluid Transients and Structural Interactions in Piping Systems (edited by P.H. Rothe and D.C. Wiggert), The American Society of Mechanical Engineers, New York (1981).

12. Hatfield, F.J., and D.C. Wiggert, "Fluid-Structure Interaction in Piping by Component Synthesis," Fluid Transients and Structural Interactions in Piping Systems (edited by P.H. Rothe and D.C. Wiggert), The American Society of Mechanical Engineers, New York (1981).

13. Rodabaugh, E.C., S.K. Iskander, and S.E. Moore, "End Effects in Elbows Subjected to Moment Loadings," Report ORNL/Sub-2913/7, Oak Ridge National Laboratory, Oak Ridge, Tennessee (1978).

14. Quezon, A.J., and G.C. Everstine, "Stress Indices and Flexibility Factors for 90-Degree Piping Elbows with Straight Pipe Extensions," DTNSRDC/-CMLD-82/05, David W. Taylor Naval Ship R&D Center, Bethesda, MD (1982).

15. Zienkiewicz, O.C., and R.E. Newton, "Coupled Vibrations of a Structure Submerged in a Compressible Fluid," Proceedings of the International Symposium on Finite Element Techniques, Stuttgart, pp. 359-379 (1969).

16. Everstine, G.C., "A Symmetric Potential Formulation for Fluid-Structure Interaction," Journal of Sound and Vibration, vol. 79, no. 1, pp. 157-160 (1981).

17. Dodge, W.G., and S.E. Moore, "ELBOW: A Fortran Program for the Calculation of Stresses, Stress Indices, and Flexibility Factors for Elbows and Curved Pipe," Report ORNL-TM-4098, Oak Ridge National Laboratory, Oak Ridge, Tennessee (1973).

18. Streeter, V.L., Fluid Mechanics, third edition, McGraw-Hill Book Company, Inc., New York (1962).

19. Krause, N., W. Goldsmith, and J.L. Sackman, "Transients in Tubes Containing Liquids," International Journal of Mechanical Sciences, vol. 19, no. 1, pp. 53-68 (1977).

20. Joukowsky, N., "Uber den Hydraulischen Stoss in Wasserleitungsrohren," Memoir de l'Academie, vol 9, 8 Ser., no. 5 (1900).

21. Gantayat, A.N., and G.H. Powell, "Stress Analysis of Tee Joints by the Finite Element Method," Report US SESM 73-6, Structural Engineering Laboratory, University of California, Berkeley, California (1973).

22. Quezon, A.J., and G.C. Everstine, "Comparison of Finite Element Analyses of a Piping Tee Using NASTRAN and CORTES/SA," Ninth NASTRAN Users' Colloquium, NASA CP-2151, National Aeronautics and Space Administration, Washington, DC, pp. 224-242 (1980).

23. Ross, D., Mechanics of Underwater Noise, Pergamon Press, Inc., New York (1976).

24. Hamdi, M.A., Y. Ousset, and G. Verchery, "A Displacement Method for the Analysis of Vibrations of Coupled Fluid-Structure Systems," International Journal for Numerical Methods in Engineering, vol. 13, no. 1, pp. 139-150 (1978).

25. Everstine, G.C., "Structural Analogies for Scalar Field Problems," International Journal for Numerical Methods in Engineering, vol. 17, no. 3, pp. 471-476 (1981).

26. Everstine, G.C., E.A. Schroeder, and M.S. Marcus, "The Dynamic Analysis of Submerged Structures," *NASTRAN: Users' Experiences*, NASA TM X-3278, National Aeronautics and Space Administration, Washington, DC, pp. 419-429 (1975).

27. Everstine, G.C., "Finite Element Solution of Torsion and Other 2-D Poisson Equations," *Tenth NASTRAN Users' Colloquium*, NASA CP-2249, National Aeronautics and Space Administration, Washington, DC, pp. 153-164 (1982).

28. Everstine, G.C., "Structural-Acoustic Finite Element Analysis, with Application to Scattering," Proceedings of the Sixth Invitational Symposium on the Unification of Finite Elements, Finite Differences, and Calculus of Variations (edited by H. Kardestuncer), University of Connecticut, Storrs, CT, pp. 101-122 (1982).

29. Den Hartog, J.P., *Mechanical Vibrations*, fourth edition, McGraw-Hill Book Company, Inc., New York (1956).

30. American Society of Mechanical Engineers, "ASME Boiler and Pressure Vessel Code. Section III, Rules for Construction of Nuclear Power Plant Components" (1980 edition).

31. Lyon, R.H., *Statistical Energy Analysis of Dynamical Systems: Theory and Applications*, MIT Press, Cambridge, Massachusetts (1975).

N84
15601

UNCLAS

N84 15601 D11

PROPAGATING PLANE HARMONIC WAVES THROUGH FINITE LENGTH PLATES OF VARIABLE THICKNESS USING FINITE ELEMENT TECHNIQUES

J. H. Clark, A. J. Kalinowski, C. A. Wagner

NAVAL UNDERWATER SYSTEMS CENTER
NEW LONDON, CONNECTICUT 06320

SUMMARY

Closed form solutions exist in the literature for propagating plane harmonic waves through infinitely long uniformly thick plates which are immersed in fluids. These solutions fail to account for the edge effects present in finite length plates and address only plates of uniform thickness. This paper presents an analysis using finite element techniques which addresses the propagation of a uniform incident pressure wave through a finite diameter axisymmetric tapered plate immersed in a fluid. The approach utilized in developing a finite element solution to this problem is based upon a technique for axisymmetric fluid structure interaction problems presented in the Tenth NASTRAN Conference (ref. 1).

The problem addressed in this paper is that of a 10 inch diameter axisymmetric fixed plate totally immersed in a fluid. The plate increases in thickness from approximately 0.01 inches thick at the center to 0.421 inches thick at a radius of 5 inches. Against each face of the tapered plate a cylindrical fluid volume has been represented extending five wavelengths off the plate in the axial directon. The outer boundary of the fluid and plate regions have been represented as a rigid encasement cylinder as was nearly the case in the physical problem.

The primary objective of the analysis is to determine the form of the transmitted pressure distribution on the downstream side of the plate. A secondary purpose is to demonstrate the feasibility of employing the ref. 1 fluid-structure interaction technique on a large D.O.F. problem, and in fact running this large problem uncovered a basic error in the NASTRAN coding for 32 bit machines (e.g., VAX or IBM 360, 370, or 3033) when employing MPC or DMIG cards. These errors could impact any rigid format.

The finite element model used consists of 7455 nodes comprising 7191 axisymmetric ring elements. Both the fluid and the plate structure have been represented using axisymmetric CTRAPAX and CTRIAAX elements. The fluid (seawater) elements and structure (plate) elements are linked together along their boundary by utilizing a duplicate set of nodes and a direct matrix insertion capability within NASTRAN. This enables the incorporation of the stiffness and mass coupling terms in the stiffness and mass matrices respectively.

The plate is loaded with a uniform harmonic pressure wave (f = 100,000 Hz)

which propagates axially through the incident side fluid, into the plate, and then out into the transmitted side fluid.

Presented results consist of plots of pressure along both the incident and transmitted surfaces of the tapered plate. In addition, pressure and phase contours throughout the modeled fluids are presented.

SYMBOLS

Values are given in both SI and U.S. Customary Units. The measurements and calculations were made in U.S. Customary Units.

ΔA = associated area (eq. (1))

c = value of term entered on diagonal of damping matrix

c_f = sound wave velocity in fluid

f = frequency of propagating wave

k_f = bulk modulus of the acoustic fluid

n_r = normal to a surface in radial direction

n_z = normal to a surface in axial direction

U_z = displacement in axial direction

ρ_f = mass density of acoustic fluid

INTRODUCTION

Sternberg, et al., (ref. 2) have experimentally demonstrated the frequency independent characteristics of acoustic filter plates with regards to beamforming characteristics. Mathematical approaches have been undertaken to analytically account for this phenomena with varying degrees of success. The objective of this project was to utilize the finite element method to model the transmission of a plane harmonic wave through a filter plate of variable thickness immersed in sea water. This filter plate effect, if used in conjunction with an acoustic lens, develops beams which are independent of frequency and of constant width. A typical configuration is shown in Figure 1 and has been experimentally tested.

The analysis presented accounts for the rigid containment cylinder, the tapered circular steel filter plate, the transmission side fluid inside the containment cylinder and the incident side fluid which theoretically extends to infinity. The rubber acoustic lens discussed briefly above has been excluded from this analysis in order to isolate the effects of the filter plate.

Since the actual structure is axisymmetric the finite element model utilized is also axisymmetric. The filter plate has been analyzed by using the displacement method within NASTRAN. The fluid has been modeled in accordance with an axisymmetric pressure analogy (ref. 1). The driving force consists of a plane harmonic wave at 100 kHz at normal incidence to the steel plate. Pressure and phase distributions throughout the incident and transmitted fluid volumes are to be computed. To enhance the presentation of the rather extensive pressure and phase data, pressure and phase contours throughout the internal and external fluid have been presented. In addition, plots of pressure along the incident and transmitted surfaces of the filter plate are presented.

Model Development

As detailed in ref. 1 the development of a finite element model for any axisymmetric fluid structure interaction problem requires several steps. For large degree of freedom problems model sizing, element sizing, and element selection are reasonably straightforward, however, they must be addressed cautiously in order to avoid both technical misjudgments and excessive computer cost.

I. Sizing. The particular piece of hardware modeled is well defined. As shown in Figure 2 the encasement cylinder is 5" (12.7 cm) in length and 0.5" (1.27 cm) thick. The filter plate is 10" (25.4 cm) in diameter and tapers from .08" (0.203 cm) at the center to 0.421" (1.06 cm) at a 4" (10.16 cm) radius. The location of the driving surface is 2.5" (6.35 cm) away from the filter plate surface and at the end of the containment cylinder. The area between the filter plate and driving surface is fluid filled. On the downstream side the modeled fluid extends to the end of the containment cylinder. The fluid within the containment cylinder extends 4 wavelengths off the plate.

The important aspect relating to element sizing for steady state fluid structure interaction problems is that the distribution of nodes throughout the model be such that plane harmonic waves at the frequency of interest can adequately be described. As developed in ref. 3 adequate representation of the pressure waves is ensured by using ten nodes per wavelength or in this case where f = 100 kHz the node spacing becomes 0.06" (0.152 cm). This is based upon a wave propagation velocity in seawater of 60000 in/sec (152400 cm/sec). With node spacings this small and a model geometry as described above, the number of degrees of freedom approaches the limits of COSMIC NASTRAN on the VAX 11/780.

Since an axisymmetric pressure analogy solution has been invoked for the fluid elements, the selection of mating element type is limited. Several axisymmetric elements exist within COSMIC NASTRAN, however, previous success with CTRAPAX and CTRIAAX elements determined selection. These elements have been used to represent both the fluid and filter plate. As will be discussed in the next section, the containment cylinder and driving surfaces are represented as boundary or load conditions. The finite element model developed according to the above discussion is shown in Figure 3.

II. Boundary Condition. The boundary condition addressed next is the coupling of the fluid elements (modeled within an axisymmetric pressure analogy) to the structure elements (modeled within the displacement method). This coupling when using axisymmetric elements requires duplicate nodes along any fluid structure boundary. These duplicate nodes are then utilized in formulating the off diagonal coupling terms within both the mass and stiffness matrices for each of the elements involved. The details of the coupling proocedure are given in ref. 1 and are not repeated here.

The mass terms are given as, $- A^{w} \rho_f k_f n_r$ and $- A^{w} \rho_f k_f n_z$ (1)

and stiffness terms are given as, $\Delta A \, n_r$ and $\Delta A \, n_z$

The physical nature of the filter plate hardware enables representation of the cylindrical containment cylinder as a rigid outer fluid boundary condition, and is expressed as

$$\frac{\partial p}{\partial n} = 0$$

where p is the fluid pressure.

This boundary condition is implemented within the pressure analogy by freeing all constraints along the containment cylinder/fluid interface (i.e., no surface tractions).

The external fluid boundary is terminated with fluid dampers in such a way that the fluid appears to extend to mathematical infinity. Since NASTRAN does not contain any axisymmetric dashpot elements, this effect was developed using a direct matrix insertion technique similar to that required along the fluid/structure boundary. To each node along the fluid boundary the magnitude of the lumped damping term to be inserted in the damping matrix is given as

$$c = \frac{\Delta A^{b} k_f}{c_f}$$

As with the stiffness and mass terms described previously, the location of the damping term within the damping matrix is developed in ref. 1.

III. Loading. Plane harmonic pressure waves will be the predominant load type seen by the filter plate. The plane harmonic wave utilized in this problem is at a frequency of 100 kHz and has a magnitude of 1 psi (6895 P). This wave emanates from the outer fluid boundary parallel to the flat metal surface and impinges on the filter plate at normal incidence. The boundary conditions and loading scheme are shown in Figure 3.

DISCUSSION

Initial attempts to execute NASTRAN and develop solutions for the pressure field resulting from the tapered filter plate were unsuccessful. Several out of the ordinary problems were encountered while making these initial checkout computer runs. The first of these relates to the use of the DMIG card or MPC card option with larger problems on a 32 bit machine (in this case the VAX 11/780).

After considerable time and expense, it was discovered that the problem arises when a model has a large number of nodes such that the combined row and column internal node number exceeds 2^{32} (the 32 bit word can no longer represent an unsigned integer of this size). As a result when NASTRAN attempts to order the list of row and column ID's in a monitonically increasing order, the large internal node numbers actually appear as smaller negative numbers because the sorting routine processes the 32nd bit as a plus or minus sign. As a result the DMIG card coupling terms were arbitrarily associated with a node elsewhere in the matrix thus voiding the coupling effect. Coding changes were suggested by RPK Corporation and ultimately corrected this error. The coding change alters the internal node sorting routine in such a way that the 32nd bit is read as part of the node number and not as a plus (+) or minus (-) sign. Subsequent runs demonstrated proper placement of the DMIG card coupling terms.

The second, less serious problem encountered relates to the mass distribution for elements which are very close to the centerline.

NASTRAN calculates the lumped mass of any axisymmetric element by first determining the centroid of the elements nodes. This radius is then used to determine the circumference of the ring element. Knowing the length and height of the element then enables a determination of the area and therefore mass of the entire ring element. This mass is allocated equally to each of the four nodes comprising the elements connectivity. For large radii this allocation scheme is very accurate, however, when the radius to the centroid of the element is less than five times the node spacing significant errors result (as much as 40%). This error has been corrected by using the elements outer and inner radii to calculate ring areas relative to the centroidal radius. This divides each ring element into an outer annulus and an inner annulus. The mass of the outer annulus is allocated to the two outer annulus nodes. The mass of the inner annulus is allocated to the two inner nodes. The FORTRAN coding changes made to the TRAPAD and TRIAAD subroutine in NASTRAN are shown in Figures 4 and 5. The lines that have changes are mainly in the lines without the column 73-80 card number designators.

RESULTS

The NASTRAN solution to a steady state fluid structure interaction problem consists of the pressure and phase distribution throughout the fluid. For very large problems this data is cumbersome to interpret, consequently two data presentations have been developed. The first consists of a plot of the pressure along the upstream and downstream sides of the tapered metal plate. This data shown in Figures 6 and 7 show several areas of higher pressure transmission through the tapered plate. The major peak to peak fluxuations along the plate surface in the pressure plots correlate with the submerged plate flexure wavelengths existing in a constant-thickness submerged plate whose thickness is the average type thickness.

A finer mesh distribution radially along the centerline is needed in order to properly model the stiffness in the plate and thus pick up the transmitted pressure. This is why the transmitted and incident pressures are too large at the centerline. Subsequent runs with a fluid plate (field solution is known) demonstrated that this error near the centerline was localized to two or three elements.

A second and, in this case, more useful presentation of this data is a color graphics format of pressure and phase contours. Pressure contours are shown in Figure 8. A noticeable effect depicted by these pressure contours is the redirection or focusing of the pressure towards the centerline. Equally important, the appearance of annular regions of increased energy transmission are evident. There are regions where more energy transmits through the plate than in similar neighboring regions. The phase contour shown in Figure 9 is evidence of the transmission of an actual plane wave from the driving boundary through the incident side fluid. The bands of constant and repeating phase angles verify this plane wave. The discontinuities in the phase contours in the downstream fluid correlate with certain redirected pressure contours evident in Figure 8. These acoustic characteristics of filter plates, while experimentally verified, have not been readily predictable. The technique utilized here establishes a reasonable prediction capability. The development of a predictive capability for both the redirection of the pressure field and the regions of higher energy transmission were objectives of this effort.

REFERENCES

1. Kalinowski, A. J., and Nebelung, C. W., "Solution of Axisymmetric Fluid Structure Interaction Problems with NASTRAN" (U), 10th NASTRAN User's Colloquium, NASA CONF Publication 2249, 1982.

2. Sternberg, R. L., and Anderson, W. A., "A Comparison of the Useful Aperture Diameter, Directivity Index and Beam Width for an Acoustic Lens and an Acoustic Lens-Acoustic Filter Plate Combination", Naval Underwater Systems Center Technical Memorandum No. 771187.

3. Kalinowski, A. J., and Nebelung, C. W., "Media-Structure Interaction Computation Employing Frequency Dependent Mesh Sizes with the Finite Element Method", Shock and Vibration Bulletin, Vol. 51, 1981.

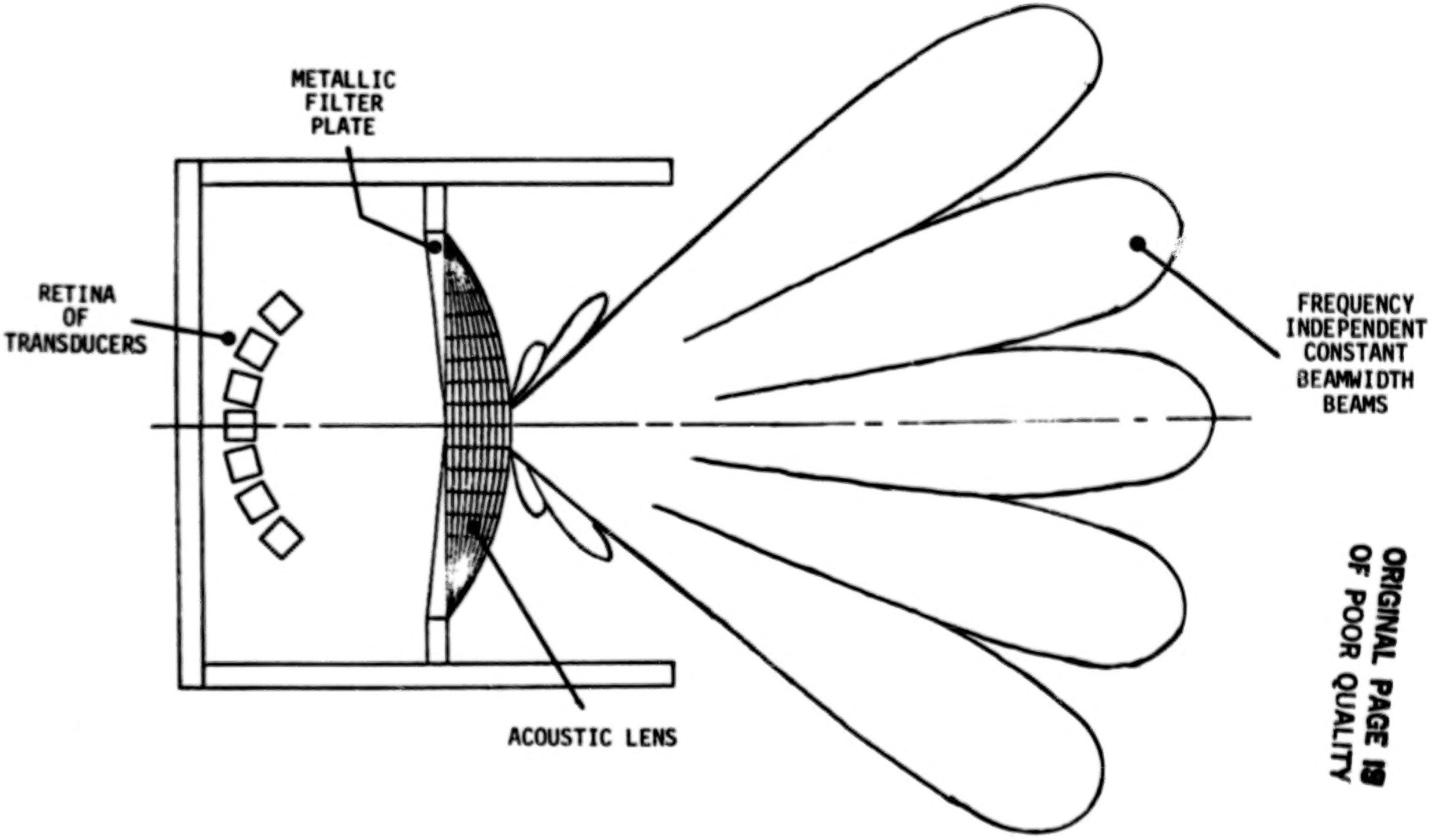
METALLIC FILTER PLATE
RETINA OF TRANSDUCERS
FREQUENCY INDEPENDENT CONSTANT BEAMWIDTH BEAMS
ACOUSTIC LENS

FIGURE 1 A TYPICAL TAPERED FILTER PLATE AND ACOUSTIC LENS CONFIGURATION

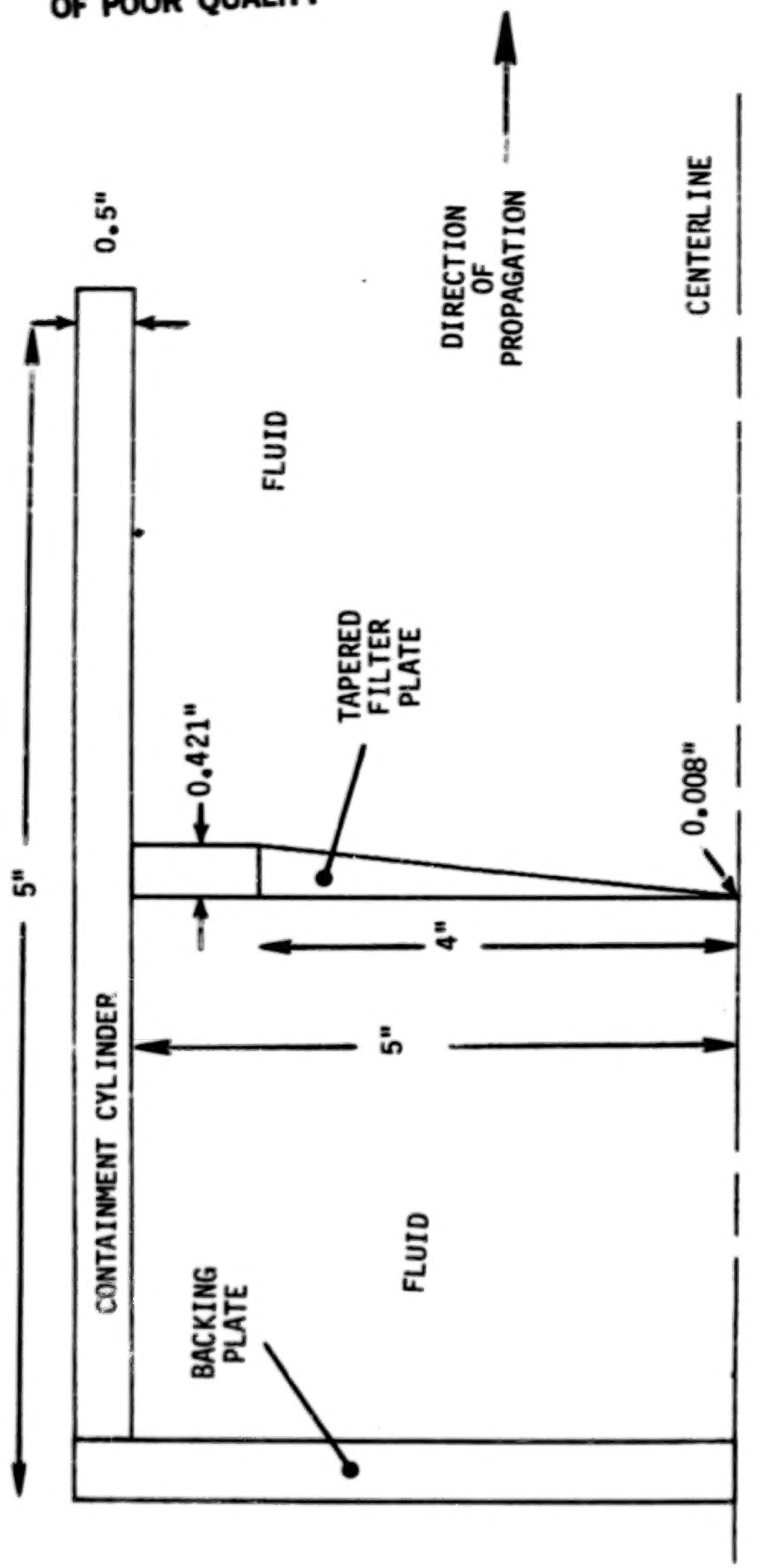
0.5"
5"
DIRECTION OF PROPAGATION
CENTERLINE
FLUID
TAPERED FILTER PLATE
0.421"
0.008"
4"
5"
CONTAINMENT CYLINDER
FLUID
BACKING PLATE

FIGURE 2. THE TAPERED FILTER PLATE AND ASSOCIATED HARDWARE

ORIGINAL PAGE IS
OF POOR QUALITY

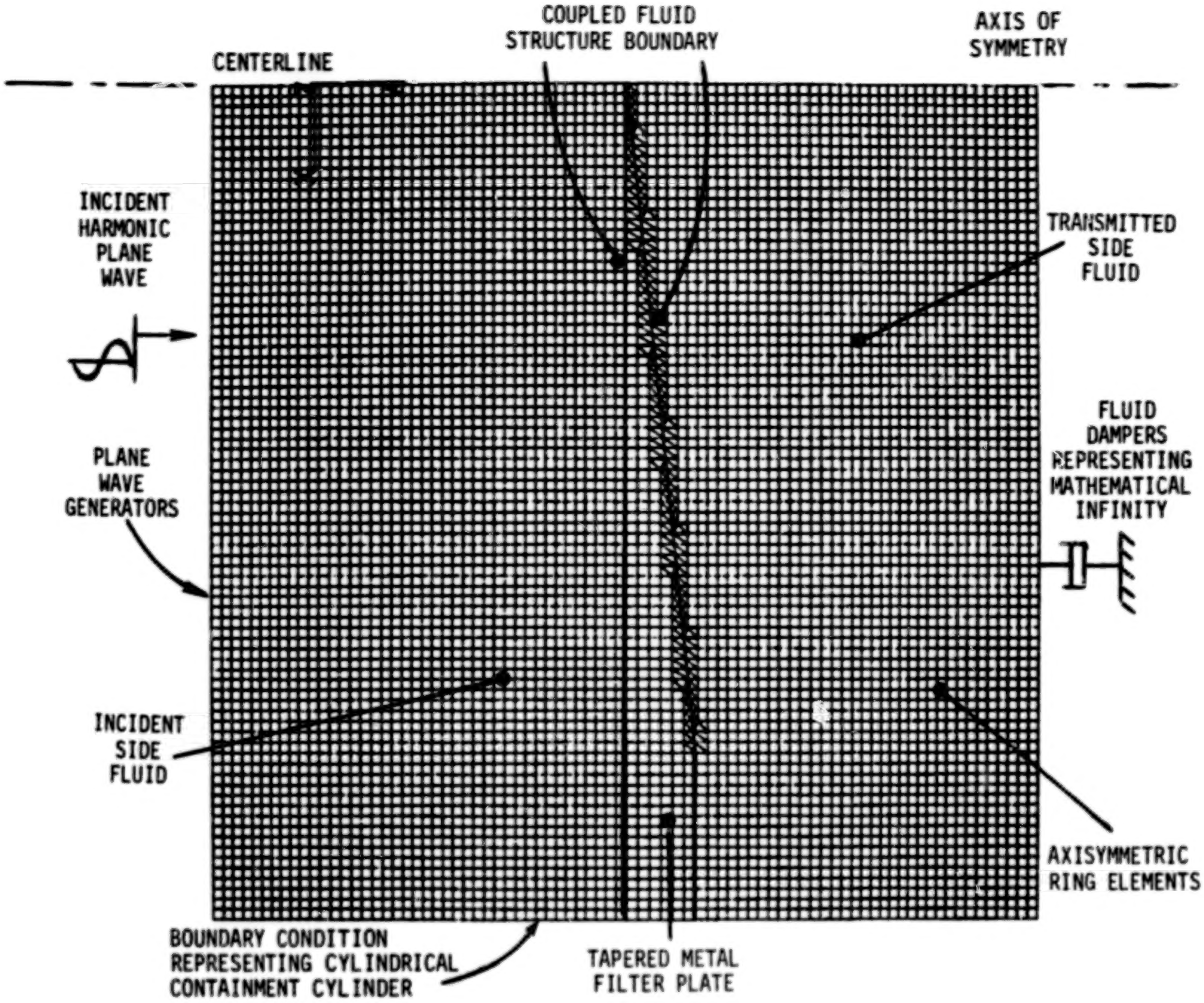
COUPLED FLUID
STRUCTURE BOUNDARY
AXIS OF
SYMMETRY
CENTERLINE
INCIDENT
HARMONIC
PLANE
WAVE
TRANSMITTED
SIDE
FLUID
FLUID
DAMPERS
REPRESENTING
MATHEMATICAL
INFINITY
PLANE
WAVE
GENERATORS
INCIDENT
SIDE
FLUID
AXISYMMETRIC
RING ELEMENTS
BOUNDARY CONDITION
REPRESENTING CYLINDRICAL
CONTAINMENT CYLINDER
TAPERED METAL
FILTER PLATE

FIGURE 3. A FINITE ELEMENT MODEL OF THE TAPERED FILTER PLATE, SURROUNDING FLUID, AND STRUCTURAL BOUNDARIES

```
 ..                      ,.ZS2,C2,S2,C4,..,..  . . ..,AUJPO,RHOD       00000420
5,                       AR, SKI                                       00000430
6,R2P,R3P,Z2P,Z3P,AR14,FMAST,FMAS14,FMAS23,FNMASS(4)
 DIMENSION  IECPT(30),ICS(4),ECPT(20),NODNUM(4),JECPT(5)               00000440
                      ..R(14) ..                                       00000450

 EQUIVALENCE (ECPT(..,     ....,IDEL),(BMASS(1,..,..KI(1)),BMBSS(1))00000680
 EQUIVALENCE (DICT5,DICT(5))                                           00000690
 EQUIVALENCE (IBADEL,ECPT(1))
 EQUIVALENCE (JECPT(2),ECPT(2)),(JECPT(3),ECPT(3)),(JECPT(4),
1ECPT(4)),(JECPT(5),ECPT(5))
 ISORT = 0                                                             00000700
 MASO.                                                                 0000071


C                                                                      00004670
C         GENERATE LUMPED MASS MATRIX HERE                             00004680
C                                                                      00004690
 670      JFILL=0
      DO 680 I=1,3                                                     00004700
C*****
C       CHANGES AS PER AJK 10/12/82
C*****
      NMINXX=MINO(NODNUM(1),NODNUM(2),NODNUM(3))
      DO 9999 JJ=1,3
C*****
C       SORT NODE NUMBERS ACCORDING TO SIZE - SMALLEST FIRST
C*****
      IF (NMINXX.EQ.NODNUM(JJ)) GO TO 9998
      GO TO 9999
 9998 JFILL=JFILL+1
      JFIL2=JJ
      GO TO 9997
 9999 CONTINUE
      WRITE(6,9992)JFIL2,IBADEL
 9992 FORMAT(1X,' HAVING TROUBLE FILLING LUMPED MASS MATRIX IN TRIAAD SU
     1BROUTINE,  JFILL =',I20,4X,'EL NUMBER =',I20)
 9997 AKJM((JFILL-1)*3+1)=FNMASS(JFIL2)
      AKJM((JFILL-1)*3+2)=FNMASS(JFIL2)
      AKJM((JFILL-1)*3+3)=FNMASS(JFIL2)
C*****
C       STRIKE NODE OUT OF ORDERING (LOW TO HIGH) OPERATION
C*****
      NODNUM(JFIL2)=1E+9




C*****
C       END CHANGES
C*****
 680  CONTINUE
      DICT(2) = 2                                                      00004720
C                                                                      00004730
      CALL EMGOUT(AKJM,AKJM,9,1,DICT ..                                00004740
      RETURN                                                           0000..
```

FIGURE 4 FORTRAN CODING CHANGES IN NASTRAN SUBROUTINE TRAPAD FOR CTRAPAX ELEMENTS

ORIGINAL PAGE IS
OF POOR QUALITY

```
C     LUMPED MASS CALCULATIONS HANDLED HERE
C
  900 AR= (R(1)*(Z(2)-Z(4)) + R(2)*(Z(3)-Z(1)) + R(3)*(Z(4)-Z(2))+
     X      R(4)*(Z(1)-Z(3)))/ 2.
C *** AKJ(1) = RHOD*(R(1)+R(2)+R(3)+R(4))/4. * AR
C *** AKJ(1)=AKJ(1)/4.0D0
C *** DO  920  I=2,12
C 920 AKJ(I) = AKJ(1)
C
C
C FMAS14 = MASS OF HALF NEAR CENTERLINE
C FMAS23 = MASS OF HALF AWAY FROM CENTERLINE
C
      R3P = (R(4) + R(3))/2.0D0
      R2P = (R(1) + R(2))/2.0D0
      Z3P = (Z(4) + Z(3))/2.0D0
      Z2P = (Z(1) + Z(2))/2.0D0
      AR14 = (R(1)*(Z2P - Z(4)) + R2P*(Z3P - Z(1))
     $       + R3P*(Z(4) - Z2P)  + R(4)*(Z(1) - Z3P))/2.0D0
      FMAST = RHOD*(R(1) + R(2) + R(3) + R(4))*AR/4.0D0
      FMAS14 = RHOD*(R(1) + R2P + R3P + R(4))*AR14/4.0D0
      FMAS23 = FMAST - FMAS14
C*****
C        CHANGES AS PER AJK 10/12/82
C*****
C        COMPUTE LUMPED MASS AT NODES A,B,C,D (I.E.  1,2,3,4)
      FNMASS(1)=FMAS14/2.0D0
      FNMASS(2)=FMAS23/2.0D0
      FNMASS(3)=FMAS23/2.0D0
      FNMASS(4)=FMAS14/2.0D0
      NODNUM(1)=JECPT(2)
      NODNUM(2)=JECPT(3)
      NODNUM(3)=JECPT(4)
      NODNUM(4)=JECPT(5)
C      WRITE(6,*)'  NODNUM IN TRAPAD',NODNUM(1),NODNUM(2),NODNUM(3),
C     1NODNUM(4)
      JFILL=0
      DO 920 I=1,4
      NMINXX=MINO(NODNUM(1),NODNUM(2),NODNUM(3),NODNUM(4))
      DO 9999 JJ=1,4
C*****
C        SORT NODE NUMBER ACCORDING TO SIZE (SMALLEST FIRST)
C*****
      IF(NMINXX.EQ.NODNUM(JJ)) GO TO 9998
      GO TO 9999
 9998 JFILL=JFILL+1
      JFIL2=JJ
      GO TO 9997
 9999 CONTINUE
      WRITE(6,9992)JFIL2,IPADEL
 9992 FORMAT(1X,' HAVING TROUBLE FILLING LUMPED MASS MATRIX IN TRAPAD SU
     1BROUTINE',I20,4X,'EL NUMBER',I20)
 9997 AKJ((JFILL-1)*3+1)=FNMASS(JFIL2)
      AKJ((JFILL-1)*3+2)=FNMASS(JFIL2)
      AKJ((JFILL-1)*3+3)=FNMASS(JFIL2)
C*****
C        STRIKE NODE OUT OF ORDERING (LOW TO HIGH) OPERATION
C*****
      NODNUM(JFIL2)=1E+9
  920 CONTINUE
 ***
       END THIS SET OF CHANGES

        (1)= ESTID
```

FIGURE 4 FORTRAN CODING CHANGES IN NASTRAN SUBROUTINE TRAPAD FOR CTRAPAX ELEMENTS

```
     4,                  [illegible]                                   00000400
     5,                  GOR,GZO,GRZ,VOR,VZO,VRZ,DEL,DKL,C4,S2,S4 ,DGAMR  00000410
     6,                  AJHO,AJJHO,RHOD,DGAMAR,CONVM,AREA,C2S2          00000420
C*****
C       CHANGES AS PER AJK FOR REDISTRIBUTING MASS 10/13/82
C*****
     7,ZBAR1,ZBAR2,ZBAR3,RBAR1,RBAR2,RBAR3,AREA12,AREA23,AREA13
     8,RAVAG12,RAVAG23,RAVAG13,CONM12,CONM23,CONM13,FNMASS(3)
C                                                                        00000430
      INTEGER DICT(11),ELID,ESTID,ISORT(3)                               00000440
      DOUBLE PRECISION CONSTS                                            00000450
      LOGICAL NOGO, HEAT

      EQUIVALENCE [illegible],LABEL), (DICT(5),                           00000730
      EQUIVALENCE (Z(1),Z1), [illegible],Z2), (Z(3),Z3)                  00000740
      EQUIVALENCE (AKI(1),GABABQ(1,1)),(RMASS(1,1),AKM(1))               00000750
      EQUIVALENCE (CONSTS(1),PI), (CONSTS(4),DEGRAD)                     00000760
      EQUIVALENCE (IRADEL,ECPT(1))
     1,              (CONSTS(2),TWOPI)                                   00000770
      EQUIVALENCE (JECPT(1),ECPT(2)),(JECPT(2),ECPT(3)),(JECPT(3),
     1ECPT(4))
                                                                         00000780
                                                                         00000790
      INITIALIZE                                                         00000800

         50 I=1,2

      RMASS(9,9) = [illegible]
      GO TO 400                                                          00003810
C 350 AREA = (R1*(Z2-Z3) + R2*(Z3-Z1) + R3*(Z1-Z2))/2.                  00003820
C     CONVM =  RHOD*(R1 + R2 + R3)/3.*AREA                               00003830
350   ZBAR1=(Z(1)+Z(2)+Z(3))/3.0
      ZBAR2 = ZBAR1
      ZBAR3 = ZBAR1
      RBAR1 = (R(1) + R(2) + R(3))/3.0
      RBAR2 = RBAR1
      RBAR3 = RBAR1
      AREA12 = (R(1)*(Z(2) - ZBAR3) + R(2)*(ZBAR3 - Z(1))
     $         +RBAR3*(Z(1) - Z(2)))/2.0
      AREA23 = (RBAR1*(Z(2) - Z(3)) + R(2)*(Z(3) - ZBAR1)
     $         +R(3)*(ZBAR1 - Z(2)))/2.0
      AREA13 = (R(1)*(ZBAR2 - Z(3)) + RBAR2*(Z(3) - Z(1))
     $         +R(3)*(Z(1) - ZBAR2))/2.0
      RAVAG12 = (R(1) + R(2) + RBAR3)/3.
      RAVAG23 = (RBAR1 + R(2) + R(3))/3.
      RAVAG13 = (R(1) + RBAR2+ R(3))/3.
      CONM12 = RHOD*RAVAG12*AREA12
      CONM23 = RHOD*RAVAG23*AREA23
      CONM13 = RHOD*RAVAG13*AREA13
C*****
C       CHANGES FOR MASS CALCULATION AJK 10/12/82 -
C*****
C       COMPUTE LUMPED MASS AT NODES A,B,C (I.e. 1,2,3)
      FNMASS(1)=(CONM12+CONM13)/2.0
      FNMASS(2)=(CONM12+CONM23)/2.0
      FNMASS(3)=(CONM23+CONM13)/2.0
      NODNUM(1)=JECPT(1)
      NODNUM(2)=JECPT(2)
      NODNUM(3)=JECPT(3)
C      WRITE(6,*)ZBAR1,ZBAR2,ZBAR3,RBAR1,RBAR2,RBAR3,AREA12,AREA23,
C     1AREA13,RAVAG12,RAVAG23,RAVAG13,CONM12,CONM23,CONM13,
C     2FNMASS(1),FNMASS(2),FNMASS(3),NODNUM(1),NODNUM(2),NODNUM(3)
C*****
C       END CHANGES
C*****
```

FIGURE 5 FORTRAN CODING CHANGES IN NASTRAN SUBROUTINE TRIAAD FOR CTRIAAX ELEMENTS

```
      AREA = AREA12 + AREA23 + AREA13
      CONVM = CONM12 + CONM23 + CONM13
      IF(AREA.LT.0.0) GO TO 7171
      GO TO 7172
 7171 PRINT 7173, AREA,IECPT(1)
 7173 FORMAT(1X,'NEGATIVE AREA = ',E11.5,2X,'IN ELEMENT NUMBER',
     $I15,2X,'DID YOU NUMBER ELEMENT COUNTER CLOCKWISE AS REQUIRED ??'//
     $)
C       STOP
 7172 CONTINUE
C                                                                       00003840
                                                                        0000385
   RANSFORM THE ELEMENT STIFFNE                   SYSTEM                00003
     RID POINT DEGREES
```

FIGURE 5 FORTRAN CODING CHANGES IN NASTRAN SUBROUTINE TRIAAD FOR CTRIAAX ELEMENTS

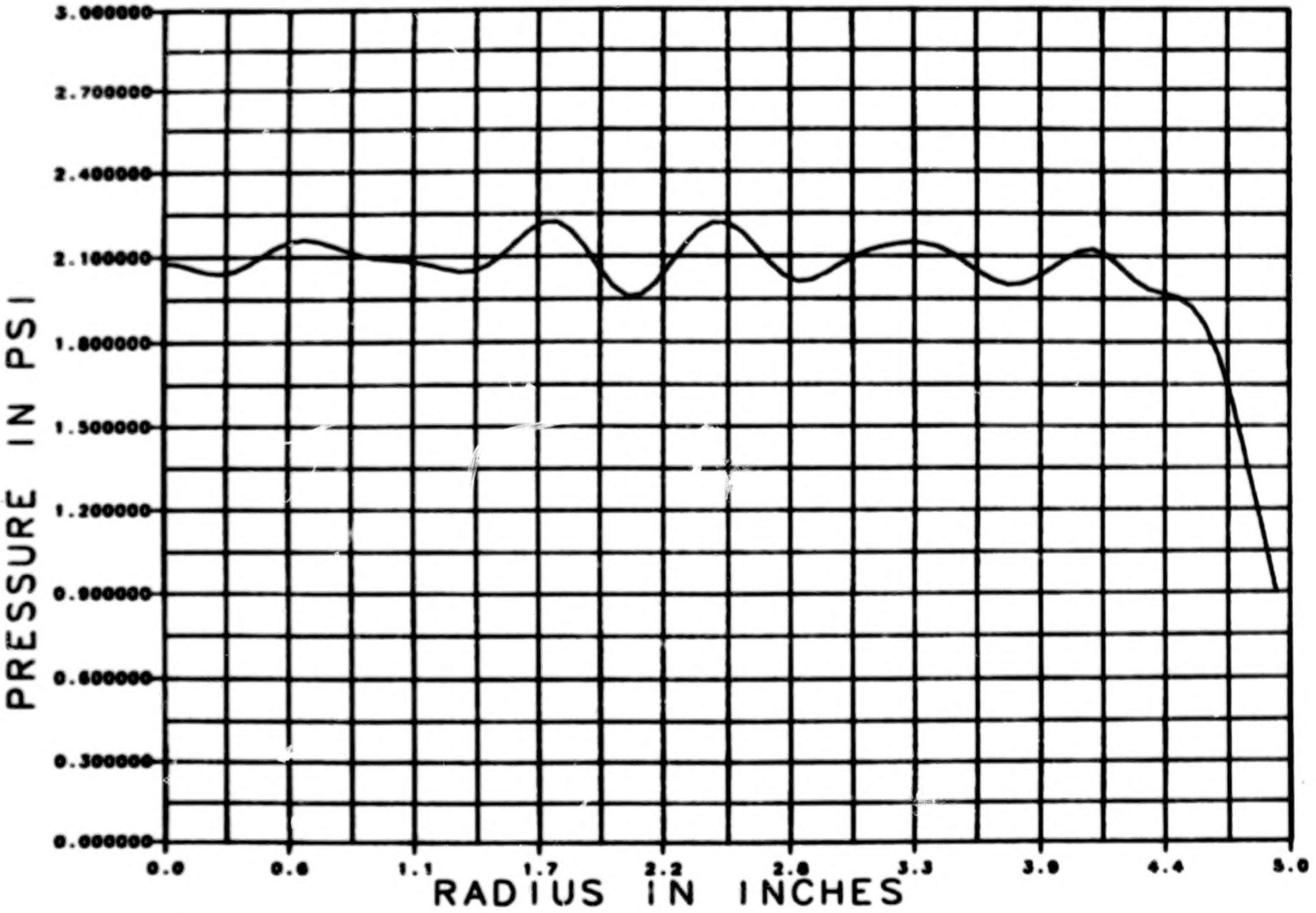

FIGURE 6 THE PRESSURE DISTRIBUTION AS A FUNCTION OF RADIUS ALONG THE INCIDENT FACE OF THE TAPERED FILTER PLATE

ORIGINAL PAGE IS
OF POOR QUALITY

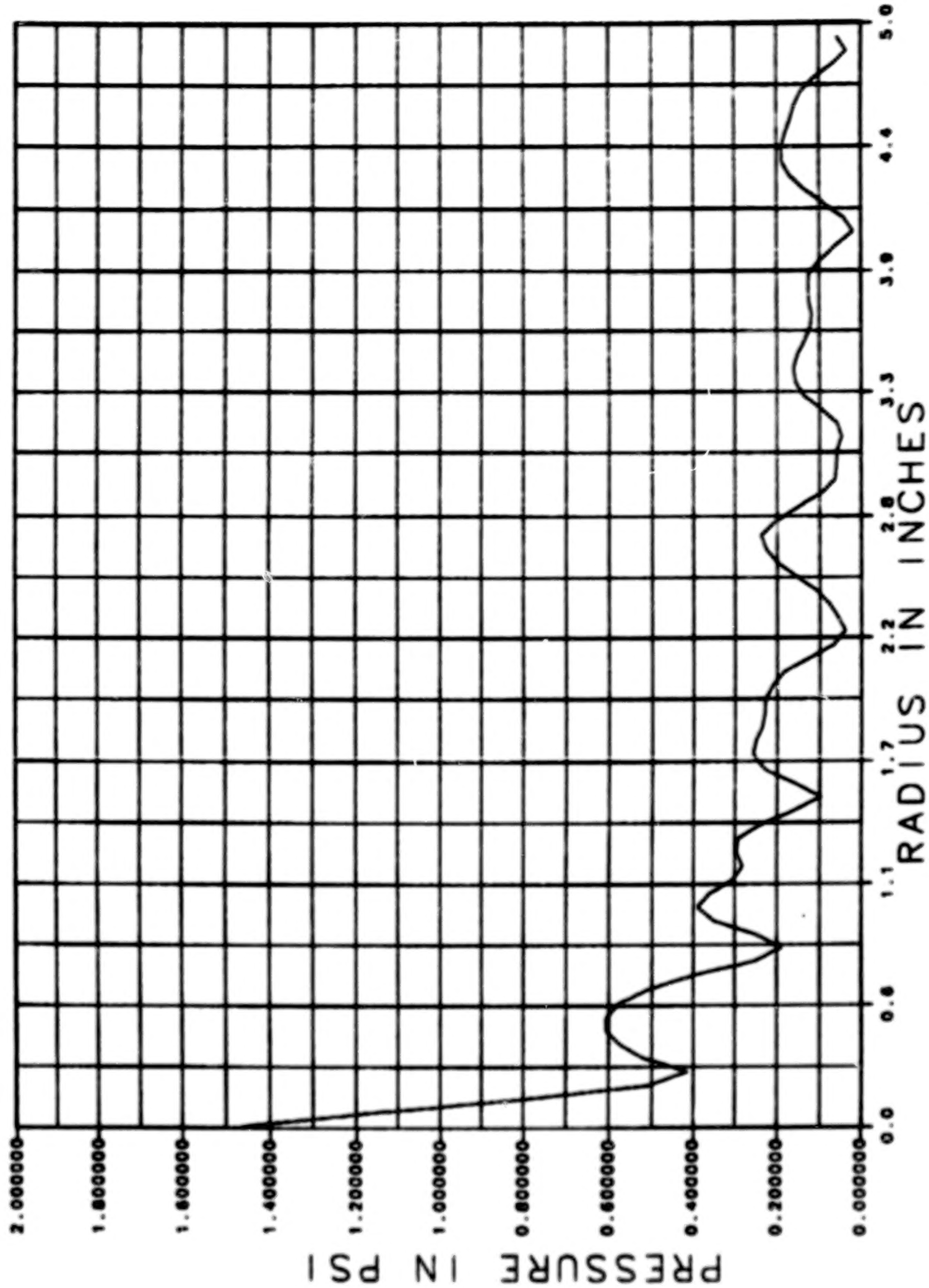

FIGURE 7 THE PRESSURE DISTRIBUTION AS A FUNCTION OF RADIUS ALONG THE TRANSMITTED FACE OF THE TAPERED FILTER PLATE

ORIGINAL PAGE IS
OF POOR QUALITY

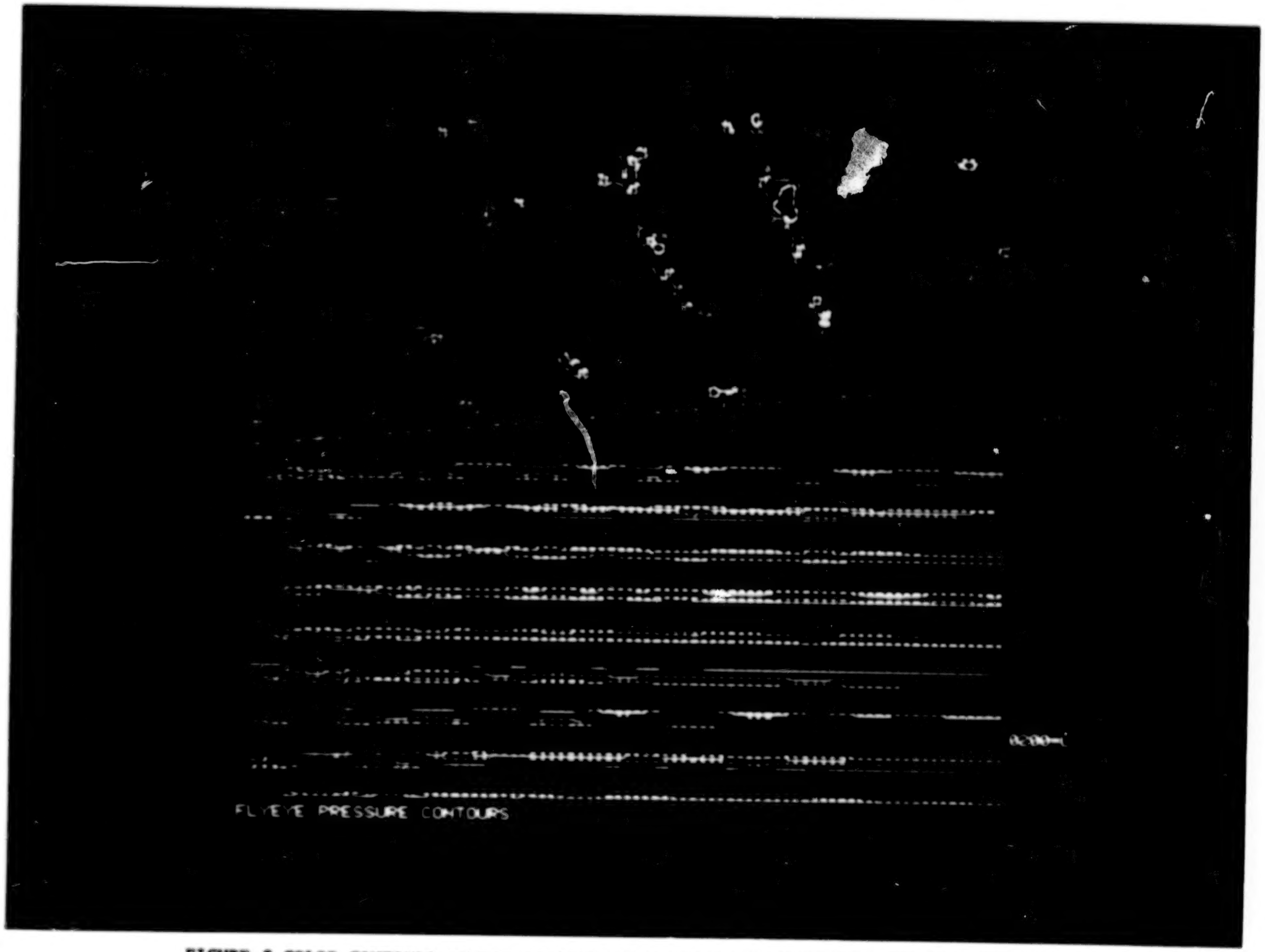

FIGURE 8 COLOR CONTOURS OF THE PRESSURE DISTRIBUTION THROUGHOUT THE TAPERED FILTER PLATE MODEL

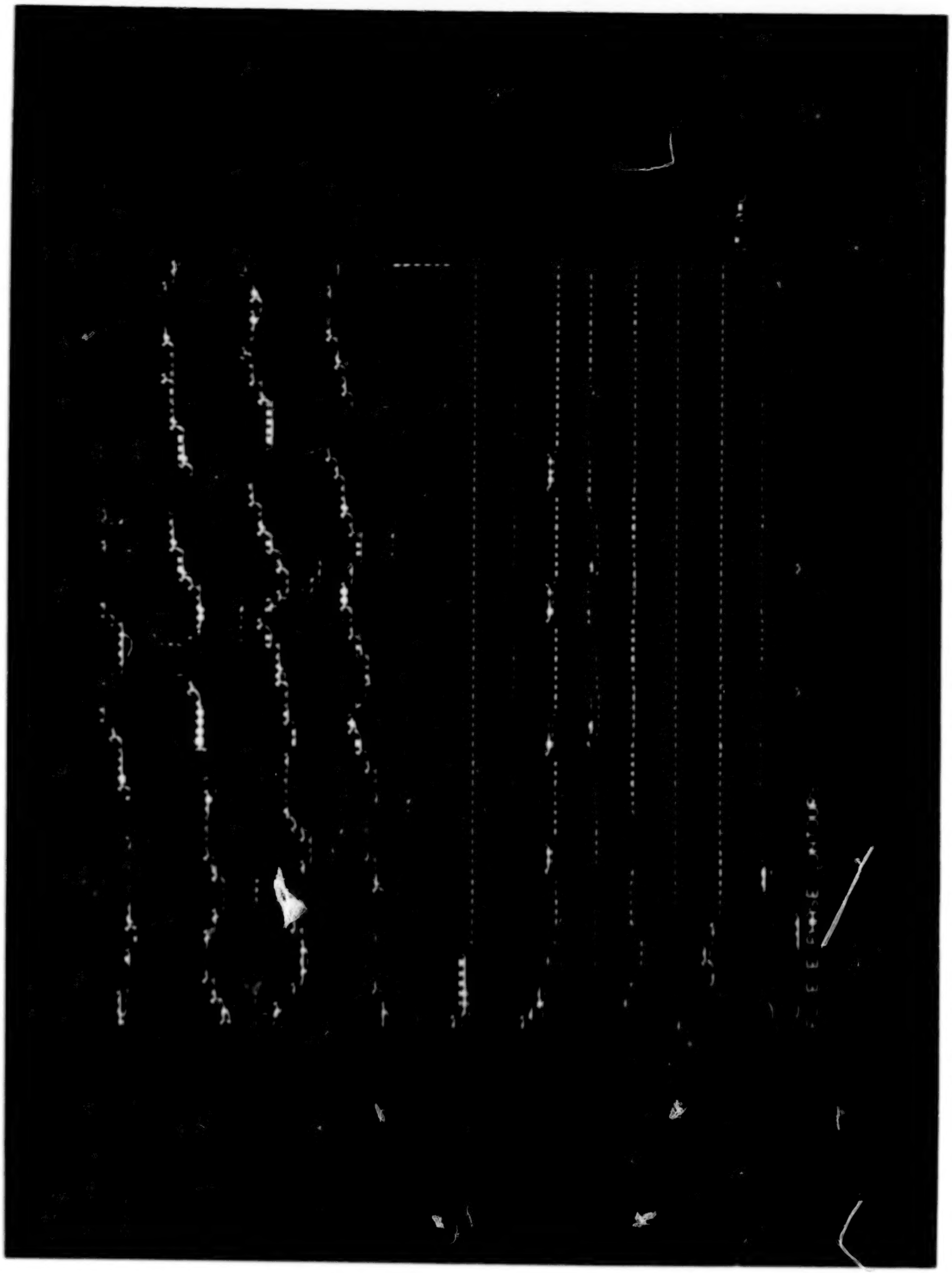

FIGURE 3 COLOR CONTOURS OF THE PHASE DISTRIBUTION THROUGHOUT THE TAPERED FILTER PLATE MODEL

N84
15602

UNCLAS

D12

N84 15602

PROPAGATION OF FLEXURAL AND MEMBRANE WAVES WITH FLUID LOADED NASTRAN PLATE AND SHELL ELEMENTS

A. J. Kalinowski and C. A. Wagner

NAVAL UNDERWATER SYSTEMS CENTER
NEW LONDON, CONNECTICUT 06320

SUMMARY

This paper is concerned with modeling flexural and membrane type waves existing in various submerged (or in vacuo) plate and/or shell finite element models that are excited with steady state type harmonic loadings proportioned to $e^{i\omega t}$. Only thin walled plates and shells are treated wherein rotary inertia and shear correction factors are not included. More specifically, the issue of determining the shell or plate mesh size needed to represent the spatial distribution of the plate or shell response is of prime importance towards successfully representing the solution to the problem at hand. To this end, a procedure is presented for establishing guide lines for determining the mesh size based on a simple test model that can be used for a variety of plate and shell configurations such as, (1) cylindrical shells with water loading, (2) cylindrical shells in vacuo, (3) plates with water loading, and (4) plates in vacuo. The procedure for doing these four cases is given, with specific numerical examples present only for the cylindrical shell case.

INTRODUCTION

This paper addresses the topic of modeling flexural waves and membrane waves present in various types of shell and plate type structural configurations. The issue at hand is arriving at a simple procedure for determining a mesh size adequate to represent the details of the spatial response distributions necessary to achieve some desired level of accuracy. To be sure, it would be too large an undertaking to answer this question for all possible plate and shell configurations that may arise, however, the selected class of thin walled cylindrical shells and flat plates are often the major building blocks of a good deal of structures. Therefore, the paper will focus on these two configurations, with the major emphasis on the cylindrical shell employing CCONEAX elements with axisymmetrical loading. Physical problems with finite length dimensions exhibit solution responses that often have the form of standing wave patterns as a result of reflections from the shell boundaries. Further, these solutions do not have a single clearly defined constant amplitude traveling wave component as one would have, in say, an infinitely long

C-3

shell or plate. A constant amplitude traveling wave (propagating in the x direction at frequency ω) response, R, of the form $R = R_0 e^{i(-\gamma x+\omega t)}$ is a desirable form to seek because the constant amplitude R_0 and associated spatial wave length $\lambda_\gamma = 2\pi/\gamma$ can then be used as a measure for determining the ability of a particular element to represent the desired wave propagation phenomenon. Deviations of the finite element amplitude response from the exact response constant R_0 and/or deviatons of the finite element response phase angle period from the exact spatial period can be used to judge the mesh refinement necessary to achieve a desired level of accuracy. The thrust of this paper is not to give a hard and fast rule for the number of elements per wavelength necessary to achieve some desired level of accuracy, but rather to provide a procedure for allowing one to establish his own level of accuracy. We take this approach because rules of thumb are often dangerous, particularly in the area of wave propagation in plate and shell structures. There are cases, for example, in a plate or cylindrical shell where a cutoff point exists such that the particular problem parameters (geometry, frequency, and physical constants) result in a situation where there is no traveling wave. If the problem parameters happen to be such that the traveling wave root is close to the cut-off point, a finer mesh size might be needed to properly represent the propagating wave situation.

The symmetrically loaded (θ independent loading) infinitely long cylinder shell (with or without fluid external fluid present) is selected as the model for examining flexural and membrane traveling waves (see Figure 1). This same model can be used to treat all four plate and shell cases (with and without water) discussed above. The plate cases can be realized by letting $a \to \infty$ and the in vacuo cases achieved by setting the density of the fluid equal to zero.

SYMBOLS

a = radius of cylindrical shell (in)

c = fluid sound speed (in/sec)

c_s = shear velocity = $\sqrt{G/\rho_s}$ psi

c_p = in vacuo plate wave speed, $\sqrt{E/(\rho_s(1-\nu^2))}$ (in/sec)

c_γ = propagating wave phase velocity, ω/γ

c_{fp} = in vacuo plate wave speed, $\sqrt[4]{h\rho_s\omega^2/D}$ (in/sec)

D = plate modulus = $Eh^3/[12\ (1-\nu^2)]$ of rigidity (lb/in)

f = harmonic frequency (Hz)

G = shear modulus of elasticity (psi)

$H_0^{(1)}(\ );\ H_1^{(1)}(\ )$ = Hankel Bessel functions of the first kind order 0 and 1

h = plate or shell thickness (in)

$i = \sqrt{-1}$ complex number

$K_o(); K_1()$ = modified Bessel functions of order 0 and 1

$k = \omega/c$ acoustic wave number (in^{-1})

$k_{fp} = \omega/c_{fp}$ in vacuo plate wave number (in^{-1})

$k_p = \omega/c_p$ in vacuo plate wave number (in^{-1})

L = finite element model length (in)

M_z = shell line moment (lb/in/in)

N_z = axial line membrane force (lb/in)

p = fluid pressure (psi)

Q = transverse shell line shear force (lb/in)

r = radial cylindrical coordinate (in)

t = time variable (sec)

u = axial motion of plate or shell (in)

U_o = amplitude of u (in)

w = radial motion of plate or shell (in)

W_o = amplitude of w (in)

x = plate coordinate direction normal to plate (in)

z = axial cylindrical coordinate variable (in)

λ_γ = wavelength of propagating wave

γ = traveling wave number for z direction (in^{-1})

γ_r = real part of γ

γ_i = imaginary part of γ

ρ = mass density of fluid (lb/sec^2 in^{-4})

ρ_s = mass density ofstructure (lb/sec^2 in^{-4})

ν = Poisson's ratio of structure

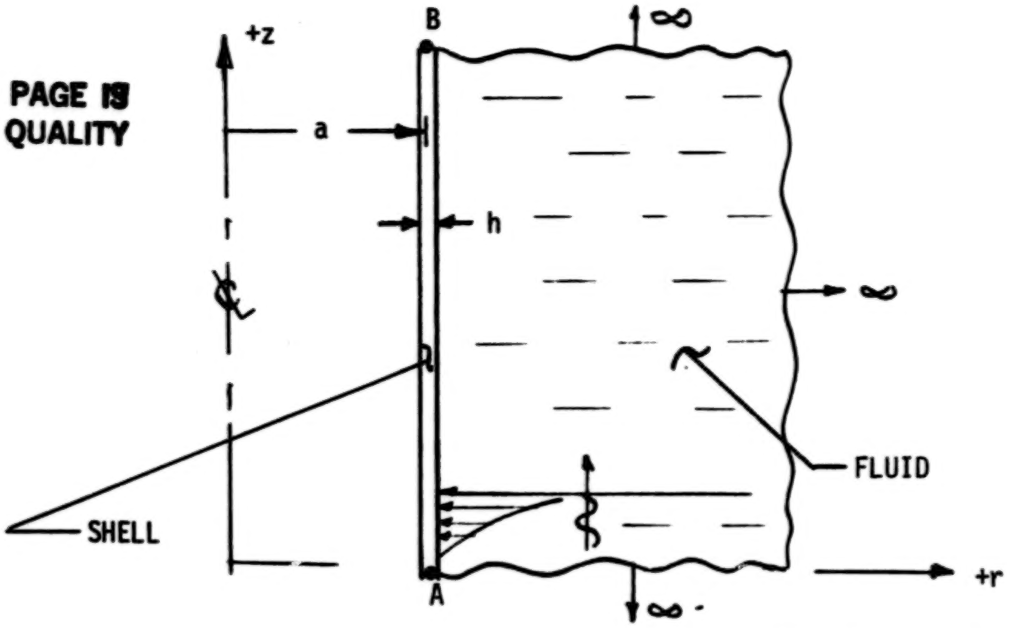
+z
B
∞
a
h
℄
∞
SHELL
FLUID
A
∞
+r

FIGURE 1. FLEXURAL WAVE MODEL FOR SUBMERGED CYLINDRICAL SHELL

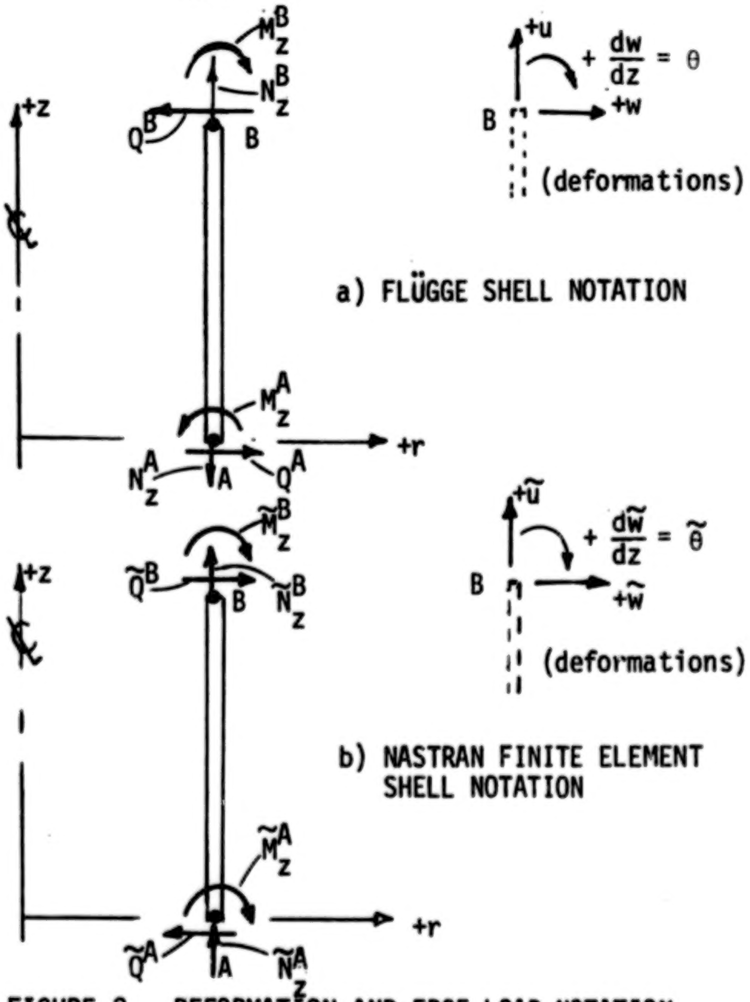

a) FLÜGGE SHELL NOTATION

b) NASTRAN FINITE ELEMENT SHELL NOTATION

M_z^B
N_z^B
+z
Q^B
B
+u
$+ \frac{dw}{dz} = \theta$
+w
(deformations)
℄
M_z^A
+r
N_z^A
A
Q^A
$\tilde{M}_z^B$
+z
$\tilde{Q}^B$
B
$\tilde{N}_z^B$
$+\tilde{u}$
$+ \frac{d\tilde{w}}{dz} = \tilde{\theta}$
$+\tilde{w}$
(deformations)
℄
$\tilde{M}_z^A$
+r
$\tilde{Q}^A$
A
$\tilde{N}_z^A$

FIGURE 2. DEFORMATION AND EDGE LOAD NOTATION

$\omega = 2\pi f$ = harmonic frequency (rad/sec)

ANALYTICAL WAVELENGTH FORMULATION FOR PLATES AND CYLINDRICAL SHELLS

The analytical formulation employed for determining the exact relationship for freely propagating waves in plate and cylindrical shell structures is important for its own sake, however, the formulation also directly leads to the procedure employed to set up the NASTRAN wavelength accuracy demonstration models. Consequently, some of the important details of the development for the freely propagating wave characteristics equation are given. The procedure given will closely follow the one given in ref. 2, except that freely propagating rather than standing wave configurations are considered by changing the axial variation as a complex exponential variation in z rather than a cosine variation.

Of eventual interest is both the flexural wave and axial (membrane) wavelengths for plates (with and without water present) and for infinitely long cylindrical shells (with and without water present). This constitutes 2 x 2 x 2 = 8 different situations. However, we can treat the eight cases at the same time by first treating the most complex case of the submerged infinitely cylindrical shell. By taking appropriate limits of this case (i.e., water density → 0 or shell radius → ∞) we can recover the other cases of interest without requiring any new analyses.

We start with the governing simplified thin wall shell field equations for the cylindrical shell (ref. 1) and corresponding wave equation for the external fluid, namely

$$\frac{\partial^2 u}{\partial z^2} + \frac{\nu}{a}\frac{\partial w}{\partial z} - \frac{\partial^2 u}{\partial t^2} \cdot \frac{1}{c_p^2} = 0 \tag{1}$$

$$\frac{\nu}{a}\frac{\partial u}{\partial z} + \frac{w}{a^2} + \frac{h^2}{12}\frac{\partial^4 w}{\partial z^4} + \frac{\partial^2 w}{\partial t^2} \cdot \frac{1}{c_p^2} = - p\Big|_{r=a} \cdot (1-\nu^2)/(Eh)$$

$$\nabla^2 p - \frac{1}{c^2}\frac{\partial^2 p}{\partial t^2} = 0 \tag{2}$$

subject to the usual boundary condition relation relating the pressure gradient normal to the shell and the shell acceleration,

$$\frac{\partial p}{\partial r}\Big|_{r=a} = -\rho\,\frac{\partial^2 w}{\partial t^2} \tag{3}$$

where u, w are the axial, and radial displacements of the shell (see Figure 2a for positive sense); p is the pressure in the fluid; h the shell thickness; a the radius of the cylindrical shell; r, z are the radial axial cylindrical coordinates; E, ν are Young's modulus and Poisson's ratio of the shell; c_p is the plate wave speed parameter ($\sqrt{E/(\rho_s(1-\nu^2))}$); and c is the acoustic wave speed of the fluid. The shell equations (1) are for classical thin wall plate and shell theory and do not have rotary inertia and shear correction factors included. Consequently, the area of interest focused on herein will be in a frequency range of ω such that the above two methods correction factors are not necessary. This point will be expanded upon later in the paper.

The θ symmetrical shell motion representing propagating waves in the +z direction are assumed to take the form

$$\begin{aligned} u &= U_o\, e^{i\gamma z}\, e^{-i\omega t} \\ v &= 0 \qquad \text{(no hoop motion)} \\ w &= W_o\, e^{i\gamma z}\, e^{-i\omega t} \end{aligned} \tag{4}$$

where U_o and W_o are the yet to be determined wave amplitudes, and γ is the propagating wave number. For outward going waves, the form of the pressure solution identically satisfying the wave equation (2) is given by ref. 2,

$$p(r,z) = P_o\, H_o^{(1)}(r\sqrt{k^2-\gamma^2})e^{i\gamma z}\, e^{-i\omega t} \tag{5}$$

which can be easily verified by direct substitution of equation (5) into equation (2), where P_o is the yet unknown pressure amplitude, and $H_o^{(1)}(\ )$ is the Hankel function of the first kind of order zero. A similar expression for p with $H_o^{(2)}(\ )$ (Hankel functions of the second kind) also satisfies the wave equation, but represents inward coming waves (when $k^2 > \gamma^2$) or results in an ever increasing exponential increasing pressure field with increasing r when $k^2 < \gamma^2$. Neither of these situations corresponds to the physical problem at hand, thus only the Hankel function of the first kind is retained.

The characteristic equation resulting in an interaction equation relating the driving frequency ω and admissible propagating wave numbers, γ, is obtained by substituting equations (4) and (5) into equation (1), subject to the boundary condition (3): actually substituting equations (4) and (5) into condition (3) leads to the relation between the surface motion amplitude W_o and the pressure amplitude P_o, namely

$$P_o = \frac{-\rho\, W_o\, \omega^2}{\sqrt{k^2-\gamma^2}\; H_1^{(1)}(a\sqrt{k^2-\gamma^2})} \tag{5a}$$

Thus the resulting two linear equations in the W_o, U_o coefficients is given by

$$\begin{aligned} &U_o i\left(\frac{\omega^2}{c_p^2} - \gamma^2\right) + W_o\left(-\frac{\nu\gamma}{a}\right) = 0 \\ &U_o i\left(\frac{\nu\gamma}{a}\right) + W_o\left[\frac{1}{a^2} + \frac{h^2}{12}\gamma^4 - (\omega/c_p)^2 - \frac{(1-\nu^2)\rho\omega^2 H_0^{(1)}(a\sqrt{k^2-\gamma^2})}{Eh\sqrt{k^2-\gamma^2}\; H_1^{(1)}(a\sqrt{k^2-\gamma^2})}\right] = 0 \end{aligned} \tag{6}$$

The nontrivial solution is obtained by setting the determinant of the amplitude coefficients equal to zero resulting in

$$\left(\frac{\omega^2}{c_p^2} - \gamma^2\right)\left[\frac{1}{a^2} + \frac{h^2}{12}\gamma^4 - (\omega/c_p)^2 - \frac{(1-\nu^2)\rho\omega^2\, H_0^{(1)}(a\sqrt{k^2-\gamma^2})}{Eh\sqrt{k^2-\gamma^2}\; H_1^{(1)}(a\sqrt{k^2-\gamma^2})}\right] + \left(\frac{\nu\gamma}{a}\right)^2 = 0 \tag{7a}$$

for $k^2 > \gamma^2$

or in another equivalent form of

$$\left(\frac{\omega^2}{c_p^{\,2}} - \gamma^2\right)\left[\frac{1}{a^2} + \frac{h^2}{12}\gamma^4 - (\omega/c_p)^2 - \frac{(1-\nu^2)\rho\omega^2 K_0\left(a\sqrt{\gamma^2-k^2}\right)}{Eh\sqrt{\gamma^2-k^2}\;K_1\left(a\sqrt{\gamma^2-k^2}\right)}\right] + \left(\frac{\nu\gamma}{a}\right)^2 = 0 \tag{7b}$$

for $\gamma^2 > k^2$

where the $K_0()$ and $K_1()$ are modified Bessel functions and are related to the Hankel functions by the identity

$$K_n\ (X) = \frac{\pi}{2}\, i^{n+1}\ H_n^{(1)}(iX) \tag{8}$$

Noting that the in vacuo flexural wave number, k_{fp}, formula for a plate is given by

$$k_{fp} = \sqrt[4]{\frac{h\ \rho_s\omega^2}{D}} \tag{9}$$

and the in vacuo membrane compressional wave number, k_p, given by

$$k_p = \frac{\omega}{c_p} = \frac{\omega}{\sqrt{\dfrac{E}{(1-\nu^2)\rho_s}}} \tag{10}$$

and finally the acoustic wave number by

$$k = \frac{\omega}{c} \tag{11}$$

where c is the acoustic wave speed of the fluid medium; the characteristic equation for the traveling wave number, non-dimensionalized with respect to the acoustic wave number k, can algebraically be rewritten as

$$\left((k_p/k)^2-(\gamma/k)^2\right)\left[\frac{1}{(ka)^2} - \left(\frac{k_p}{k}\right)^2\left\{1- \frac{(\gamma/k)^4}{(k_{fp}/k)^4} + \frac{\left(\frac{\rho a}{\rho_s h}\right) H_0^{(1)}\left(ka\sqrt{1-\left(\frac{\gamma}{k}\right)^2}\right)}{(ka)\sqrt{1-\left(\frac{\gamma}{k}\right)^2}\ H_1^{(1)}\left(ka\sqrt{1-\left(\frac{\gamma}{k}\right)^2}\right)}\right\}\right]$$

$$+ \frac{\nu^2(\gamma/k)^2}{(ka)^2} = 0 \tag{12a}$$

For $\left(\frac{\gamma}{k}\right)^2 < 1$

or

$$\left((k_p/k)^2-(\gamma/k)^2\right)\left[\frac{1}{(ka)^2} - \left(\frac{k_p}{k}\right)^2\left\{1- \frac{(\gamma/k)^4}{(k_{fp}/k)^4} + \frac{\frac{\rho a}{\rho_s h} K_0\left(ka\sqrt{\left(\frac{\gamma}{k}\right)^2-1}\right)}{ka\sqrt{\left(\frac{\gamma}{k}\right)^2-1}\ K_1\left(ka\sqrt{\left(\frac{\gamma}{k}\right)^2-1}\right)}\right\}\right]$$

$$+ \frac{\nu^2(\gamma/k)^2}{(ka)^2} = 0 \tag{12b}$$

For $\left(\frac{\gamma}{k}\right)^2 > 1$

The original dimensional form of the characteristic equation (7) depended on the eight parameters h, ω, E, ν, ρ, ρ_s, a, c, for the resulting wave number γ; however, the above equation (12) form only depends on the reduced number of 5 non-dimensional parameters, namely k_p/k, ka, ρ/ρ_s, a/h, and ν for the resulting non-dimensional wave numbers γ/k. The term (k_{fp}/k) is not an independent parameter since it can be expressed in terms of the other ones through the relation

$$\frac{k_{fp}}{k} = (12)^{\frac{1}{4}} \sqrt{(k_p/k)\left(\frac{a}{h}\right)/(ka)} \tag{13}$$

Roots of Characteristic Equation and Mode Shapes

The roots of the frequency equation (12) cover several special cases and require further elaboration. The roots of interest for freely propagating waves are those for which $\gamma = \gamma_r$ is a real quantity, wherein the shell response has arguments (see equation (4)) of the traveling wave form $i(\gamma_r z - \omega t)$ and corresponds to a wave propagating in the +z direction and the corresponding wavelength is given by

$$\lambda = \frac{2\pi}{\gamma_r} \tag{14}$$

Possibly roots of the characteristic equation are complex (e.g., this could be the case when employing equation (12a) due to the complex form of the Hankel functions $H_n(\ ) = J_n(\ ) + i\, Y_n(\ )$). In these situations, the complex root can be written in the form $\gamma = \gamma_r + i\gamma_i$ and substitution of this quantity into the shell response equation (4), shows that the axial z response is proportional to $e^{i(\gamma_r + i\gamma_i)z} = e^{i\gamma_r z}\, e^{-\gamma_i z}$. Thus the solution amplitude would either reduce $(\gamma_i > 0)$ or grow indefinitely $(\gamma_i < 0)$ with z according to the sign of γ_i. The wavelength of the reducing (or growing) fluxuations is still given by $\lambda_r = 2\pi/\gamma_r$.

The case of interest in the remainder of this paper is the one for which there are freely propagating waves of constant amplitude. This situation will result when $(\gamma/k)^2 > 1$ wherein the modified Bessel functions K_0 and K_1 have real arguments and consequently equation (12b) usually results in real roots for γ. The situation $(\gamma/k)^2 > 1$ implies the acoustic wavelength $\lambda_a = 2\pi/k$ is longer than the propagating wavelength, $\lambda_r = 2\pi/\gamma_r$.

For cylindrical shells, unlike the infinite plate, the axial membrane force N_z, will also result in a radial component of motion. Consequently, the axial and radial motions for the membrane propagation or the flexural wave propagation are coupled. In fact, the same characteristic equation (12b) can be used to determine both the membrane and flexural propagating wave numbers γ_{ax}, γ_{fl}. Whether a given root, γ, corresponds to the membrane or flexural wave can be established by examining the mode shape. More specifically, the ratio of U_0/W_0 can be solved from either of the two homogenous equations (6); upon substituting the root, γ, into say the first of equations (6) yields

$$\frac{U_o}{W_o} = \frac{\nu\gamma/a}{i\left(\frac{\omega^2}{c_p{}^2} - \gamma^2\right)} \equiv \frac{\nu(\gamma/k)\ e^{i\pi/2}}{\left(\left(\frac{\gamma}{k}\right)^2 - \left(\frac{k_p}{k}\right)^2\right)(ka)} \tag{15}$$

Upon subsituting the γ/k root in question into equation (15), the size of U_o relative to W_o can be established, wherein $|U_o/W_o| >> 1.0$ implied a dominant axial motion hence signifying a membrane propagating wave and $|U_o/W_o| << 1.0$ implies a dominant radial motion hence signifying a flexural propagating wave.

Limiting Cases of General Characteristic Equation

Several limiting cases of the general characteristic equation (12b) not only provide useful information by their own merit (i.e., the traveling wave characteristic equation of a plate in fluid or air; or, the case of a cylinder in air) but at the same time provide insight with regard to where (i.e., the range of (γ/k)) to search for the root. It is instructive to start with the simplest case of an infinite flat plate in vacuo and build up to the more general case of a submerged infinite cylinder.

- infinite plate in vacuo

This situation is realized by taking the limit as the fluid to structure mass ratio goes to zero, $\rho/\rho_s \rightarrow 0$, and as the non-dimensional frequency parameters $ka \rightarrow \infty$. It is noted that $ka \rightarrow \infty$ can be realized by having the radius $a \rightarrow \infty$ at a finite frequency $\omega = k/c$. Thus equation (12b) reduces to

$$\left[k_p^2 - \gamma^2\right]\left[1 - \left(\frac{\gamma}{k_{fp}}\right)^4\right] = 0 \tag{16}$$

which by inspection has the roots

$$\gamma = k_p \quad \text{and} \quad \gamma = k_{fp}$$

Substituting $\gamma = k_p$ into equations (6) shows that

$$U_o\ i(0) + W_o \cdot (\nu k_p/\infty) = 0$$

$$U_o\ i(0) + W_o \cdot \underbrace{[h^2\ k_p^4/12 - (\omega/c_p)^2]}_{\neq 0} = 0 \tag{17}$$

thus, $W_o = 0$ and U_o is any constant, and hence this mode corresponds to pure axial motion with no radial motion, thus indicating the $\gamma = k_p$ root is for the membrane traveling wave. Similarly, substituting $\gamma = k_{fp}$ into equations (6) yields

$$U_o i\ \overbrace{[\omega^2/c_p{}^2 - k_{fp}^2]}^{\neq 0} + W_o \cdot (0) = 0$$

$$U_o i\ [0] + W_o \cdot [0] = 0 \tag{18}$$

ORIGINAL PAGE IS
OF POOR QUALITY

thus $U_o = 0$, and W_o is any constant and hence corresponds to pure flexural motion with no axial motion.

- infinite plate in fluid

This situation is similarly obtained by passing to the limit as $a \to \infty$ in equation (12b) and noting that $(K_0(x)/K_1(x)) \to 1$ as $x \to \infty$. Thus equation (12b) reduces to

$$\left[\left(\frac{k_p}{k}\right)^2 - \left(\frac{\gamma}{k}\right)^2\right]_1 \left[1 - \frac{\left(\frac{\gamma}{k}\right)^4}{\left(\frac{k_{fp}}{k}\right)^4} + \frac{\left(\frac{\rho}{\rho_s}\right)}{kh\sqrt{\left(\frac{\gamma}{k}\right)^2 - 1}}\right]_2 = 0 \tag{19}$$

where again separate membrane traveling waves and flexural traveling waves result by separately equating the $[\ ]_1$ and $[\ ]_2$ terms to zero in quation (19). Thus by inspection, as in the in vacuo plate case,

$$\frac{\gamma}{k} = \frac{k_p}{k}$$

is again a root for the membrane propagating wave and the root of

$$\left[1 - \frac{\left(\frac{\gamma}{k}\right)^4}{\left(\frac{k_{fp}}{k}\right)^4} + \frac{(\rho/\rho_s)}{kh\sqrt{\left(\frac{\gamma}{k}\right)^2 - 1}}\right]_2 = 0 \tag{19a}$$

provides the flexural wave root. It is noted that equation (19a) is algebraically equivalent to equation (7.10) of ref. 2. Upon inspecting equation (19a), it is seen that the effect of the water presence is to make the γ/k root a larger value (i.e., the flexural wavelength is smaller) than what would have been the case in the absence of external water. Thus the water has no effect on the membrane wave root, however the flexural wave root is effected and must be solved numerically with some sort of root searching scheme.

- infinite in vacuo cylindrical shell

The characteristic equation is again obtained from the general (12b) case, by passing to the limit as $(\rho/\rho_s) \to 0$, thus obtaining

$$(k_p^2 - \gamma^2)\left[\frac{1}{a^2} - k_p^2\left\{1 - \left(\frac{\gamma}{k_{fp}}\right)^4\right\}\right] + \frac{\nu^2\gamma^2}{a^2} = 0 \tag{20}$$

which corresponds to a cubic equation in the desired γ^2 root and consequently can be solved for exactly without resorting to a numerical root finder. Due to the presence of the last term in equation (20), $\gamma = k_p$ is no longer the exact root for the membrane traveling wave, however, the $(\nu\gamma/a)^2$ does not usually shift the membrane wave number root very far from the plate solution, $\gamma = k_p$ as can be seen after solving for the exact roots of equation (20). Only positive values for γ^2 obtained from the cubic solution will correspond to freely propagating waves. Although the exact membrane and flexural roots are coupled through the last term in equation (20), an approximation of the root, say for roughing out the mesh size needed, can be obtained from the approximations obtained after dropping the normally small $(\nu\gamma/a)^2$ term, hence

$$\gamma \approx k_p$$

for membrane waves, and

$$\gamma \approx k_{fp}\sqrt[4]{1-\frac{1}{(k_p a)^2}}$$

for flexural waves.

MODELING FLEXURAL AND MEMBRANE WAVES WITH NASTRAN

A simplified model is needed for the determination of the necessary number of elements per wavelength required to accurately model the membrane and/or flexural freely propagating waves in NASTRAN type elements. The procedure used here is to cut a segment (say at least one wavelength long) out of the infinitely long model. At one cut of the model (call it the starting end "A"), moments and forces existing in the freely propagating wave are applied explicitly; at the other end (call it the termination end "B"), an appropriate absorbing boundary conditions is applied (dampers that relate shell edge velocities to edge moments and forces). The boundary absorbers implicitly apply the appropriate amount of moment or force that would have been present internally at that section of the shell. In theory, it would be possible to apply explicit appropriately phased mements and forces at the termination end as well, however, this is not done for two reasons. First, there is a certain amount of phase angle drift (an amount beyond the expected termination phase of γL) that exists as the wave propagates along the axis of the shell (or plate) and it is not known a priori what the phase drift is so that the termination moments and forces can't be appropriately adjusted; the application of boundary absorbers, however, does not require any phase drift adjustment. Secondly, the implementation of the absorbers gives future insight on how to truncate finite element shells or plates in such a manner that large problems requiring premature model termination can be made.

In Vacuo Cylindrical Shell

- determination of edge loading moments and forces

The appropriate moments and forces at the starting end A can be determined from the relationships relating the shell motion u, w to the shell edge loads N_Z^A, Q^A, M_Z^A and are given by the shell theory relations (ref. 1)

$$M_Z^A = D\,\frac{\partial^2 w}{\partial z^2} \qquad Q^A = D\frac{\partial^3 w}{\partial z^3} \qquad N_Z^A = \frac{Eh}{(1-\nu^2)}\left(\frac{\partial u}{\partial z} + \nu\frac{w}{a}\right) \tag{21}$$

where the equation (21) moments and forces are line loads (i.e., loads per unit circumferential arc length) obeying the shell sign convention of Figure 2a. Upon substituting equations (4) into equations (21), it follows that

**ORIGINAL PAGE IS
OF POOR QUALITY**

$$M_Z^A = -\gamma^2 D\, W_o\, e^{i(\gamma z-\omega t)} \qquad Q^A = -i\,\gamma^3 D\, W_o\, e^{i(\gamma z-\omega t)}$$
$$N_Z^A = \frac{Eh}{(1-\nu^2)}\left[i\,\gamma\, U_o\, e^{i(\gamma z-\omega t)} + \frac{\nu}{a} W_o\, e^{i(\gamma z-\omega t)}\right] \tag{22}$$

where the relation between U_o and W_o is governed by equation (15) for cylindrical shells. For plates ($a \to \infty$), U_o and W_o are independent, where for membrane waves U_o denotes the wave amplitude with $W_o = 0$ and for flexural waves W_o is the wave amplitude with $U_o = 0$.

Equations (22) are not in a form ready to use in NASTRAN CCONEAX elements for three reasons: first, NASTRAN input is not in the usual line load form as is the case with shell theory, but rather are total values wherein the line loads must be multiplied by $2\pi a$; second, the finite element type sign convention (like quantities at both ends of the member are positive in the same sense) is different from the shell theory convention (e.g., compare Figures 2a and 2b) and; third, NASTRAN has an $e^{+i\omega t}$ hardwired into the code, consequently an adjustment in the analytical solution is necessary to compensate for this point. Specifically, a wave traveling in the +z direction also can be represented with an $i(-\gamma z + \omega t)$ type argument, thus by replacing γ with $-\gamma$ and ω with $-\omega$ in the analytical solutions will accomplish the corresponding correction. Thus accounting for all three compensations and also incorporating equation (15), the NASTRAN loading for the cylindrical shell at the starting cut A, evaluated at $z = 0$, is given by:

$$\tilde{M}_Z^A = 2\pi a\, \gamma^2\, D\, W_o\, e^{+i\omega t}$$
$$\tilde{Q}^A = 2\pi a\, \gamma^3\, D\, W_o\, e^{+90^\circ i}\, e^{+i\omega t} \qquad \text{NASTRAN cut-A loading for cylinder} \tag{23}$$
$$\tilde{N}_Z^A = \frac{2\pi a\, \rho_s\, \omega^2 \nu}{(a/h)}\left(\frac{W_o}{\gamma^2 - k_p^2}\right) e^{+i\omega t}$$

where W_o is any suitable displacement amplitude factor that is selected by the user, and γ is the root directly from the appropriate frequency equation (sign changes in γ and ω have already been compensated for in setting up equation (23)). The $e^{+i\omega t}$ factors are of course omitted when entered data into NASTRAN since this factor is automatically accounted for internal to the program.

- determination of shell edge termination absorbers

The membrane or flexural wave incident upon the shell termination will reflect from the end unless the appropriate boundary condition is inserted to simulate the effect of having an infinitely long shell. Here the appropriate boundary absorber is developed for each of the three shell edge loads. Following the same procedure used to setup equations (23), the internal moments and forces at the termination end are given by

$$\tilde{M}_Z^B = -2\pi a\ \gamma^2\ D\ W_0\ e^{+i\omega t}\ e^{-\gamma L}$$

$$\tilde{Q}^B = -2\pi a\ \gamma^3\ D\ e^{+i90^0}\ W_0\ e^{+i\omega t}\ e^{-i\gamma L} \tag{24}$$

$$\tilde{N}^B = \frac{-2\pi a\ h\ \rho_S\ \omega^2 e^{+i90^0}}{\gamma}\ U_0\ e^{+i\omega t}\ e^{-i\gamma L}$$

The equations (24) can be written in terms of velocity, by noting $\dot{u} = +i\omega u$ $\dot{w} = i\omega w$, $dw/dx = \dot{\theta} = (-i\gamma)(i\omega w)$ thus equations (24) become

$$\tilde{M}_Z^B = \frac{-2\pi a\ \gamma\ D}{\omega}\,(\dot{\theta}) \qquad \tilde{Q}^B = \frac{-2\pi a \gamma^3 D}{\omega}\,(\dot{w}) \qquad \tilde{N}^B = \frac{-2\pi a\ h\ \rho_S \omega}{\gamma}(\dot{u}) \tag{25}$$

where the above forces are the forces on the shell edge B. Dampers attached to the end of the shell would have an internal force or moment equal and opposite to the value at the shell edge, thus the forces and moments internal to the damper are given by

$$M_d^B = C_\theta \cdot (\dot{\theta}) \qquad Q = C_Q \cdot (\dot{w}) \qquad W = C_N \cdot (\dot{u}) \tag{26}$$

where the damper values are given by

$$C_\theta = \frac{2\pi a\ D}{c_\gamma} \qquad C_Q = \frac{2\pi a\ D\ \gamma^2}{c_\gamma} \qquad C_N = 2\pi a h\ \rho_S c_\gamma \left.\right\} \begin{array}{l}\text{NASTRAN}\\ \text{CCONEAX}\\ \text{DAMPERS}\end{array} \tag{27}$$

where the propagation phase velocity, c_γ, is defined by

$$c_\gamma = \frac{\omega}{\gamma} \tag{28}$$

where γ is the root of the characteristic equation. In the case of a plate, the same dampers can be used, except the $2\pi a$ would be replaced by the width of the plate (perpendicular to the direction of propagation) and appropriately subdivided between the element termination nodes (two termination nodes for actual plate elements and one termination node for beam elements with a plane strain correction on the Young's modulus).

Submerged Cylindrical Shell

- determination of edge loading moments and forces

The appropriate moments and forces employed to drive the shell edge employ the same equation (23) formulas, except that the propagating wave number root, γ must be determined from equations (12b) in this case.

- determination of shell edge termination dampers

Again equations (27) can be used, except that γ as determined from equations (27) is employed.

- determination of fluid loading on face z = 0

The appropriate fluid loading can be obtained by substituting equation (5a) into (5) (and converting into the $-i\gamma z + \omega t$ form by letting $\gamma = -\gamma$ and $\omega = -\omega$) to obtain

$$p(r,z) = \frac{-\rho W_0 \omega^2 H_0^{(1)} (r\sqrt{k^2-\gamma^2})}{\sqrt{k^2-\gamma^2}\, H_1^{(1)} (a\sqrt{k^2-\gamma^2})} e^{-i\gamma z + i\omega t} \tag{29}$$

Employing the large argument Bessel function approximations (ref. 5) of

$$H_0^{(1)}(X) \approx \sqrt{(2/(\pi X)}\, e^{i(X-\pi/4)} \qquad H_1^{(1)}(X) \approx H_0(X) e^{-\pi/2} \tag{30}$$

the equation (29) can be rewritten for, $|r\sqrt{\gamma^2 - k^2}| > 10.0$, in the form

$$p(r,z) \approx \frac{-W_0 \rho\omega^2 e^{-(r/a-1)(a\sqrt{\gamma^2-k^2}}}{\sqrt{\gamma^2-k^2}\,\sqrt{r/a}} e^{-i\gamma z} e^{+i\omega t} \tag{31}$$

where equation (31) can be used as the enforced pressure at the face z = 0.

Equation (31) can also be used to drive plate models by first making a change in variable $r = x + a$ (where x is the outward distance measured from the middle surface of the shell) and then appropriately passing to the limit as $a \to \infty$ to obtain

$$p(x,z) = \frac{-W_0 \rho\omega^2 e^{-x\sqrt{\gamma^2-k^2}}}{\sqrt{\gamma^2-k^2}} e^{-i\gamma z} e^{+i\omega t} \tag{32}$$

- determination of fluid loading on face z = L

On this face we choose to absorb the incident pressure wave with an absorber type boundary condition rather than load it explicitly with equation (29) evaluated at z = L. This approach is consistent with the manner in which the shell was terminated. The relationship between pressure and applied forces in a finite element formulation is that the normal gradient of the pressure is proportional to the finite element model force. Therefore, the gradient of pressure normal to the cut, z = L is needed and given by (with equation (5) $i(+\gamma z-\omega t)$ arguments)

$$\frac{\partial p}{\partial z} = i\gamma p(r,z) \tag{34}$$

and since for steady state problems,

$$\frac{\partial p}{\partial t} = -i\omega p$$

it follows

$$\frac{\partial p}{\partial z} = \frac{-\gamma}{\omega}\frac{\partial p}{\partial t} \equiv \frac{-\gamma}{\omega}\dot{p} \tag{35}$$

is the boundary condition to employ along the vertical fluid cut z = L. For direct acoustic fluid elements (ref. 6), the finite element nodal force is related to the normal gradient by the relation

$$F_n = \int_S [N]^T \frac{\partial p}{\partial n'} \, dS \tag{36}$$

where [N] is the element shape function. For lumped force applications, equation (36) is represented as, (where n' is the unit normal to the fluid and ΔA is an appropriate amount of area surrounding the node at the point of the F_n application)

$$F_n = \Delta A \frac{\partial p}{\partial n'} \tag{37}$$

and upon substituting equation (35) into (37) one obtains

$$F_n = -\Delta A \frac{\gamma}{\omega} \dot{p} \tag{38}$$

and represents the nodal force on the fluid as being proportional to the pressure time rate of change. Thus the internal force in a damper attached to the node would be equal and opposite in value and given by

$$F_n^{damp} = +\Delta A \frac{\gamma}{\omega} \dot{p}$$

where the damper value would be

$$C_d^p = \frac{\Delta A \gamma}{\omega} \qquad \text{direct pressure method damper (no analogy) for } z = L \text{ face} \tag{39}$$

In the case of NASTRAN, the acoustic fluid is modeled by way of an analogy which reduces the elasticity equations to the Helmholtz equation by way of introducing dummy constants into the material matrix and allowing the displacement variable, u_z, occupy the pressure variable (see ref. 3 for details). The analogy has been adopted herein, consequently, an additional factor of ρc^2 appears in equation (37), and consequently the frequency dependent NASTRAN axial damper needs to be modified by this same factor and thusly equation (39) is replaced by (replacing $\omega \to -\omega$, $\gamma \to -\gamma$ converts to NASTRAN convention; this results in the same damper since signs cancel)

$$\tilde{C}_d^p = \frac{\Delta A \gamma}{\omega} \rho c^2 \qquad \text{NASTRAN (ref. 3) analogy damper for } z = L \text{ face, with } \gamma \text{ directly from appropriate characteristic equation.} \tag{40}$$

It is noted, that so long as γ is a real quantity (e.g., characteristic root equation for γ is obtained from equation (12b)), the termination condition in the z direction is a pure damper. However, where γ is complex (e.g., root from equation (12a)) substitution of γ into the equation (40) damper will result in a complex damper. The real part can be treated as above, but the complex part will end up looking like a resistance (spring) when combined with the $+i\omega$ appearing as a multiplier in the assembled damping matrix in NASTRAN. Thus, the imaginary part of the damper (if it is present) can be applied as a nodal spring whose spring constant is

$$\left(\frac{i \Delta A (-\gamma^i)}{(-\omega)} \rho c^2 \right) (+i\omega) = -\Delta A \, \rho c^2 \, \gamma^i \qquad \text{NASTRAN analogy spring (with } \gamma^i \text{ directly from appropriate characteristic equation)}$$

wherein for decaying waves, γ^i will be a positive number making the spring constant positive.

Equation (40) can equally be applied to plate model problems, upon properly interpreting ΔA.

- determination of fluid loading on outer face $r = r_0$

Here on the outer radial fluid face, the boundary condition is developed just as in the previous case, except that now the gradient has to be taken in the direction of the outward normal ($n' = r$). Thus operating on equation (29) with $\partial(\ )/\partial r$ and then employing the equation (30) large argument relations, the following result is obtained

$$\frac{\partial p}{\partial r} \approx -\sqrt{\gamma^2-k^2}\, p(r,z) \tag{41}$$

Unlike equation (34), this result does not have a factor i relating the gradient of p and p itself, consequently, upon substition of equation (41) into equation (37), one obtains

$$F_n = -\Delta A \sqrt{\gamma^2-k^2}\; p \tag{42}$$

and represents the nodal force on the fluid as being proportional to the pressure. Thus the internal force in a spring attached to the node would be equal and opposite in value and is given by

$$F_n^{spg} = +\Delta A \sqrt{\gamma^2-k^2}\; p$$

where the spring constant value would be

$$K^p = \Delta A \sqrt{\gamma^2-k^2} \qquad \text{direct pressure method spring (no analogy) for } r = r_0 \text{ face} \tag{43}$$

and in the case of employing the ref. 3 pressure analogy, the counterpart of equation (43) is

$$\tilde{K}^p = \Delta A\, \rho c^2 \sqrt{\gamma^2-k^2} \qquad \text{NASTRAN (ref. 3) analogy spring for } r = r_0 \text{ face} \tag{44}$$

When γ is a root of equation (12b) ($\gamma^2 > k^2$), equation (44) implies a real spring is all that is needed. However, when $\gamma^2 < k^2$, and equation (12a) is employed, the roots, γ, are, in general, complex which implies that equation (44) will have a real and imaginary part. The real part of $\tilde{K}^p$ is still a spring, however the imaginary portion can be converted into a damper by dividing the imaginary part coefficient (not including i) of equation (44) by ω (to compensate for the ω multiplied in by the complex stiffness formation).

Equation (44) can equally be applied to plate model problems, upon appropriately interpreting ΔA.

Limitations of Membrane and Flexural Wave Modeling

The scope of this study is limited to a driving frequency region where the influence of plate rotary inertia and shear deformation on the flexural motions are not important. In fact, this is the limitation of the propagating wavelength formulas given earlier. The ability of NASTRAN to account for these higher order effects is a topic all in itself and will not be addressed in this paper wherein stiffness and mass formulations along the lines given in ref. 7 must be considered.

Although we are interested in both plate and shell propagating waves, the classical plate theory (CPT) can provide insight with regard to the point at which the above mentioned correction factors are needed. The CPT is defined here as the special case of equation (1) with $a \to \infty$. Midlin's classical paper (ref. 4) provides a guideline for when the characteristic wave equations presented herein no longer predicts the proper waves number roots, γ. As pointed out in ref. 4, the exact elasticity solution to the same problem shows that CPT can predict the correct flexural wave numbers when the corresponding $2\pi/\gamma$ wavelengths are long in comparison with the thickness of the plate. As the wavelength gets smaller, the exact elasticity solution traveling wave phase velocity (ω/γ), has as its upper limit, the velocity of the Rayleigh surface wave. Hence the CPT cannot be expected to give good results for the wave numbers, γ, as the driving frequencies get increasingly large. Reference 4 provides a plot of propagating phase velocity $c_\gamma = \omega/\gamma$ (non-dimensionalized with respect to the shear wave velocity $c_s = \sqrt{G/\rho_s}$) versus the plate thickness (non-dimensionalized with respect to the flexural wavelength, $2\pi/\gamma$ for a fixed Poisson's ratio ($\nu = 0.5$) and is reproduced here as Figure 3. The CPT straight line plot, curve II, is nothing more than equation (9) rewritten in the form

$$\frac{c_\gamma}{c_s} = \frac{h}{\lambda_\gamma} \cdot \frac{2\pi}{\sqrt{6(1-\nu)}} \tag{44a}$$

and is compared against curve I, the exact elasticity solution. Curves III, IV, and V are different combinations of adding rotary interior and shear correction factors. Figure 3 suggests that the shear correction addition has the biggest impact on correcting the CPT case. The shear thickness parameter T2, in the NASTRAN CCONEAX elements appears to attempt to account for shear effects, however, this point has not been pursued with regard to attempting to make NASTRAN propagate flexural waves for $h/\lambda_\gamma > 0.15$.

The results in Figure 3 suggest that a h/λ_γ (plate thickness-to-flexural wavelength ratio) of limit of 0.15 be maintained, i.e.,

$$\frac{h}{\lambda_\gamma} \leq 0.15 \tag{45}$$

or equivalently,

$$\frac{\gamma h}{2\pi} \leq 0.15 \tag{45a}$$

where γ is the flexural wave number root of the problem at hand. The limit given by equation (45a) employed Figure 3 which is a plot based on a fixed Poisson's ratio (i.e., $\nu = 0.5$). The guideline formula can still be used for other values of Poisson's ratio due to the weak dependence of the plots on ν. In fact, for the common case of $\nu = 0.3$, a value of $h/\lambda_\gamma = 0.15$ implies a c_γ/c_s ordinate of 0.4598 for the CPT case and a value of 0.4032 in the exact

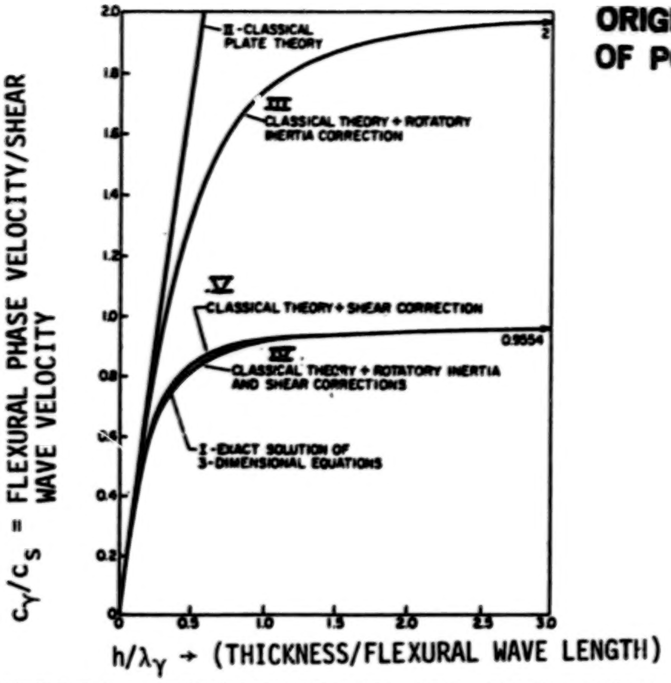

FIGURE 3. DEVIATION OF THIN WALL PLATE THEORY FROM EXACT THEORY

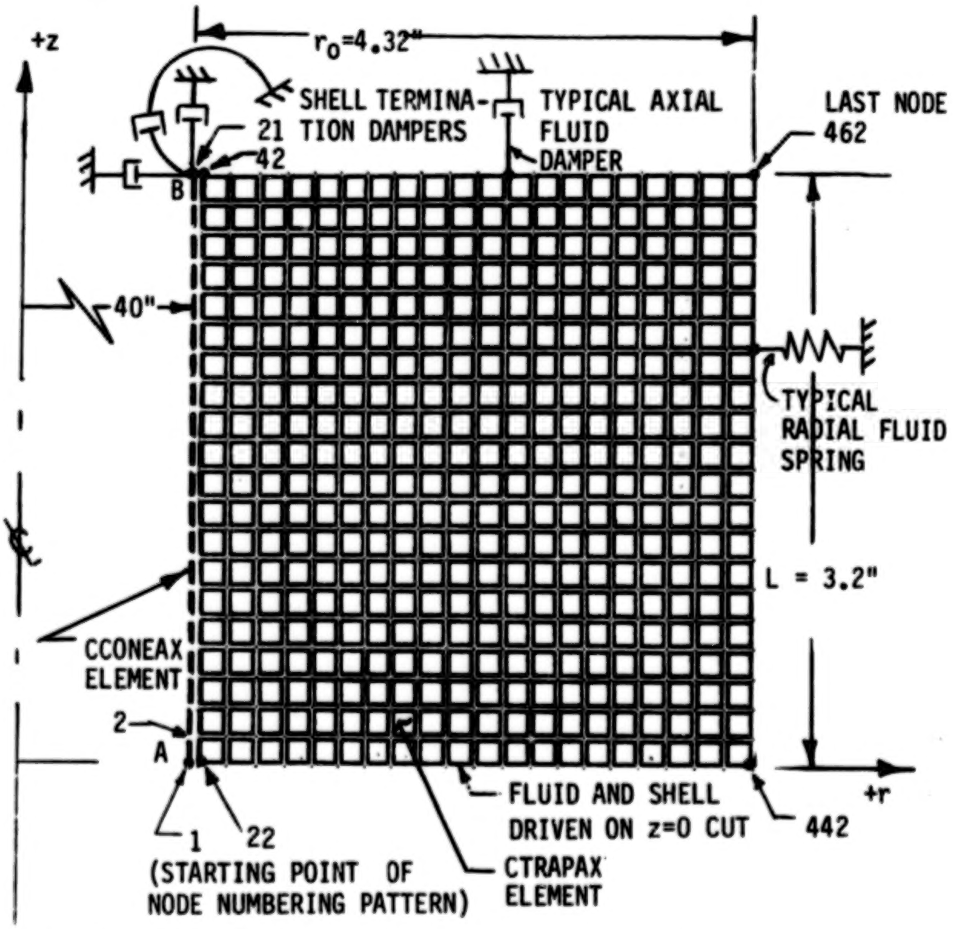
+z
r_0=4.32"
SHELL TERMINATION DAMPERS
21
42
TYPICAL AXIAL FLUID DAMPER
LAST NODE 462
B
40"
TYPICAL RADIAL FLUID SPRING
℄
L = 3.2"
CCONEAX ELEMENT
2
A
FLUID AND SHELL DRIVEN ON z=0 CUT
+r
1
22
(STARTING POINT OF NODE NUMBERING PATTERN)
CTRAPAX ELEMENT
442

FIGURE 4. FINITE ELEMENT MESH (20-ELEMENT SHELL)

theory case. However, for $\nu = 0.5$, a $h/\lambda_\gamma = 0.15$ implies a c_γ/c_s ordinate of 0.5441 in the CPT case and a value of 0.4629 in the exact theory case (computed from equation (40) of ref. 4). Thus, illustrating the Figure 3 $\nu = 0.5$ case is an extreme case (e.g., 17.5% deviaton for $\nu = 0.5$ compared to 14.0% for $\nu = 0.3$) with regard to the point at which CPT deviates from the exact theory.

Thus, to test inequality (45a), one simply employs the appropriate characteristic equation developed (e.g., equation (12b)) and after obtaining the flexural wave root γ, verify whether in equation (45a) is satisfied.

Comments on Mass Matrix

The issue of an appropriate mass matrix for dynamics problems has long been a topic of discussion in the literature on finite elements. Here we take the simpliest approach, namely that of a diagonal lumped mass matrix for the shell. Upon employing the lumped approach, for say CCONAX elements, NASTRAN generates zero valued rotary inertia mass matrix contributions. To fill this void, the work by ref. 8 was employed wherein the suggested diagonal rotary inertia terms at a node would be given by

$$I_r = \frac{m^e \ell^2}{24}\left[\frac{1}{10} + \left(\frac{h}{\ell}\right)^2\right] \tag{46}$$

for the single element contribution at a rotation degree-of-freedom node where m^e is the total mass of the element, ℓ is the element length, h the element thickness. Thus end point nodes with one element framing into the node employs equation (46) once and internal nodes with two elements framing into the same node applys equation (46) twice.

DEMONSTRATION PROBLEMS

A series of limited, yet fully representative, demonstration problems are presented here to illustrate the use of the procedures discussed in the theoretical section. First an in vacuo cylindrical shell is treated employing three different mesh distributions. Secondly, the same shell (employing the finer mesh distribution) is solved with external water present. All solutions are obtained with COSMIC SOL-8 employing the VAX computer version of NASTRAN.

In Vacuo Cylinder Example

An infinite cylindrical shell is excited and is propagating a constant amplitude harmonic wave in the plus z direction. The shell (shown in Figure 1) is cut at points A and B and is modeled as a 3.2 inch long, 20 element CCONEAX finite element model shown in Figure 4 (in the in vacuo case considered here, the fluid is omitted in the model). The point A (incident side of the shell) is driven with equations (23) and is terminated with three boundary dampers sized according to equations (27). The problem parameters correspond to the following data

$$a = 40.0'' \quad , \quad h = 0.20'' \quad , \quad E = 154{,}149.39 \text{ psi}$$
$$\nu = 0.3 \quad , \quad \rho_s = 0.000048, \quad \omega = 9749.99 \text{ rad/sec} \tag{47}$$

wherein the corresponding wave number roots to the characteristic equation (20) are given by

$$\gamma = 0.163949685 \quad \text{for the membrane root}$$
and
$$\gamma = 1.67707302 \quad \text{for the flexural wave root} \tag{48}$$

hence the membrane wavelength is 12.566 inches and the flexural wavelength is 3.7465 inches.

- flexural wave example

The shell termination dampers at cut B are computed upon substitution of the equation (48) flexural wave root into equations (27) to obtain

$$C_\theta = 4.8819909 \qquad C_Q = 13.7309605 \qquad C_N = 14.0269417 \tag{49}$$

and the shell edge forces, for an arbitrarily selected driven amplitude of $W_o = 1.0 \times 10^{-6}$, at the driver cut end A are obtained by substituting the flexural wave root into equations (23) to obtain (supressing the exponential time factor where dampers are installed with DMIG cards):

$$\tilde{M}_Z^A = 7.9827681 \times 10^{-2} \qquad \tilde{Q}^A = 0.1338768\ e^{i\pi/2}$$
$$\tilde{N}_Z^A = 6.175285 \times 10^{-4} \tag{50}$$

The rotary inertia mass entries are computed with equation (46). The corresponding NASTRAN input is given in Figure 5 for reference purposes. The exact solution is a constant amplitude displacement wave varying as

$$w = W_o\, e^{i(-\gamma z + \omega t)}$$

Consequently, the exact solution is easy to plot and is simply a constant magnitude radial displacement of magnitude $W_o = 1 \times 10^{-6}$ and whose phase angle rolls off linearly with z and reploting with spatial period $2\pi/\gamma$. The exact solution versus the NASTRAN solution is given in Figure 6 and shows good agreement between the exact solution and the corresponding NASTRAN solution. Since the model element spacing is 0.16 inches, the solution model is a 23½ element per wavelength case. In order to investigate the influence of mesh size on solution accuracy, the same 3.2 inch model was run for two coarser meshes; one having 5 elements and the other having only 3 elements. The same dampers and edge loads are reapplied to the coarser models. The resulting solutions are shown in Figure 7 and as can be seen, the quality of the solution (i.e., the ability of the cylindrical shell to propagate flexural waves) has degraded over the finer mesh example, particularly for the three element shell.

```
ID NUSC, FLEX WAVE IN SHELL WITH FORCE LOADING
DIAG 8,14
APP DISP
SOL 8
TIME 2400
CEND
TITLE= FLEX WAVE IN SHELL WITH FORCE LOADING
P2PP=DASH
M2PP=MASS
AXISYMMETRIC=COSINE
SDISPLACEMENTS(PHASE)=ALL
FREQUENCY=100
MAXLINES=600000
OLOAD=ALL
DLOAD=100
BEGIN BULK
AXIC           0
FREQ         100 1551.76
MAT1         6001554149.6                   .3 .000048
PCONEAX      160     600     .20     600.0006667     600    .167     0.0+PCON
+PCON         1.     -1.      0.      90.    180.
RLOAD2       400     101             103    1000
TABLED1     1000                                                     +TAB1
+TAB1        1.0     1.0  10000.     1.0    ENDT
DLOAD        100      1.      1.     400      1.     401
RLOAD2       401     889                    1000
DAREA*               889         1000001                       5     7.9827681-2
DPHASE       103 1000001       1     90.
DAREA*               101         1000001                       1      .1338768
DAREA*               889         1000001                       3     6.175285-4
DMIG    DASH       0       1       1       1
DMIG*               DASH         1000021                       1             *DASH1
*DASH1           1000021               1      13.7309605
DMIG*               DASH         1000021                       3             *DASH3
*DASH3           1000021               3      14.0269417
DMIG*               DASH         1000021                       5             *DASH2
*DASH2           1000021               5       4.8819909
DMIG    MASS       0       1       1       1
DMIG        MASS 1000001       5         1000001       5 6.988-7
DMIG        MASS 1000002       5         1000002       5 1.397-6
DMIG        MASS 1000003       5         1000003       5 1.397-6
DMIG        MASS 1000004       5         1000004       5 1.397-6
DMIG        MASS 1000005       5         1000005       5 1.397-6
DMIG        MASS 1000006       5         1000006       5 1.397-6
DMIG        MASS 1000007       5         1000007       5 1.397-6
DMIG        MASS 1000008       5         1000008       5 1.397-6
DMIG        MASS 1000009       5         1000009       5 1.397-6
DMIG        MASS 1000010       5         1000010       5 1.397-6
DMIG        MASS 1000011       5         1000011       5 1.397-6
DMIG        MASS 1000012       5         1000012       5 1.397-6
DMIG        MASS 1000013       5         1000013       5 1.397-6
```

```
DMIG        MASS 1000014       5         1000014       5 1.397-6
DMIG        MASS 1000015       5         1000015       5 1.397-6
DMIG        MASS 1000016       5         1000016       5 1.397-6
DMIG        MASS 1000017       5         1000017       5 1.397-6
DMIG        MASS 1000018       5         1000018       5 1.397-6
DMIG        MASS 1000019       5         1000019       5 1.397-6
DMIG        MASS 1000020       5         1000020       5 1.397-6
DMIG        MASS 1000021       5         1000021       5 6.988-7
RINGAX         1           40.00    0.00                     246
RINGAX         2           40.00    0.16                     246
RINGAX         3           40.00    0.32                     246
RINGAX         4           40.00    0.48                     246
RINGAX         5           40.00    0.64                     246
RINGAX         6           40.00    0.80                     246
RINGAX         7           40.00    0.96                     246
RINGAX         8           40.00    1.12                     246
RINGAX         9           40.00    1.28                     246
RINGAX        10           40.00    1.44                     246
RINGAX        11           40.00    1.60                     246
RINGAX        12           40.00    1.76                     246
RINGAX        13           40.00    1.92                     246
RINGAX        14           40.00    2.08                     246
RINGAX        15           40.00    2.24                     246
RINGAX        16           40.00    2.40                     246
RINGAX        17           40.00    2.56                     246
RINGAX        18           40.00    2.72                     246
RINGAX        19           40.00    2.88                     246
RINGAX        20           40.00    3.04                     246
RINGAX        21           40.00    3.20                     246
CCONEAX        1     160       1       2
CCONEAX        2     160       2       3
CCONEAX        3     160       3       4
CCONEAX        4     160       4       5
CCONEAX        5     160       5       6
CCONEAX        6     160       6       7
CCONEAX        7     160       7       8
CCONEAX        8     160       8       9
CCONEAX        9     160       9      10
CCONEAX       10     160      10      11
CCONEAX       11     160      11      12
CCONEAX       12     160      12      13
CCONEAX       13     160      13      14
CCONEAX       14     160      14      15
CCONEAX       15     160      15      16
CCONEAX       16     160      16      17
CCONEAX       17     160      17      18
CCONEAX       18     160      18      19
CCONEAX       19     160      19      20
CCONEAX       20     160      20      21
ENDDATA
```

FIGURE 5. TWENTY ELEMENT CYLINDRICAL SHELL EXAMPLE DATA FOR FLEXURAL WAVE RUN

ORIGINAL PAGE IS
OF POOR QUALITY

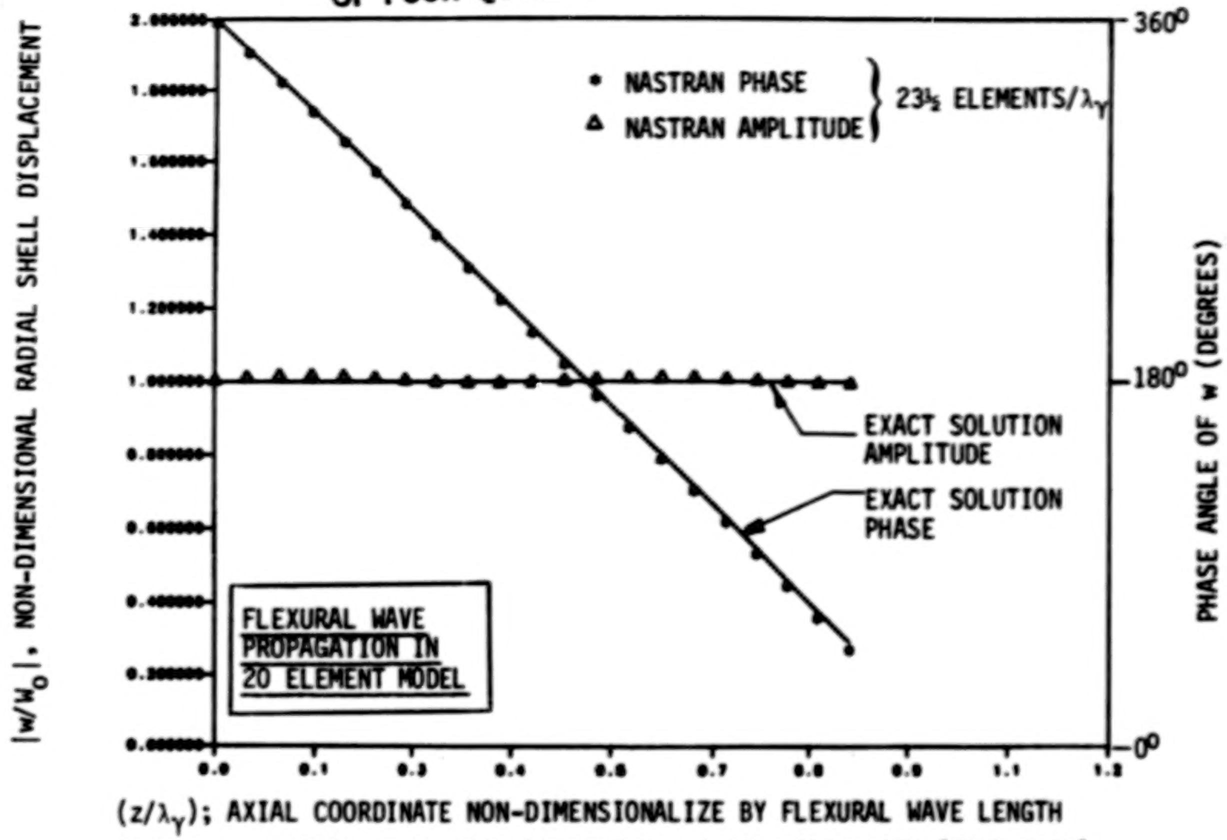

FIGURE 6. RADIAL SHELL DISPLACEMENT VS. AXIAL COORDINATE (FINE MESH) FOR 23½ FLEXURAL WAVE LENGTHS PER ELEMENT

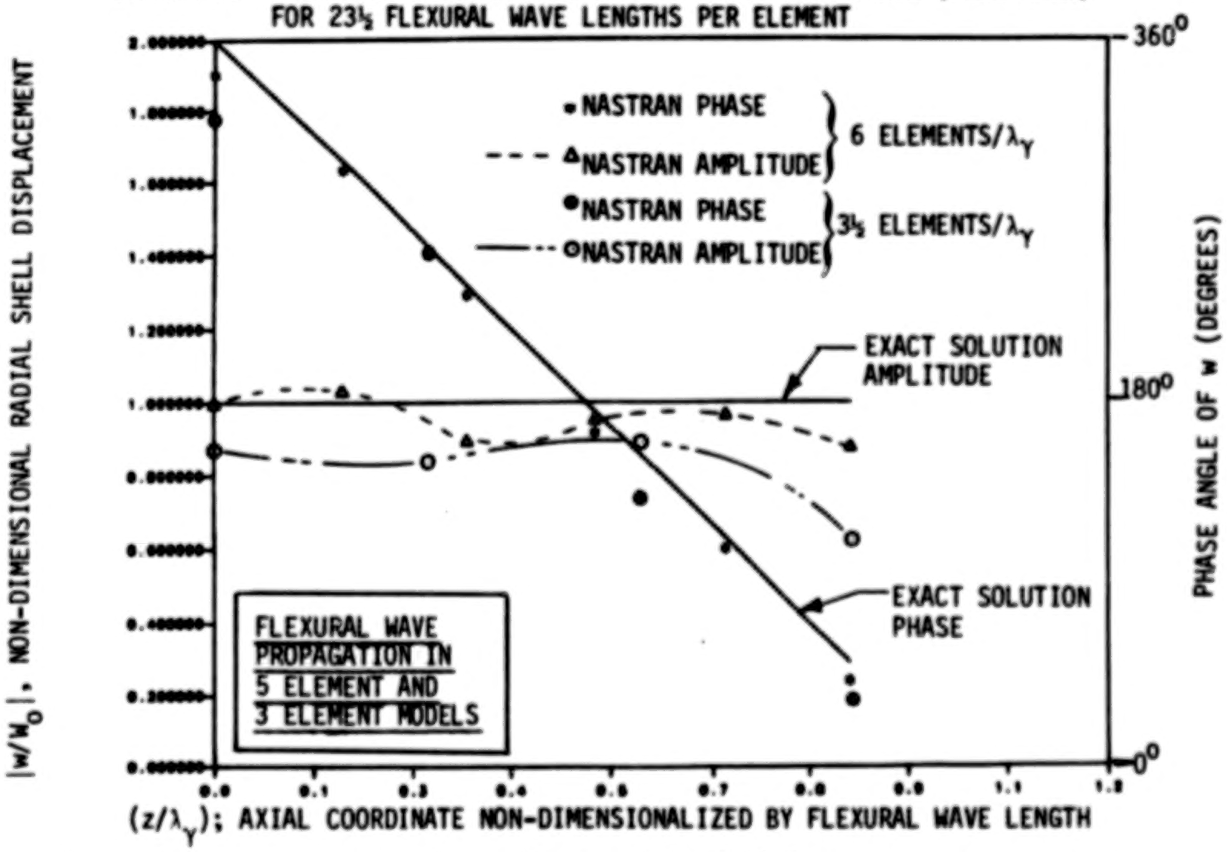

FIGURE 7. RADIAL SHELL DISPLACEMENT VS. AXIAL COORDINATE (COARSE MESH) FOR 6 AND FOR 3½ FLEXURAL WAVE LENGTHS PER ELEMENT

- membrane wave example

Again, the 20 element model is considered, except in this case, we propagate a membrane wave along the +z direction of the same cylindrical shell considered for the flexural wave example. The procedure is exactly the same here, except that the membrane root (first of equations (48)) is employed to compute the shell termination dampers and driving moments and forces. Thus, substituting the membrane root into equations (27) and (23), the model dampers and edge loads are in this case:

$$C_\theta = 0.4772607 \qquad C_Q = 0.012828529 \qquad C_N = 143.484479$$

and

$$\tilde{M}_Z^A = 7.6290549 \times 10^{-4} \qquad \tilde{Q}^A = 1.2507811 \times 10^{-4}\, e^{i\pi/2}$$

$$\tilde{N}_Z^A = -29.909871$$

The solution response for the dominant axial motion is plotted in Figure 8 and is non-dimensionalized with respect to the, U_0, axial wave amplitude magnitude (by equation (15), $|U_0| = 21.37985 \times 10^{-6}$ when $W_0 = 1.0 \times 10^{-6}$). The radial deflection, non-dimensionalized with respect to W_0, is given in Figure 9. The quality of the solution is seen to be very accurate, as would be expected since the wavelength is substantially longer than the flexural wave example (e.g., $(2\pi/.0163949)/0.16 = 239\frac{1}{2}$ elements per wavelength.

Submerged Cylinder Example (Flexural Wave)

Again, the same 20 element cylindrical shell is considered, except here, the shell is submerged in water (external water only where $c = 60{,}000.$ in/sec and $\rho = 0.000096$). Substituting the equation (47) parameters into equation (7b), and solving for the wave number roots, it is found that

$$\begin{aligned} \gamma &= 0.164124528 && \text{for the membrane root} \\ \text{and} \\ \gamma &= 2.51631787 && \text{for the flexural root.} \end{aligned} \tag{51}$$

Comparing the second of equations (51) to the in vacuo wave number, it is noted that the presence of the fluid shortened the wavelength by a factor of $\approx 2/3$. Substituting the flexural root into equations (27) and (23), the model dampers and edge loads (for a $W_0 = 1 \times 10^{-6}$ shell amplitude) are given by

$$C_\theta = 7.32505101 \quad , \quad C_Q = 46.3811654 \quad , \quad C_N = 9.34867391$$

and

$$\tilde{M}_Z^A = 0.179713448 \quad , \quad \tilde{Q}_A = 0.452216160\, e^{i\pi/2} \quad ,$$

$$\tilde{N}_Z^A = 2.7283602 \times 10^{-4}$$

In addition, the $z = L$ boundary cut damper is given through equation (40), the $= r_0 = 43.2$ inch fluid boundary spring by equation (44) and the $z = 0$ pressure loading by equation (31). The pressure values are enforced by applying the stiff spring approach, where the stiff spring constant is sized to be 1000

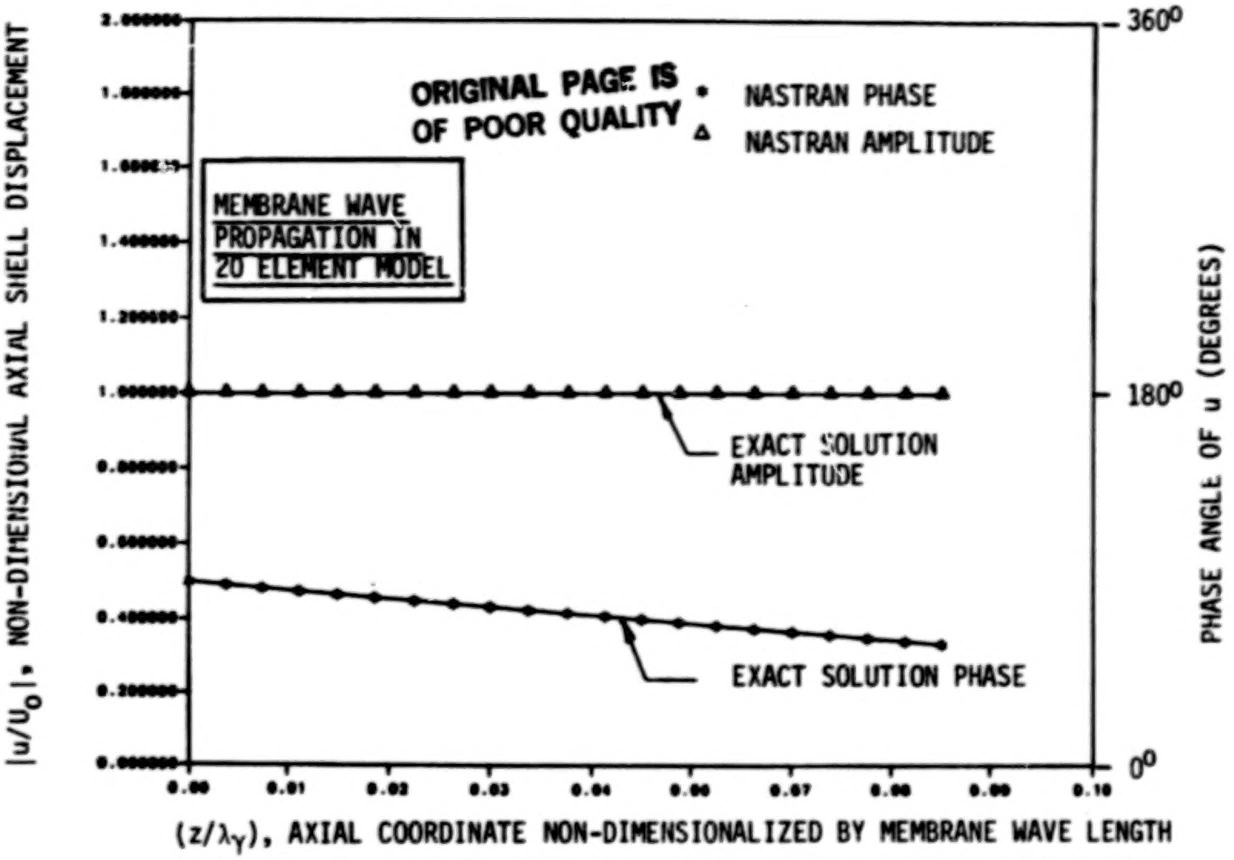

FIGURE 8. AXIAL SHELL DISPLACEMENT VS. AXIAL COORDINATE (FINE MESH)

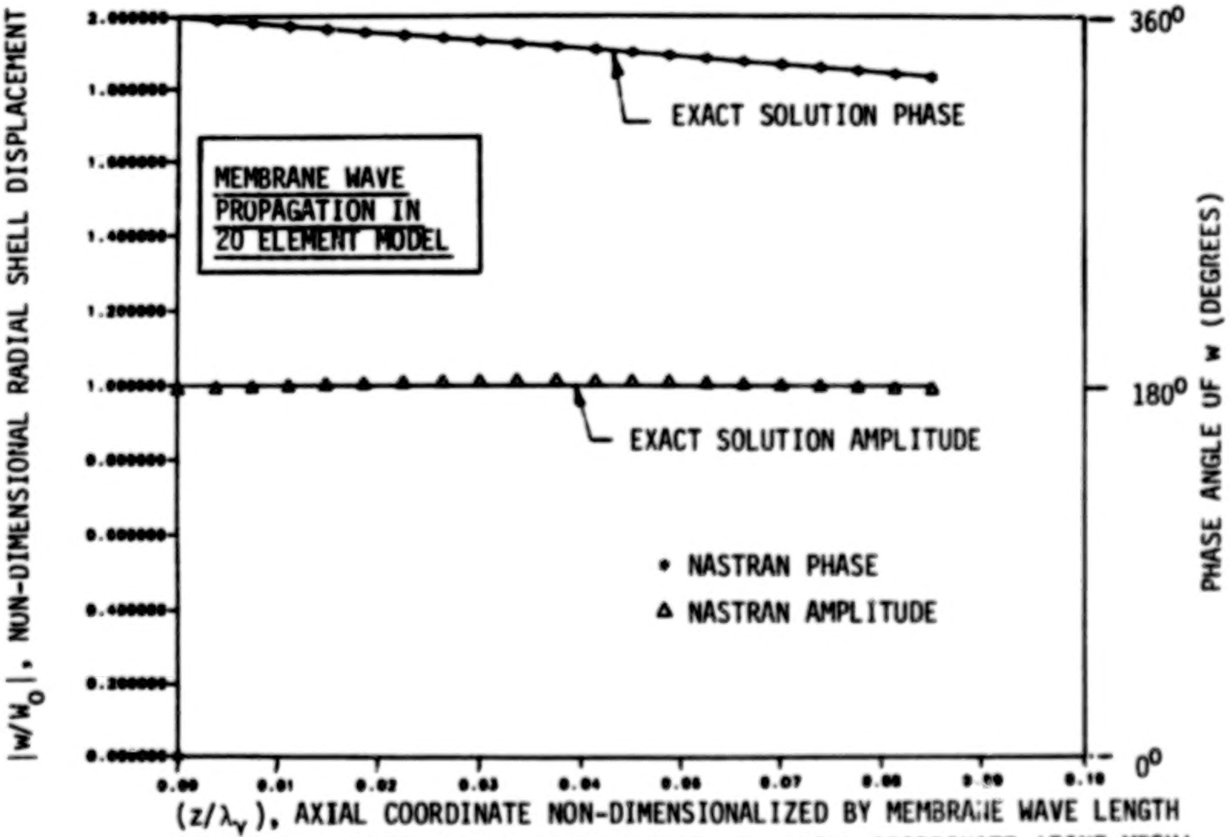

FIGURE 9. RADIAL SHELL DISPLACEMENT VS. AXIAL COORDINATE (FINE MESH)

times the regular pressure element stiffnesses and the applied force is the pressure times the stiff spring. The actual data input is shown in Figure 10, where the obvious repetitive pattern to the numbering system of Figure 4, permits us to leave out most of the grid coordinate cards, element cards, and fluid-to-structure DMIG connection cards while leaving behind representative examples of each kind. The resulting response for the radial deflection is plotted in Figure 11 and the corresponding pressure in the fluid (at the surface of the structure) is plotted in Figure 12. Both the deformation and pressure are seen to track the exact solution closely. A graphical representation of the entire pressure field amplitude is shown in Figure 13 through employing the PATRAN fringe color plotting feature. Plotting data in this fashion shows bands of data having the same magnitude spread, as a single color. Narrow bands at the surface spreading outward radially to increasingly wider bands show the exponential type decay in the pressure field.

CONCLUDING REMARKS

The results in this paper demonstrate a procedure by which the NASTRAN computer program can be employed to check the ability of the NASTRAN program to model membrane and flexural waves existing in both in vacuo and submerged cylindrical shells and flat plates. The study is limited to a range of frequencies where rotary inertia and shear correction factors are not necessary to model the corresponding wave propagation. For the demonstration problems considered, the wave propagation ability of the elements considered appears to fall off rapidly, once lessthan 6 elements per wavelength are considered. For example, in the 6 element per flexural wavelength problem, the worse nodal point magnitude was in error by 12 % for the radial deflection, whereas the error was 36.7% for the 3½ element per wavelength example. It is recommended that the user make his own test with regard to mesh fineness necessary to achieve a particular level of accuracy. For example, when the propagating wave root is in the neighborhood of a cutoff frequency (i.e., a condition where no propagating wave exists), finer meshes than experineced in the demonstration considered in this paper may be needed. For most cases experienced by the authors, however, 10 elements per wavelength appears to provide good results for properly modeling the wave propagation for flexure and membrane waves in the kinds of elements considered herein.

ORIGINAL PAGE IS
OF POOR QUALITY

```
ID NUSC, FLEX WAVE WITH WATER LOADING
DIAG 8,14
APP DISP
SOL 8
TIME 240
CEND
TITLE= FLEX WAVE WITH WATER LOADING FREQUENCY=15517.41 HZ
B2PP=DAMP
M2PP=MASS
K2PP=STIF
AXISYMMETRIC=COSINE
DISPLACEMENTS(PHASE)=ALL
FREQUENCY=100
MAXLINES=600000
OLOAD=ALL
DLOAD=100
BEGIN BULK
AXIC           0
FREQ         100 1551.76
MAT1         600154149.6                     .3 .000048
PCONEAX      100     600     .20     600.0008667     600    1.67   0.0+PCOP
+PCOP         1.     -1.      0.     90.    180.
RLOAD2       600     106                    1000
TABLED1     1000                                                   +TAB1
+TAB1        1.0     1.0  10000.     1.0    ENDT
DLOAD        100      1.      1.     600      1.     602
PTRAPAX      150             500
MAT1         500         145600.  50000. .000096
RLOAD2       602     800             103    1000
DAREA        106 1000001       5.1797134
DPHASE       103 1000001       1     90.
DAREA        800 1000001       1.4522162
DAREA        106 1000021       32.7284-6
DMIG        MASS 1000021       1         1000021         146.38117
DMIG        MASS 1000021       3         1000021         39.368674
DMIG        MASS 1000021       5         1000021         57.329051
DMIG    STIF       0       1       1       1
DMIG    MASS       0       1       1       1
DMIG    DAMP       0       1       1       1
DAREA*                   106         1000022               3    -.363431E+11
DAREA*                   106         1000043               3    -.242700E+11
DAREA*                   106         1000064               3    -.162076E+11
DAREA*                   106         1000085               3    -.108236E+11
DAREA*                               1000106               3    -.7726
DAREA*
DM
*       175      1000358          10
DMIG*   STIF                     1000379                      3     *    185
*       185      1000379                3         1.E+13
DMIG*   STIF                     1000400                      3     *    195
*       195      1000400                3         1.E+13
DMIG*   STIF                     1000421                      3     *    205
*       205      1000421                3         1.E+13
DMIG*   STIF                     1000442                      3     *    215
*       215      1000442                3         1.E+13
DMIG*   STIF                     1000443                      3     *    A25
*       A25      1000443                3 87689064.000000
DMIG*   STIF                     1000444                      3     *    A35
*       A35      1000444                3 87689064.000000
DMIG*   STIF                     1000445                      3     *    A45
*       A45      1000445                3 87689064.000000
DMIG*   STIF                     1000446                      3     *    A55
*       A55      1000                   3     68.000000

*
DMIG*                            1000461                            *    A205
*   A205         1000461                3 87689
DMIG*   STIF                     1000462                      3     *    A215
*   A215         1000462                3 10844567.000000
DMIG*   DAMP                     1000462                      3     *    AB15
*   AB15         1000462                3     1933.227905
DMIG*   DAMP                     1000441                      3     *    AB25
*   AB25         1000441                3     3859.287471
DMIG*   DAMP                     1000470                      3     *    AB35
*   AB35         1000470                3     3844.935547
DMIG*   DAMP                     1000399                      3     *    AB45

*   AB20
DMIG*   DAMP                     1000042                      3     *    AB2
*   AB215        1000042                3     1796.933472
DMIG*   STIF                     1000022                      1     *     10
*        10      1000001                1       20.108194
DMIG*   STIF                     1000022                      3     *     11
*        11      1000001                3        0.000001
DMIG*   MASS                     1000001                      1     *     12
*        12      1000022                3     -667.075256
DMIG*   MASS                     1000001                      3     *     13
*        13      1000022                3       -0.000078
DMIG            1000017       5                 1       5 1.397-6
DMIG        MASS 1000018       5         1000018       5 1.397-6
DMIG        MASS 1000019       5         1000019       5 1.397-6
DMIG        MASS 1000020       5         1000020       5 1.397-6
DMIG        MASS 1000021       5         1000021       5 6.990-7
RINGAX         1           40.00    0.00                     246
RINGAX         2           40.00    0.16                     246
RINGAX         3           40.00    0.32                     246
RINGAX         4           40.00    0.48                     246
RINGAX         5           40.00    0.64                     246
               6                    0.80                     246
RI
RINGAX         :           43.20                           12456
RINGAX       460           43.20    2.88                   12456
RINGAX       461           43.20    3.04                   12456
RINGAX       462           43.20    3.20                   12456
CCONEAX        1     100       1       2
CCONEAX        2     100       2       3
CCONEAX        3     100       3       4
CCONEAX        4     100       4       5
CCONEAX        5     100       5
               6     100
CCON           :              18      19
CCONEAX       19     100      19      20
CCONEAX       20     100      20      21
CTRAPAX       21     150      22      43      44      23
CTRAPAX       22     150      23      44      45      24
CTRAPAX       23     150      24      45      46      25
CTRAPAX       24     150      25      46      47      26
              25     150      26      47      48      27
                     150                      49      28
                                              460
CTRAPAX      419     150     439     460      461     440
CTRAPAX      420     150     440     461      462     441
ENDDATA
```

FIGURE 10. TWENTY ELEMENT SUBMERGED SHELL EXAMPLE DATA FOR FLEXURAL WAVE RUN

ORIGINAL PAGE IS
OF POOR QUALITY

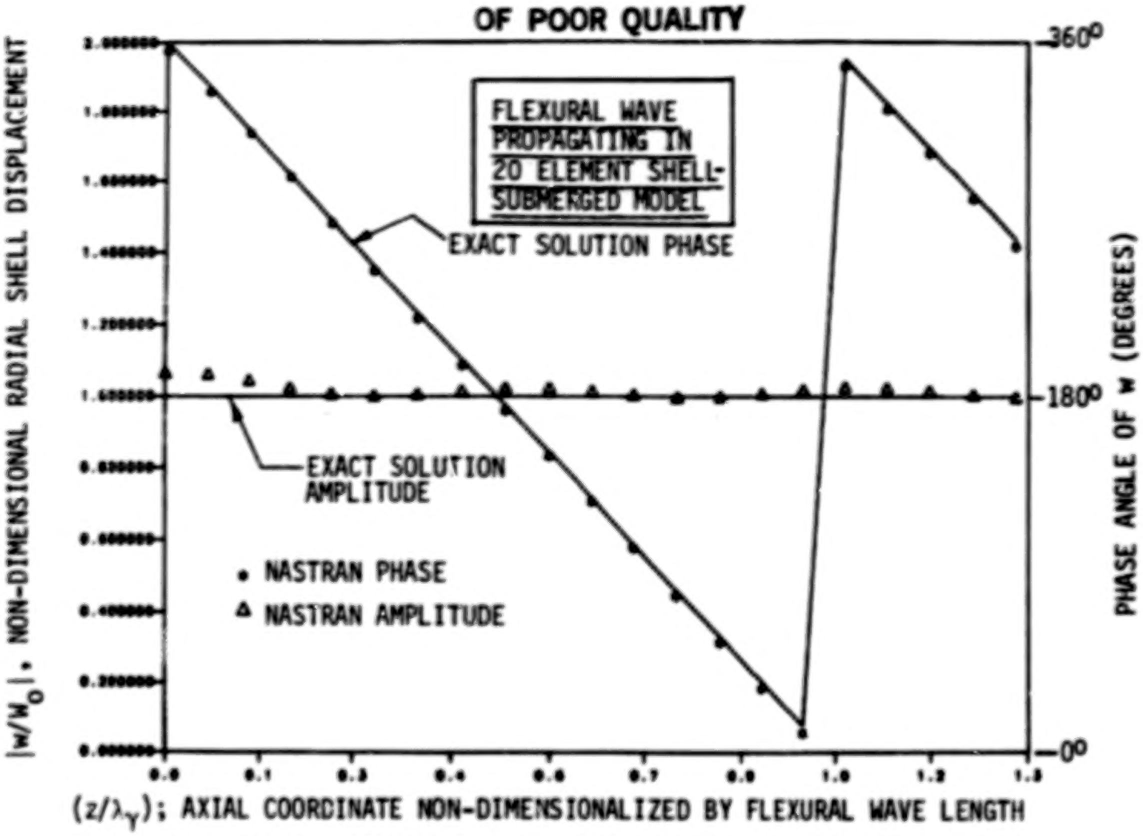

FIGURE 11. RADIAL DISPLACEMENT VS. AXIAL COORDINATE FOR 15½ FLEXURAL WAVE LENGTHS PER ELEMENT (SUBMERGED SHELL)

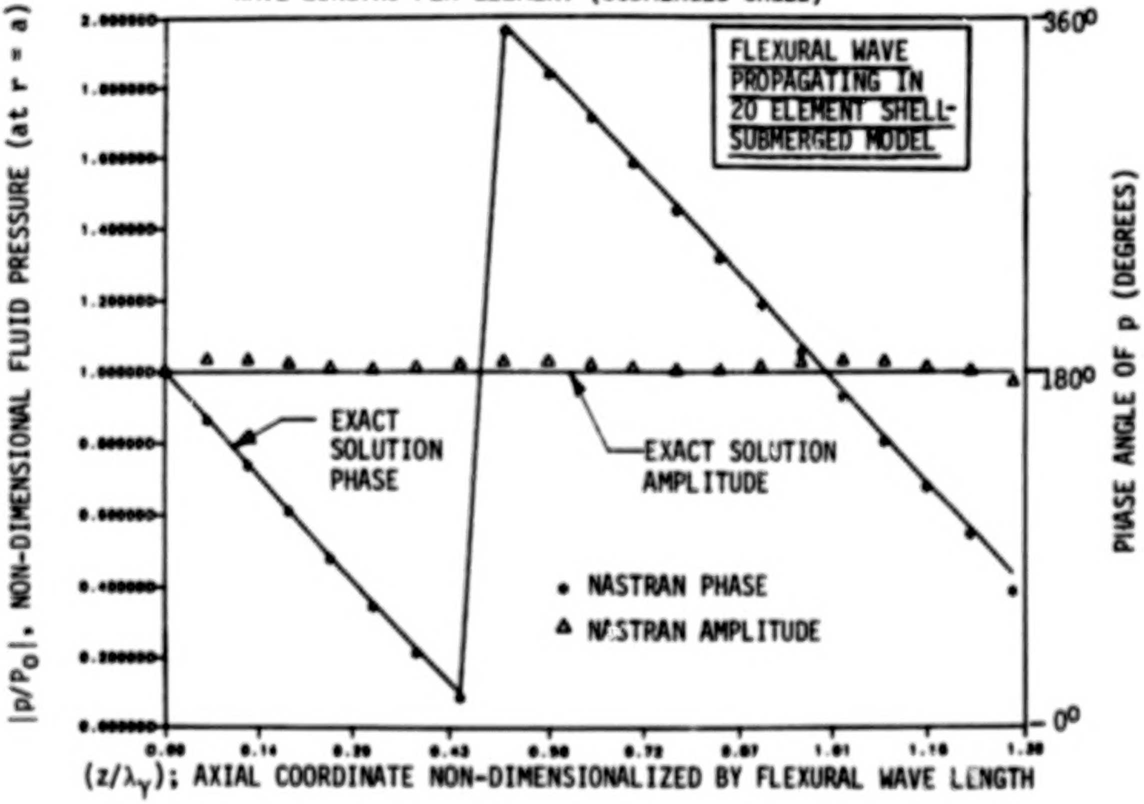

FIGURE 12. SURFACE PRESSURE VS. AXIAL COORDINATE FOR 15½ FLEXURAL WAVE LENGTHS PER ELEMENT (SUBMERGED SHELL)

ORIGINAL PAGE IS
OF POOR QUALITY

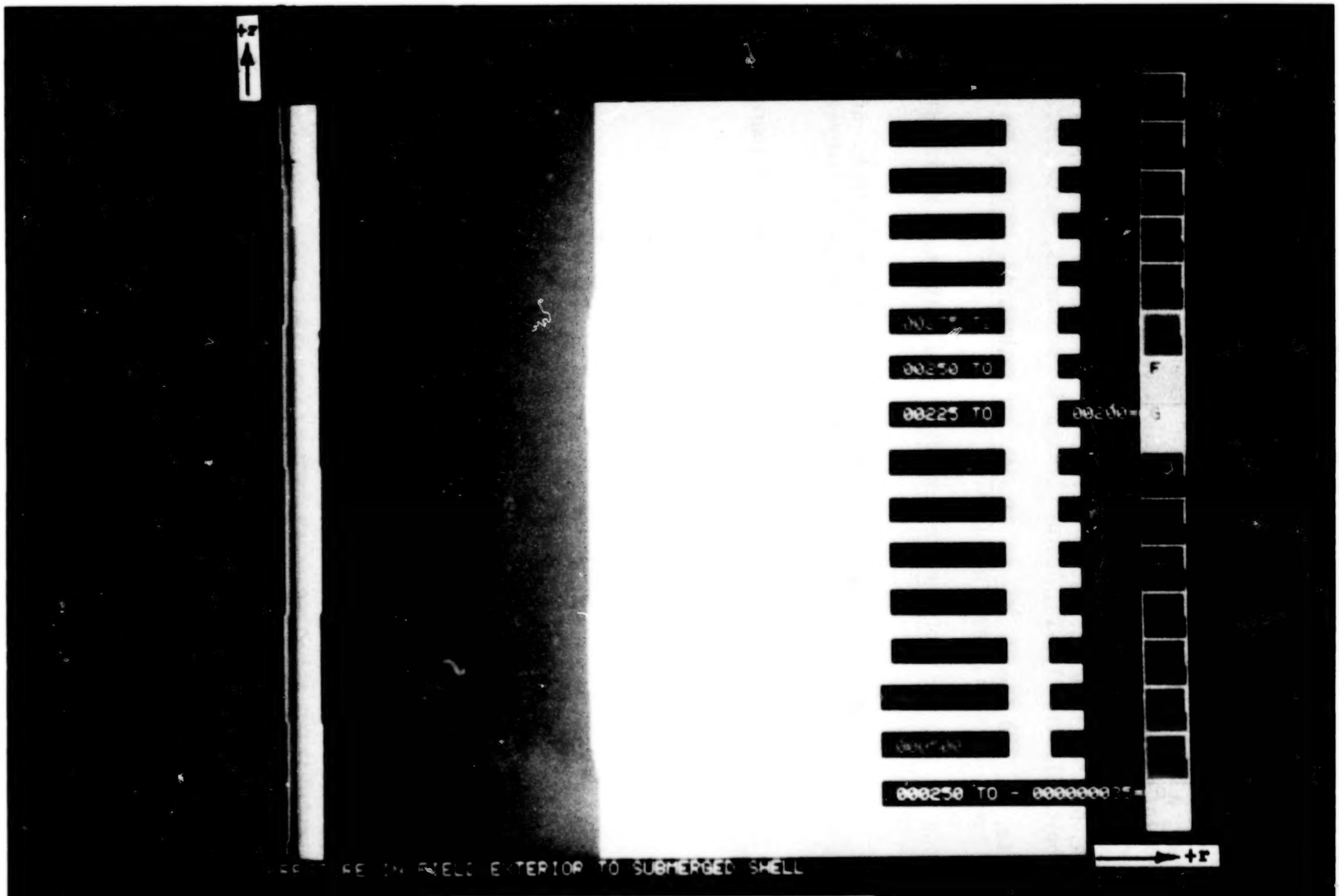

FIGURE 13. FRINGE PLOTS FOR PRESSURE AMPLITUDE IN FLUID FIELD

REFERENCES

1. Flügge, W., Stresses in Shells, Springer-Verlag, 1962.

2. Junger, M. C., and Feit, D., Sound, Structures, and Their Interaction, MIT Press, Cambridge, 1972.

3. Kalinowski, A. J., and Nebelung, C. W., "Solution of Axisymmetric Fluid Structure Interaction Problems", Tenth NASTRAN User's Colloquium, NASA Conference Publication 2249, May 1982.

4. Midlin, R. D., "Influence of Rotary Inertia and Shear on Flexural Motions of Isotropic, Elastic Plates", Journal of Applied Mechanics, March 1951.

5. Abramowitz, M., and Stegun, I. A., Handbook of Mathematical Functions, National Bureau of Standards, June 1964.

6. Zienkiewicz, O. C., The Finite Element Method, (3rd Edition), McGraw-Hill Book Company, 1977.

7. Pica, A., and Hinton, E., "Transient and Pseudo-Transient Analysis of Mindlin Plates", International Journal for Numerical Methods in Engineering, Vol. 15, 1980.

8. Cook, R. D., "Remarks About Diagonal Mass Matrices", International Journal for Numerical Methods in Engineering, Vol. 17, 1981.

N84
15603

UNCLAS

D/13

N84 15603

DYNAMIC CERTIFICATION OF A THRUST-MEASURING SYSTEM FOR LARGE SOLID ROCKET MOTORS*

R. A. LeMaster and R. B. Runyan
Sverdrup Technology, Inc./AEDC Group

INTRODUCTION

The J-4 Rocket Test Cell and its Thrust Measuring System (TMS) at Arnold Engineering Development Center (AEDC) were modified to provide multicomponent force measurement of large solid rocket motors having nozzle gimbaling capability. To verify the structural integrity of a combined TMS and motor system, a large finite element model of the TMS and motor was developed using the MSC/NASTRAN computer program. Due to the importance of obtaining accurate estimates for the dynamic force levels, it was necessary to certify that the model adequately simulated the physical system. This was accomplished by performing a modal analysis test on the TMS and motor combination. The objectives of this paper are: (1) to discuss the physical characteristics of the TMS and motor that influence the MSC/NASTRAN model; (2) to compare the frequency response characteristics computed using the MSC/NASTRAN model to those obtained from the modal analysis test; (3) to discuss the experiences gained in modal analysis testing; and (4) to demonstrate how state-of-the-art experimental and analytical methods are used in the design of ground test facilities.

Due to economic and/or time constraints associated with performing experimental investigations on large, complex structures, the structural analyst rarely has the opportunity to determine how well his finite element representation simulates the characteristics of the actual structure. Finite element calculations have been shown to agree very well with experimental data for simple components. However, little data is available concerning how well they agree for complex structures comprised of many components. Since the TMS and motor combination are comprised of structural components from aerospace, mechanical, and civil engineering disciplines, the methods, results, comparisons, and conclusions drawn from this activity will be of interest to the dynamics and structures community in general.

In the following sections, descriptions of the TMS, finite element model, and modeling assumptions will be given in conjunction with the analysis methods. Subsequent sections will discuss the experimental effort and compare the experimental data to the computed results.

---

[*] The work reported herein was performed by the Arnold Engineering Development Center (AEDC), Air Force Systems Command (AFSC). Work and analysis for this research were done by personnel of Sverdrup Technology, Inc., operating contractor of the AEDC Engine Test Facility. Further reproduction is authorized to satisfy the needs of the U. S. Government.

THRUST-MEASURING SYSTEM

During simulated altitude testing, the motor is restrained by a large fixture which is referred to as the Thrust-Measuring System. The TMS is designed to react and measure the six components of thrust developed by the motor, and is rated at 2.2 MN (500,000 lb) axial force and 222.2 kN (50,000 lb) side force. The TMS is very massive, using eight W 36 x 400 beams to react the primary forces. The location of the TMS within the J-4 Rocket Test Cell is shown in figure 1. Figure 2 shows the main thrust stand structure prior to installation in the test cell.

During testing, the TMS is required to withstand large dynamic forces created by ignition and gimbaling transients. The magnitude of the dynamic forces may be several times the static values and is a function of the motor dynamics and its interaction with the TMS.

The TMS contains a large number of structural connections, many of which contain secondary members which intersect with primary members at odd angles. In general, the depth of the secondary members is significantly less than that of the primary member, and the secondary members are welded only to the flange or web of the frame member. Consequently, the mechanical behavior of the connections is quite complex. Three typical connections are shown in figures 3a, b, and c.

Figure 3a shows one of eight connections where the main thrust-measuring system structure connects to a 3.048-m (10 ft) support column. The support column is made from 0.91-m (36 in.)-diameter thick-walled pipe and has longitudinal stiffeners located every 36 deg around its circumference. As seen in figure 3a, several secondary support and bracing members attach to the main girder and intersect it at odd angles at various locations (i.e., flange or web). Since the secondary member intersecting the main girder web is much smaller than the main girder, the plate behavior of the main girder web will influence the stiffness of the connection.

Figure 3b shows another connection used several times in the TMS. Again, note the relative size of the main girder and secondary member; the plate behavior of the web will influence the connection stiffness characteristics. Also shown in figure 3b is a typical triaxial strain gage accelerometer and mounting block installation. The orientation and positioning of the accelerometers and mounting blocks are discussed in a subsequent section.

Figure 3c shows another typical connection in which the secondary members intersect the main girder at odd angles, and are much smaller than the main girder. Clearly, the load-deflection behavior of these connections will be quite complex.

FINITE ELEMENT ANALYSIS

Experience has shown that significant dynamic interactions may develop during ignition and gimbaling transients. The magnitudes of the dynamic interactions are influenced by coupling between the vertical and lateral motion of the TMS as it responds to the load transients. Therefore, it is necessary that the complicated modes of vibration characterizing the TMS be adequately defined.

A large finite element model of the TMS and motor combination was developed using the MSC/NASTRAN computer program. The finite element model of the TMS (shown graphically in figure 4) is comprised primarily of beam elements. Truss elements were used to represent the load-measuring column behavior; the flexures were treated as pinned connections. Experimentally obtained axial stiffness coefficients for the load-measuring columns were used to establish the equivalent properties of the truss elements.

The magnitude of the effort required to model the connections using three-dimensional continuum or plate elements dictated that assumptions be made regarding the kinematic behavior of the connections. It was often necessary to idealize a connection as being either fixed or pinned; in some cases linear constraint equations were written to describe the kinematic behavior of the connections. This type of connection idealization is universally used in the day-to-day application of finite element programs to the analysis of frame structures; it is also one of the more significant approximations. In later sections, the impact of the connection modeling assumptions will be discussed in light of the accuracy of the computed modes.

Mass and stiffness matrices of the solid rocket motor were obtained from the motor manufacturer and added to the structural model of the TMS. The case of the motor was represented using shell elements, and the propellant was represented by three-dimensional, continuum-type elements. A simplified material representation of the propellant was used which represented its anticipated frequency response characteristics. However, the viscous character of the propellant was not considered.

The motor and TMS models were combined using standard substructuring methods (references 1 and 2). Since the two models were developed by two different companies, it was not possible to use the automated substructuring techniques available in the MSC/NASTRAN computer program. Therefore, the partitioning and merging matrix operations necessary to combine the two models were implemented through direct matrix abstraction program (DMAP) modifications to the appropriate rigid format solution modules. The partitioning vectors for both the motor and TMS matrices were supplied as input in the bulk data decks. The mass and stiffness matrices representing the motor were transmitted to and from permanent disc storage using the INPUT4 and OUTPUT4 IO modules.

The combined TMS and motor model was used to compute the first thirty natural frequencies and mode shapes of the system. The system response to various excitation sources was obtained through superposition of the modal responses. To make the analysis more manageable, the integration of the uncoupled equations and the subsequent summation of the modal responses were performed outside of NASTRAN, using in-house software as illustrated in figure 5. Using this technique, stresses were obtained in an interactive manner on an element-by-element basis. When it was determined that the stress history in a particular element was required, the stress-displacement matrix for that element was created using the geometric and material data from the NASTRAN bulk data deck. The appropriate modal displacements were subsequently determined using the eigenvalues and time histories of the generalized coordinates; the appropriate stresses were then computed. This technique proved to be very efficient and significantly decreased the amount of peripheral storage required to retain the dynamic stress and displacement histories. The only quantities saved were the time histories of the generalized coordinates and the mode shapes, or eigenvectors. It was also very convenient since the analyst did not have to specify which displacements and stresses he wished to have printed out or retained prior to executing the actual analysis (as required by many finite element programs). This method also significantly reduced royalty costs associated with using MSC/NASTRAN, since NASTRAN was used only to assemble the component matrices and compute the natural frequencies and mode shapes; all remaining computations were performed outside of NASTRAN.

EXPERIMENTAL MODAL SURVEY

In recent years an impact testing technique commonly referred to as "modal analysis testing" has been developed which enables the natural frequencies and modal properties of a system to be determined experimentally. In addition, the mode shapes may be displayed in animated motion on a graphics computer terminal. The modal analysis methods enable the structural analyst to study a particular mode of the structure and to compare the frequency and mode shape to those obtained from a finite element analysis. In addition, the damping associated with a particular mode can be obtained and used as input to the finite element model. One benefit of the modal analysis method is that it provides experimental data in a form directly compatible with the results of a finite element analysis. The analyst may then evaluate which modes are accurately represented, and may gain insight as to how the finite element model may be improved.

Modal testing requires both the excitation and the response of the structure to be recorded. The excitation and response time histories are transformed to the frequency domain, and the frequency response function relating the response to the excitation is obtained. The selective acquisition of a family of frequency response functions having a common excitation point enables the modal parameters of the structure to be obtained. For detailed treatments on modal analysis methods, the interested reader is referred to references 2 through 10.

To adequately define the complicated mode shapes of the TMS and the motor combination, three-dimensional accelerometer readings were required at 54 different locations on the structure. This resulted in having accelerometer response data at almost every major connection on the structure (figure 6). An actual motor having an inert propellant was used to insure that the dynamic characteristics of the motor were properly represented.

The quality of the modal analysis results is directly proportional to the quality of the excitation and response time history data. A major problem at the onset of the modal analysis effort was to determine how to excite the structure to such an extent that the low-frequency response (1-30 Hz) of the structure could be measured. It is a relatively easy matter to excite the high-frequency modes of a structure, but to adequately excite the low-frequency modes of massive structures is not as simple. In addition, a time constraint required that the modal testing be completed within a short time, including instrumentation and hardware setup.

Impact Method No. 1

Two different instrumentation and impact device configurations were tried. The basic idea behind the first setup was to obtain accelerometer response data at as many locations as possible for each impact. The advantage of this approach is that it enabled the experimental data to be obtained quickly. A major disadvantage is that every channel of the data cannot easily be visually inspected on an oscilloscope as the data are being recorded. Therefore, it is not known until the data are being reduced whether all channels contain good data.

Accelerometers available for this test were in the 5- and 10-G range and were of the strain gage type. Computations performed using the finite element representation of the structure indicated that a 400-kN (90,000 lb) impact force would be required to excite the low-frequency modes sufficiently to obtain a good signal. A device designed to deliver the impact force, shown in figure 7, consisted of a pendulum having a swing radius of 3.048m (10 ft). The pendulum bob [a 10.16-cm (4 in.)-diam by 60.96-cm (24 in.)-long steel cylinder] was allowed to swing free and impact on the anvil containing a quartz force ring; it was manually caught on rebound to prevent multiple impacts. The pendulum impact device was designed to excite modes having a significant participation in the lateral direction.

Several problems were encountered which limited the usefulness of the pendulum impact device and associated instrumentation. These are listed below:

1. The impact device did not yield clean impulse time domain profiles and corresponding frequency spectra. Discontinuities in the impact anvil and force ring assembly resulted in partial reflection of the impact force, and the "hammer" chattered with the anvil surface during contact. Details of the anvil assembly are shown in figure 8.

2. Instrumentation problems prevented obtaining good data on all recorder channels for a given impact.

3. The accelerometers were not sensitive enough to obtain good signal-to-noise ratio signals.

Impact Method No. 2

To overcome the problems encountered with the high energy impact setup, a commercially available instrumented sledge hammer and a high sensitivity seismic accelerometer, shown in figure 9, were used. The sledge hammer is capable of developing up to a 22-kN (5,000 lb) impact load, and provided a flat impulse spectrum over the frequency range of interest. The seismic accelerometer has a rated sensitivity down to 10^{-6} G, and weighs approximately one-half kilogram (one pound). Response data obtained using this hardware were on the order of 10^{-3} G. Compared to the first impact device, the instrumented sledge hammer provided a relatively low level energy input into the system.

The data were obtained using a roving accelerometer procedure in which a single accelerometer was moved to the various response locations; the impact location was considered the reference point throughout the modal analysis. To obtain accelerometer response data in three orthogonal directions of each data location on the structure, it was necessary to install mounting blocks at each location. The mounting blocks were fabricated to provide a flat surface perpendicular to each of the three measurement directions. A typical mounting block is shown in figure 3b, with a triaxial accelerometer mounted on its top face.

Since only one single-axis high sensitivity accelerometer was available, it was necessary to relocate the accelerometer in each of the three measurement directions at each measurement location. This was the most time-consuming operation of the entire job. To ensure that all modes of the structure had been excited, three different impact points having different impact directions were utilized. All three impact points were located on the aft firing ring of the motor.

This method requires considerably more time than the previous method. However, since only one pair of response and impact time signals was being recorded simultaneously, it was possible to view both the input and response signals on an oscilloscope as they were being recorded. This made it possible to ensure that good data were obtained at each response location. This proved to be a very important feature.

COMPARISON OF EXPERIMENTAL AND ANALYTICAL RESULTS

A comparison of the computed and experimentally determined frequencies and mode shapes is shown in Table I. As seen in Table I, the frequencies and general shape of the modes agreed very well for most of the modes. An evaluation of the results of this comparison shows that the finite element model was capable of computing those modes which were associated with the load-measuring columns and motor combination. In addition, the shell-type modes of the motor were represented well. However, modes controlled by the accumulated flexibility of the large structural beam connections (4, 5, and 8 of Table I) were not in good agreement.

CONCLUSIONS

This investigation concludes that state-of-the-art structural analysis computer programs such as NASTRAN can be used to successfully represent the dynamic characteristics of large thrust-measuring systems. The finite element model must include accurate representations of all major components comprising the system (i.e., thrust butt, load-measuring columns, motor, and propellant). However, it was also observed that the finite element models of frame structures which utilize kinematic constraints to represent complex connections may not represent all modes of the structure accurately. Fortunately, for the situation under consideration, the inaccurately represented modes did not contribute significantly to the response of the critical members.

The dynamic certification effort was considered successful since the experimental data indicated that the dominant modes expected to respond to the ignition and gimbaling transients were adequately represented by the combined finite element model of the motor and TMS.

The modal analysis results identified areas in the TMS which were "dynamically sensitive," and a careful review of the animated mode shapes suggested design changes which would improve the dynamic characteristics of the TMS.

The commercially available instrumented sledge hammer and seismic accelerometer combination provided the highest quality data, and enabled the data to be reviewed as it was being taken. The ability to inspect the data in the field proved to be very desirable when this type of experiment is performed. It was concluded that relatively low input force levels can be used to excite the low-frequency modes of massive structures by tuning the impact spectrum of the hammer.

The quality of the animated mode shape displays was adequate to determine the basic motion of the structure. However, in most cases one or more of the points in the animated display of the structure were in obvious error. In addition, it was difficult to discern exactly how the structure was deforming during some of the higher frequency modes.

Modal testing is a valuable tool for discerning the adequacy of a finite element representation, and can be successfully applied to very large structures used in ground test facilities.

REFERENCES

1. Przemieniecki, J. S.: Theory of Matrix Structural Analysis. McGraw-Hill, 1968.

2. Bathe, K. J. and Wilson, E. L.: Numerical Methods in Finite Element Analysis. Prentice-Hall, 1976.

3. Kennedy, C. C., and Pancu, C. D. P.: "Use of Vectors in Vibration Measurement and Analysis." Journal of the Aeronautical Sciences, Vol. 14, No. 11, November 1947, pp. 603-625.

4. Pendred, J. W. and Bishop, R. E. D.: "A Critical Introduction to Some Industrial Resonance Testing Techniques." Journal of Mechanical Engineering Science," Vol. 5, No. 4, 1963, pp. 345-367.

5. Klosterman, A. L.: "Determining Dynamic Information by Use of Vector Components of Vibration." M.S. Thesis in Mechanical Engineering, University of Cincinnati, 1968.

6. Klosterman, A. L.: "On the Experimental Determination and Use of Modal Representations of Dynamic Characteristics." Ph.D. Dissertation, University of Cincinnati, 1971.

7. Brown, D. L.: "Grinding Dynamics." Ph.D. Dissertation, University of Cincinnati, 1976.

8. Halversen, W. G. and Brown, D. L.: "Impulse Technique for Structural Frequencies Response Testing." Sound and Vibration, November 1977, pp. 8-21.

9. Tomlinson, G. R. and Hibbert, J. H.: "Identification of the Dynamic Characteristics of a Structure with Coulomb Friction." Journal of Sound and Vibration, Vol. 64, No. 2, 1979, pp. 233-242.

10. Goyder, H. G. D.: "Methods and Application of Structural Modeling from Measured Structural Frequency Response Data." Journal of Sound and Vibration, Vol. 68, No. 2, 1980, pp. 209-230.

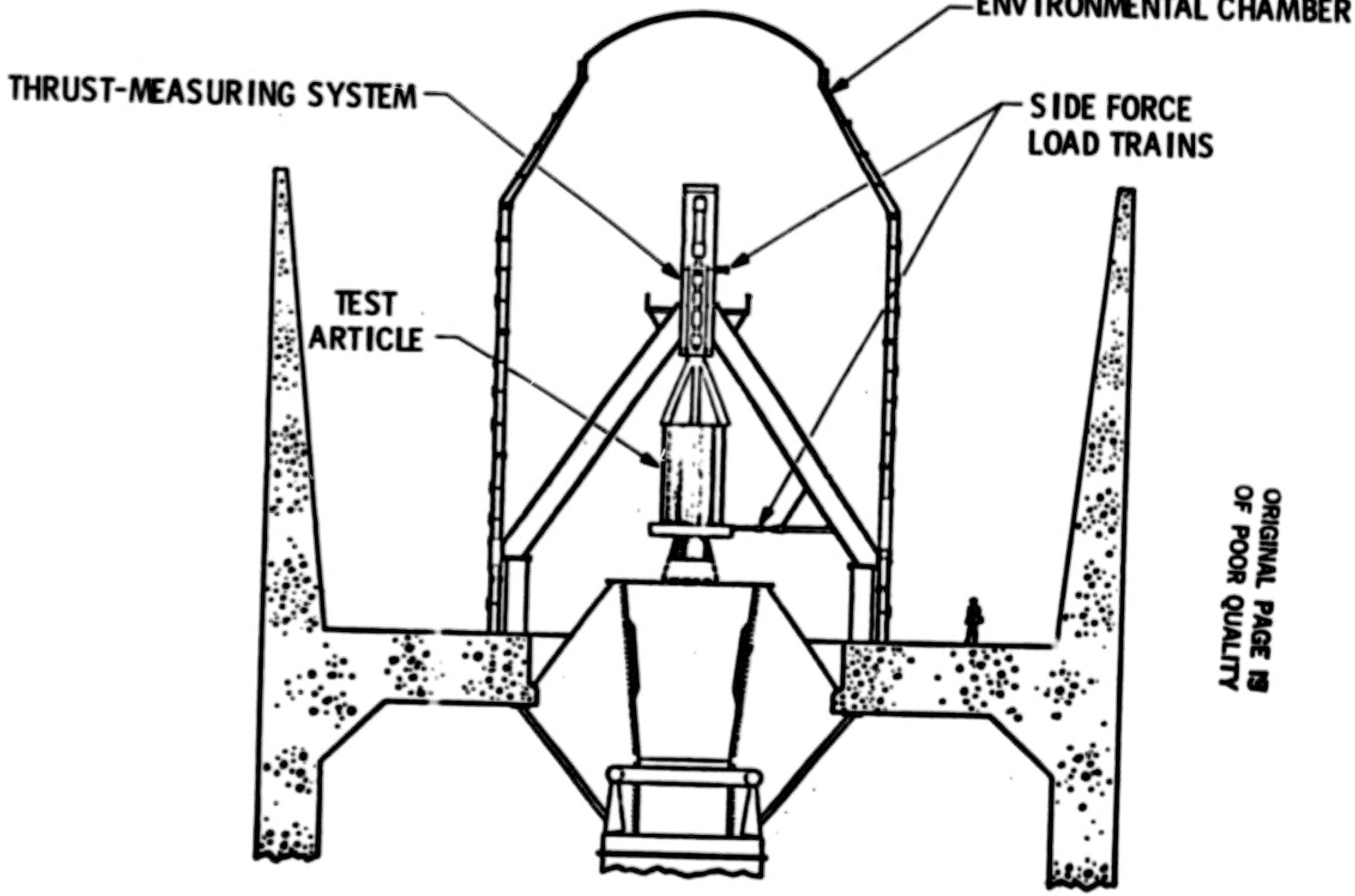
ENVIRONMENTAL CHAMBER
THRUST-MEASURING SYSTEM
SIDE FORCE LOAD TRAINS
TEST ARTICLE

Figure 1. Thrust-Measuring System Installation

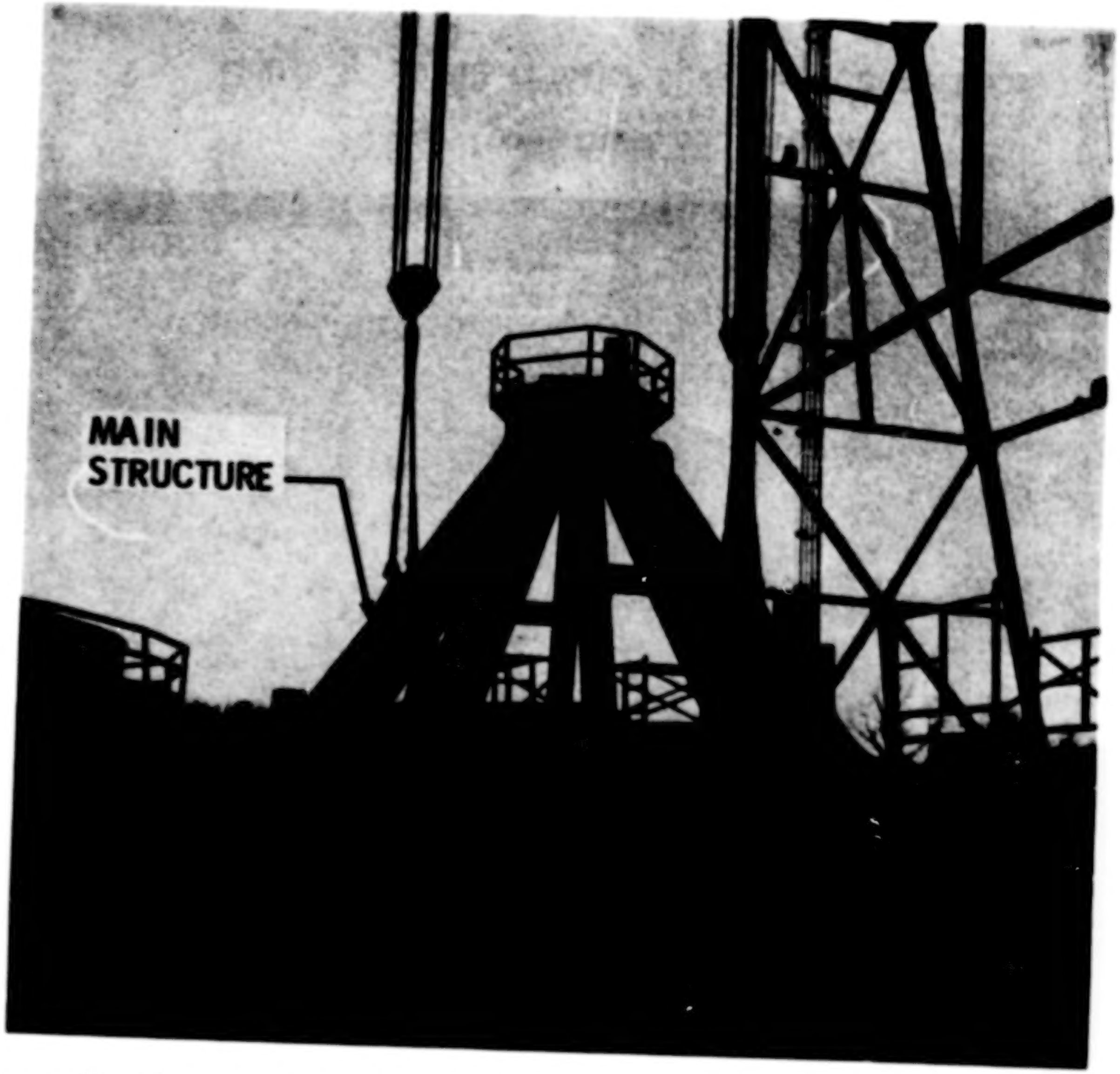
MAIN
STRUCTURE

Figure 2. Thrust-Measuring System, Main Structure Pre-Installation

ORIGINAL PAGE IS
OF POOR QUALITY

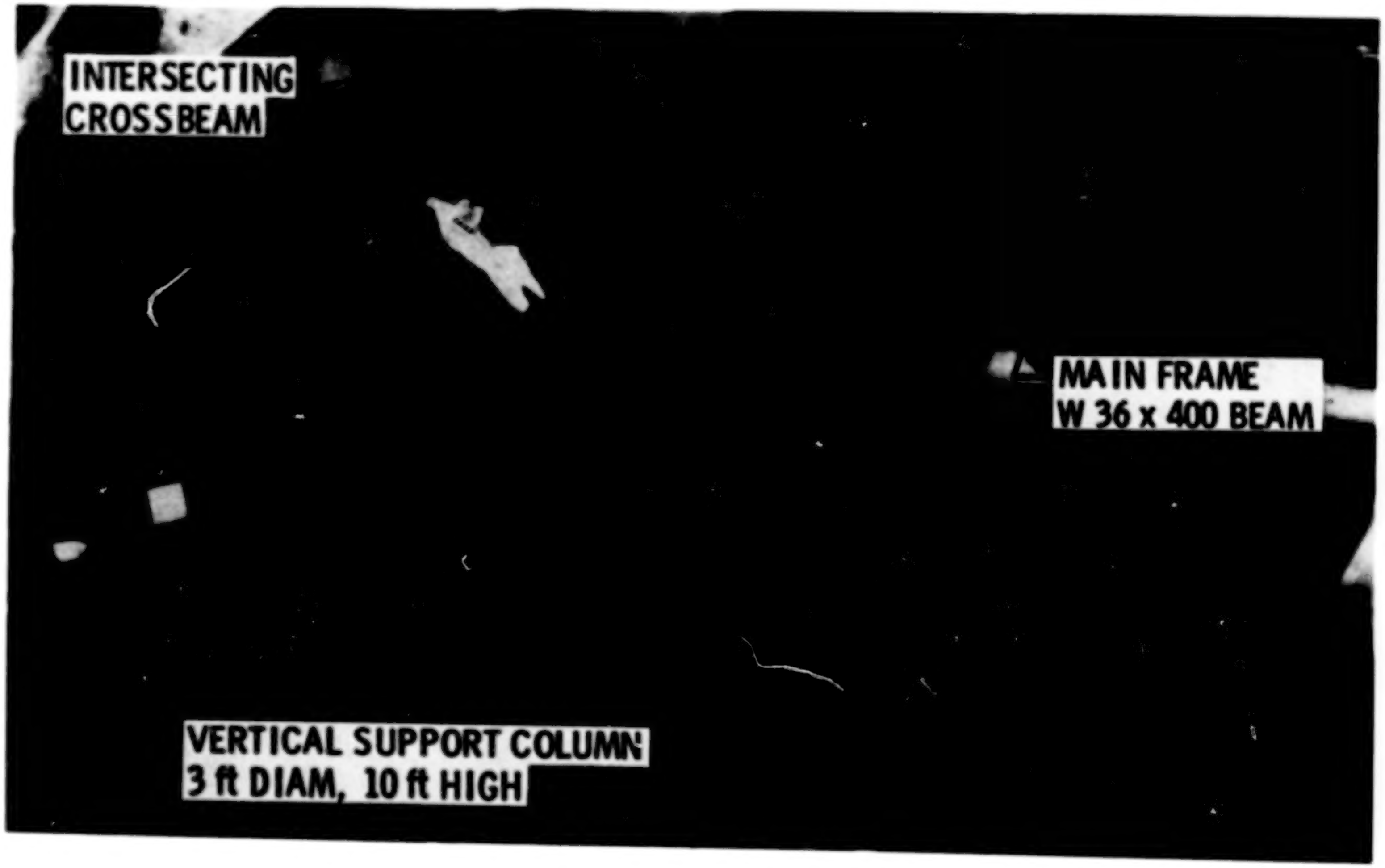
INTERSECTING
CROSSBEAM
MAIN FRAME
W 36 x 400 BEAM
VERTICAL SUPPORT COLUMN
3 ft DIAM, 10 ft HIGH

a. Lower frame connection

Figure 3. Details of Major Structural Connections

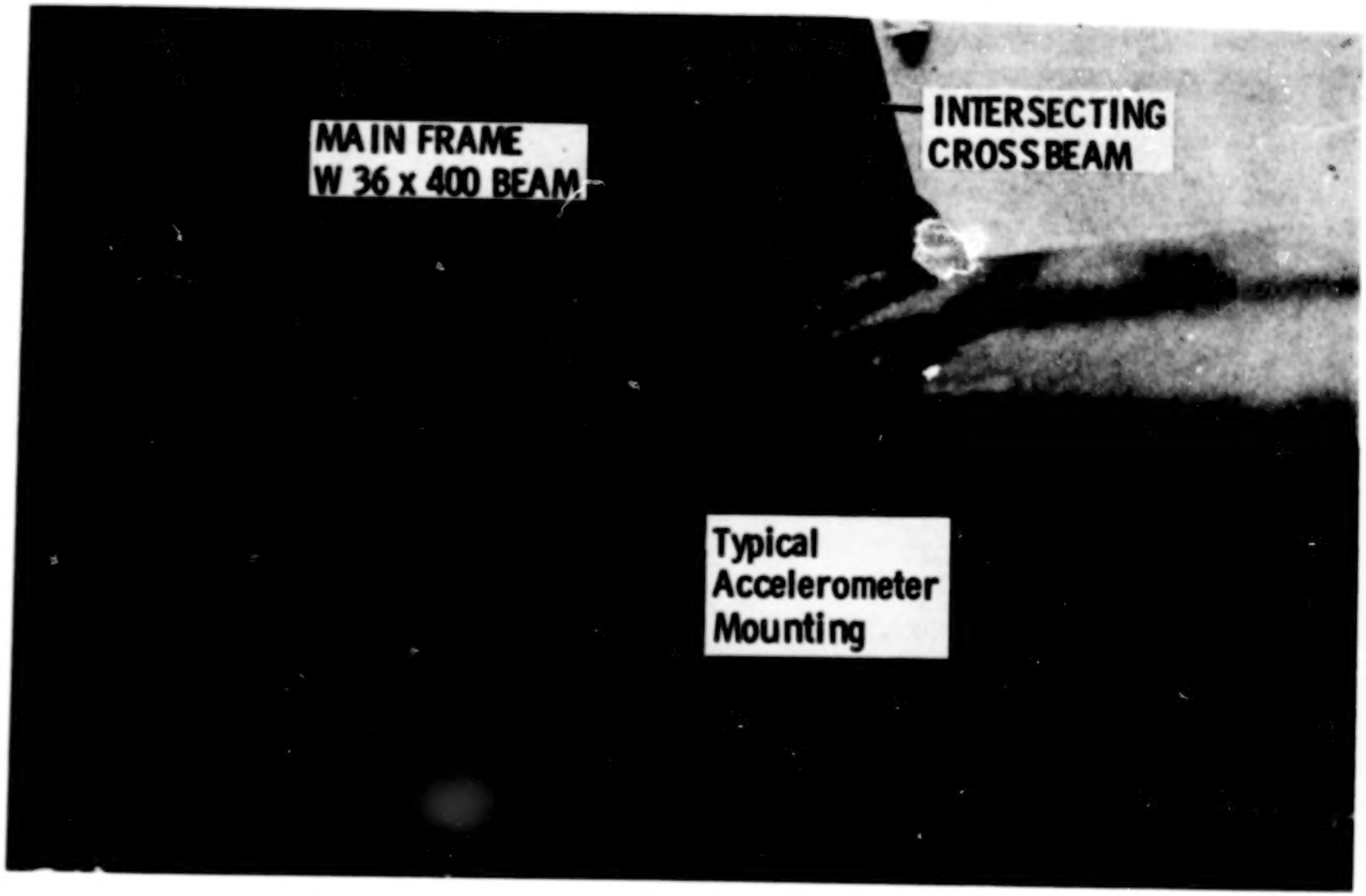
MAIN FRAME
W 36 x 400 BEAM
INTERSECTING
CROSSBEAM
Typical
Accelerometer
Mounting

b. Mid frame 90-deg connection

Figure 3. Continued

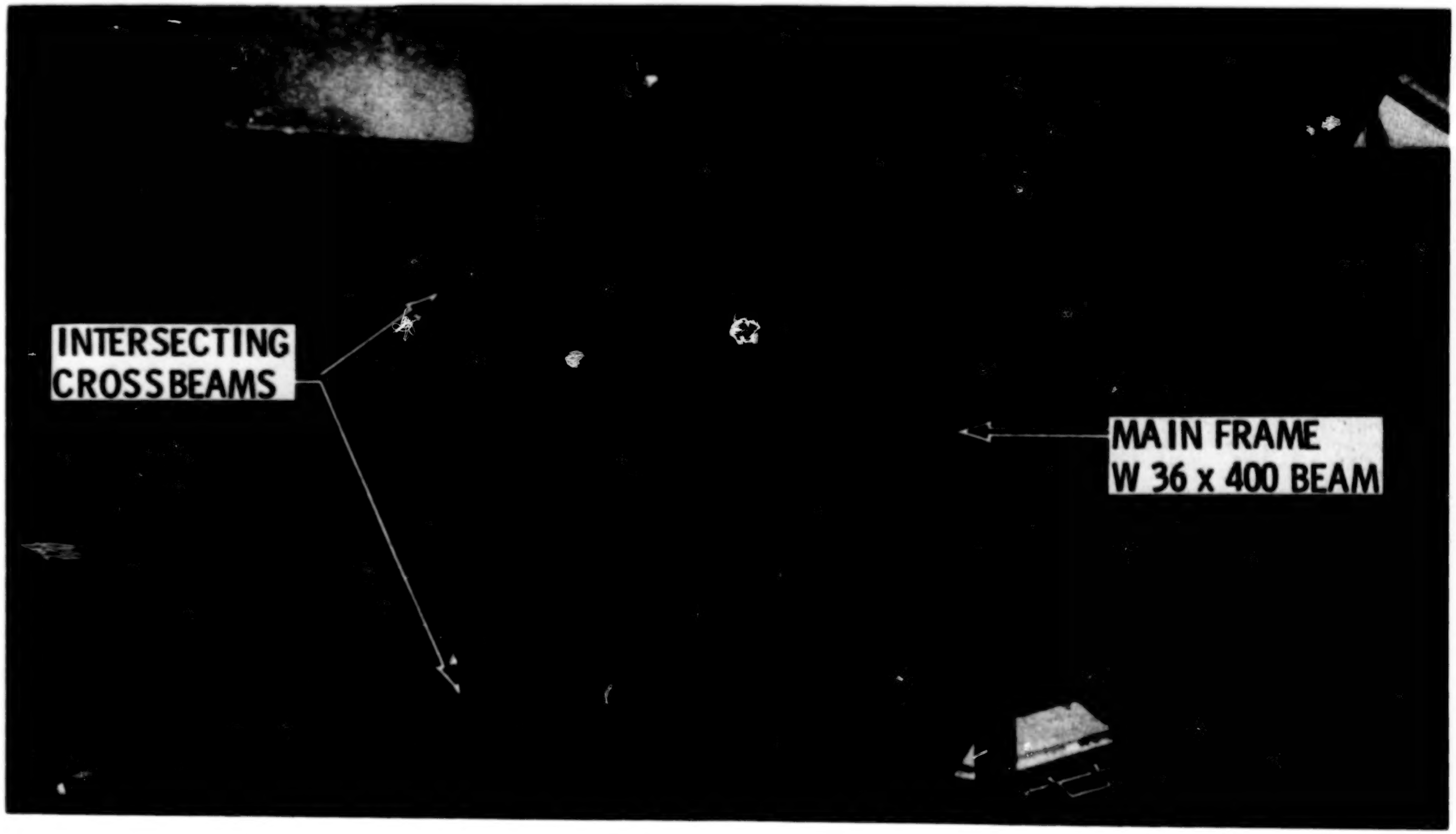
INTERSECTING
CROSSBEAMS
MAIN FRAME
W 36 x 400 BEAM

c. Mid frame double connection

Figure 3. Concluded

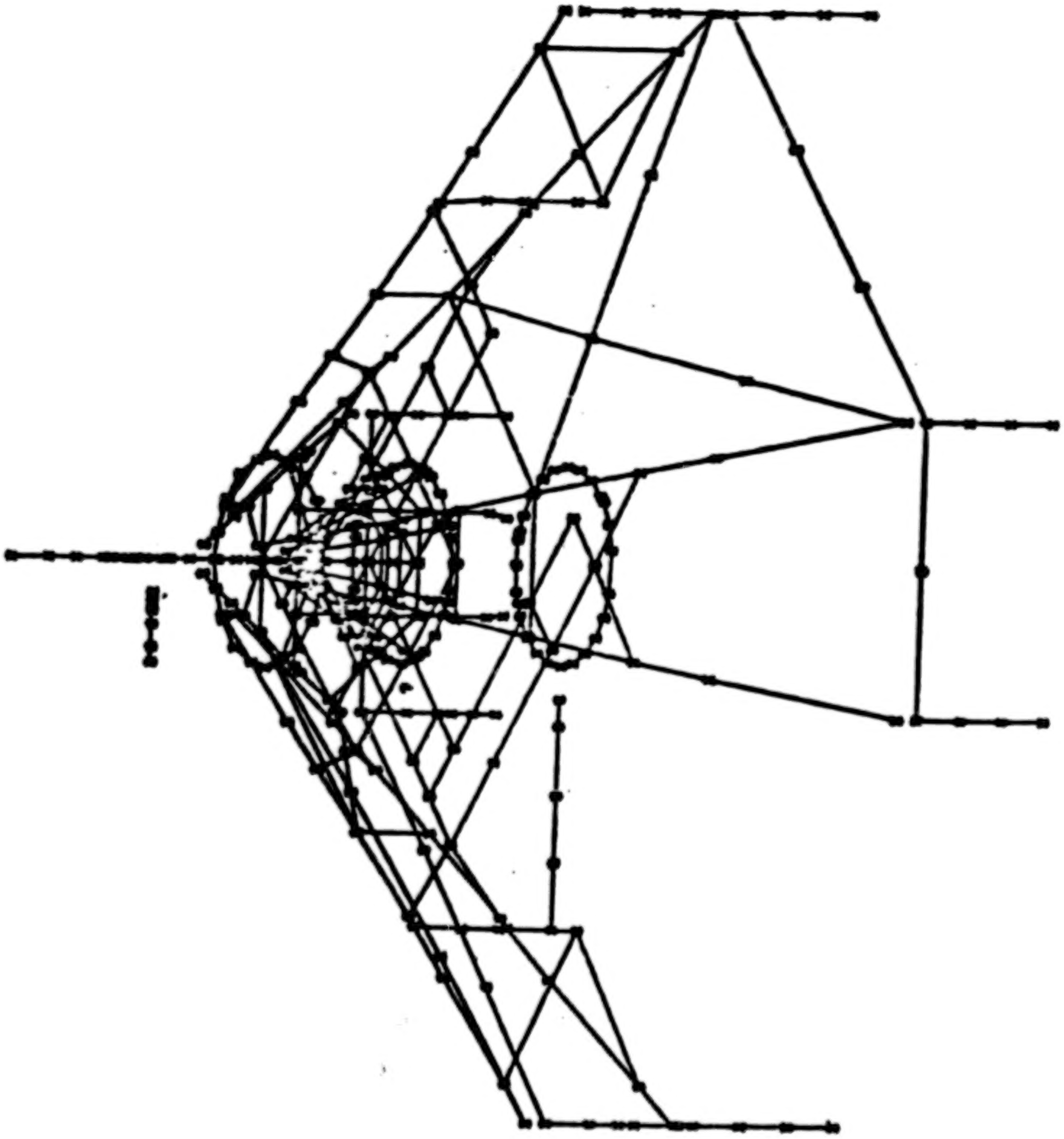

Figure 4. NASTRAN Finite Element Geometry Plot

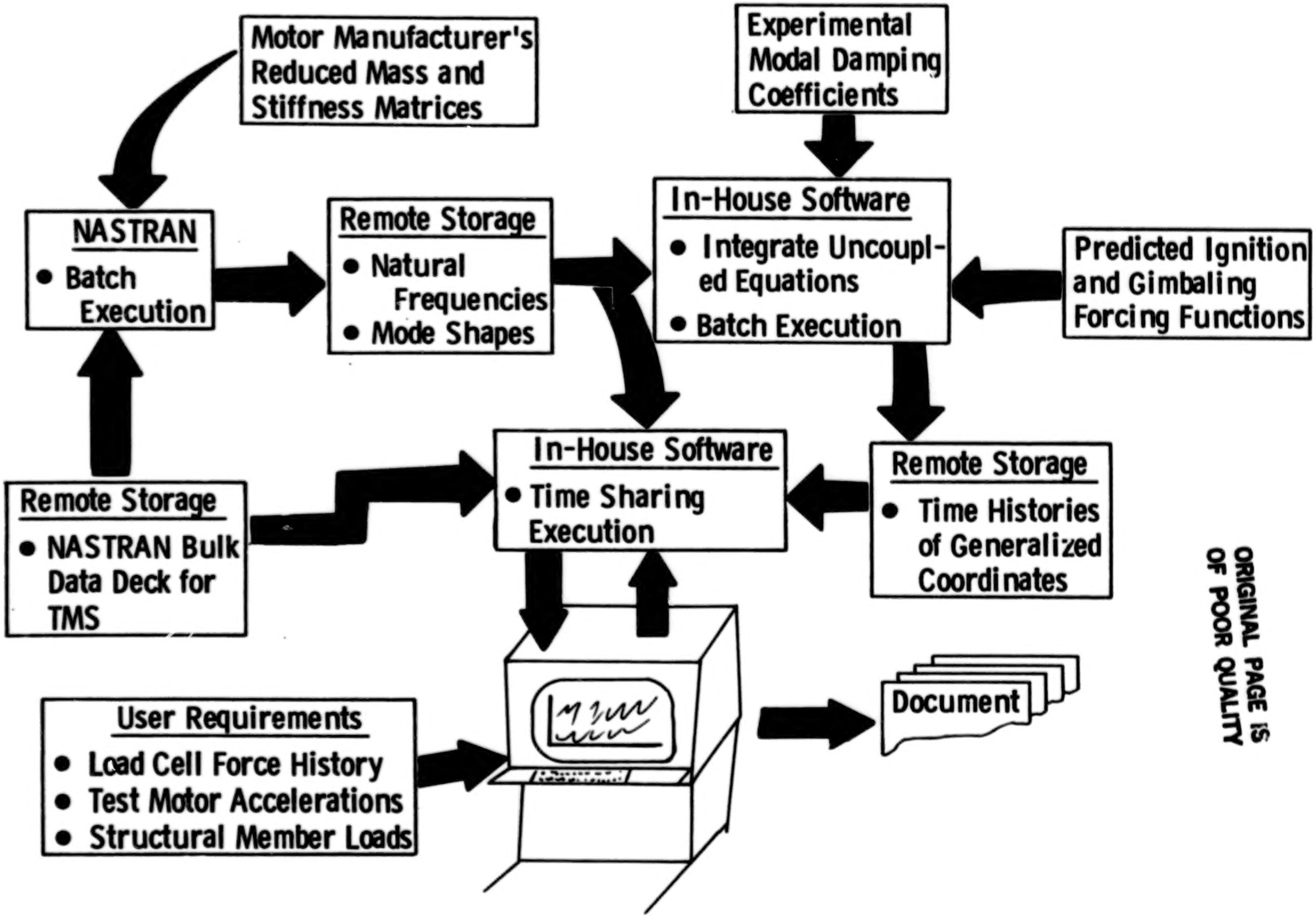
Motor Manufacturer's Reduced Mass and Stiffness Matrices
Experimental Modal Damping Coefficients
NASTRAN
• Batch Execution
Remote Storage
• Natural Frequencies
• Mode Shapes
In-House Software
• Integrate Uncoupled Equations
• Batch Execution
Predicted Ignition and Gimbaling Forcing Functions
In-House Software
• Time Sharing Execution
Remote Storage
• Time Histories of Generalized Coordinates
Remote Storage
• NASTRAN Bulk Data Deck for TMS
User Requirements
• Load Cell Force History
• Test Motor Accelerations
• Structural Member Loads
Document

Figure 5. Flow of Information During Computational Study

ORIGINAL PAGE IS
OF POOR QUALITY

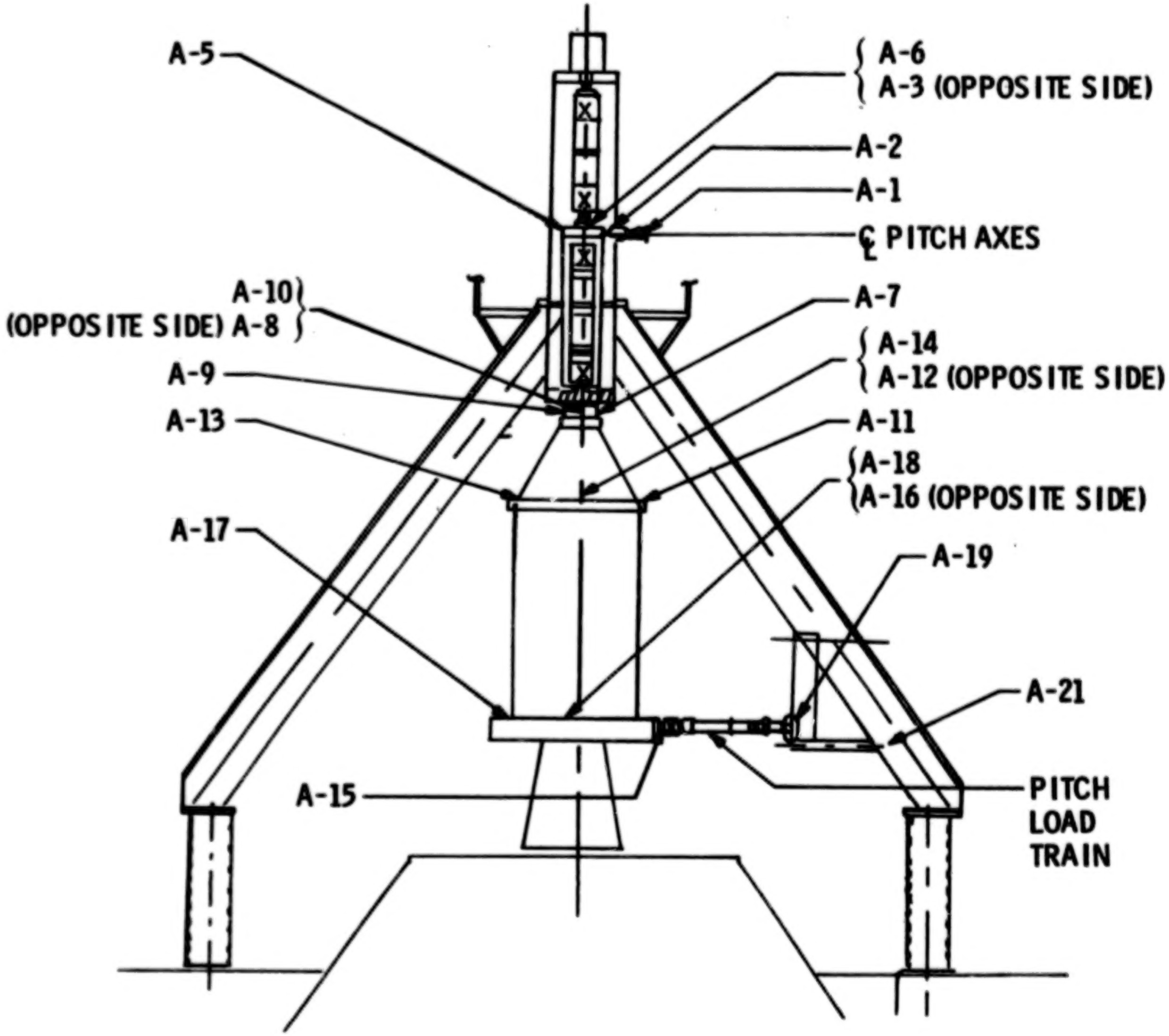
A-5
A-6
A-3 (OPPOSITE SIDE)
A-2
A-1
℄ PITCH AXES
A-10
(OPPOSITE SIDE) A-8
A-7
A-9
A-14
A-12 (OPPOSITE SIDE)
A-13
A-11
A-18
A-16 (OPPOSITE SIDE)
A-17
A-19
A-21
A-15
PITCH
LOAD
TRAIN

Figure 6. Accelerometer Locations, Elevation View, Pitch Plane

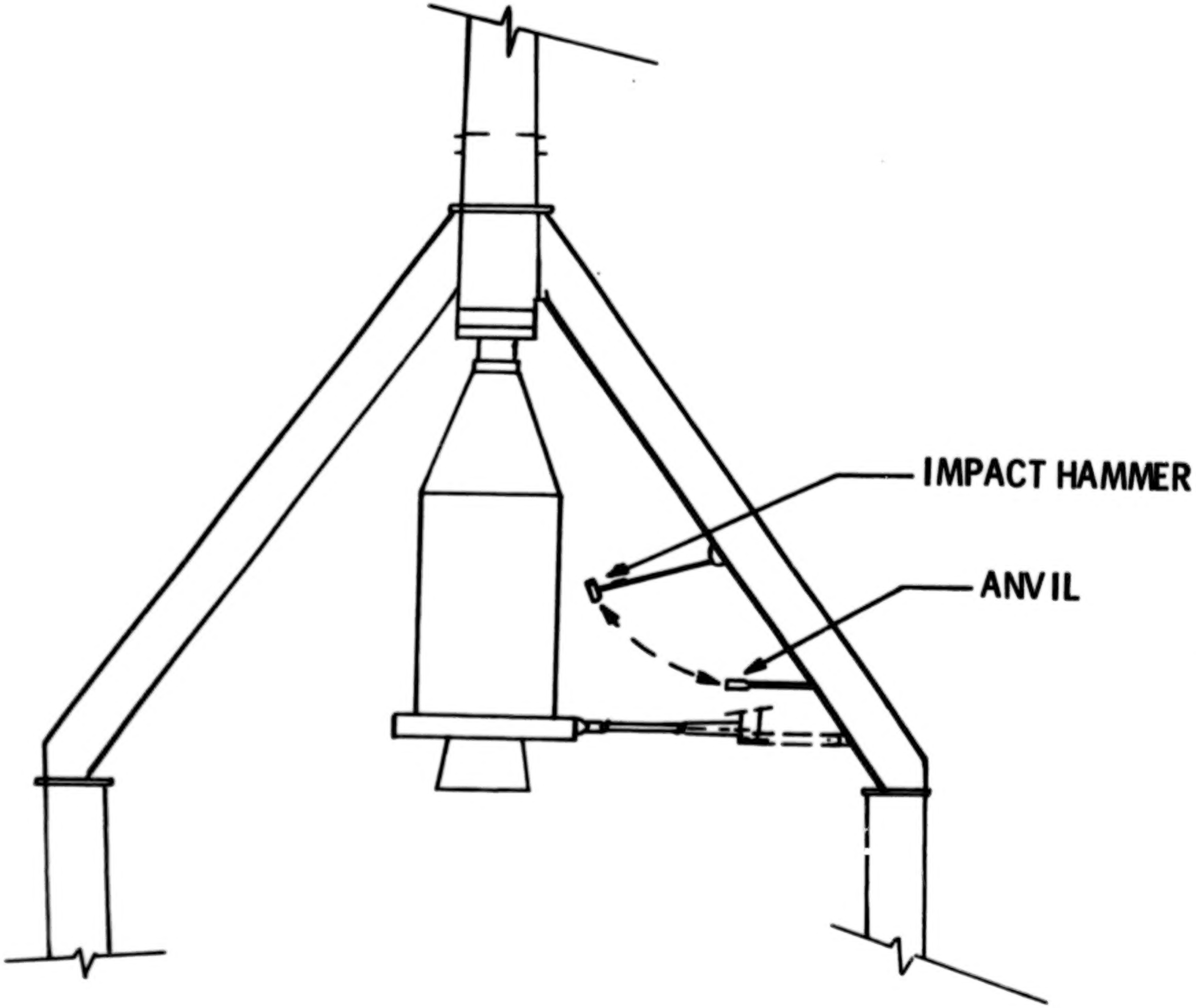
IMPACT HAMMER
ANVIL

Figure 7. High Energy Impact Device Installation

ORIGINAL PAGE IS
OF POOR QUALITY

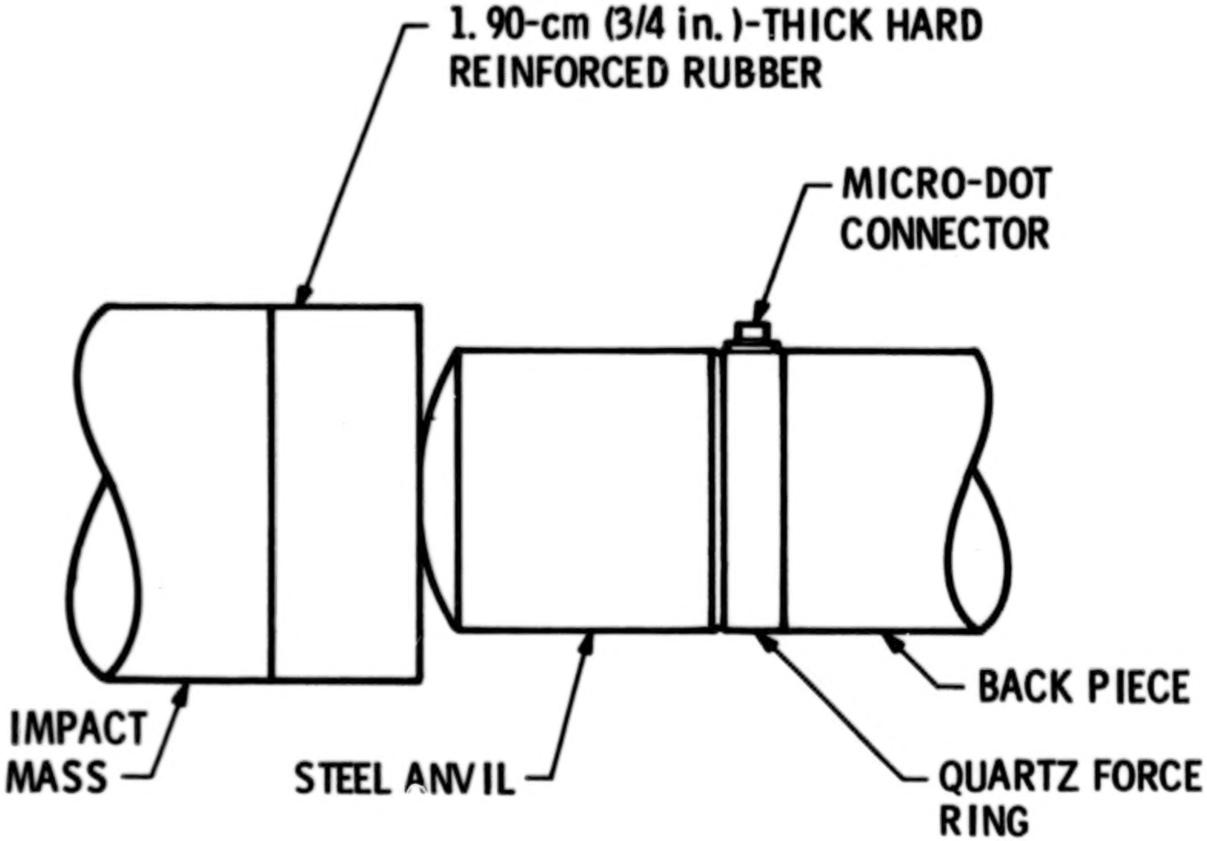
1.90-cm (3/4 in.)-THICK HARD REINFORCED RUBBER
MICRO-DOT CONNECTOR
IMPACT MASS
STEEL ANVIL
BACK PIECE
QUARTZ FORCE RING

Figure 8. Impact Anvil Details

ORIGINAL PAGE IS
OF POOR QUALITY

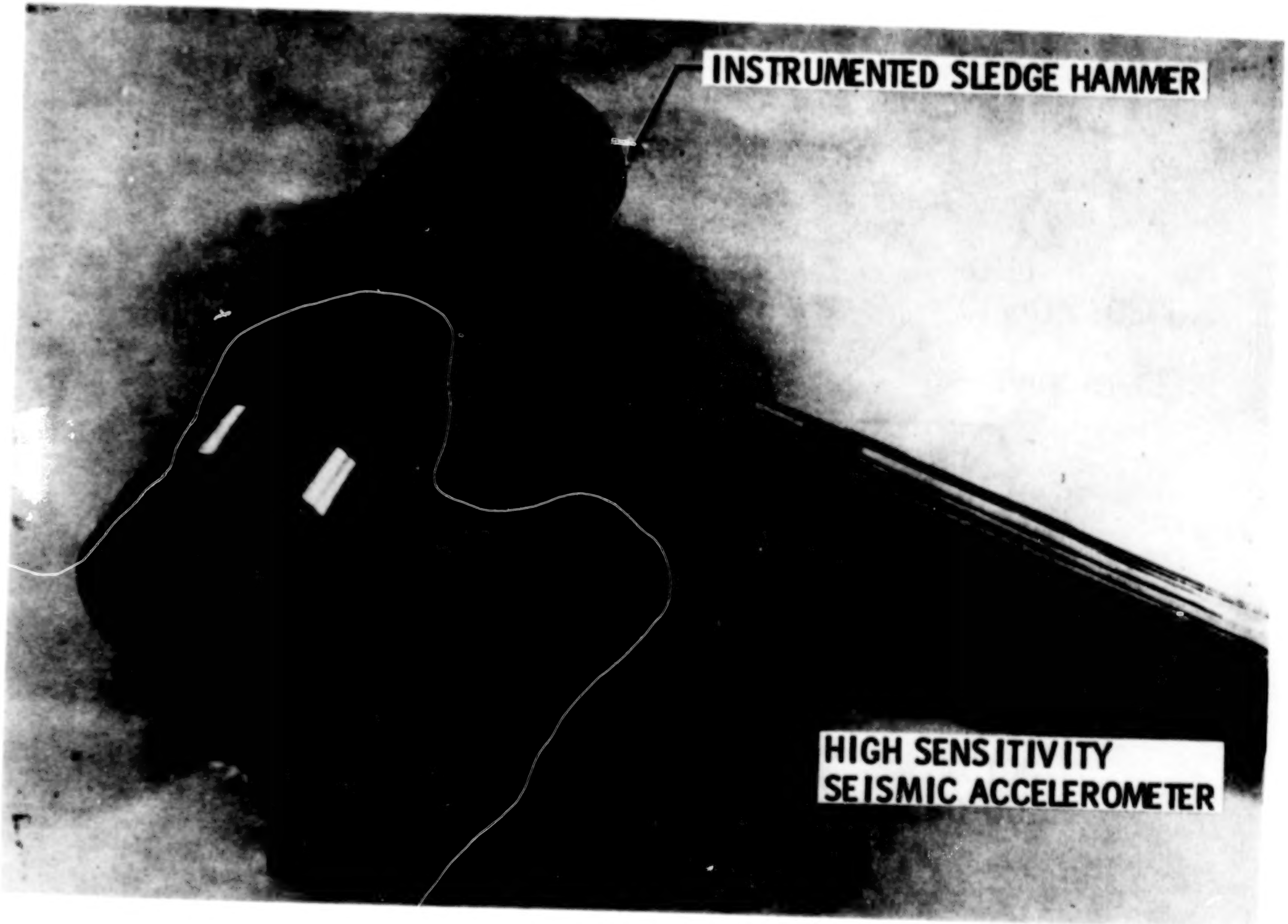
INSTRUMENTED SLEDGE HAMMER
HIGH SENSITIVITY
SEISMIC ACCELEROMETER

Figure 9. Impact and Measurement Devices

Table I. - Experimental and Computed Natural Frequencies

MODE NUMBER	EXPERIMENT (Hz)	COMPUTED (Hz)	DESCRIPTION OF MODE SHAPE
1	5.2	5.2	First lateral mode of motor in yaw direction.
2	5.6	5.6	First lateral mode of motor in pitch direction.
3	6.5	6.9	First rotational mode of motor.
4	7.5	*	Out-of-phase bending of inner thrust butt girders.
5	8.8	16.4	Breathing motion of thrust butt girders.
6	10.8	11.9	Vertical motion of motor on axial load column.
7	12.2	12.7	Second lateral mode of motor in yaw direction.
8	13.4	18.1	Out-of-phase bending of thrust butt main girders.
9	14.0	14.7	Second lateral mode of motor in pitch direction.
10	18.2	18.2	Lateral bending of X bracing and first bending mode of motor.

*Was not computed.

N84
15604

UNCLAS

D/14

N84 15604

DETERMINATION OF ELEVATOR AND RUDDER HINGE FORCES ON THE LEARJET MODEL 55 AIRCRAFT

Robert R. Boroughs and Viswa Padmanabhan
Gates Learjet Corporation

SUMMARY

The empennage structure on the Learjet 55 aircraft was quite similar to the empennage structure on earlier Learjet models. However, due to an important structural change in the vertical fin along with the new loads environment on the 50 series aircraft, a structural test was required on the vertical fin, but the horizontal tail was substantiated by a comparative analysis with previous tests. NASTRAN analysis was used to investigate empennage deflections, stress levels, and control surface hinge forces. The hinge force calculations were made with the control surfaces in the deflected as well as undeflected configurations. A skin panel buckling analysis was also performed, and the non-linear effects of buckling were simulated in the NASTRAN model to more accurately define internal loads and stress levels. Comparisons were then made between the Model 55 and the Model 35/36 stresses and internal forces to determine which components were qualified by previous tests. Some of the methods and techniques used in this analysis have been described in the following paragraphs.

INTRODUCTION

Features in the 55 empennage section that were identical to previous Learjet models included the horizontal tail, elevators, and the upper portion of the vertical fin and rudder (see figure 1). The most significant change in the empennage occurred in the lower portion of the vertical fin and rudder which were expanded using the same taper ratio and airfoil contour as the upper portion so that the total height of the vertical fin and rudder was increased by approximately 15 inches. Since the vertical tail increased in size and the vertical fin spar depths and spacings changed at the intersection with the tailcone, an entirely new tailcone section was designed to support the empennage section. Control systems for the elevators and rudder were nearly the same as the previous controls in this area with the exception of the 15 inch height increase in the vertical tail and the geometry changes in the tailcone.

Construction in the vertical tail consisted of five spars and eight ribs made of bent up aluminum sheet metal covered with an aluminum skin. The rudder was assembled with one spar, eleven ribs, and a thin skin cover, all of which were aluminum sheet metal fabrication. Support for the rudder was accomplished through three hinge points. Two of these hinges, the top and center attachments, connected the rudder leading edge to the rear spar of the vertical stabilizer while the third hinge point, or bottom support, was attached to the aft side of frame 48 through a torque tube and bracket support assembly (see figure 2). Near the lower end of this torque tube was mounted a bellcrank assembly which provided the means for actuating and controlling the rudder surface.

Structural arrangement of the horizontal tail included a forward and rear spar with three intermediate stringers on both the upper and lower surfaces, seven ribs per side, and upper and lower skin panels. The elevators were one spar airfoil sections with nine ribs per side which were covered with an aluminum skin. Each elevator was attached to the horizontal stabilizer by three hinge points along the elevator leading edge. The tip and center span hinges both connected directly to the rear spar of the horizontal stabilizer, but the inboard hinge attachment was very similar to the lower hinge on the rudder. The elevator inboard hinge consisted of a torque tube assembly which was supported at the horizontal stabilizer rear spar and aircraft center line by a bracket assembly. This bracket installation served as a support for both the right hand and left hand elevators at the inboard end (see figure 3). Actuation and control of the elevators was achieved through individual bellcranks on the inboard end of each torque tube. These bellcrank assemblies were then connected by a push rod linkage system which extended through the vertical stabilizer to a control system sector in the fuselage tailcone.

SYMBOLS

A_i	X, Y, and Z components of a point at the origin for a CORD2R card
α	rotation about the x axis for element internal forces
B_i	X, Y, and Z components of a point on the Z axis for a CORD2R card
β	rotation about the Y axis for element internal forces
C_i	X, Y, and Z components of a point in the X-Z plane for a CORD2R card
F_{iE}	internal force component
γ	rotation about z axis for element internal forces
H_G	coordinate values of a deflected control surface transformed to the basic system
H_L	coordinate values of a deflected control surface in a local system
H_λ	coordinate values corrected for hinge line sweep
H_θ	coordinate values corrected for control surface rotation
λ	hinge line sweep
$T\lambda$	transformation matrix for hinge line sweep
$T\theta$	transformation matrix for control surface rotation
θ	control surface rotation
x	first coordinate of a point in a local rectangular system
y	second coordinate of a point in a local rectangular system

z	third coordinate of a point in a local rectangular system
X	first coordinate of a point in the basic rectangular system
Y	second coordinate of a point in the basic rectangular system
Z	third coordinate of a point in the basic rectangular system

BACKGROUND

Since the Model 55 empennage structure was very similar to the Model 35/36 empennage structure and other earlier empennage structures, Learjet was faced with the situation on the 50 series development program of determining which structural items were qualified by previous certification tests and which structural items needed to be requalified. The vertical tail and tailcone support structure was obviously one area which had to be qualified by structural test, since the height of this component had been increased on the 50 series aircraft. A portion of the NASTRAN analysis on that structure has been detailed in NASA CP-2151 (see ref. 1) and consequently has not been addressed in this text. However, a description of the NASTRAN analysis performed on the rudder and rudder hinges was not covered in that document and has been incorporated in the body of this paper.

A review of the loads for the 50 series aircraft helped to further clarify some of these questions, but for some structural components the answer was not obvious and more study was necessary. One area where this was particularly true was the horizontal tail installation. This situation was mainly due to a revised loads definition for the horizontal tail where the combination of new loads was not directly comparable to the older load conditions. Also, a faster method was needed for calculating elevator hinge forces for the various load conditions and deflected elevator configurations. Previously, hinge forces had been calculated using methods which were very tedious, time consuming, and not very adaptable to changes in elevator position.

To help clarify these questions a NASTRAN analysis was performed on the empennage structure for the various load conditions and control surface positions so that a comparison could be made between the deflections, stresses, and internal loads on the 55 empennage with the 35/36 empennage. Previous structural tests had demonstrated that the horizontal stabilizer and elevators on the 35/36 aircraft had the capability to sustain 150% of ultimate load (not limit load) for two of the more critical conditions on that airplane. The 150% of ultimate load tests were performed to more accurately define the strength of the horizontal stabilizer and elevators as well as establish the growth capability of this structure. Consequently, a portion of the NASTRAN analysis was spent simulating the 35/36 load conditions in order to establish a baseline for the 50 series analysis. Then the 50 series loads were applied to the NASTRAN model and a comparison was made between these data and the 35/36 data. Using this approach Learjet was able to more clearly define which elements were qualified by previous certification tests and which members, if any, need to be qualified in the 50 series substantiation program. This data base would also help to establish what components needed to be qualified in future growth versions and/or modifications to the existing configuration.

MODELING CRITERIA

The NASTRAN model used to represent the empennage section included the vertical stabilizer, rudder, horizontal stabilizer, elevators, and tailcone section (see figure 1). The tailcone was utilized in the model to more accurately describe the flexibility and stiffness of the vertical tail, since the spars from the vertical tail extended into and were attached to the tailcone. A significant portion of the control system connecting the rudder and elevators was also modeled to more accurately define the effect of control system flexibility on the deflection of the control surfaces and hinge forces.

Since this structure was geometrically quite complex, multiple local coordinate systems were used to simplify the modeling and to make the analysis easier to perform for the different control system deflected configurations. Each frame in the tailcone section was modeled in a local cylindrical coordinate system while the vertical fin and horizontal stabilizer were modeled in a local rectangular coordinate system. The rudder and elevators were all modeled in local rectangular systems with the Y axis of each coordinate system defined along the hinge line. This type of coordinate system definition permitted the rotation of each control surface about the hinge line by simply transforming the CORD2R card (see ref. 2) rather than changing all of the grid point coordinates in the control surface to reflect the deflected position. Rotation of the control surface about the hinge line thus permitted the calculation of hinge forces for various control surface movements. This technique also facilitated a study of vertical fin and horizontal stabilizer internal forces and stresses for various control surface positions.

The model for this structure was approximately 5700 degrees of freedom in size with 950 nodes and 2800 elements. Local coordinate systems totaled seventeen which consisted of both rectangular and cylindrical reference systems. Since the results of previous static tests had indicated that skin panel buckling was present, a buckling analysis was implemented to identify buckled skin panels and to simulate this non-linear phenomenon in the NASTRAN analysis (see ref. 3). This buckling simulation was achieved by replacing the original skin thickness of the buckled panel with an effective skin thickness which represented the stiffness of the buckled configuration. The buckling analysis and effective skin thickness calculation were performed by a computer program which was set up to run as a post processor to the NASTRAN program. This process generally had to be repeated several times in order to obtain a convergent solution. A more detailed description of the theory behind this analysis has been presented in NASA TMX 3428 and further discussion will not be covered in this text.

TAILCONE

Incorporation of the tailcone section with the empennage model was done to more accurately define the stiffness relationship between these two components. Representation of the tailcone section included the structure from frame 39 to frame 48 (see figure 1). The modeling of this structure was accomplished by defining the grid points at each frame and stringer intersection in a local cylindrical coordinate system in the plane of the frame using CORD2C cards (see ref. 2). NASTRAN members used to model this structure were BAR elements for the frames, CONROD elements for [illegible] elements for the skin panels and doublers. A baggage door on the left hand side of the tailcone did not have significant structural carry through capability and was omitted to conserve degrees of freedom. The keel beam structure that extended from frame 39 to 41 in this section was modeled using CONROD elements for the caps, SHEAR elements for the side webs, and QDMEM2 elements for the horizontal webs.

VERTICAL TAIL

Two separate local rectangular coordinate systems were used to facilitate the definition of grid point locations in the vertical fin and rudder (see figure 2). The local rectangular coordinate system for the vertical fin was defined using a CORD2R card with the origin located on the center line of the airplane at the intersection of the vertical tail leading edge and the tailcone upper surface. The X axis was defined as positive aft, the Y axis was defined as positive up, and the Z axis was defined as positive left hand outboard. The local rectangular coordinate system for the rudder was defined using a CORD2R card with the origin on the rudder hinge line at the lower end of the rudder torque tube. Orientation of the X axis was positive aft and slightly down (for zero degree rudder deflection), the Y axis was positive up along the rudder hinge line, and the Z axis was positive left hand outboard.

Grid points were located at the intersection of the spar caps and rib caps on both the right hand and left hand outer contours of the vertical tail. The spar caps in the region of the fuselage frames were modeled using BAR elements while the remainder of the spar caps and rib caps were simulated by CONROD elements. Skin panels were represented by QDMEM2 members, although there were some triangular, TRMEM, membrane elements used to describe intricate corners. SHEAR elements were used to represent the spar and rib webs.

Attachment of the rudder to the vertical fin was accomplished through two hinges from the aft spar of the vertical fin to the leading edge of the rudder. The hinge model consisted of a framework of eight CONRODs that connected the hinge point to a rudder rib on the aft side and to a vertical fin rib on the forward side. The first group of four CONRODs, or the aft hinge, connected the hinge point to four points on the adjacent rudder rib, while the second group of four CONRODs, or the forward hinge, connected the hinge point to four grid points on the adjacent vertical fin rib (see figure 2). This method of modeling facilitated an easier computation of hinge loads through a resolution of forces in the CONRODs into forces in a predefined coordinate system by using a series of transformation equations. The torque load in the rudder was restrained by a bellcrank mounted on a torque tube whose axis coincided with the hinge line of the rudder. This torque tube was attached to the bottom of the rudder on one end and to a bracket support on the aft side of frame 48 on the other end. BAR elements were used to model the torque tubes and the bellcrank assembly which actuated and controlled the rudder rotation at the bottom of the torque tube. Modeling of the bracket support on frame 48 was accomplished using CONRODs for the stiffeners and QDMEM2 membranes for the webs.

HORIZONTAL TAIL

The horizontal tail consisted of the horizontal stabilizer and right hand and left hand elevators. Attachment of the horizontal stabilizer to the vertical fin was accomplished through a hinge point on the top of the vertical fin between spars three and four and a screwjack attached to the horizontal stabilizer apex and spar two of the vertical fin. Rotation of the horizontal tail could then be achieved through actuation of this screwjack. The elevators were attached to the rear spar of the horizontal stabilizer through three hinges on each side.

Three separate local rectangular coordinate systems were created using the CORD2R facility in NASTRAN to model the horizontal tail structure. These local coordinate systems were used to describe the horizontal stabilizer, right hand elevator, and left hand elevator. Layout of the horizontal stabilizer local rectangular coordinate systems was established with the origin located at the horizontal stabilizer apex with the X axis positive aft, the Y axis positive left hand outboard, and the Z axis positive down. Orientation of the left hand elevator local rectangular coordinate system was defined with the origin at the intersection of the hinge line and aircraft center plane with the X axis perpendicular to the hinge line and positive aft, the Y axis coincident with the hinge line and positive left hand outboard, and the Z axis perpendicular to the X-Y plane and positive down. The right hand elevator local rectangular coordinate system was similar to the left hand elevator with some differences in positive axes directions. The origin for the right hand elevator coordinate system was the same as the left hand elevator; however, the X axis was perpendicular to the right hand hinge line and positive forward, the Y axis coincided with the right hand hinge line and was positive right hand outboard, and the Z axis was perpendicular to the X-Y plane and was positive up. One important advantage of the separate coordinate systems for the elevators was the ease and improved flexibility of analyzing the elevators and horizontal stabilizer with the elevators in various deflected positions.

Grid points in the horizontal tail were specified in relation to the appropriate coordinate system depending on whether the point was in the horizontal stabilizer, right hand elevator, or left hand elevator. Location of the grid points was defined by the intersection of the spars and stringers with the ribs and by the exterior contour. As in the vertical fin, the spar caps, stringers and rib caps were represented by CONRODs, the spar and rib webs were SHEAR elements and the skin panels were modeled using QDMEM2 and TRMEM members in the horizontal stabilizer while QUAD2 and TRIA2 elements were used in the elevators. BAR elements were used to simulate the elevator trailing edges.

Attachment of the elevators to the horizontal stabilizer rear spar was accomplished by three hinges on each elevator. These hinges were designated by the spanwise location and were referred to as the inboard hinge, center hinge, and tip hinge (see figure 3). The center and tip hinges were modeled as a framework of eight CONRODs that connected the hinge point to an elevator rib and a horizontal stabilizer rib. The first group of four CONRODs, or aft hinge, connected the hinge point to four grid points on an elevator rib, while the second group of four CONRODs, or forward hinge, connected the hinge point to four grid points on a horizontal stabilizer rib (see figure 3). The torque load on the elevator was reacted by a bellcrank mounted on a torque tube whose axis coincided with the elevator hinge line. There were two of these bellcrank/torque tube assemblies, one for each side. The torque tube attached to the elevator on the tube's outboard end and to a bracket support mounted on the horizontal stabilizer's rear spar on the airplane center line on the tube's inboard end. Both torque tubes and bellcranks were modeled using BAR elements, while the center line bracket support assembly was modeled using CONRODs.

CONTROL SYSTEM

A portion of the control system connecting the rudder and elevator has also been included in the modeling of the empennage section to more accurately define the effect of control system stiffness on the deflection of these control surfaces and in particular the associated hinge forces. Rudder motion on the Learjet M55 aircraft was accomplished by rudder pedal movement which was transferred by a closed loop cable assembly which drove a bellcrank mounted on the rudder torque tube (see figure 4). The aft portion of this cable system was included in the finite element model and was represented by CONROD elements with the side of the closed loop cable system that was not in tension removed. The CONROD elements representing the cables were extended into the tailcone section where the forward end of this member was attached to a pulley which was restrained against rotation.

Elevator deflection on this aircraft was achieved by control column movement which was transferred through a closed loop cable assembly and a push-pull rod linkage system. The upper portion of the push rod system consisted of two round tubes which were attached to the bellcranks on the left and right elevators respectively. The other end of these two push rods were joined to a down spring linkage mounted on the aft side of spar three in the vertical fin. A single round tube was used in the lower portion of the push rod system. This shaft was connected to the down spring linkage on the top end and to a sector on the bottom end (see figure 5). The portion of the elevator control system that was included in the empennage model consisted of the elevator bellcranks, upper push rods, down spring linkage, and lower push rod which was constrained at the lower end for the NASTRAN analysis. The grid points that defined the top and bottom points of the lower push rod were defined in separate local cylindrical coordinate systems. This was done so that these grid points could be moved with the elevator motion by using a simple set of transformation equations. The push-pull rods were modeled with CONRODs, whereas the bellcranks and down spring linkage were represented by an assemblage of BAR elements.

The horizontal stabilizer rotation about the hinge point between spar three and four on top of the vertical fin was achieved by a screwjack actuator attached to the horizontal stabilizer apex. A BAR element was used to represent the screwjack. One end of this BAR element was attached to a fitting on the forward side of spar two in the vertical fin, and the other end was connected to a fitting mounted on the horizontal stabilizer center line. The fittings that attached the screwjack actuator at both ends were also modeled using BAR elements.

LOADS AND CONSTRAINTS

Many different load conditions were analyzed using the NASTRAN empennage model. A correlation analysis was performed on the horizontal tail using a positive gust with top roll moment load condition from the 35/36 fatigue test spectrum. This load case was selected basically because earlier tests did not have sufficient instrumentation to perform a correlation analysis, and this particular case was one of the higher load conditions in the 35/36 fatigue test spectrum. Since the correlation analysis for the vertical tail was described in a previous NASA paper (See ref. 1), the results of that work were not presented here. The analysis of the Learjet 55 vertical tail described in this paper was directed mainly at rudder hinge force calculations. The load case applied to the vertical tail for these rudder hinge force calculations was a maximum side bending with rudder kick load condition.

NASTRAN runs were made for all of the 35/36 horizontal tail static test loads. These conditions were run in order to establish a baseline for the Model 55 analysis so that a determination could be made as to whether any of the 55 horizontal tail internal loads and stresses exceeded those on the 35/36 horizontal tail. Since some of the 35/36 load cases were tested to 150% ultimate load, there was good reason to believe that the 55 horizontal tail load conditions were covered by the previous 35/36 static tests. The 35/36 loads were applied to the horizontal stabilizer and elevators with the elevators in the neutral, or undeflected position, the 15° up position and the 15° down position. The loads definition for the Model 55 horizontal tail was somewhat different from the 35/36 horizontal tail. There were many more load cases for the Model 55 airplane than for the 35/36 airplane, and a direct comparison was not easily achievable for many of these conditions. Consequently, internal loads and stresses were determined for the 55 horizontal tail load conditions with the elevators in the undeflected and deflected positions using NASTRAN analysis in order to establish a common basis for comparison with the 35/36 internal loads and stresses.

Loads were applied to the vertical fin, rudder, horizontal stabilizer and elevators using FORCE card images (See ref. 2). These forces were applied at the grid points to simulate the shear, bending and torque envelopes for these airfoil surfaces. A computer program was written which accepted concentrated forces from the test loads data as input and redistributed these forces proportionately to the four nearest grid points according to the distance from those nodes and generated FORCE card images as output.

Constraints for the empennage model were applied at several locations. The majority of constraints were applied along the perimeter of frame 39 (See figure 2) in all three translational degrees of freedom at the frame and stringer intersections. Other constraints were applied to the rudder control system and elevator control system. The rudder control system was constrained by attaching the forward end of the tailcone rudder cable to a frame in the tailcone section. The elevator control system was restrained by using SPC, single point constraints, (See ref. 2) on the three translational degrees of freedom at the bottom end of the lower push rod (See figure 2).

CONTROL SURFACE ROTATION

ORIGINAL PAGE IS
OF POOR QUALITY

Grid coordinates on the control surfaces were specified with respect to the appropriate rudder or elevator local rectangular coordinate system. These local coordinate systems were initially defined for the control surface in the undeflected position. However, the control surface could be deflected or rotated without changing the grid point coordinates merely by rotating the local coordinate system. This was accomplished by modifying the CORD2R card image in the bulk data deck by transforming the original axes reference to a new axes reference.

The CORD2R card image in the bulk data deck for each control surface defined a rectangular coordinate system by reference to three points. The first point "A" (A1, A2, A3) defined the origin of the local coordinate system (See figure 6). The second point "B" (B1, B2, B3) defined the direction of the "Z" axis, and the third point "C" (C1, C2, C3) defined a point in the X-Z plane. The basic coordinate system was used as the reference system for these points (See ref. 2). The origin for the basic system was defined at fuselage station (F.S.) 0.00, butt line (B.L.) 0.00, and waterline (W.L.) 0.00 with the "X" axis positive aft, "Y" axis positive left hand outboard, and the "Z" axis positive down. Components of A, B, and C were defined on the CORD2R card image by means of a simple series of transformations described by the following matrix equations.

$$\left[H_\theta\right] = \left[T_\theta\right] \times \left[H_L\right] \tag{1}$$

The equation shown above converts coordinates in a swept deflected control surface to coordinates in a swept undeflected control surface. Equation (2) shown below transformed the coordinates in equation (1) to coordinates parallel to a fuselage reference system corrected for the hinge line sweep angle λ.

$$\left[H_\lambda\right] = \left[T_\lambda\right] \times \left[H_\theta\right] \tag{2}$$

Substituting equation (1) into equation (2) and then referencing these values to the basic system with an H_{GO} matrix resulted in equation (3).

$$\left[H_G\right] = \left[T_\lambda\right] \times \left[T_\theta\right] \times \left[H_L\right] + \left[H_{GO}\right] \tag{3}$$

Equation (3) was used to calculate the components of points "B" and "C" on the CORD2R card which defined the rotated control surface.

HINGE LOAD CALCULATION

As indicated previously, the hinges were modeled using CONRODS and/or Bar elements. Since the hinge point had to be in equilibrium under the action of the internal element forces, the resultant of the forces from the elements on the aft side of the hinge line must be equal and opposite to the resultant from the elements on the forward side of the hinge line. This force on the forward hinge member was defined as the hinge force for each of the control surface support points.

Internal forces in the CONRODs and BARs were extracted from the NASTRAN output for a given load case. The forces in the hinge elements were then rotated into a common coordinate system through a series of transformations (See figure 7). The three force components in the element coordinate system were then defined as F_{xE}, F_{yE}, and F_{zE}. Orientation of the element coordinate system was defined by the two end points of the member and a $\vec{V}$ vector, if the element was a BAR (See ref. 2). Element grid point components x_A, y_A, z_A and x_B, y_B, z_B (See figure 7) established the basis for transforming the element forces to a common coordinate system. This was accomplished by rotating, or transforming, these forces through three angles α, β, and γ. Upon calculation of these three rotations, the transformation matrices were formed as shown in figure 7. The element forces F_{xE}, F_{yE}, and F_{zE} were then resolved in the common X, Y, Z directions, and then the hinge force components were determined by summing the resolved individual element forces.

A small computer program was written to perform the transformation from the element coordinate system to the common reference coordinate system. This program also accounted for the effect of control surface rotation. Hinge loads were computed on both sides of the hinge line as a check on the transformation calculations. The hinge loads at all the hinge points plus the loads at the intersection of the torque tubes and bellcranks were also summed to check the equilibrium of these hinge loads with the control surface applied loads.

BUCKLING ANALYSIS

A comparison of skin cover compressive stresses with the corresponding panel buckling allowables indicated the presence of skin panel buckling for several load cases. Consequently, an automated buckling analysis was implemented to identify buckled skin panels and to simulate this non-linear phenomenon in the NASTRAN analysis. The buckling simulation was achieved by replacing the original skin thickness of the buckled panel with an effective skin thickness which represented the stiffness of the buckled configuration. A detail description of the theory for this analysis has been described in reference 3. The buckling analysis and effective skin thickness calculation were coded into a computer program which was set up to run as a post processor to the NASTRAN program. This NASTRAN analysis with the buckled effective skin thickness generally had to be repeated several times in order to obtain a convergent solution. Since some of the loading cases on the horizontal tail were combined conditions, the buckling analysis was performed on both the upper and lower surfaces simultaneously.

ANALYTICAL RESULTS

After extensive analysis and study, the applied loads on the Model 55 horizontal tail were determined to be less than the maximum tested loads on the 35/36 horizontal tail which was identical to the 55 in structural detail. Consequently, no static test was performed on this structure during the 55 testing program.

However, in order to establish a correlation between the horizontal tail portion of the NASTRAN empennage model and the structural test data, a positive gust condition with top roll moment load case was used from the Model 35/36 fatigue test program as was mentioned previously. The results of this test along with the NASTRAN data have been exhibited in figures 8 through 11. Figures 8 and 9 show the correlation on the horizontal stabilizer forward spar upper cap and lower cap respectively while figures 10 and 11 show the correlation on the rear spar upper cap and lower cap respectively. Most of the experimental points agree with the NASTRAN data very closely with the exception of the most inboard point on the rear spar lower cap. This gage was very near an access door in the skin panel and appeared to be affected by the stress gradient due to this cutout. As mentioned earlier, no correlation was presented on the vertical tail, since this was performed in an earlier paper (See ref. 1).

CONCLUDING REMARKS

A method has been demonstrated for calculating control surface hinge forces using a Learjet Model 55 empennage NASTRAN analysis. Hinge element internal forces were extracted from the NASTRAN analysis and converted to a common coordinate system using a set of transformation equations to define the individual hinge forces. Since each control surface was defined in a local rectangular coordinate system, rotation of the control surface could be easily accomplished by transforming the components on the CORD2R card. This control surface rotation capability permitted Learjet to investigate the impact of control surface movement on the hinge attachments in more detail than was previously possible. A buckling analysis was also performed to determine the non-linear effect of skin panel buckling on stringer and spar cap stresses. These techniques proved to be a valuable asset to Learjet in studying the structural operating characteristics of the Model 55 empennage structure and associated control surfaces and for substantiating the horizontal tail structure by comparison with previous tests.

REFERENCES

1. Boroughs, Robert R.; Paramasivam, Sivam; and Werner, Joanna K: Development and Analysis of the Learjet 54/55 Fuselage NASTRAN Model Using Substructure Techniques, Ninth NASTRAN user's Colloquium, NASA CP 2151, October 1980, pp. 201-223.

2. The NASTRAN User's Manual (Level 17.5), NASA SP-222 (05), Washington, D.C., December 1978.

3. Abla, Mike H.; Boroughs, Robert R.; and Cook, Everett L.: Analysis of The Learjet 35/36 Wing and Correlation With Experimental Results, NASTRAN User's Experiences, NASA TMX-3428, Otober 1976, pp. 331-352.

ORIGINAL PAGE IS
OF POOR QUALITY

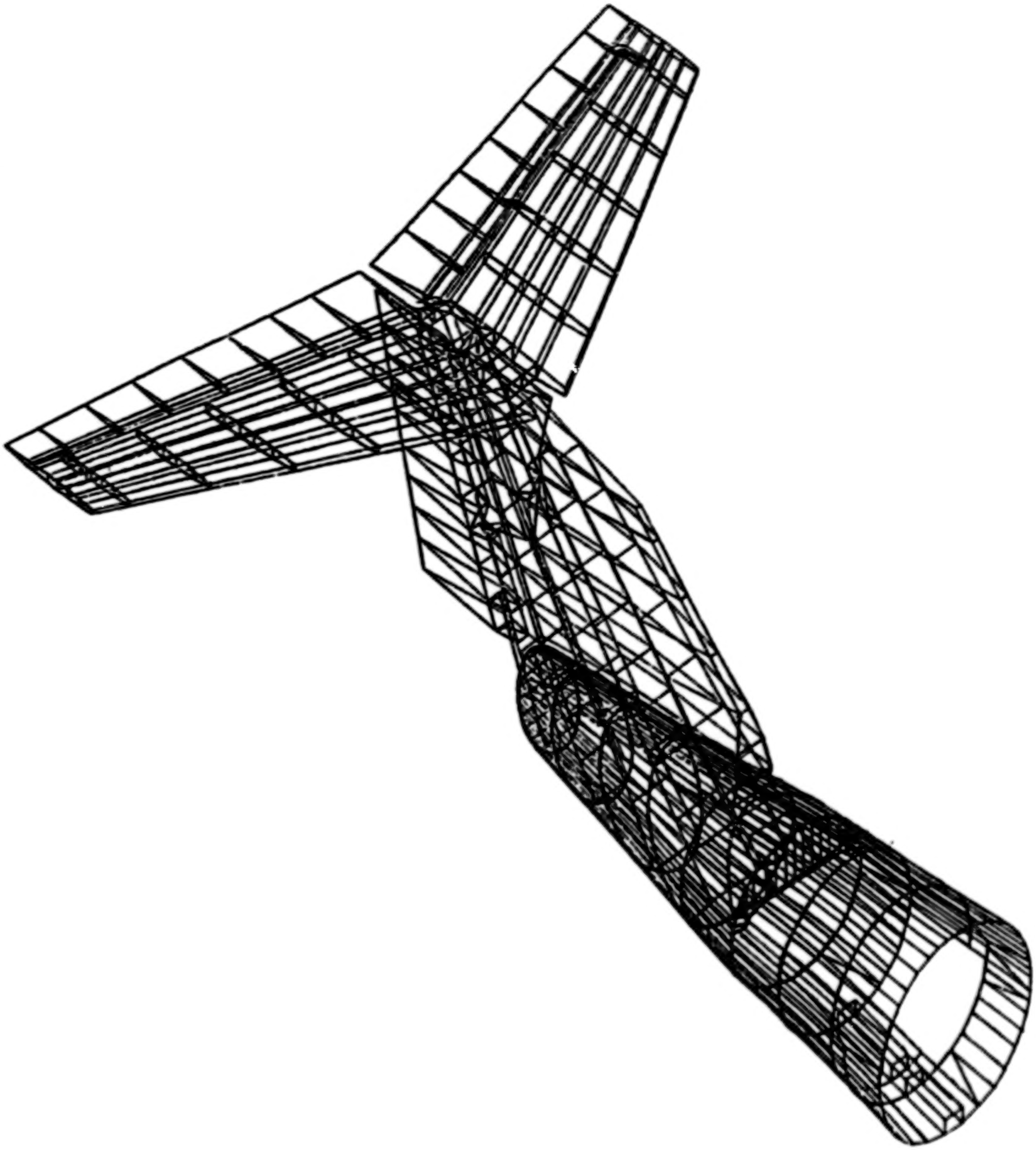

FIGURE 1 - NASTRAN 55 EMPENNAGE MODEL

ORIGINAL PAGE IS
OF POOR QUALITY

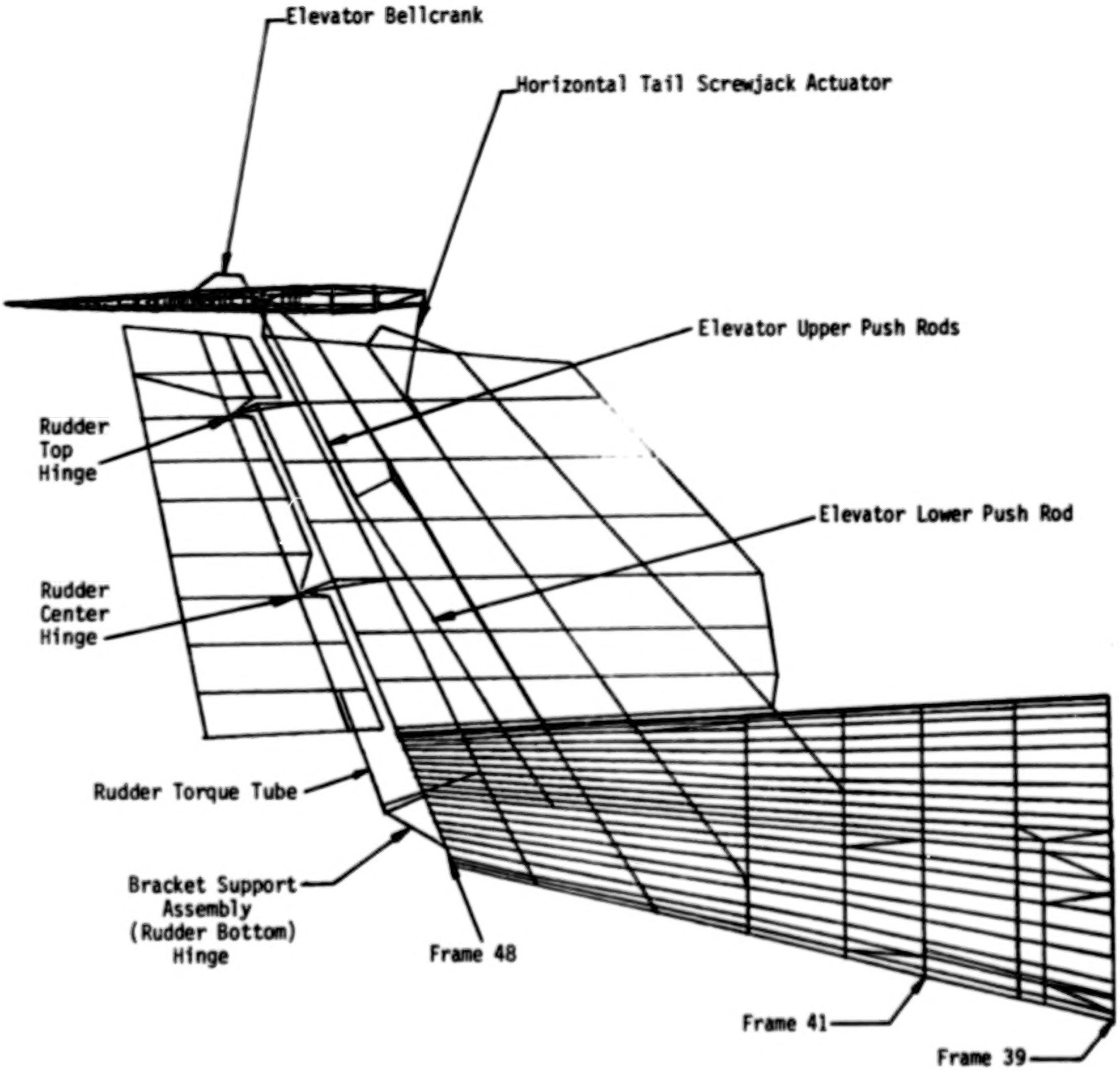
Elevator Bellcrank
Horizontal Tail Screwjack Actuator
Elevator Upper Push Rods
Rudder Top Hinge
Elevator Lower Push Rod
Rudder Center Hinge
Rudder Torque Tube
Bracket Support Assembly (Rudder Bottom) Hinge
Frame 48
Frame 41
Frame 39

FIGURE 2 - VERTICAL TAIL STRUCTURE

ORIGINAL PAGE IS
OF POOR QUALITY

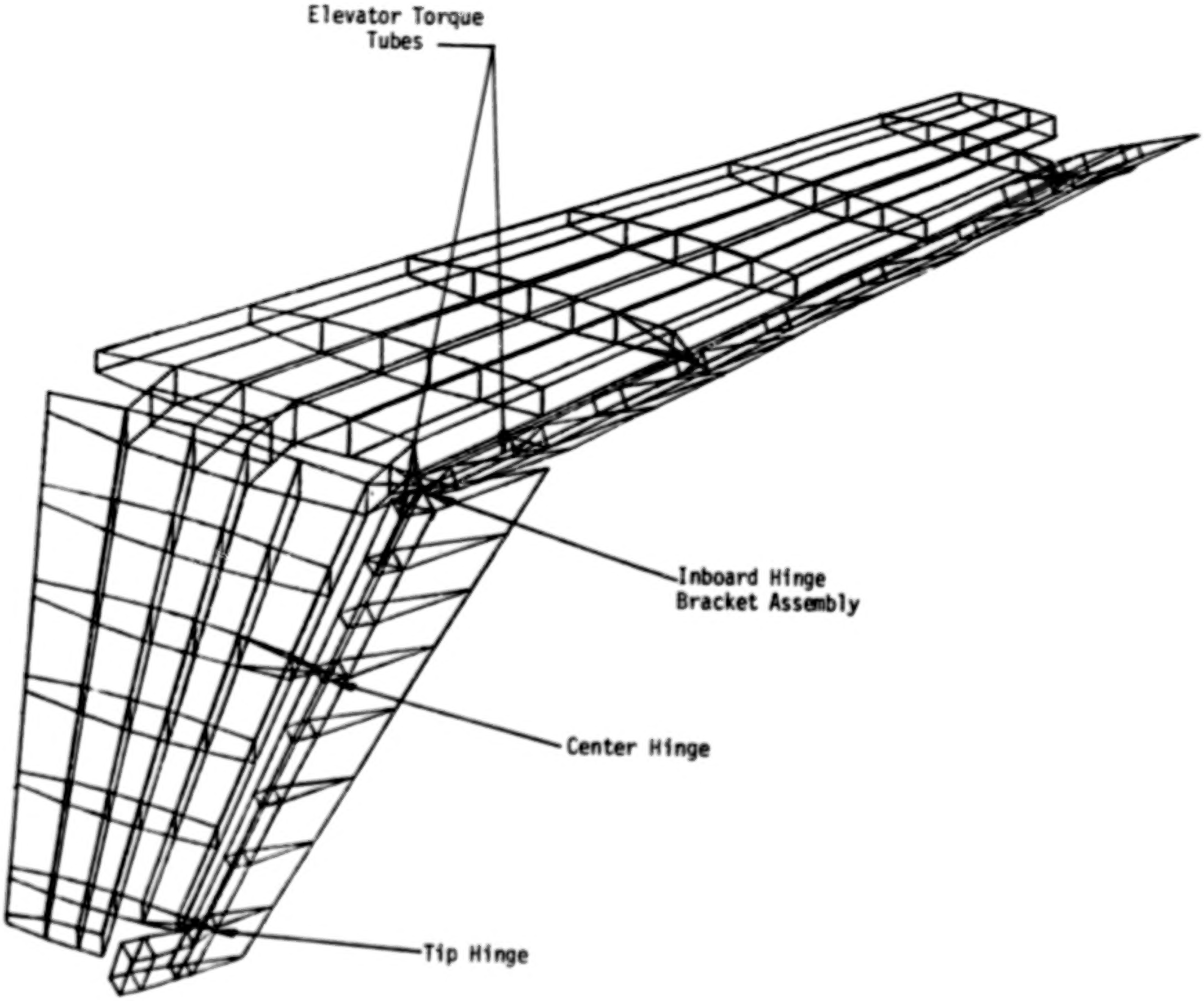
Elevator Torque Tubes
Inboard Hinge Bracket Assembly
Center Hinge
Tip Hinge

FIGURE 3 - HORIZONTAL TAIL STRUCTURE

ORIGINAL PAGE IS
OF POOR QUALITY

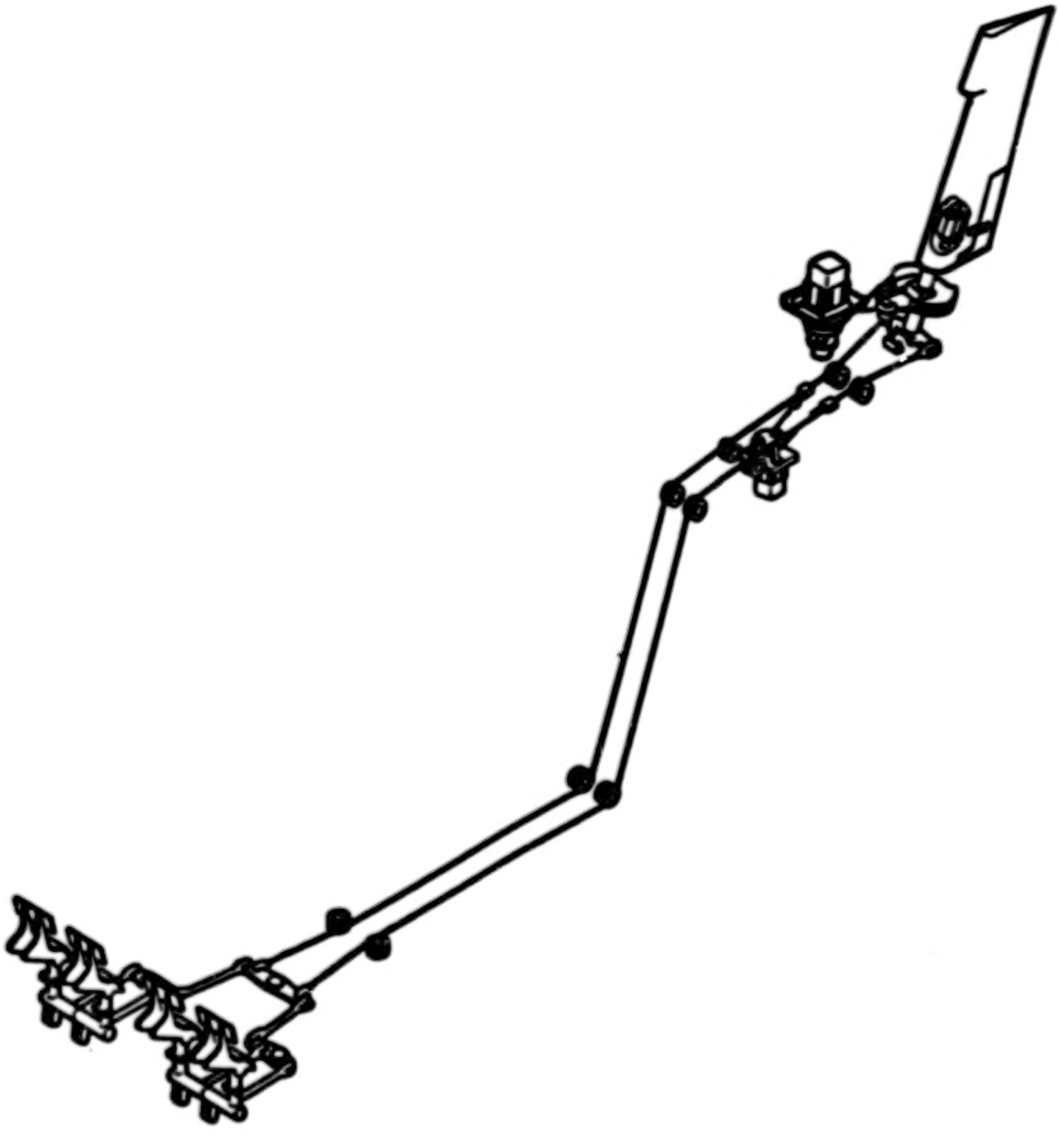

FIGURE 4 - RUDDER CONTROL SYSTEM

ORIGINAL PAGE IS
OF POOR QUALITY

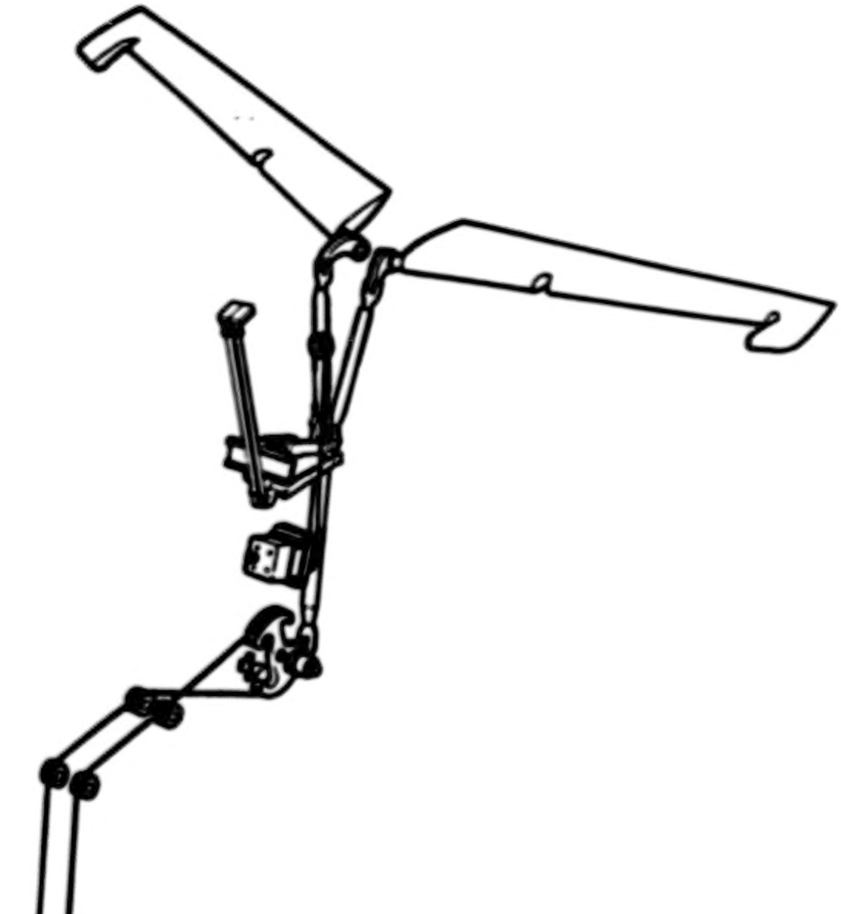

FIGURE 5 - ELEVATOR CONTROL SYSTEM

ORIGINAL PAGE IS
OF POOR QUALITY

Input Data Card CØRD2R   Rectangular Coordinate System Definition

Description: Defines a rectangular coordinate system by reference to the coordinates of three points. The first point defines the origin. The second point defines the direction of the z-axis. The third point defines a vector which, with the z-axis, defines the x-z plane. The reference coordinate must be independently defined.

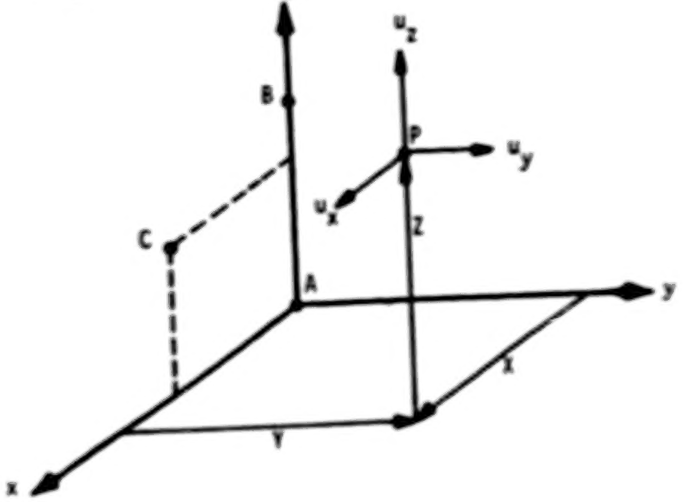

Format and Example:

1	2	3	4	5	6	7	8	9	10
CØRD2R	CID	RID	A1	A2	A3	B1	B2	B3	ABC
CØRD2R	3	17	-2.9	1.0	0.0	3.6	0.0	1.0	123
+BC	C1	C2	C3						
+23	5.2	1.0	-2.9						

Field	Contents
CID	Coordinate system identification number (Integer > 0)
RID	Reference to a coordinate system which is defined independently of new coordinate system (Integer ≥ 0 or blank)
A1,A2,A3 B1,B2,B3 C1,C2,C3	Coordinates of three points in coordinate system defined in field 3 (Real)

Remarks:

1. Continuation card must be present.
2. The three points (A1, A2, A3), (B1, B2, B3), (C1, C2, C3) must be unique and noncollinear. Noncollinearity is checked by the geometry processor.
3. Coordinate system identification numbers on all CØRD1R, CØRD1C, CØRD1S, CØRD2R, CØRD2C, and CØRD2S cards must all be unique.
4. An RID of zero references the basic coordinate system.
5. The location of a grid point (P in the sketch) in this coordinate system is given by (X, Y, Z).
6. The displacement coordinate directions at P are shown by (u_x, u_y, u_z).

FIGURE 6 - CORD2R COORDINATE SYSTEM CARD IMAGE

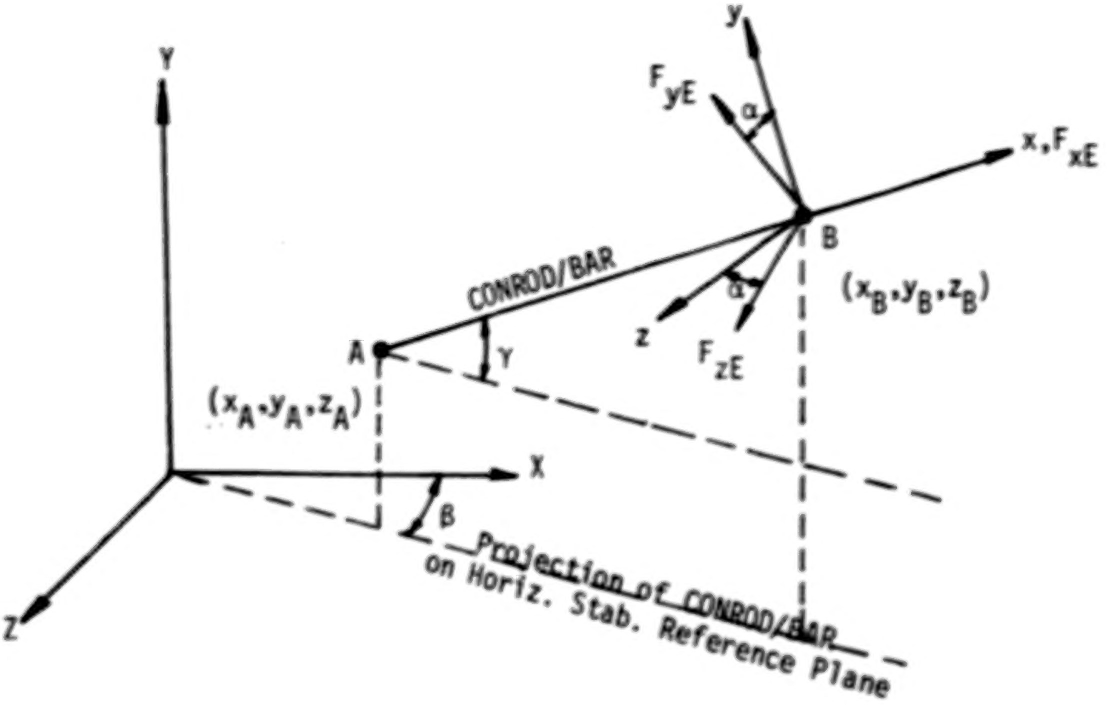
Y
y
F_{yE}
α
x, F_{xE}
B
CONROD/BAR
(x_B, y_B, z_B)
α
A
γ
z
F_{zE}
(x_A, y_A, z_A)
X
β
Projection of CONROD/BAR
on Horiz. Stab. Reference Plane
Z

$$\begin{bmatrix} F_{XE} \\ F_{YE} \\ F_{ZE} \end{bmatrix} = \begin{bmatrix} \cos\beta & 0 & -\sin\beta \\ 0 & 1 & 0 \\ \sin\beta & 0 & \cos\beta \end{bmatrix} \begin{bmatrix} \cos\gamma & -\sin\gamma & 0 \\ \sin\gamma & \cos\gamma & 0 \\ 0 & 0 & 1 \end{bmatrix} \begin{bmatrix} 1 & 0 & 0 \\ 0 & \cos\alpha & -\sin\alpha \\ 0 & \sin\alpha & \cos\alpha \end{bmatrix} \begin{bmatrix} F_{xE} \\ F_{yE} \\ FzE \end{bmatrix}$$

FIGURE 7 - HINGE FORCE TRANSFORMATION

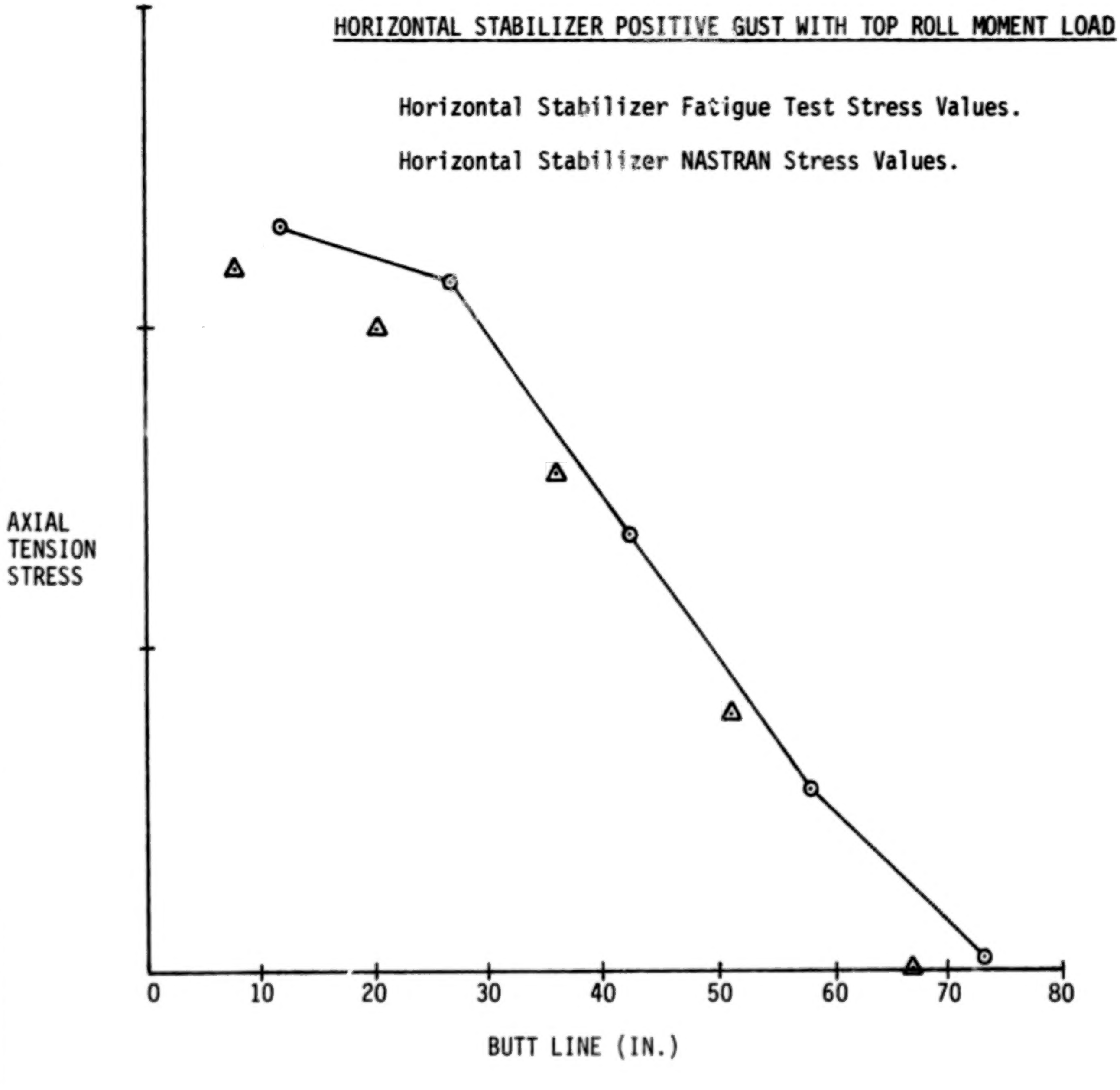

FIGURE 8 - HORIZONTAL STABILIZER FORWARD SPAR UPPER CAP STRESSES

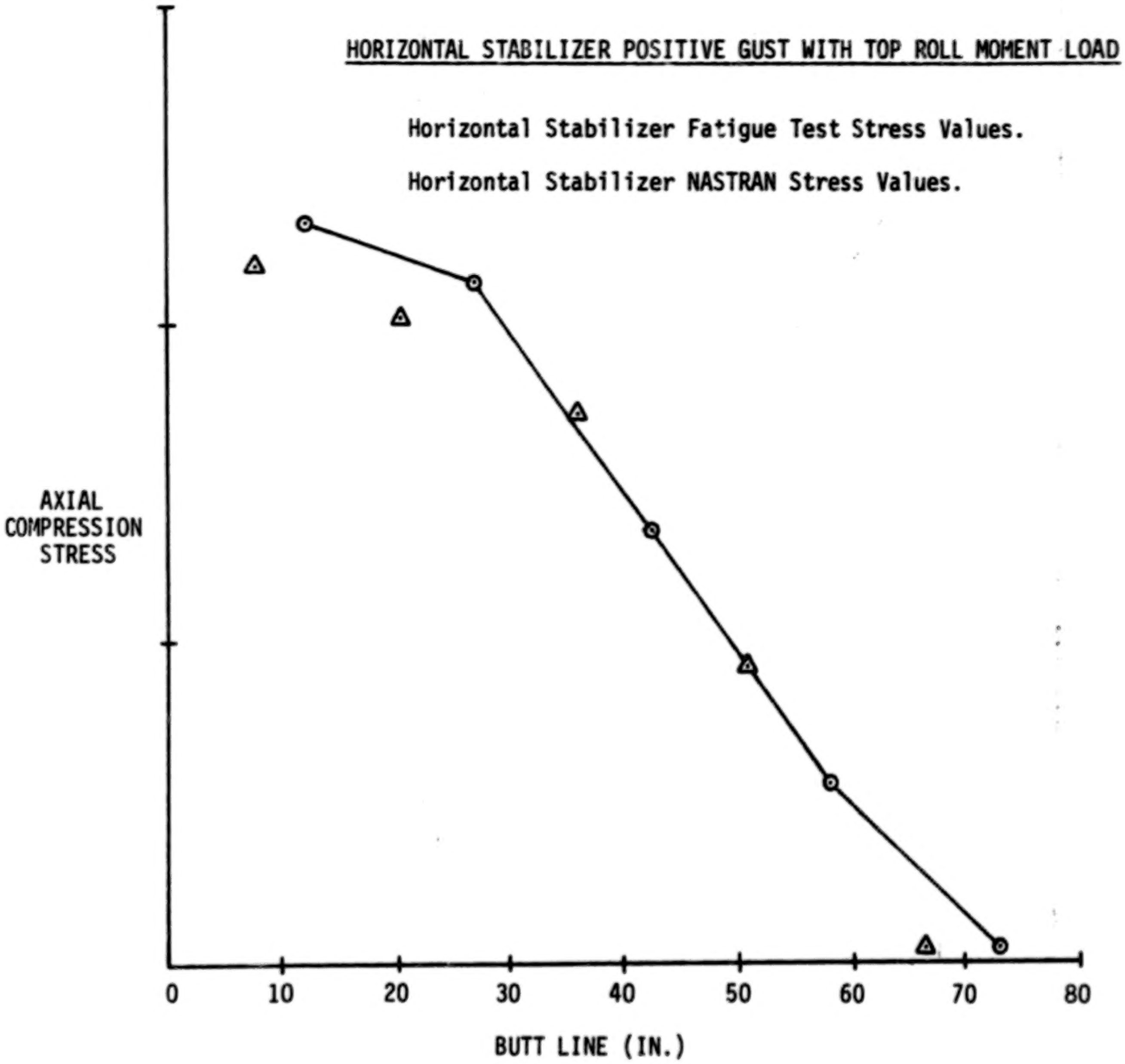

FIGURE 9 - HORIZONTAL STABILIZER FORWARD SPAR LOWER CAP STRESSES

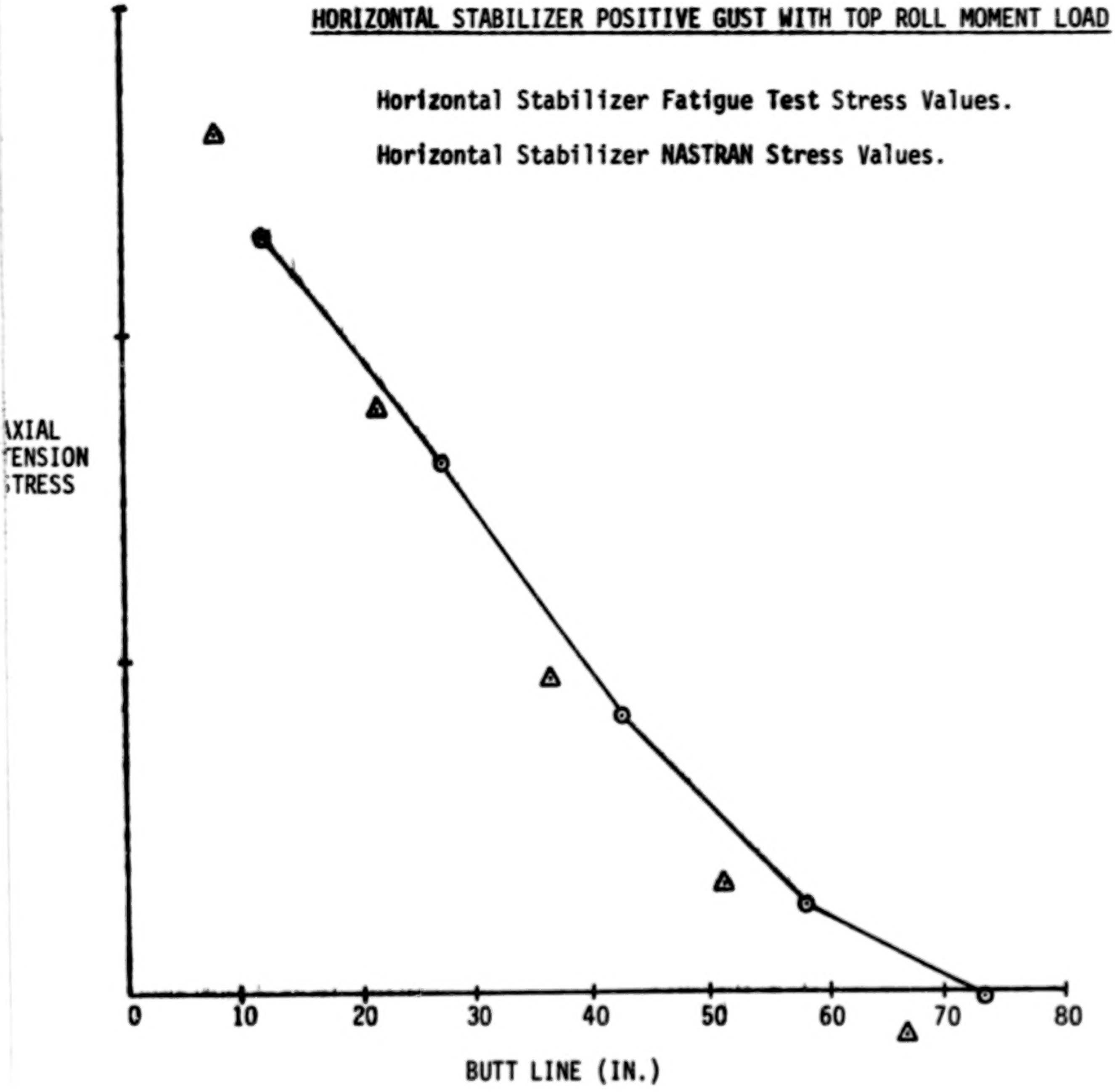

FIGURE 10 - HORIZONTAL STABILIZER REAR SPAR UPPER CAP STRESSES

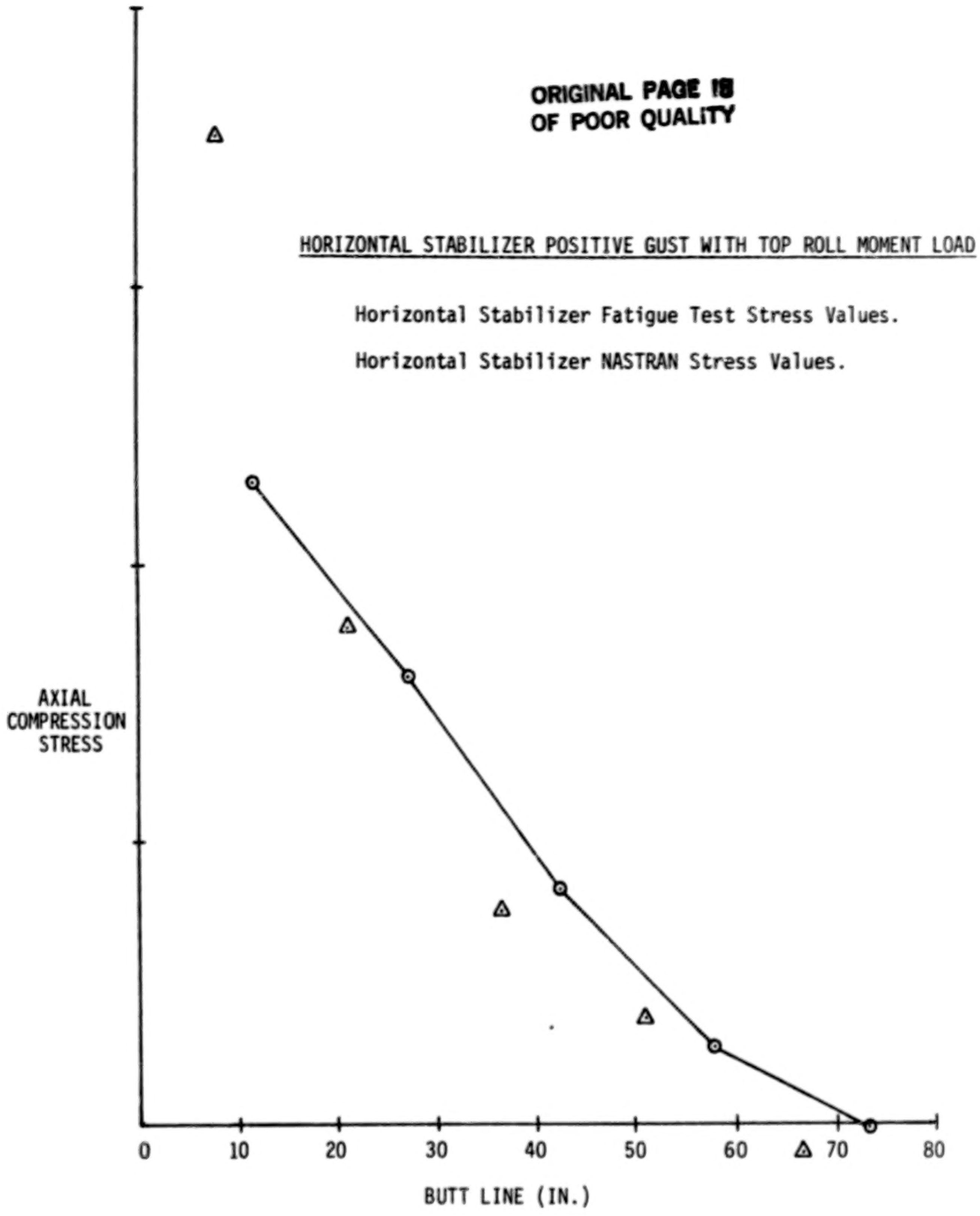

FIGURE 11 - HORIZONTAL STABILIZER REAR SPAR LOWER CAP STRESSES

N84
15605

UNCLAS

N84 15605 D15

ORIGINAL PAGE IS OF POOR QUALITY

A NEW METHOD FOR GENERATING AND MAINTAINING RIGID FORMATS IN NASTRAN

By

P. R. Pamidi and W. Keith Brown
RPK CORPORATION

SUMMARY

Since all NASTRAN users are most likely to use some of the Rigid Formats, it is important that a convenient means of updating these Rigid Formats be available. This benefits both the NASTRAN maintenance contractor and the NASTRAN user community. With this in view, RPK Corporation is currently developing a new method for generating and updating Rigid Formats in NASTRAN. The heart of this method is a Rigid Format data base that is in card-image format and that can therefore be easily maintained by the use of standard text editors. Each Rigid Format entry in this data base will contain the Direct Matrix Abstraction Program (DMAP) for that Rigid Format along with the related restart, subset and substructure control tables. NASTRAN will read this data base directly in every NASTRAN run and perform the necessary transformations to allow the DMAP to be processed and compiled by the NASTRAN executive. This approach will permit Rigid Formats to be changed without unnecessary compilations and relinking of NASTRAN. Furthermore, this approach will also make it very easy for users to make permanent changes to existing Rigid Formats as well as to generate their own Rigid Formats. This new method will be incorporated in a future release of the public version of NASTRAN.

INTRODUCTION

The popularity and longevity of NASTRAN are due to the many types of analyses that it supports and the generality and flexibility that it offers to the user to perform these analyses. The analyses are implemented in NASTRAN by the use of many functional modules each of which can be considered as an independent program. These functional modules interface with one another through executive parameter flags and a local data base called the File Allocation Table (FIAT). The FIAT and the flags are maintained by the NASTRAN executive. The order in which the functional modules are executed and the definition of the files and flags to be read or written by these functional modules are specified by means of a higher level language called the Direct Matrix Abstraction Program (DMAP). The DMAP is compiled and processed by the NASTRAN executive.

The most general way of using NASTRAN is with a user written DMAP program. However, in order to relieve the user of the burden of writing DMAP sequences for the most commonly used analyses (e.g., static analysis, normal mode analysis, etc.), a number of standard DMAP sequences (with sophisticated restart capabilities and subset features) have been developed and included in NASTRAN. These standard DMAP sequences are collectively called the NASTRAN Rigid Formats. There are currently twenty (20) Rigid Formats in NASTRAN. They are very valuable to the user as they are in a readily available and useable form and offer the user the flexibility for performing a variety of analyses. Modifications to the Rigid Formats can be easily made by the user by means of the ALTER feature described in Section 2.2 of the NASTRAN User's Manual (Reference 1).

PRESENT METHOD FOR GENERATING AND MAINTAINING RIGID FORMATS

At present, the Rigid Formats exist in NASTRAN in the form of subroutines. These subroutines are called the LDxx (LD01, LD02, etc.) subroutines and are described in Section 6.6 of the NASTRAN Programmer's Manual (Reference 2). There is one LDxx subroutine for each Rigid Format in NASTRAN. The bulk of the code in these subroutines is in the form of Fortran DATA statements consisting mainly of Hollerith values of the type 4Hxxxx. This format is very awkward. Consequently, making updates to these subroutines is an extremely tedious, time-consuming and error-prone procedure. In order to overcome this serious problem, a utility program called the Rigid Format Generation (RFGEN) program was developed for use by the maintenance contractor to automatically generate the LDxx subroutines. The RFGEN program requires the maintenance of a separate data base of Rigid Formats and their associated restart tables. This data base is read by the RFGEN utility to generate the desired LDxx subroutines.

The current practice of generating and maintaining Rigid Formats has many serious drawbacks. These are discussed in detail below.

1. Because of the nature of the LDxx subroutines, the use of the RFGEN utility is absolutely essential when major changes (e.g., extensive changes to the DMAP) need to be made to any Rigid Format. However, the RFGEN utility is currently operational only on the CDC machine. Hence, the maintenance contractor cannot generate the LDxx subroutines directly on another machine which he may be using as the primary machine for NASTRAN maintenance.

2. The Rigid Format information is currently contained both in the external data base used by the RFGEN utility as well as in the LDxx subroutines of NASTRAN. This is not only wasteful and cumbersome, but has also caused serious problems. Occasionally, updates were

made directly to an LDxx subroutine (for example, correction of a restart table) but never incorporated into the RFGEN data base. Consequently, these updates were lost when the RFGEN utility was used at a later date to generate replacement LDxx subroutines.

3. Permanent changes to a Rigid Format require the updating and recompiling of the appropriate LDxx subroutine as well as the relinking (or rebuilding) of Link 1. This is very inconvenient and annoying both to the maintenance contractor and users.

4. Users do not have access to the RFGEN utility which is available only to the maintenance contractor. They, therefore, cannot make major permanent changes to Rigid Formats at their local sites and are thus forced to use the ALTER capability in order to incorporate the desired changes. However, this has the disadvantage that the ALTER packet has to be included in every run in which the user needs the changes. This can be particularly inconvenient when the ALTERs are extensive.

   An extension of the above problem is that sophisticated users cannot generate new Rigid Formats of their own except by means of inserting the DMAP on a temporary basis through the NASTRAN DMAP approach. However, this has the same limitation that the ALTER cards have in that the DMAP has to be included in every run in which the user needs it. This can be particularly cumbersome when the DMAP contains many statements.

5. The substructuring capability of NASTRAN causes the automatic generation of DMAP ALTERs in those Rigid Formats that support this capability. Currently, Rigid Formats 1, 2, 3, 8 and 9 support this feature. These automatic ALTERs are currently specified in the Fortran subroutines ASCM01, ASCM05, ASCM07 and ASCM08. These ASCMxx subroutines must, therefore, be appropriately updated whenever changes to Rigid Formats 1, 2, 3, 8 and 9 affect their DMAP statement numbers and hence the DMAP ALTERs specified in these ASCMxx subroutines.

6. The data base currently used by the RFGEN utility is not in a very convenient format. Making changes to this data base is therefore not very easy, particularly when changes need to be made to the restart tables.

NEW METHOD FOR GENERATING AND MAINTAINING RIGID FORMATS

All of the above problems can be eliminated by having a Rigid Format data base that is read by NASTRAN directly and that can be maintained easily by means of standard text editors already available on the host computers. The important and distinct advantages to be derived from this approach are discussed below.

1. The need for the RFGEN utility and its associated data base will be eliminated and updating of Rigid Formats will become equally easy on all machines.

2. The LDxx subroutines in their current form will be eliminated from NASTRAN and the entire information about Rigid Formats will be contained in the new Rigid Format data base. This will greatly facilitate the maintenance effort.

3. Permanent changes to a Rigid Format can be incorporated simply by suitably updating the new data base by means of a text editor. The need for compilations and the relinking of Link 1 will thus be eliminated, thereby greatly aiding both users and the maintenance contractor.

4. It will become very easy for users to test and incorporate major changes to existing Rigid Formats at their local sites without having to use the ALTER feature in every run. Similarly, sophisticated users will be able to generate new Rigid Formats (complete with the associated restart tables) with relative ease.

5. By incorporating controls for substructure DMAP ALTERs in the new data base, the need for the possible updating of the ASCMxx subroutines every time the associated Rigid Formats are changed will be eliminated. This will greatly reduce chances for error since all information about the substructure DMAP ALTERs will be contained in the new data base instead of being spread over several ASCMxx subroutines.

6. The format of the new data base will be designed to be user-friendly and to be easily amendable.

IMPLEMENTATION OF THE NEW METHOD

The Rigid Format data base will be in a card-image format and will contain entries for all 20 Rigid Formats in NASTRAN. Each Rigid Format entry will contain the following items of information:

1. DMAP statements
2. Card Name Restart Table
3. File Name Restart Table
4. Rigid Format Change Restart Table
5. Subset flags
6. Controls for substructure DMAP ALTERs

The format of the data base will be designed to be user-friendly and to be easily amendable. All DMAP statements will be in a format similar to the format in which NASTRAN prints the DMAP. All restart tables, subset flags and substructure controls will be defined so as to permit easy editing.

The Rigid Format entries will be implemented as follows on the four computer systems on which NASTRAN is currently supported:

1. IBM - Each entry will be a member of a partitioned dataset
2. UNIVAC - Each entry will be an element of a file
3. CDC - Each entry will be a separate file
4. DEC VAX - Each entry will be a separate file

An I/O interface will be designed on all of the four computer systems to read the Rigid Format entries. This interface will be written in machine-dependent code. Additional subroutines in machine-independent code will be designed to perform the necessary transformations to allow for the processing and compilation of the DMAP by the NASTRAN executive. The current LDxx subroutines will thus no longer be used and will therefore be deleted from the code.

In addition, documentation updates will be provided for the NASTRAN User's Manual and the NASTRAN Programmer's Manual. The User's Manual updates will contain a definition of the format of the new Rigid Format data base and also a description of how to maintain and update the data base. The Programmer's Manual updates will include a description of all subroutines and COMMONs that are added to NASTRAN as part of this new capability.

CONCLUDING REMARKS

The new method of generating and maintaining Rigid Formats described in this paper should be welcomed by both the NASTRAN maintenance contractor and the NASTRAN user community. It will, for the first time, make it possible for the maintenance contractor to update and modify existing Rigid Formats without the use of a utility program and without unnecessary compilations and relinking of NASTRAN. It will also, for the first time, make it possible and practicable for users not only to make permanent changes to existing Rigid Formats, but also to create new Rigid Formats of their own. This will greatly enhance the flexibility and attractiveness of NASTRAN.

REFERENCES

1. The NASTRAN User's Manual, NASA SP-222(05), December 1978.
2. The NASTRAN Programmer's Manual, NASA SP-223(05), December 1978.

N84
15606

UNCLAS

N84 15606 D16

IMPLEMENTATION OF
ELASTIC-PLASTIC STRUCTURAL ANALYSIS
INTO NASTRAN †

Alvin Levy, A. B. Pifko and P. L. Ogilvie

Grumman Aerospace Corporation, Bethpage N.Y

SUMMARY

Elastic-plastic analytic capabilities have been incorporated into the NASTRAN program. The present implementation includes a general rigid format and additional bulk data cards as well as two new modules. The modules are specialized to include only perfect plasticity of the CTRMEM and CROD elements but can easily be expanded to include other plasticity theories and elements. The practical problem of an elastic-plastic analysis of a ship's bracket connection is demonstrated and compared to an equivalent analysis using Grumman's PLANS program. The present work demonstrates the feasibility of incorporating general elastic-plastic capabilities into NASTRAN.

INTRODUCTION

A feasibility study on incorporating state-of-the-art nonlinear capabilities into NASTRAN has been conducted and reported on in ref. 1. It was pointed out that each class of nonlinear behavior has a "best" solution strategy. For an elastic-plastic analysis, the "initial-strain" approach is the most efficient finite element analytic method. In this approach, an incremental pseudo-load vector is formulated assuming an initial strain equal to the sum of the estimated plastic strain for the current increment and an equilibrium correction term which corrects for the difference between the resulting plastic strain and assumed plastic strain of the previous incremental step. This method, characterized by the plastic behavior being incorporated into an incremental pseudo-load vector, leaves the stiffness matrix unaltered from step to step. Thus, the stiffness matrix need only be decomposed once. Consistent with the initial-strain approach, ref. 2 provides the pseudo-load vector formulation due to plastic behavior for a number of elements in the NASTRAN library. The general approach is to transfer the integral form of the pseudo-load vector into a numerical representation by utilizing various integration schemes. For many of the finite elements the choice of the number and type of integration points is left to the user. The choice of integration points for the integration of the pseudo-load vector determines the allowable variation of the plastic strain within each element. This allowable variation can be changed by choosing a different set of integration points. This may eliminate the costly process of changing the finite element idealization if the plastic strain variation was more complex than originally modeled for. One may only have to change the choice of integration points. A more complete discussion of these methods is given in ref. 3.

---

† Partially funded by David W. Taylor Naval Ship Research and Development Center, Bethesda, Maryland.

The initial-strain approach, as outlined above, has been incorporated into the NASTRAN program. This has been done by writing a new rigid format along with two new modules. Also included are three new bulk data cards. Although the methods are general, only perfectly-plastic behavior of a membrane and a rod element have been initially considered. This first step is sufficient to examine the feasibility and efficiency of the implemented techniques within the NASTRAN framework.

The practical problem of an elastic-plastic structural analysis of a ship's bracket connection has been carried out using the implemented NASTRAN program and the results have been compared to those obtained from the PLANS finite element computer program (ref. 4). The results are in exact agreement and the cpu time and associated costs are approximately the same.

ELASTIC-PLASTIC FORMULATION

The initial-strain method is chosen to solve small displacement plasticity problems. The governing equation, derived from energy principles, is written in incremental form as follows:

$$[K]\{\Delta U\}_i = \{\Delta P\}_i + \{\Delta Q\}_i + \{R\}_i \tag{1}$$

where

$[K]$ ≡ elastic stiffness matrix

$\{\Delta U\}_i$ ≡ incremental displacement of i^{th} step

$\{\Delta P\}_i$ ≡ incremental external load of i^{th} step

$\{\Delta Q\}_i$ ≡ incremental pseudo load based on predicted inelastic strain of i^{th}step

$\{R\}_i$ ≡ equilibrium correction term representing any balancing force due to drift from equilibrium during the incremental application of the load

The elastic stiffness matrix is found to be

$$[K] = \int [B]^T [E] [B] \, dV \tag{2}$$

where $[B]$ is obtained from the strain-displacement relation

$$\{\Delta \epsilon\}_i = [B]\{\Delta U\}_i \tag{3}$$

and [E] is obtained from the stress-strain relation

$$\left\{\Delta\sigma\right\}_i = [E]\left(\left\{\Delta e\right\}_i - \left\{\Delta\epsilon^P\right\}_i\right) \tag{4}$$

with

$\left\{\Delta\sigma\right\}_i$ ≡ incremental stress

$\left\{\Delta e\right\}_i$ ≡ incremental total strain

$\left\{\Delta\epsilon^P\right\}_i$ ≡ incremental plastic strain

Plasticity enters the analysis through the increment in plastic strain, $\Delta\epsilon^P$. These as well as other path dependent quantities depend on the implemented plasticity theory.

The predicted pseudo-load vector for the $(i+1)^{st}$ step is found to be

$$\left\{\Delta Q\right\}_{i+1} = \frac{\delta_{i+1}}{\delta_i}\int [B]^T [E]\left\{\Delta\epsilon^P\right\}_i dV \tag{5}$$

where δ_{i+1} and δ_i correspond to the $(i+1)^{st}$ and i^{th} step sizes respectively. We can expect the successive linearization procedure to drift from a true equilibrium position for the nonlinear response. This drifting is a combined result of truncation, the successive linearization procedure and the fact that information not yet available is required for a true solution (in Eq (5) the predicted pseudo-load vector is based on the incremental plastic strains of the preceding step rather than on the current step). The simplest corrective procedure involves the introduction of an equilibrium correction term that may be added as a load vector in the incremental procedure. The equilibrium correction term is defined as

$$\left\{R\right\}_{i+1} = \int [B]^T [E]\left(\left\{\Delta\epsilon^P\right\}_i - \left\{\Delta\epsilon^P\right\}_{i-1}\right) dV \tag{6}$$

This is a simpler method than a complete iterative scheme and in effect the equilibrium correction term represents a one step iteration.

The pseudo-load vector is computed by various integration schemes (e.g., trapezoidal and Gaussian) in which Eqs (5) and (6) are combined and written as

$$\left\{\Delta Q\right\}_{i+1} + \left\{R\right\}_{i+1} = \sum_{J=1}^{n} A_j [B(\tau_j)]^T [E(\tau_j)]\left(\left(1 + \frac{\delta_{i+1}}{\delta_i}\right)\left\{\Delta\epsilon^P\right\}_i - \left\{\Delta\epsilon^P\right\}_{i-1}\right) \tag{7}$$

where n represents the number of integration points, τ_j represents the spatial location of the jth integration point and A_j corresponds to an integration weight factor for the jth integration point. The derivation of the pseudo-load vector for many of the NASTRAN elements is presented in ref. 2. The present study utilizes only the triangular membrane element (CTRMEM) and the extensional rod element (CROD).

IMPLEMENTATION OF ELASTIC-PLASTIC ANALYSIS INTO NASTRAN

Elastic-plastic capabilities have been incorporated into the NASTRAN program. A flow diagram, representing the intital-strain method, is shown in Appendix A. The function of each step in the flow diagram is explained. A corresponding rigid format was written as a modification to rigid format 1 (Level 17.0). The ALTER package and resulting new rigid format are shown in Appendices B1 and B2, respectively.

Some of the important features of the new rigid format will be mentioned. Firstly, two new modules have been written, PLANS1 and PLANS2. PLANS1 determines the critical load, i.e., the lowest load amplitude for which at least one element stress point has become plastic. In addition a new table, PLI, is initialized. This table contains the last known field quantities such as stress, strain and plastic strain. PLANS2 implements the elastic-plastic constitutive equations for incremental stress, strain and plastic strain. Initially only perfect plastic behavior of the CTRMEM and CROD elements have been included. In addition PLANS2 updates the PLI table and forms the pseudo-load vector the the next plastic increment. The calculations needed to perform an elastic-plastic analysis are divided into those that are performed one time and those that are performed in each incremental step. Among those that are performed once are all the usual functions necessary in an elastic finite element analysis, i.e., reading input, all global functions such as setting up data tables, and solving for the elastic displacement field. These functions are performed by the operational sequence currently in rigid format 1 and are represented by the first block of the flow diagram. In addition, the critical load calculation and some preliminary plastic analysis definitions are carried out as shown in the flow diagram above LOOPA, which is the start of the plasticity loop. The calculations performed during each incremental step are contained in the plasticity loop as shown in the flow diagram. During each pass through the plasticity loop the SSG3 module solves for the incremental displacements due to the plastic pseudo-load only. The incremental displacement due to the external load or prescribed displacements are known and are added to the incremental displacements due to the pseudo-load vector. The plasticity constitutive equations are implemented and the new pseudo-load vector, to be used in the next incremental step, is formed (PLANS2). The plasticity loop is repeated for each incremental step.

Three new bulk data cards have been added for later use in a general elastic-plastic analytic capability program. These are described in Appendix C. The MATS2 bulk data card defines the plastic material properties; the PLFAC2 bulk data card defines the load history and step size information; and the TABLEY1 bulk data card defines the yield stress as a function of accumulated plastic strain.

SAMPLE PROBLEM

In order to validate the implemented NASTRAN capability an elastic-plastic analysis of a typical structural detail of a ship, namely a bracket connection, was performed using NASTRAN and the Grumman PLANS program. Figure 1 shows the intersection of a horizontal girder with a transverse bulkhead. The shaded area represents the structural component that was analyzed. Loads and boundary displacements on this section were provided from a finite element model of the entire structure. The finite element model consisted of 657 membrane triangles for the webs, 103 rod elements for the flanges (shown as dotted lines in Fig. 3) resulting in 704 degrees of freedom with a semi-band width of 40. Figures 2 and 3 show the details of the finite element model. Figure 4 shows the resulting growth of the plastic region of the highest stressed section.

The NASTRAN analysis was performed on a CDC cyber 172 computer and required 20 cpu seconds for each incremental step. The PLANS program,run on an IBM 370/3033 computer, used 5 cpu seconds for each incremental step. The results from each program were identical. Taking into account the difference between computational speed of each computer (about 5:1), the running time for the NASTRAN program is competitive with the PLANS program.

CONCLUSIONS

The present work demonstrates the feasibility of incorporating elastic-plastic capabilities into NASTRAN. The present implementation included a general new rigid format and bulk data cards as well as two new modules. The modules are specialized to include only perfect plasticity of the CTRMEM and CROD elements.

An extension of these capabilities to include general plastic behavior of the complete NASTRAN element library should present no new pitfalls and will be briefly outlined. Firstly, an extension to the flow chart and ALTER package would include one new module, PLA5, used to accumulate the total displacements (Table UGVPAC) as well as stress, strain and plastic strain (Table PLIAC) at the end of each increment. It would apear as

```
PLA5   UGVP, PLI/UGVPAC,PLIAC/V,N,PLACOUNT/V,N,P
```

In addition, new tables would be set up in PLANS1 and would contain element integration point information. To form these tables, user specified information would be supplied on bulk data cards through new element property cards.

Module PLANS2 must be generalized to build a pseudo-load vector, Eq (7), from the new tables set up in PLANS1. In addition, the plasticity theory contained in PLANS2 should be expanded to include, in addition to perfect plasticity, linear strain-hardening, nonlinear strain-hardening using either a Ramberg-Osgood function or a stress-strain table, or any other theory consistant with the initial strain approach that the developer wants to incorporate.

REFERENCES

1. Levy, A., and Pifko, A.B., "Feasibility Study for the Incorporation of Nonlinear Capability into NASTRAN," Grumman Research Department Report, RE-593, Grumman Aerospace Corporation, January 1980.

2. Crouzet-Pascal, J., and Levy, A., "Pseudo-Load Formulation for NASTRAN material Nonlinear Analysis using Initial-Strain Method," Grumman Research Department Report, RE-594, Grumman Aerospace Corporation, March 1980.

3. Levy, A., and Pifko, A.B., "On Computational Strategies for Problems involving Plasticity and Creep," International Journal for Numerical Methods in Engineering, Vol. 17, pp. 747-771 (1981).

4. Pifko, A.B., Levine, H.S., Armen, Jr., H., and Levy, A., "PLANS - A finite element program for nonlinear analysis of structures," ASME Preprint 74-WA/PVP-6(1974).

ORIGINAL PAGE IS
OF POOR QUALITY

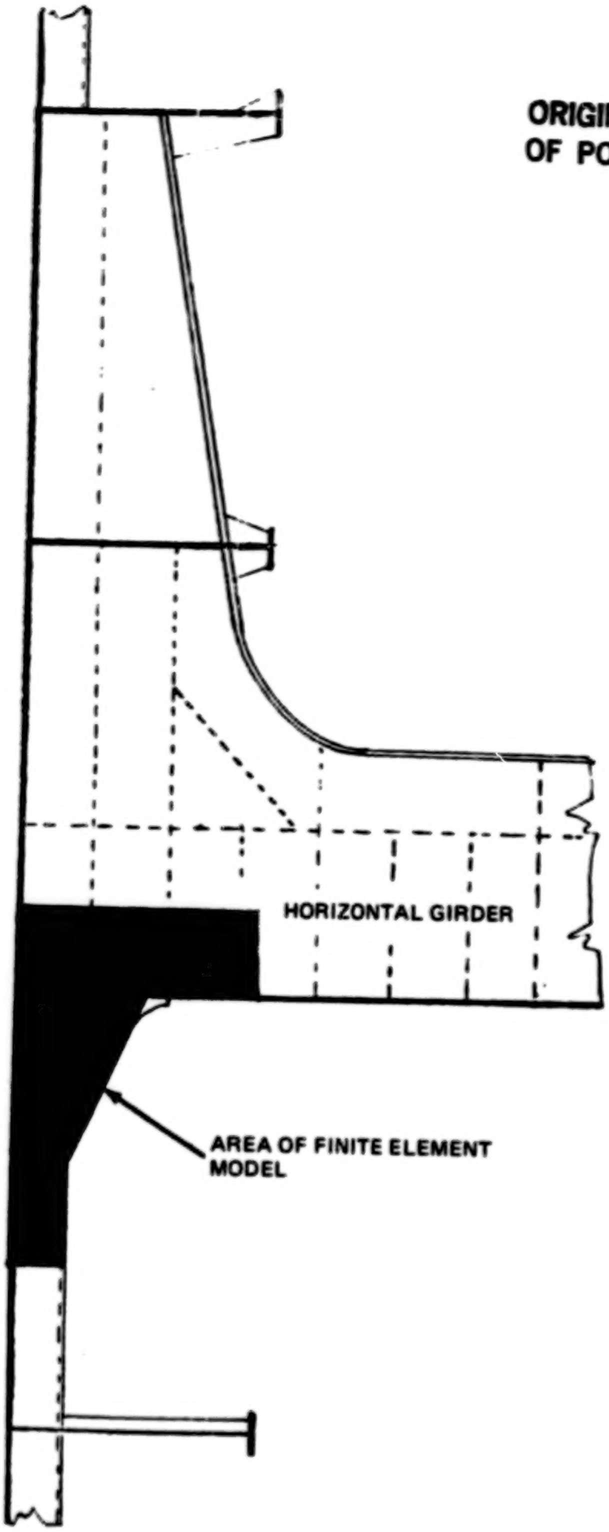
HORIZONTAL GIRDER
AREA OF FINITE ELEMENT MODEL

Fig. 1 Structural Detail of Bracket Connection

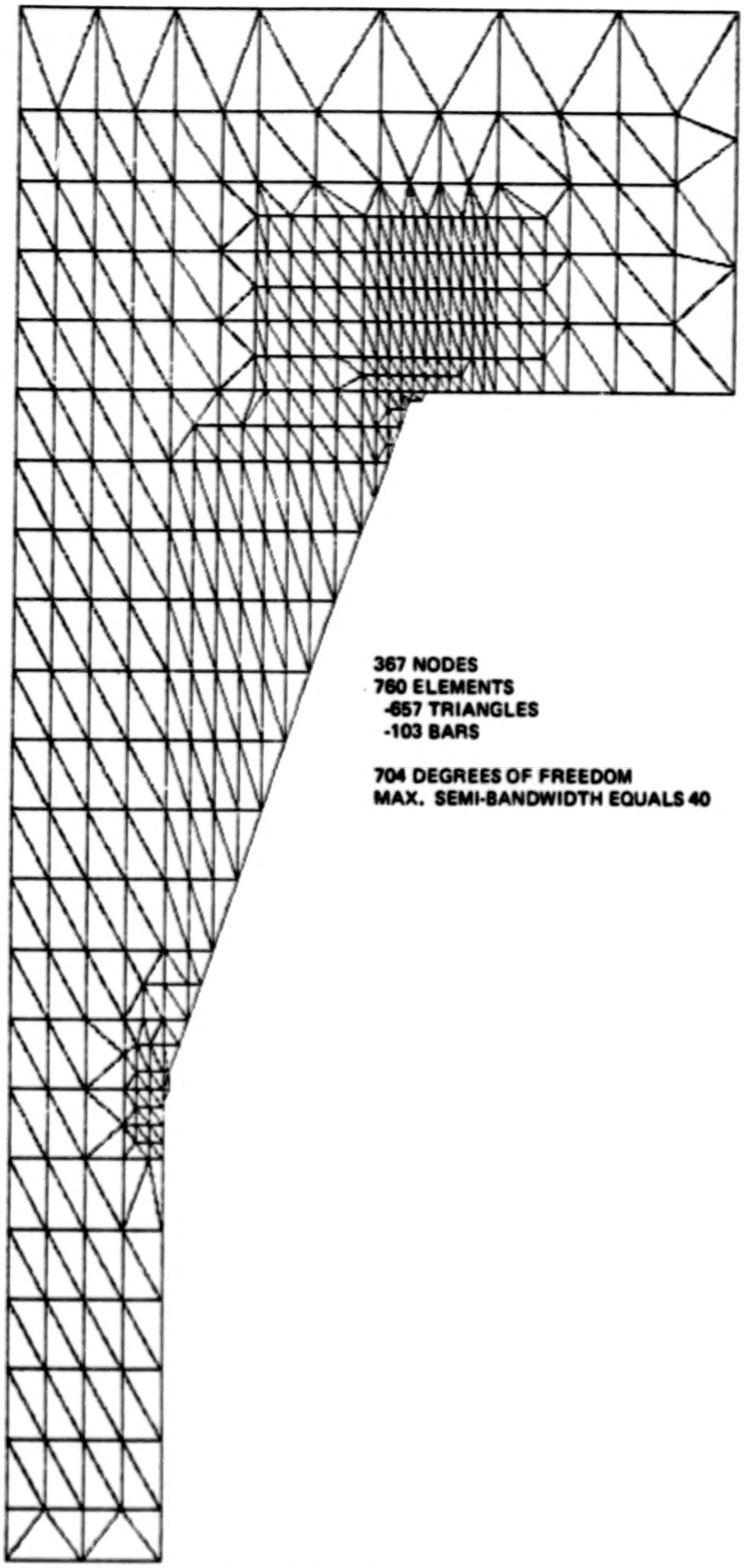

367 NODES
760 ELEMENTS
-657 TRIANGLES
-103 BARS

704 DEGREES OF FREEDOM
MAX. SEMI-BANDWIDTH EQUALS 40

Fig. 2 Finite Element Model of Bracket Detail
- CTRMEM Elements

ORIGINAL PAGE IS
OF POOR QUALITY

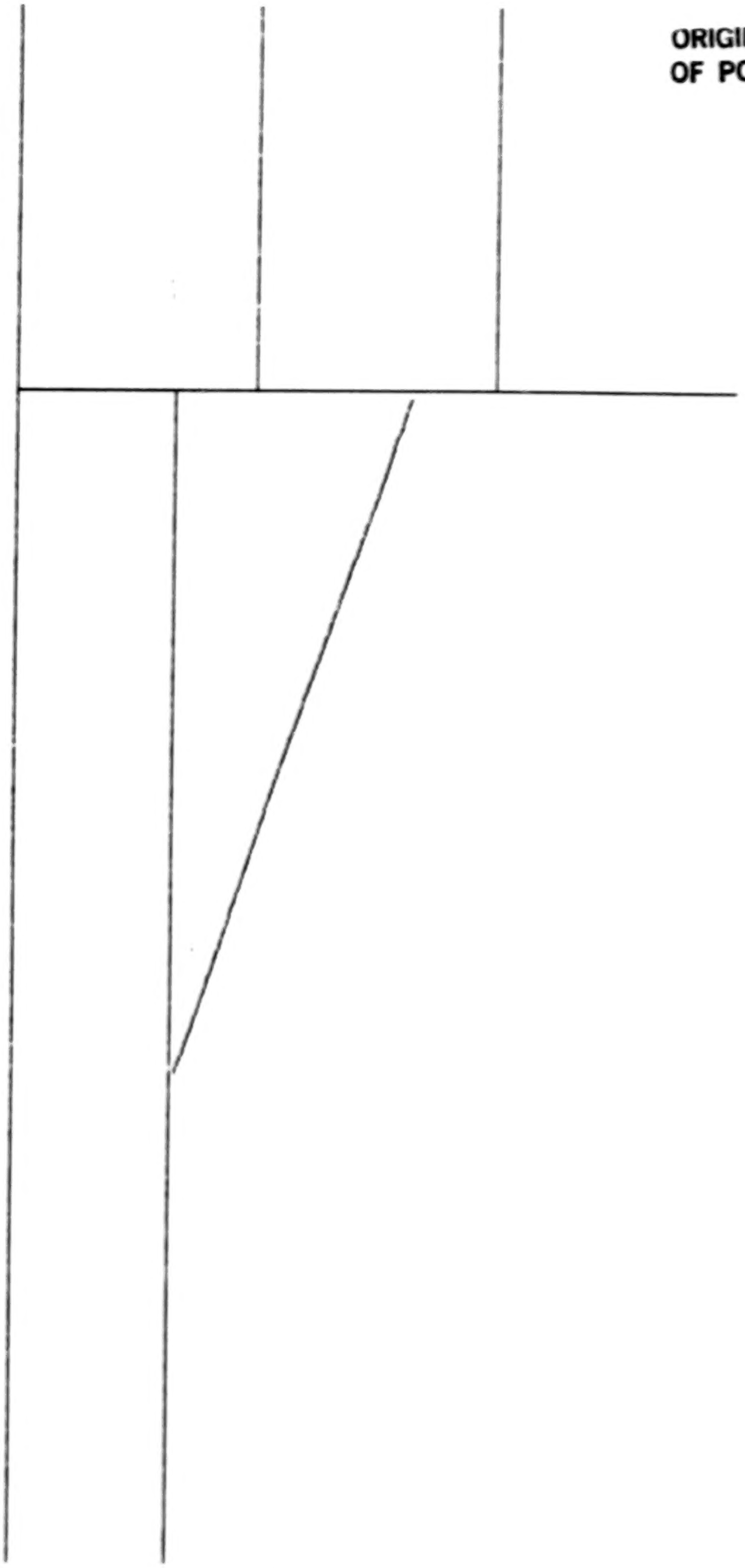

Fig. 3 Finite Element Model of Bracket Detail
- CROD Elements for Flanges

ORIGINAL PAGE IS
OF POOR QUALITY

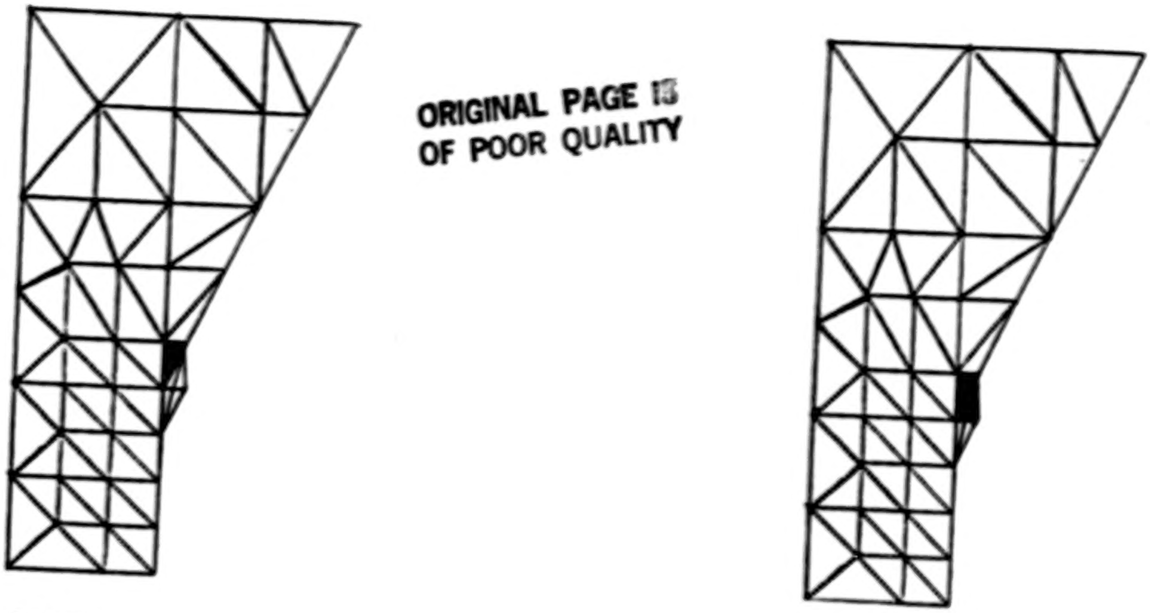

P = .3155
INITIAL YIELD

P = .3375

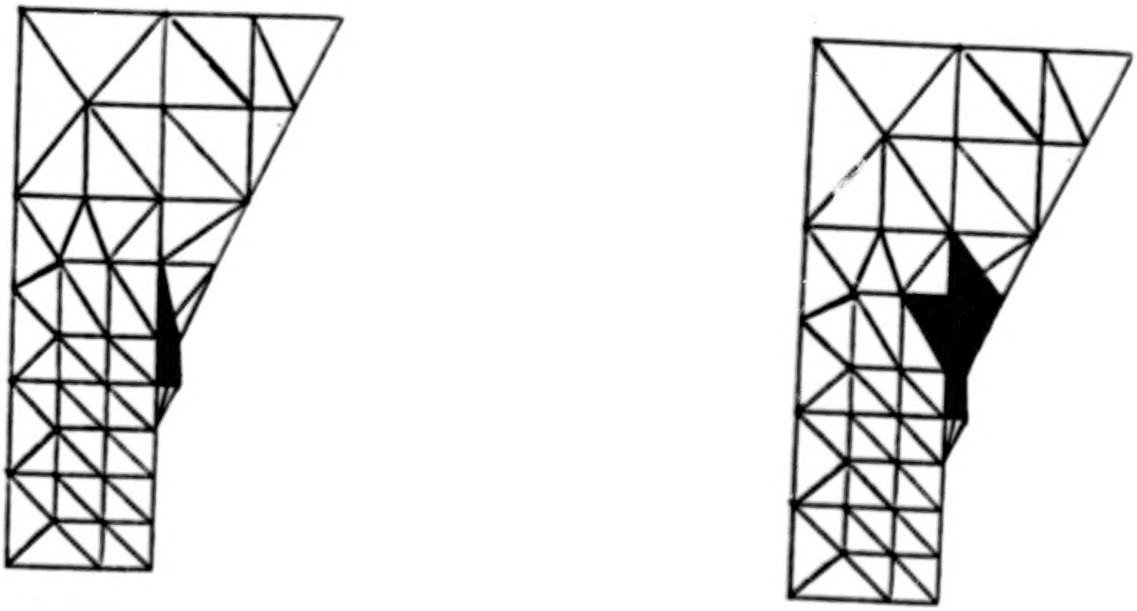

P = .3786

P = .4417
INITIAL PLASTICITY IN FLANGE

Fig. 4 Growth of the Elastic-Plastic Boundary in Region of Largest Stress

APPENDIX A

FLOW DIAGRAM OF MAIN FEATURES OF ELASTO-PLASTIC ANALYSIS

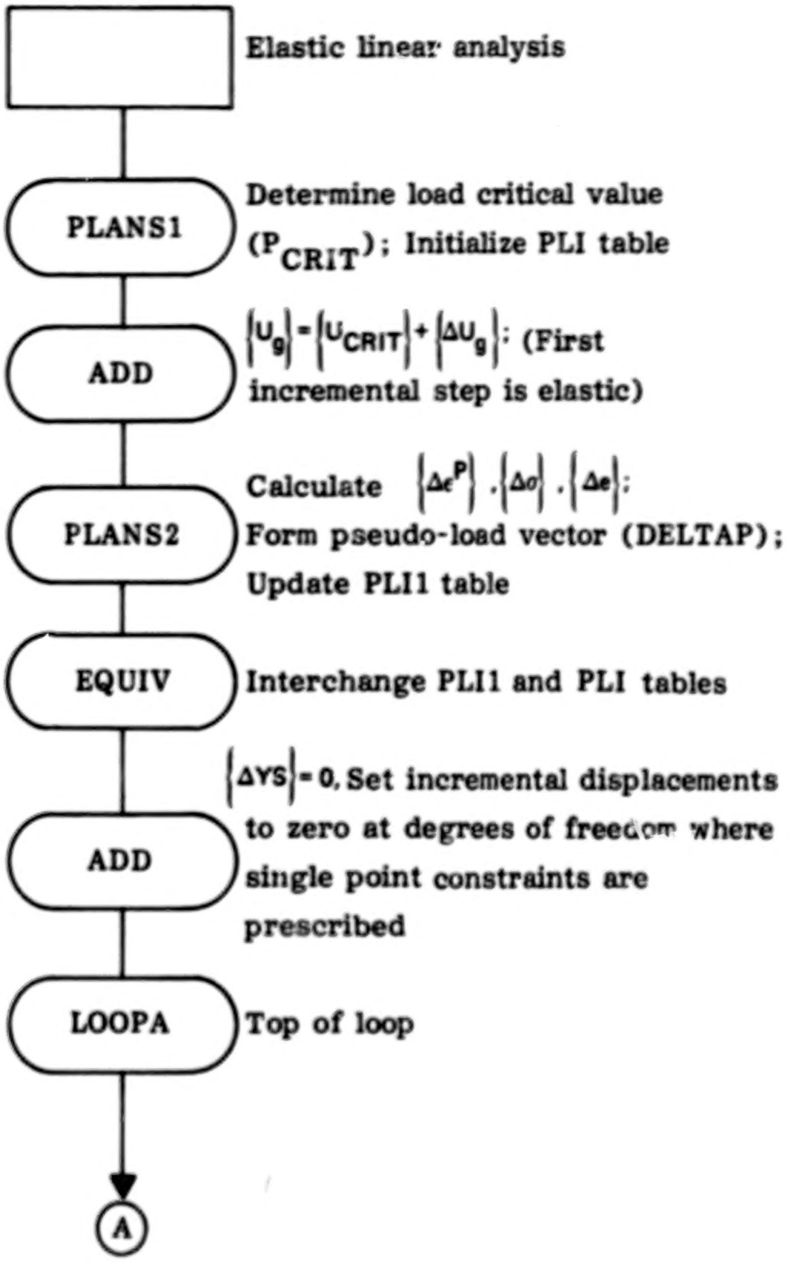

Elastic linear analysis

Determine load critical value (P_{CRIT}); Initialize PLI table

$\{U_g\} = \{U_{CRIT}\} + \{\Delta U_g\}$; (First incremental step is elastic)

Calculate $\{\Delta\epsilon^P\}, \{\Delta\sigma\}, \{\Delta\epsilon\}$; Form pseudo-load vector (DELTAP); Update PLI1 table

Interchange PLI1 and PLI tables

$\{\Delta YS\} = 0$, Set incremental displacements to zero at degrees of freedom where single point constraints are prescribed

Top of loop

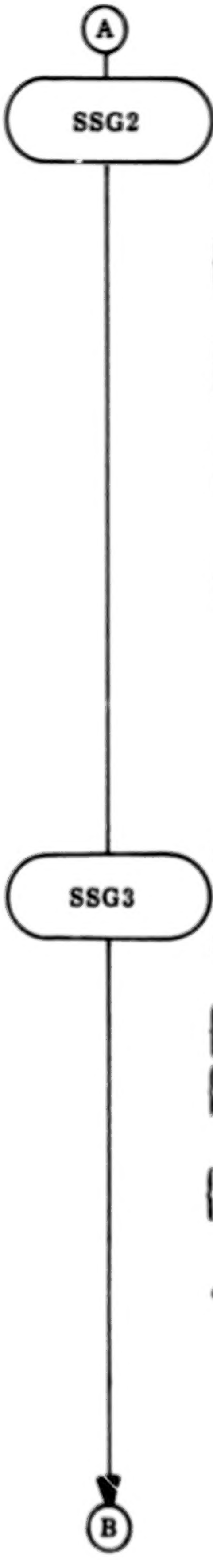

Apply constraints to incremental pseudo-load vector (DELTAP $\equiv \{\Delta P_g\}$).

$$\{\Delta P_g\} = \left\{\frac{\Delta \bar{P}_n}{\Delta P_m}\right\}, \{\Delta P_n\} = \{\Delta \bar{P}_n\} + [G_m]\{\Delta P_m\}$$

$$\{\Delta P_n\} = \left\{\frac{\Delta \bar{P}_f}{\Delta P_s}\right\}, \{\Delta P_f\} = \{\Delta \bar{P}_f\} - [K_{fs}]\{\Delta YS\}$$

$$\{\Delta P_f\} = \left\{\frac{\Delta \bar{P}_a}{\Delta P_o}\right\}, \{\Delta P_a\} = \{\Delta \bar{P}_a\} + [G_o]^T\{\Delta \bar{P}_o\}$$

$$\{\Delta P_a\} = \left\{\frac{\Delta P_l}{\Delta P_r}\right\}$$

Solve for independent degree of freedom displacements due to incremental pseudo-load,

$$\{\Delta U_l\} = [K_{ll}]^{-1}\{\Delta P_l\}$$

$$\{\Delta U_o^o\} = [K_{oo}]^{-1}\{\Delta P_o\}$$

$$\{\delta \Delta P_l\} = \{\Delta P_l\} - [K_{ll}]\{\Delta U_l\}$$

$$\epsilon_l = \frac{\{\Delta U_l\}^T\{\delta \Delta P_l\}}{\{\Delta U_l\}^T\{\Delta P_l\}}$$

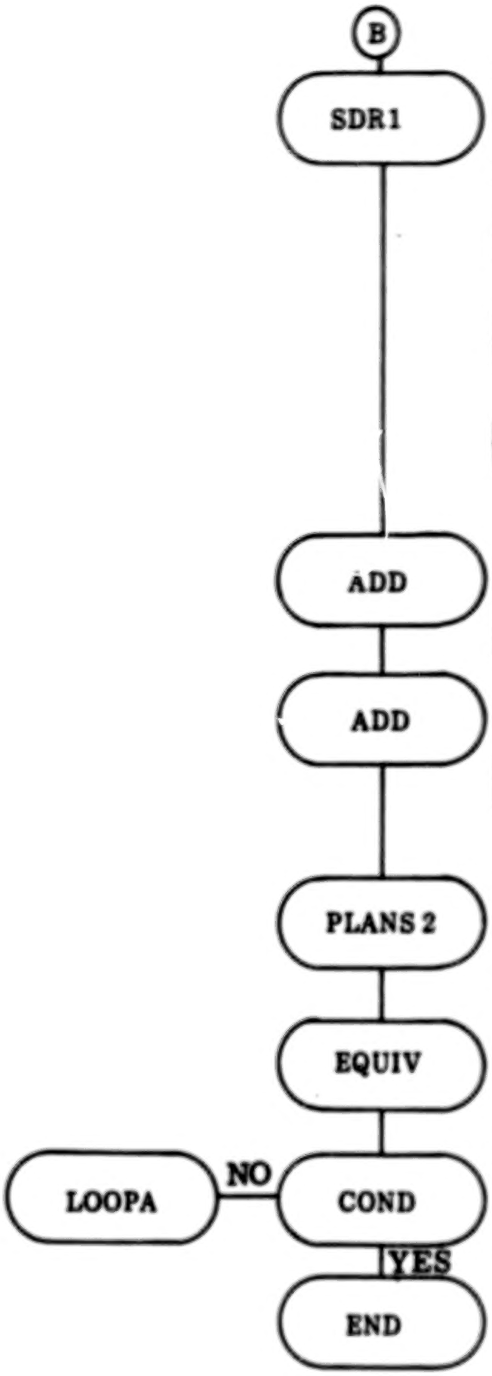

Recover dependent incremental displacements due to incremental pseudo-load,

$$\left\{\frac{\Delta U_l}{\Delta U_r}\right\} = \left\{\Delta U_a\right\}, \left\{\Delta U_o\right\} = [G_o]\left\{\Delta U_a\right\} + \left\{\Delta U_o^o\right\}$$

$$\left\{\frac{\Delta U_a}{\Delta U_o}\right\} = \left\{\Delta U_f\right\}, \left\{\frac{\Delta U_f}{\Delta YS}\right\} = \left\{\Delta U_n\right\}$$

$$\left\{\Delta U_m\right\} = [G_m]\left\{\Delta U_n\right\}, \left\{\frac{\Delta U_n}{\Delta U_m}\right\} = \left\{\Delta U_g\right\}^p$$

Form total incremental load,

$$\left\{\Delta U_g\right\} = \left\{U_{nit}\right\} \cdot \left\{\frac{\Delta P}{P_{unit}}\right\} + \left\{\Delta U_g\right\}^i$$

Update total displacement,

$$\left\{U_g\right\} = \left\{U_g\right\} + \left\{\Delta U_g\right\}$$

Calculate $\left\{\Delta \epsilon^p\right\}, \left\{\Delta \sigma\right\}, \left\{\Delta e\right\}$;
Form pseudo-load vector (DELTAP);
Update PLI1 Table

Interchange PLI1 and PLI tables

Bottom of loop; PLAST <1 ? If YES then last step and end, if NO then not last step and continue

ORIGINAL PAGE IS
OF POOR QUALITY

APPENDIX B1

"ALTERS" TO RIGID FORMAT 1 FOR ELASTO-PLASTIC ANALYSIS

```
ALTER 1,3
BEGIN     $  ELASTIC-PLASTIC ANALYSIS - - DEVELOPED BY GAC FOR NSRDC
ALTER 33,35
ALTER 37,38
ALTER 41,41
ALTER 65,66
ALTER 128,133
ALTER 137,140
PARAM    //C,N,ADD/V,N,PLACOUNT/C,N,1/C,N,0     $
PLANS1   EST,MPT,DIT,UGV/PLI/V,Y,PPCT/V,N,PCRIT     $
SAVE     PPCT,PCRIT     $
CHKPNT   PLI     $
MATPRT   UGV//     $
PARAMR   //C,N,MPY/V,N,DELP/V,Y,PPCT/V,N,PCRIT     $
PARAMR   //C,N,ADD/V,N,P11/V,N,PCRIT/V,N,DELP     $
PARAMR   //C,N,COMPLEX//V,N,P11//V,N,P11C     $
PARAMR   //C,N,COMPLEX//V,N,PCRIT//V,N,PCRITC     $
PARAMR   //C,N,COMPLEX//V,N,DELP//V,N,DELPC     $
PARAMR   //C,N,ADD/V,N,P/V,N,PCRIT//     $
ADD      UGV,/DELTAUGP/V,N,DELPC     $
ADD      UGV,/UGVP/V,N,P11C     $
CHKPNT   DELTAUGP,UGVP     $
PARAM    //C,N,ADD/V,N,PLACOUNT/V,N,PLACOUNT/C,N,1     $
EQUIV    PLI,PLI1/NEVER     $
PLANS2   PLI,MPT,EST,DELTAUGP,DIT/PLI1,DELTAP/V,N,PLACOUNT/V,N,PLAST/
         V,N,PRINTINC/V,N,P/V,N,DELP/V,Y,PMAX     $
SAVE     PLAST,PRINTINC,P     $
EQUIV    PLI1,PLI/ALWAYS     $
CHKPNT   PLI,DELTAP     $
COND     N22,PRINTINC     $
PRTPARM  //C,N,0/C,N,P     $
MATPRT   UGVP//     $
LABEL    N22     $
ADD      YS,/DELTAYS/C,N,(0.0,0.0)     $
CHKPNT   DELTAYS     $
```

```
$
$         TOP OF LOOP
$
LABEL     LOOPA      $
SSG2      USET,GM,DELTAYS,KFS,GO,DM,DELTAP/DELTAQR,DELTAPO,DELTAPS,
          DELTAPL      $
CHKPNT    DELTAQR,DELTAPO,DELTAPS,DELTAPL      $
SSG3      LLL,KLL,DELTAPL,LOO,KOO,DELTAPO/DELTAULV,DELTAUOOV,DRULV,DRUOV/
          V,N,OMIT/V,N,IRES=-1/V,N,NSKIP/V,N,EPSI      $
SAVE      EPSI      $
CHKPNT    DELTAULV,DELTAUOOV,DRULV,DRUOV      $
COND      L22,IRES      $
MATGPR    GPL,USET,SIL,DRULV//C,N,L      $
MATGPR    GPL,USET,SIL,DRUOV//C,N,O      $
LABEL     L22      $
SDR1      USET,DELTAP,DELTAULV,DELTAUOOV,DELTAYS,GO,GM,DELTAPS,KFS,KSS,
          DELTAQR/DELTAUGV,DELTAPLG,/C,N,1/C,N,STATICS      $
CHKPNT    DELTAUGV,DELTAPLG      $
ADD       UGV,DELTAUGV/DELTAUGT/V,N,DELPC      $
ADD       DELTAUGT,UGVP/UGVPT/      $
EQUIV     UGVPT,UGVP/ALWAYS      $
CHKPNT    UGVP      $
PARAM     //C,N,ADD/V,N,PLACOUNT/V,N,PLACOUNT/C,N,1      $
EQUIV     PLI,PLI1/NEVER      $
PLANS2    PLI,MPT,EST,DELTAUGT,DIT/PLI1,DELTAP/V,N,PLACOUNT/V,N,PLAST/
          V,N,PRINTINC/V,N,P/V,N,DELP/V,Y,PMAX      $
SAVE      PLAST,PRINTINC,P      $
EQUIV     PLI1,PLI/ALWAYS      $
CHKPNT    PLI,DELTAP      $
COND      N21,PRINTINC      $
PRTPARM   //C,N,0/C,N,P      $
MATPRN    UGVP//      $
LABEL     N21      $
COND      LOOPED,PLAST      $
REPT      LOOPA,20   $
$
$         BOTTOM OF LOOP
$
LABEL     LOOPED      $
ALTER 141,164
ALTER 166,167
ALTER 174,175
ENDALTER
```

ORIGINAL PAGE IS
OF POOR QUALITY

APPENDIX B2

"ALTERED" RIGID FORMAT FOR ELASTO-PLASTIC ANALYSIS

```
LEVEL 2.0 NASTRAN DMAP COMPILER - SOURCE LISTING


  3  BEGIN      $  ELASTIC-PLASTIC ANALYSIS - - DEVELOPED BY GAC FOR NSRDC

  4  GP1        GEOM1,GEOM2,/GPL,EQEXIN,GPDT,CSTM,BGPDT,SIL/V,N,LUSET/  V,N,
                NOGPDT/V,N,ALWAYS=-1 $

  5  SAVE       LUSET $

  6  CHKPNT     GPL,EQEXIN,GPDT,CSTM,BGPDT,SIL $

  7  GP2        GEOM2,EQEXIN/ECT $

  8  CHKPNT     ECT $

  9  PARAML     PCDB//C,N,PRES/C,N,/C,N,/C,N,/V,N,NOPCDB $

 10  PURGE      PLTSETX,PLTPAR,GPSETS,ELSETS/NOPCDB $

 11  COND       P1,NOPCDB $

 12  PLTSET     PCDB,EQEXIN,ECT/PLTSETX,PLTPAR,GPSETS,ELSETS/V,N,NSIL/   V,N,
                JUMPPLOT=-1 $

 13  SAVE       NSIL,JUMPPLOT $

 14  PRTMSG     PLTSETX// $

 15  PARAM      //C,N,MPY/V,N,PLTFLG/C,N,1/C,N,1 $

 16  PARAM      //C,N,MPY/V,N,PFILE/C,N,0/C,N,0 $

 17  COND       P1,JUMPPLOT $

 18  PLOT       PLTPAR,GPSETS,ELSETS,CASECC,BGPDT,EQEXIN,SIL,,ECT,,/PLOTX1/V,N,
                NSIL/V,N,LUSET/V,N,JUMPPLOT/V,N,PLTFLG/V,N,PFILE $

 19  SAVE       JUMPPLOT,PLTFLG,PFILE $

 20  PRTMSG     PLOTX1// $

 21  LABEL      P1 $

 22  CHKPNT     PLTPAR,GPSETS,ELSETS $

 23  GP3        GEOM3,EQEXIN,GEOM2/SLT,GPTT/V,N,NOGRAV/V,N,NEVER=1 $

 24  SAVE       NOGRAV $
```

```
LEVEL 2.0 NASTRAN DMAP COMPILER - SOURCE LISTING

 25  PARAM    //C,N,AND/V,N,NOMGG/V,N,NOGRAV/V,Y,GRDPNT=-1 $
 26  CHKPNT   SLT,GPTT $
 27  TA1      ECT,EPT,BGPDT,SIL,GPTT,CSTM/EST,GEI,GPECT,/V,N,LUSET/   V,N,
              NOSIMP/C,N,1/V,N,NOGENL/V,N,GENEL $
 28  SAVE     NOSIMP,NOGENL,GENEL $
 29  PARAM    //C,N,AND/V,N,NOELMT/V,N,NOGENL/V,N,NOSIMP $
 30  COND     ERROR4,NOELMT $
 31  PURGE    KGGX,GPST/NOSIMP/OGPST/GENEL $
 32  CHKPNT   EST,GPECT,GEI,GPST,OGPST $
 36  PARAM    //C,N,MPY/V,N,CARDNO/C,N,0/C,N,0 $
 39  COND     LBL1,NOSIMP $
 40  PARAM    //C,N,ADD/V,N,NOKGGX/C,N,1/C,N,0 $
 42  EMG      EST,CSTM,MPT,DIT,GEOM2,/KELM,KDICT,MELM,MDICT,,/V,N,NOKGGX/ V,
              N,NOMGG/C,N,/C,N,/C,N,/C,Y,COUPMASS/C,Y,CPBAR/C,Y,CPROD/C,Y,
              CPQUAD1/C,Y,CPQUAD2/C,Y,CPTRIA1/C,Y,CPTRIA2/  C,Y,CPTUBE/C,Y,
              CPQDPLT/C,Y,CPTRPLT/C,Y,CPTRBSC $
 43  SAVE     NOKGGX,NOMGG $
 44  CHKPNT   KELM,KDICT,MELM,MDICT $
 45  COND     JMPKGG,NOKGGX $
 46  EMA      GPECT,KDICT,KELM/KGGX,GPST $
 47  CHKPNT   KGGX,GPST $
 48  LABEL    JMPKGG $
 49  COND     JMPMGG,NOMGG $
 50  EMA      GPECT,MDICT,MELM/MGG,/C,N,-1/C,Y,WTMASS=1.0 $
 51  CHKPNT   MGG $
 52  LABEL    JMPMGG $
 53  COND     LBL1,GRDPNT $
```

C-4

```
LEVEL 2.0 NASTRAN DMAP COMPILER - SOURCE LISTING

54  COND      ERROR2,NOMGG $
55  GPWG      BGPDT,CSTM,EQEXIN,MGG/OGPWG/V,Y,GRDPNT/C,Y,WTMASS $
56  OFP       OGPWG,,,,,// $
57  LABEL     LBL1 $
58  EQUIV     KGGX,KGG/NOGENL $
59  CHKPNT    KGG $
60  COND      LBL11A,NOGENL $
61  SMA3      GEI,KGGX/KGG/V,N,LUSET/V,N,NOGENL/V,N,NOSIMP $
62  CHKPNT    KGG $
63  LABEL     LBL11A $
64  PARAM     //C,N,MPY/V,N,NSKIP/C,N,0/C,N,0 $
67  GP4       CASECC,GEOM4,EQEXIN,GPDT,BGPDT,CSTM/RG,YS,USET,ASET/V,N,LUSET/
              V,N,MPCF1/V,N,MPCF2/V,N,SINGLE/V,N,OMIT/V,N,REACT/V,N,NSKIP/V,
              N,REPEAT/V,N,NOSET/V,N,NOL/V,N,NOA/C,Y,SUBID $
68  SAVE      MPCF1,MPCF2,SINGLE,OMIT,REACT,NSKIP,REPEAT,NOSET,NOL,NOA $
69  COND      ERROR3,NOL $
70  PARAM     //C,N,AND/V,N,NOSR/V,N,SINGLE/V,N,REACT $
71  PURGE     KRR,KLR,QR,DM/REACT/GM/MPCF1/GO,KOO,LOO,PO,UOOV,RUOV/OMIT/PS,
              KFS,KSS/SINGLE/QG/NOSR $
72  CHKPNT    KRR,KLR,QR,DM,GM,GO,KOO,LOO,PO,UOOV,RUOV,PS,KFS,KSS,QG,USET,RG,
              YS,ASET $
73  COND      LBL4,GENEL $
74  GPSP      GPL,GPST,USET,SIL/OGPST/V,N,NOGPST $
75  SAVE      NOGPST $
76  COND      LBL4,NOGPST $
77  OFP       OGPST,,,,,// $
78  LABEL     LBL4 $
```

ORIGINAL PAGE IS
OF POOR QUALITY

```
        LEVEL 2.0 NASTRAN DMAP COMPILER - SOURCE LISTING

   79  EQUIV    KGG,KNN/MPCF1 $
   80  CHKPNT   KNN $
   81  COND     LBL2,MPCF2 $
   82  MCE1     USET,RG/GM $
   83  CHKPNT   GM $
   84  MCE2     USET,GM,KGG,,,/KNN,,, $
   85  CHKPNT   KNN $
   86  LABEL    LBL2 $
   87  EQUIV    KNN,KFF/SINGLE $
   88  CHKPNT   KFF $
   89  COND     LBL3,SINGLE $
   90  SCE1     USET,KNN,,,/KFF,KFS,KSS,,, $
   91  CHKPNT   KFS,KSS,KFF $
   92  LABEL    LBL3 $
   93  EQUIV    KFF,KAA/OMIT $
   94  CHKPNT   KAA $
   95  COND     LBL5,OMIT $
   96  SMP1     USET,KFF,,,/GO,KAA,KOO,LOO,,,,, $
   97  CHKPNT   GO,KAA,KOO,LOO $
   98  LABEL    LBL5 $
   99  EQUIV    KAA,KLL/REACT $
  100  CHKPNT   KLL $
  101  COND     LBL6,REACT $
  102  RBMG1    USET,KAA,/KLL,KLR,KRR,,, $
  103  CHKPNT   KLL,KLR,KRR $
```

ORIGINAL PAGE IS
OF POOR QUALITY

```
     LEVEL 2.0 NASTRAN DMAP COMPILER - SOURCE LISTING

104  LABEL     LBL6 $
105  RBMG2     KLL/LLL $
106  CHKPNT    LLL $
107  COND      LBL7,REACT $
108  RBMG3     LLL,KLR,KRR/DM $
109  CHKPNT    DM $
110  LABEL     LBL7 $
111  SSG1      SLT,BGPDT,CSTM,SIL,EST,MPT,GPTT,EDT,MGG,CASECC,DIT/PG/V,N,
               LUSET/V,N,NSKIP $
112  CHKPNT    PG $
113  EQUIV     PG,PL/NOSET $
114  CHKPNT    PL $
115  COND      LBL10,NOSET $
116  SSG2      USET,GM,YS,KFS,GO,DM,PG/QR,PO,PS,PL $
117  CHKPNT    QR,PO,PS,PL $
118  LABEL     LBL10 $
119  SSG3      LLL,KLL,PL,LOO,KOO,PO/ULV,UOOV,RULV,RUOV/V,N,OMIT/V,Y,IRES=-1/
               V,N,NSKIP/V,N,EPSI $
120  SAVE      EPSI $
121  CHKPNT    ULV,UOOV,RULV,RUOV $
122  COND      LBL9,IRES $
123  MATGPR    GPL,USET,SIL,RULV//C,N,L $
124  MATGPR    GPL,USET,SIL,RUOV//C,N,O $
125  LABEL     LBL9 $
126  SDR1      USET,PG,ULV,UOOV,YS,GO,GM,PS,KFS,KSS,QR/UGV,PGG,QG/V,N,NSKIP/
               C,N,STATICS $
127  CHKPNT    UGV,PGG,QG $
```

```
LEVEL 2.0 NASTRAN DMAP COMPILER - SOURCE LISTING

134  CHKPNT    CSTM $
135  GPFDR     CASECC,UGV,KELM,KDICT,ECT,EQEXIN,GPECT,PGG,QG/ONRGY1,OGPFB1/
               C,N,STATICS $
136  OFP       ONRGY1,OGPFB1,,,,// $
140  PARAM     //C,N,ADD/V,N,PLACOUNT/C,N,1/C,N,0      $
140  PLANS1    EST,MPT,DIT,UGV/PLI/V,Y,PPCT/V,N,PCRIT      $
140  SAVE      PPCT,PCRIT      $
140  CHKPNT    PLI      $
140  MATPRT    UGV//      $
140  PARAMR    //C,N,MPY/V,N,DELP/V,Y,PPCT/V,N,PCRIT      $
140  PARAMR    //C,N,ADD/V,N,P11/V,N,PCRIT/V,N,DELP      $
140  PARAMR    //C,N,COMPLEX//V,N,P11//V,N,P11C      $
140  PARAMR    //C,N,COMPLEX//V,N,PCRIT//V,N,PCRITC      $
140  PARAMR    //C,N,COMPLEX//V,N,DELP//V,N,DELPC      $
140  PARAMR    //C,N,ADD/V,N,P/V,N,PCRIT//      $
140  ADD       UGV,/DELTAUGP/V,N,DELPC      $
140  ADD       UGV,/UGVP/V,N,P11C      $
140  CHKPNT    DELTAUGP,UGVP      $
140  PARAM     //C,N,ADD/V,N,PLACOUNT/V,N,PLACOUNT/C,N,1      $
140  EQUIV     PLI,PLI1/NEVER      $
140  PLANS2    PLI,MPT,EST,DELTAUGP,DIT/PLI1,DELTAP/V,N,PLACOUNT/V,N,PLAST/
               V,N,PRINTINC/V,N,P/V,N,DELP/V,Y,PMAX      $
140  SAVE      PLAST,PRINTINC,P      $
140  EQUIV     PLI1,PLI/ALWAYS      $
140  CHKPNT    PLI,DELTAP      $
140  COND      N22,PRINTINC      $
```

```
     LEVEL 2.0 NASTRAN DMAP COMPILER - SOURCE LISTING

140  PRTPARM   //C,N,0/C,N,P      $
140  MATPRT    UGVP//      $
140  LABEL     N22      $
140  ADD       YS,/DELTAYS/C,N,(0.0,0.0)      $
140  CHKPNT    DELTAYS      $
140  LABEL     LOOPA      $
140  SSG2      USET,GM,DELTAYS,KFS,GO,DM,DELTAP/DELTAQR,DELTAPO,DELTAPS,
               DELTAPL      $
140  CHKPNT    DELTAQR,DELTAPO,DELTAPS,DELTAPL      $
140  SSG3      LLL,KLL,DELTAPL,LOO,KOO,DELTAPO/DELTAULV,DELTAUOOV,DRULV,DRUOV/
               V,N,OMIT/V,N,IRES=-1/V,N,NSKIP/V,N,EPSI      $
140  SAVE      EPSI      $
140  CHKPNT    DELTAULV,DELTAUOOV,DRULV,DRUOV      $
140  COND      L22,IRES      $
140  MATGPR    GPL,USET,SIL,DRULV//C,N,L      $
140  MATGPR    GPL,USET,SIL,DRUOV//C,N,O      $
140  LABEL     L22      $
140  SDR1      USET,DELTAP,DELTAULV,DELTAUOOV,DELTAYS,GO,GM,DELTAPS,KFS,KSS,
               DELTAQR/DELTAUGV,DELTAPLG,/C,N,1/C,N,STATICS      $
140  CHKPNT    DELTAUGV,DELTAPLG      $
140  ADD       UGV,DELTAUGV/DELTAUGT/V,N,DELPC      $
140  ADD       DELTAUGT,UGVP/UGVPT/      $
140  EQUIV     UGVPT,UGVP/ALWAYS      $
140  CHKPNT    UGVP      $
140  PARAM     //C,N,ADD/V,N,PLACOUNT/V,N,PLACOUNT/C,N,1      $
```

ORIGINAL PAGE IS
OF POOR QUALITY

```
    LEVEL 2.0 NASTRAN DMAP COMPILER - SOURCE LISTING

140  EQUIV     PLT,PLT1/NEVER      $
140  PLANS2    PLT,MPT,EST,DELTAUGT,DIT/PLT1,DELTAP/V,N,PLACOUNT/V,N,PLAST/
               V,N,PRINTINC/V,N,P/V,N,DELP/V,Y,PMAX      $
140  SAVE      PLAST,PRINTINC,P      $
140  EQUIV     PLT1,PLT/ALWAYS      $
140  CHKPNT    PLT,DELTAP      $
140  COND      N21,PRINTINC      $
140  PRTPARM   //C,N,0/C,N,P      $
140  MATPRT    UGVP//      $
140  LABEL     N21      $
140  COND      LOOPED,PLAST      $
140  REPT      LOOPA,20  $
140  LABEL     LOOPED      $
165  JUMP      FINIS $
168  LABEL     ERROR2 $
169  PRTPARM   //C,N,-2/C,N,STATICS $
170  LABEL     ERROR3 $
171  PRTPARM   //C,N,-3/C,N,STATICS $
172  LABEL     ERROR4 $
173  PRTPARM   //C,N,-4/C,N,STATICS $
176  LABEL     FINIS $
177  END       $
```

NEW BULK DATA CARDS

MATS2: Material Properties - defines stress-strain function for either Ramberg-Osgood representation, linear strain hardening or perfect plasticity.

	1	2	3	4	5	6	7	8
			TABLEY1	TABLES1	n	$\sigma_{0.7}$	α	
Ramberg-Osgood	MATS2	17			12	0.6+5		
Linear Hardening	MATS2	17					0.25	
Perfect Plasticity	MATS2	17					0.0	
Tabular	MATS2	17		100				

Field **Contents**

MID - Material identification number which matches the identification number on some basic MAT1 card (Integer > 0)

n - shape parameter used in Ramberg-Osgood stress-strain function (Integer)

α - E_T/E for linear strain hardening (Real)

$\sigma_{0.7}$ - Ramberg-Osgood parameter (Real)

TABLES1- Table number for Stress-strain function - TABLES1 Table (Integer)

TABLEY1- Table number for yield stress vs. accumulated plastic strain, for near linear strain hardening (Integer)

Remarks: 1. Ramberg-Osgood representation: $\epsilon = \frac{\sigma}{E} + \frac{3\sigma}{7E}\left(\frac{\sigma}{\sigma_{0.7}}\right)^{n-1}$

2. TABLEY1 may be used with any of the options listed.

PLFAC2: Load history and step size information

1	2	3	4	5	6	7	8	9	10
PLFAC2	SID	P1	N1	NLD1	P2	N2	NLD2	☒	+abc
PLFAC2	5	1.0	5	1	2.0	10	1		ABC
+abc	☒	P3	N3	NLD3	-etc-			☒	
+BC		3.0	5	2					

Field Contents

SID - Set identification number (Integer > 0)

Pi - Load magnitude (Real)

Ni - Number of increments for current load (Integer ≥ 0)

NLDi - Load set reference (Integer)

Remarks:

1. Load history is contained with PLFAC2. Each Pi corresponds to total load for that set (NLDi).

2. One or Two sets of data may be included on each card. Fields 3, 4, and 5 must be used on each card, but fields 6, 7, and 8 may be omitted from any card even though continuation cards follow.

3. If Ni = 0, incrementation steps will be chosen automatically.

TABLEY1: Yield stress vs. accumulated plastic strain

1	2	3	4	5	6	7	8	9	10
TABLEY1	SID	σ_{yt}	σ_{ys}	$\Sigma\epsilon^P$	σ_{yt}	σ_{ys}	$\Sigma\epsilon^P$	☒	+abc
TABLEY1	10								ABC

+abc	☒	σ_{yt}	σ_{ys}	$\Sigma\epsilon^P$	-etc-			☒	
+BC									

Field	Contents
SID	- set identification number (Integer > 0)
σ_{yt}	- yield stress in tension (Real)
σ_{ys}	- yield stress in shear (Real)
$\Sigma\epsilon^P$	- accumulated plastic strain (Real)

Remarks:

1. If accumulated plastic strain is less than first value in table then first values of σ_{yt} and σ_{ys} are chosen, if accumulated plastic strain is greater than last value in table than last values of σ_{yt} and σ_{ys} are chosen, otherwise a linear interpolation is used.
2. One or two sets of data may be included on each card. Fields 3, 4, and 5 must be used on each card, but fields 6, 7, and 8 may be omitted from any card even though continuation cards follow.

N84
15607

UNCLAS

N84 15607 D17

ELASTIC-PLASTIC ANALYSIS OF ANNULAR PLATE PROBLEMS USING NASTRAN

P. C. T. Chen
U.S. Army Armament Research and Development Command
Large Caliber Weapon Systems Laboratory
Benet Weapons Laboratory
Watervliet, NY 12189

SUMMARY

The plate elements of the NASTRAN code are used to analyze two annular plate problems loaded beyond the elastic limit. The first problem is an elastic-plastic annular plate loaded externally by two concentrated forces. The second problem is stressed radially by uniform internal pressure for which an exact analytical solution is available. A comparison of the two approaches together with an assessment of the NASTRAN code is given.

INTRODUCTION

The piecewise linear analysis option of the NASTRAN code can be used to analyze quite complicated elastic-plastic plane-stress problems (refs. 1 and 2). The reliability of this code has been well demonstrated in the linear range but not so in the nonlinear range of loadings. One major reason is because exact analytical solutions for elastic-plastic problems are usually not available for comparison with approximate NASTRAN solutions.

In this paper, the plate elements of the NASTRAN code are used to solve two annular plate problems loaded beyond the elastic limit. The first problem considered is an elastic-plastic annular plate loaded externally by two concentrated forces. There is no analytical solution for this two-dimensional plane-stress problem and the NASTRAN code is used to obtain numerical results. The second problem considered is an elastic-plastic annular plate radially stressed by uniform internal pressure. This problem is chosen because an exact analytical solution is available for comparison. For ideally plastic materials, the stress solution for this statically determinate problem was first obtained by Mises (ref. 3) and the corresponding two strain solutions were obtained by the present author on the basis of both J_2 deformation and flow theories (ref. 4). For elastic-plastic strain-hardening materials, an exact complete solution was recently reported in reference 5. Analytical expressions were derived on the basis of J_2 deformation theory, the Hill's yield criterion, and a modified Ramberg-Osgood law. The validity of the above solution has been established by satisfying the Budiansky's criterion.

In the following, the theory of elastic-plastic plate elements as used in NASTRAN is briefly reviewed. In its present form, NASTRAN cannot be used for problems involving ideally plastic materials. It is shown that this limitation can be easily removed by making minor changes. For an elastic-plastic strain-hardening material, the NASTRAN solution is reported here and compared with the exact solution. The results are presented graphically and an assessment of the NASTRAN code is made.

PLASTIC PLATE ELEMENTS

The theoretical basis of two-dimensional plastic deformation as used in NASTRAN is that developed by Swedlow (ref. 6). In the development, a unique relationship between the octahedral stress, τ_o, and the plastic octahedral strain, $\epsilon_o{}^P$, is assumed to exist and the use of ideally plastic materials is excluded. The total strain components (ϵ_x, ϵ_y, ϵ_z, and γ_{xy}) are composed of the elastic, recoverable deformations and the plastic portions ($\epsilon_x{}^P$, $\epsilon_y{}^P$, $\epsilon_z{}^P$, and $\gamma_{xy}{}^P$). The rates of plastic flow, ($\dot{\epsilon}_x{}^P$, etc.), are independent of a time scale and are simply used for convenience instead of incremental values. The definitions of the octahedral stress and the octahedral plastic strain rate for isotropic materials are:

$$\tau_o = \sqrt{(s_{11}{}^2 + 2s_{12}{}^2 + s_{22}{}^2 + s_{33}{}^2)/3} \tag{1}$$

$$\dot{\epsilon}_o{}^P = \sqrt{[(\dot{\epsilon}_{11}{}^P)^2 + 2(\dot{\epsilon}_{12}{}^P)^2 + (\dot{\epsilon}_{22}{}^P)^2 + (\dot{\epsilon}_{33}{}^P)^2]/3} \tag{2}$$

where

$$s_{11} = \frac{1}{3}(2\sigma_x - \sigma_y) \quad , \quad \epsilon_{11}{}^P = \epsilon_x{}^P$$

$$s_{22} = \frac{1}{3}(2\sigma_y - \sigma_x) \quad , \quad \epsilon_{22}{}^P = \epsilon_y{}^P$$

$$s_{33} = -\frac{1}{3}(\sigma_x + \sigma_y) \quad , \quad \epsilon_{33}{}^P = \epsilon_z{}^P$$

$$s_{12} = T_{xy} \quad , \quad \epsilon_{12}{}^P = -\gamma_{xy}{}^P \tag{3}$$

The s_{ij} is called the deviator of the stress tensor; σ_x, σ_y, and T_{xy} are the cartesian stresses. The isotropic material is assumed to obey the Mises yield criterion and the Prandtl-Reuss flow rule. The matrix relationship for the plastic flow is:

$$\begin{Bmatrix} \dot{\epsilon}_x{}^P \\ \dot{\epsilon}_y{}^P \\ \dot{\gamma}_{xy}{}^P \end{Bmatrix} = \frac{1}{6\tau_o{}^2 M_T(\tau_o)} \begin{bmatrix} s_{11}{}^2 & s_{11}s_{22} & 2s_{11}s_{12} \\ s_{11}s_{22} & s_{22}{}^2 & 2s_{22}s_{12} \\ 2s_{11}s_{22} & 2s_{11}s_{12} & 4s_{12}{}^2 \end{bmatrix} \begin{Bmatrix} \dot{\sigma}_x \\ \dot{\sigma}_y \\ \dot{T}_{xy} \end{Bmatrix} \tag{4}$$

where

$$2M_T(\tau_o) = \dot{\tau}_o / \dot{\epsilon}_o{}^P \tag{5}$$

The plastic modulus, $M_T(\tau_o)$, can be related to the slope E_T, of the effective stress-strain curve by:

$$\frac{1}{3M_T(\tau_o)} = \frac{1}{E_T} - \frac{1}{E} \tag{6}$$

The total strain increments, obtained by adding the plastic and linear elastic parts, are:

$$\{\Delta\epsilon\} = ([D^P] + [G]^{-1})\{\Delta\sigma\} = [G_p]^{-1}\{\Delta\sigma\} \tag{7}$$

where [G] is the normal elastic material matrix and $[G_p]$ is the equivalent plastic material matrix. The matrices $[D^F]$ and $[G_p]^{-1}$ exist for finite values of M_T or (E_T) and $[G_p]$ can be obtained numerically. Because this procedure is chosen in developing NASTRAN program, only strain hardening materials can be considered for applications. However, it should be noted that even the matrix $[G_p]^{-1}$ does not exist when M_T or E_T is equal to zero, the matrix $[G_p]$ may still exist. In fact, the closed form of $[G_p]$ has been given in reference 7. We can express this as:

$$[G_p] = \frac{E}{Q} \begin{bmatrix} s_{22}^2+2A & & \text{SYM.} \\ -s_{11}\,s_{22}+2\nu A \;, & s_{11}^2+2A & \\ -\dfrac{s_{11}+\nu s_{22}}{1+\nu}\,s_{12} \;, & -\dfrac{s_{22}+\nu s_{11}}{1+\nu}\,s_{12} \;, & \dfrac{B}{2(1+\nu)} + \dfrac{(1-\nu)E_T}{E-E_T}\,\tau_o^2 \end{bmatrix} \tag{8}$$

where

$$A = \frac{E_T}{E-E_T}\,\tau_o^2 + \frac{s_{12}^2}{1+\nu} \;, \quad B = s_{11}^2 + 2\nu s_{11}\,s_{22} + s_{22}^2 \;, \quad Q = 2(1-\nu^2)A + B \,. \tag{9}$$

If we want to remove the limitation that the use of ideally plastic materials is excluded, we have to make minor changes in subroutines PSTRM and PKTRM of the NASTRAN program.

TWO-DIMENSIONAL PROGRAM

Consider a two-dimensional annular plate loaded externally by two concentrated forces. Figure 1 shows a finite element representation for one quarter of the annular plate. The other part is not needed because of symmetry. There are 198 grids and 170 quadrilateral elements in this model. The grids (1 through 11) along the x-axis are constrained in y-direction while those grids (188 through 198) along the y-axis are constrained in the x-direction. The concentrated force F is applied at the top of the y-axis (grid 198). The thickness of the plate is 0.1 inch. All membrane elements are stress dependent materials. The effective stress-strain curve is defined by:

$$\begin{aligned} \sigma &= E\varepsilon \quad \text{for} \quad \sigma < \sigma_o \\ (\sigma/\sigma_o)^n &= (E/\sigma_o)\varepsilon \quad \text{for} \quad \sigma > \sigma_o \end{aligned} \tag{10}$$

where

$$\sigma = (3/\sqrt{2})\tau_o \quad , \quad \varepsilon = \sigma/E + \sqrt{2}\,\varepsilon_p \tag{11}$$

n is the strain hardening parameter and the initial yield surface is defined by the ellipse $\sigma = \sigma_o$. The input parameters for the problem are:

$E = 10.5 \times 10^6$ psi , $\nu = 0.3$ (Poisson's ratio) , $\sigma_o = 5.5 \times 10^4$ psi , $n = 9$.

There is no analytical solution for the two-dimensional plane-stress problem and the NASTRAN code is used to obtain numerical results. First the stress solution in the elastic loading range is obtained and the elastic limit is determined. The corresponding F^* at initial yielding is 753.34 pounds. Then the solution beyond the elastic limit is obtained in 13 steps with the applied force given by $F_n = 753.36$ (0.95 +

0.05n) pounds for n = 1,2,...13. The vertical displacement at the point of application (V_D) and the horizontal displacement (U_B) at point B (grid 11) are shown in figure 2 as functions of the applied force F. The major principal stresses in elements near the x and y-axes are shown in figure 3 for F = 600 and 1205.38 pounds, respectively. The results indicate that the maximum tensile stress occurs at point C.

ONE-DIMENSIONAL PROBLEM

Consider a one-dimensional annular plate stressed radially by uniform internal pressure. The plate geometry and material properties are the same as the two-dimensional one. Utilizing the condition of axial symmetry, we need only a sector of the annular plate for the finite element model. There are only 10 elements with 22 grids. All grid points are constrained in the tangential direction. The applied load is the internal pressure p. If p = 1000 psi, the equivalent nodal force at each of the two interior grids is Q = 4.62329 pounds in the radial direction. The true pressure corresponding to initial yielding for this problem is p_o = 23,571 psi. The NASTRAN results will depend on the users' choice of element sizes and load increments. In the elastic range, the NASTRAN results based on two finite-element models were compared with the exact solution. For a ten-element model, the maximum error is 0.36 percent in displacements and 0.95 percent in stresses. For a twenty-element model, the maximum errors are reduced to 0.09 percent and 0.24 percent, respectively. Since we are satisfied with one percent error, the ten-element model is chosen for incremental analysis beyond the elastic limit.

In the plastic range, the user has to choose the load increments properly in order to obtain good results at reasonable cost. The values of the load factors can be normalized so its unit value corresponds to the limit of elastic solution, i.e., p_o = 23,571 psi. The load increments can be uniform or nonuniform. It seems that the size of load increments depends on the material properties and sizes of elements. In order to determine the influence of load factors on the displacements and stresses in the plastic range, four sets of load factors are chosen. The load increments for three of them are uniform with $\Delta p/p_o$ = 0.20, 0.10, and 0.05, respectively. The influence of load factor, p/p_o, on the inside radial displacement, u_1, is shown in figure 4. The effect of load factors on the major principal stresses in elements is shown in figure 5. We also show in these two figures the corresponding analytical results. On the basis of these comparisons, we can make the following conclusions. In the earlier stages of plastic deformation, larger load increments can be used to give very good results. As plastic deformation becomes bigger, smaller load increments should be used in order to get a reasonably good answer. However, for very large plastic deformation, it seems that we cannot improve the NASTRAN results much better by choosing even smaller increments. This is because there are other built-in errors in the NASTRAN program, e.g., the linear displacement function is assumed.

If uniform load increments are used, a direct comparison of the analytical and NASTRAN results is not available. The solid curves shown in figures 4 and 5 were obtained indirectly since the analytical results of the displacements, stresses, and pressure were represented as functions of elastic-plastic boundary (ref. 5). We have obtained the analytical results when the elastic-plastic boundary is located at a radial distance of 0.05, 0.15, 0.25, 0.35, 0.45, 0.55, 0.65, 0.75, 0.85, and 0.95 inch from the inside surface. The corresponding values of the pressure factor (p/p_o) are 1.095, 1.266, 1.414, 1.540, 1.646, 1.734, 1.805, 1.860, 1.901, and 1.929, respectively. This set of values is used as load factors in the input deck of the

NASTRAN program. Some of the NASTRAN results together with the corresponding analytical results are shown in figures 6 and 7. A direct comparison of the two approaches in the plastic range can be seen. The effect of load factors on the distribution of radial displacements is shown in figure 6. The distributions of major principal stresses for three load factors are shown in figure 7. As can be seen in figures 6 and 7, a direct comparison of two approaches will support the following conclusion. Even if the results in the elastic range are in excellent agreement, the differences in the plastic range can be quite big for large values of load factors. This suggests more research efforts should be given to large plastic deformation.

CONCLUSIONS

ORIGINAL PAGE IS
OF POOR QUALITY

Two elastic-plastic annular plate problems have been analyzed by using NASTRAN plate elements. One problem is loaded externally by two concentrated forces and the other by uniform internal pressure. The NASTRAN results for the second problem have been compared with an exact analytical solution. It seems that the NASTRAN code in its present form is still a valuable tool because it can be used to solve quite complicated plane stress problems provided the plastic deformation involved is not too large. The limitation that the use of ideally plastic materials is excluded can be easily removed by making minor changes.

REFERENCES

1. NASTRAN Demonstration Problem Manual, NASA SP-224 (01), 1972.

2. Chen, P. C. T: On Elastic-Plastic Analysis of an Overloaded Breech Ring Using NASTRAN, Proceedings of the Tenth NASTRAN Users' Colloquium, May 1982, pp. 100-109.

3. Mises, R. V.: Three Remarks on the Theory of Ideal Plastic Body, Reissner Anniversary Volume, 1949, pp. 415-429.

4. Chen, P. C. T.: A Comparison of Flow and Deformation Theories in a Radially Stressed Annular Plate, Journal of Applied Mechanics, vol. 40, no. 1, Trans. ASME, vol. 95, 1973, pp. 283-287.

5. Chen, P. C. T.: Elastic-Plastic Analysis of a Radially Stressed Annular Plate, Journal of Applied Mechanics, vol. 44, 1977, pp. 167-169.

6. Swedlow, J. J.: The Thickness Effect and Plastic Flow in Cracked Plates, ARL 65-216, Aerospace Research Laboratories, Office of Aerospace Research, October 1965.

7. Yamada, Y.; Yoshimura, N.; and Sakuri, T.: Plastic Stress-Strain Matrix and Its Application for the Solution of Elastic-Plastic Problems by the Finite Element Method, Int. J. Mech. Sci., vol. 10, 1968, pp. 345-354.

ORIGINAL PAGE IS
OF POOR QUALITY

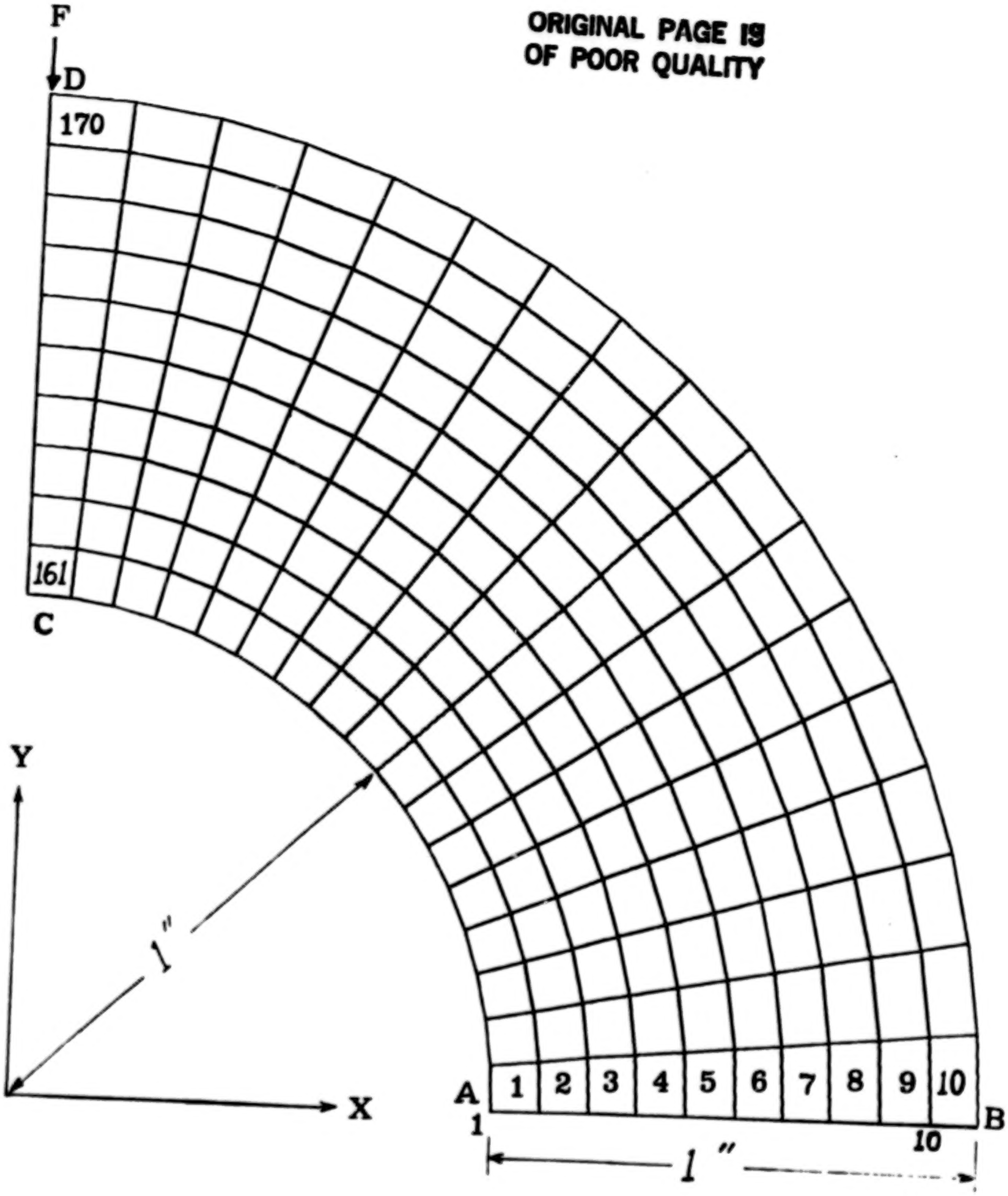
F
D
170
161
C
Y
1"
X
A
1
2
3
4
5
6
7
8
9
10
1
B
10
1"

Figure 1. Finite Element Model of an Annular Plate.

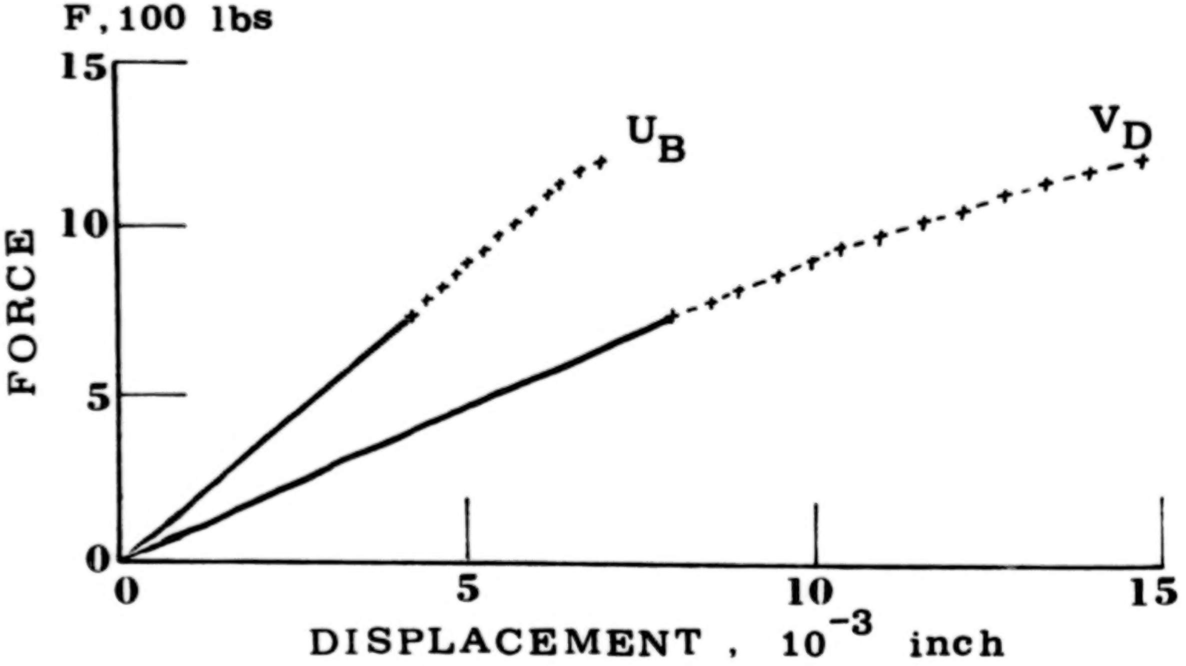

Figure 2. Vertical and Horizontal Displacements (V_D,U_B) as Functions of the Applied Force (F) - Problem 1.

ORIGINAL PAGE IS
OF POOR QUALITY

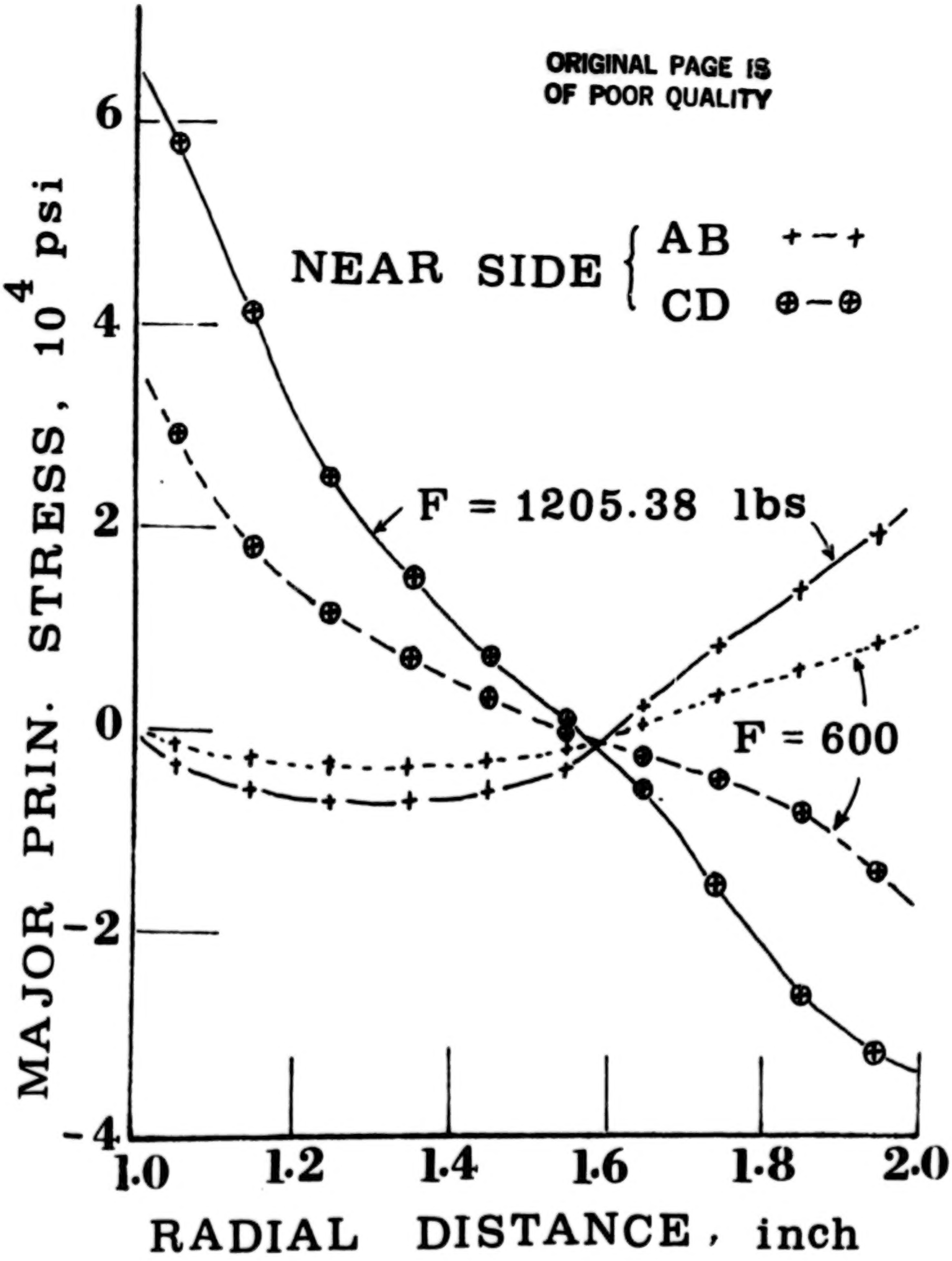

Figure 3. Distribution of Major Principal Stresses - Problem 1.

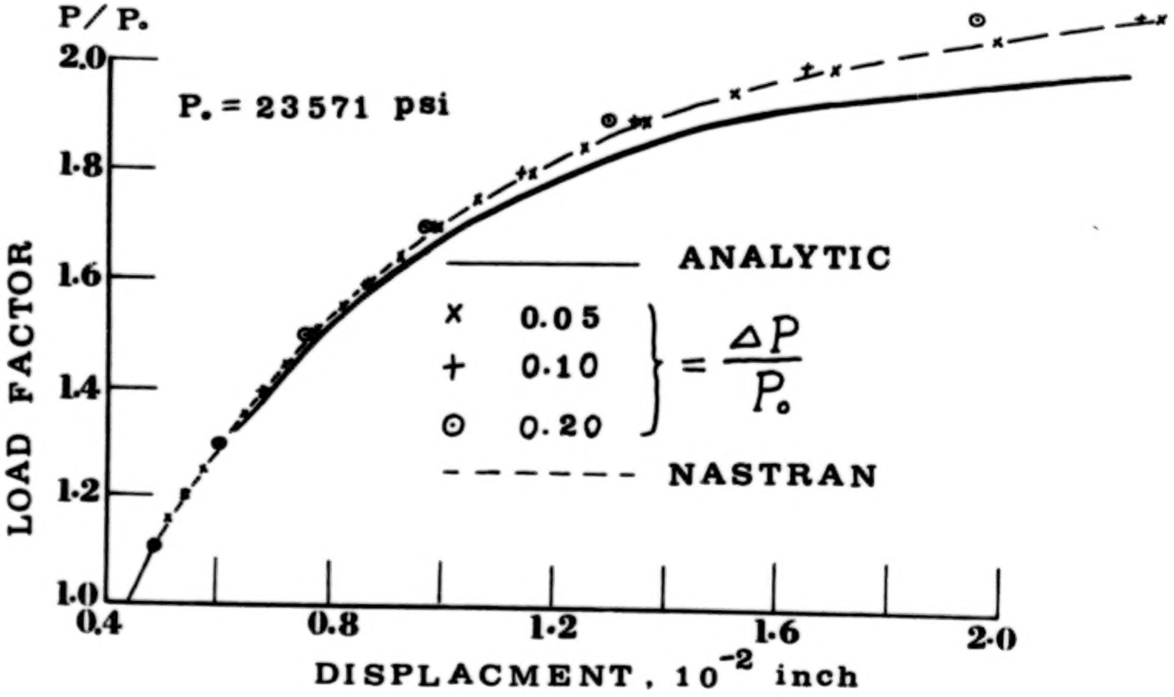

Figure 4. Influence of Load Factor on the Inside Displacements - Problem 2.

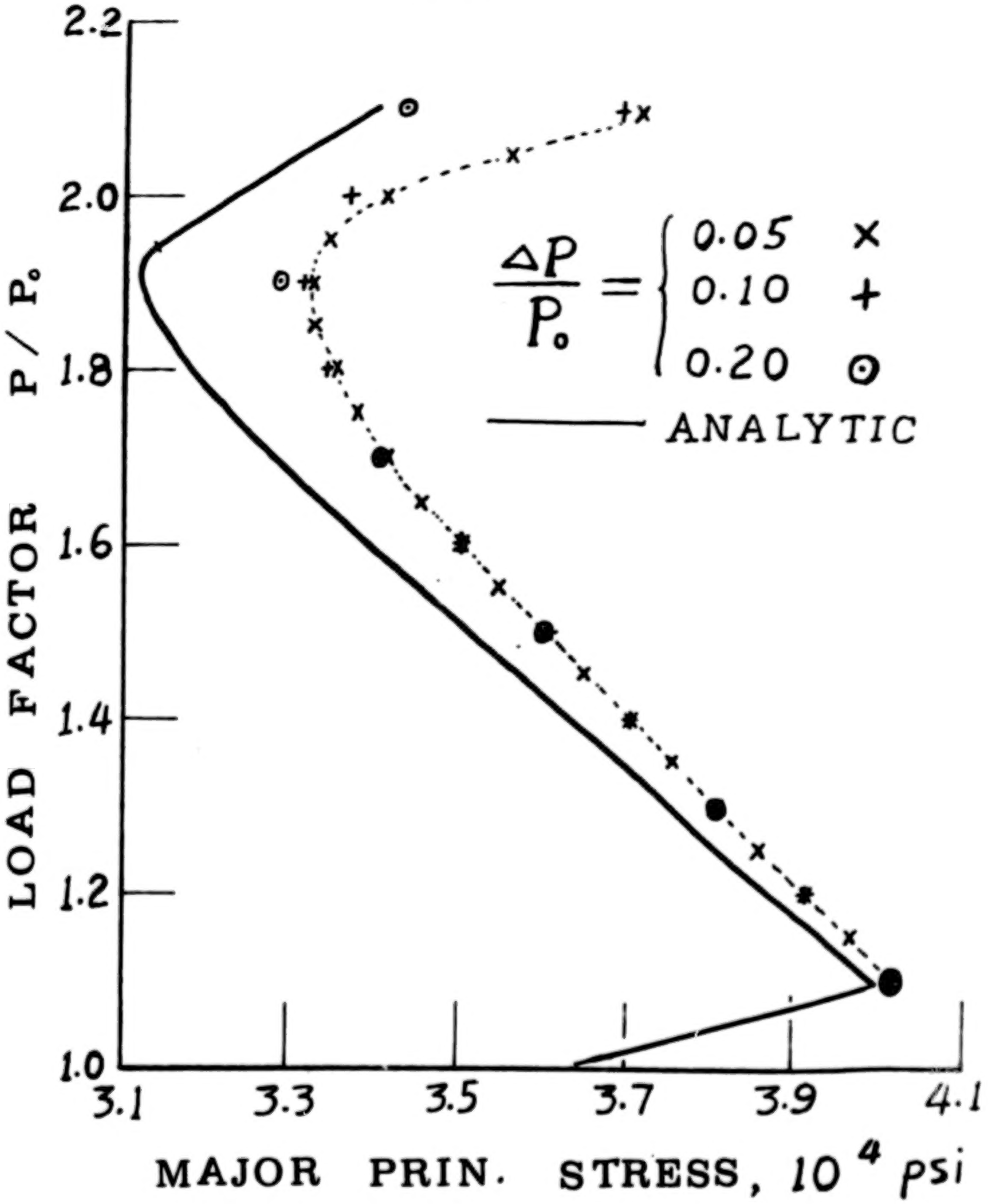

Figure 5. Influence of Load Factor on the Major Principal Stresses in Element 1 - Problem 2.

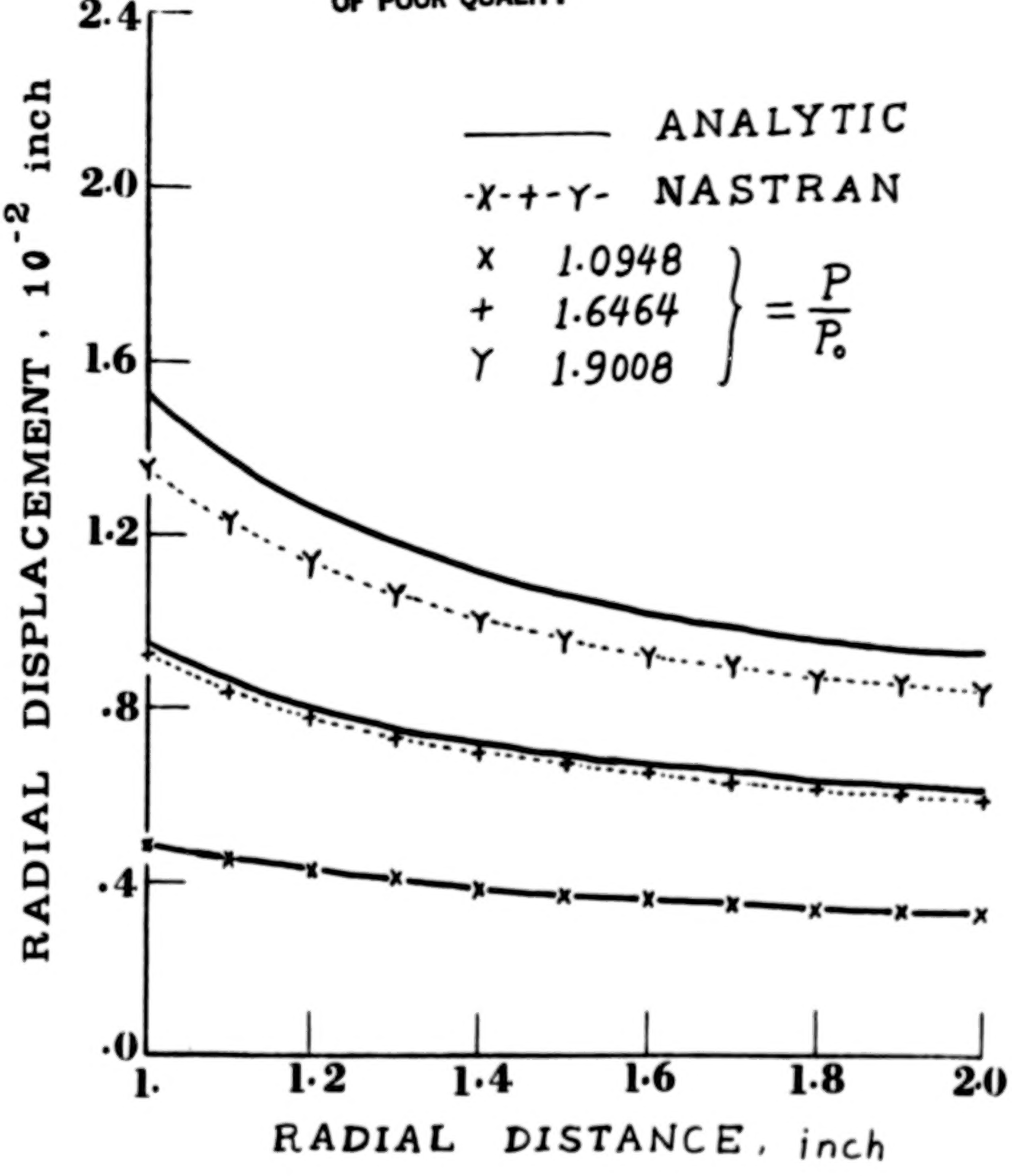

Figure 6. Distribution of Radial Displacements - Problem 2.

ORIGINAL PAGE IS
OF POOR QUALITY

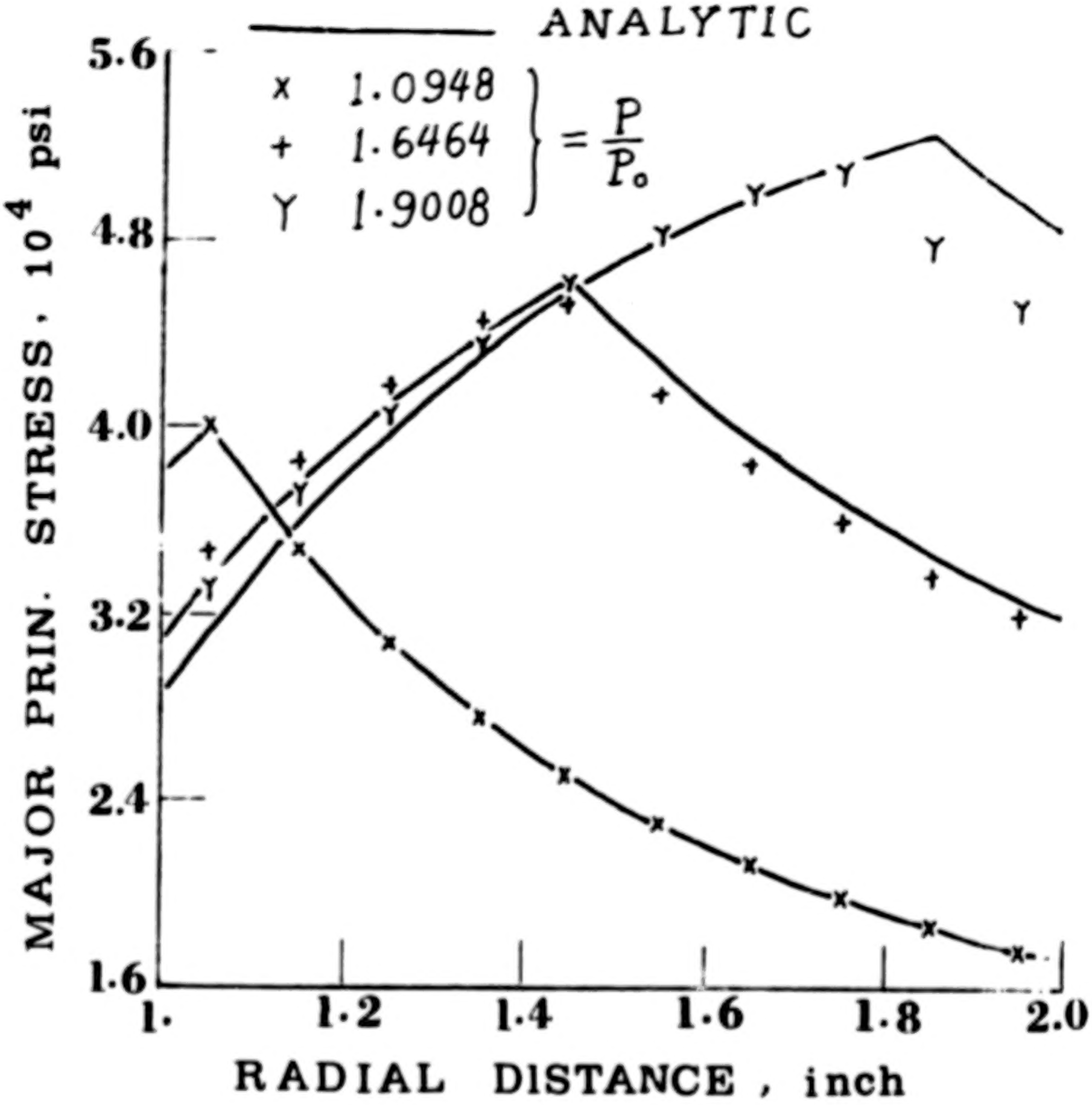

Figure 7. Distribution of Major Principal Stresses - Problem 2.

N84
15608

UNCLAS

ORIGINAL PAGE IS
OF POOR QUALITY

N84 15608 D18

BOLT IN BORE BOUNDARIES

by

T. G. Butler
BUTLER ANALYSES

INTRODUCTION

This paper discusses the factors that must be taken into consideration when applying NASTRAN's linear analysis to structures whose principle boundaries are formed by bolting, and for which localized stress peaking is important. The determination of what portion of the bolt boundary is active for a given loading is a nonlinear problem. Once the active boundaries are established for a given load, the determination of the resulting stresses is a linear problem. Does this mean that every analysis whose principle boundaries are formed by bolting are wrong if they are not treated in a nonlinear fashion? Not at all! The importance of this nonlinear condition rears its head only when the finite element mesh is so fine that the bore is no longer represented as a point. Then the particulars of the macro behavior of the bolt in the bore become important. There are two approaches to this problem: Either the employment of a set of nonlinear scalar springs at the boundaries to determine the active region for a given loading followed by a detailed linear analysis under the active bounding locales; or the pursuit of a series of boundary approximations using linear analysis, only, until admissible conditions are found. This paper deals with the second approach. An illustration of these methods is given in an application to a mounting bracket.

OPERATION

Loads applied simultaneously in 3 coordinate directions involve 3 kinds of boundaries and cause variations depending on the magnitudes of the load components. Unfortunately, it is not possible to apply a set of individual nominal loads then scale them and combine them to get a final result, because linear superposition does not work at all in this highly nonlinear problem. Changing loads causes the hold down bolts to bear on the bore surface in different locations; they cause either the bolt head or nut to make contact in different locations; they cause different edges of the bolted foot to bear on the mounting surface. In the application under consideration, there are two bolts through a single rectangular foot.

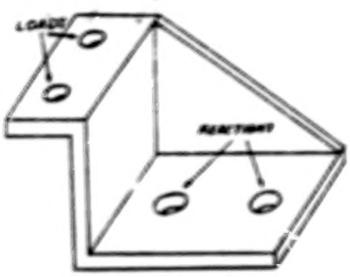

In the actual case there is a multi-fold infinity of possible bounding contacts. In the finite element case of a fine meshed model there is a high finite number of possible bounding combinations. To reduce the problem of finding admissible combinations to a manageable set, it was decided to limit the trial locations to the following:

TYPE OF BOUNDARY	DETAILS OF REPRESENTATION
Bolt Shank Against Bore Surface	Three Pairs of Points At Each Cardinal Location For Each Of Two Bores
Bolt Head Against Upper Surface Annulus	Circle Of Points About Each Of Two Bores
Bolt Nut Against Lower Surface Annulus	Circle Of Points About Each Of Two Bores
Foot Side Edge Against Mount Surface	Set Of Three Points At Each Of Two Sides Of Each Of Two Points
Foot End Edge Against Mount Surface	Set Of Points Along Entire Edge Of End Nearest Load

Sketches of these boudaries as they might behave under load are shown here.

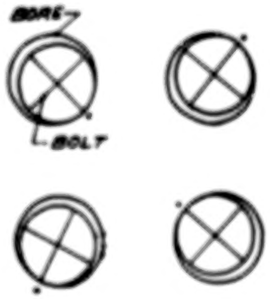

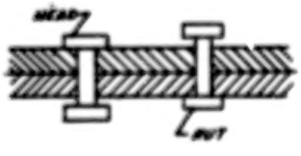

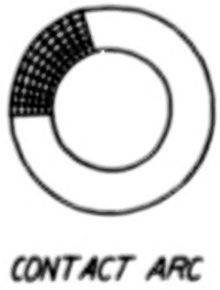

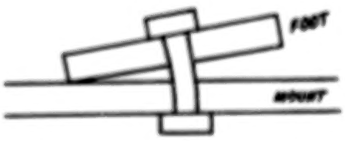

METHOD

Fools rush in where angles fear to tread. Based on the logic of rigid body actions it appeared quite reasonable to expect that one could make initial predictions that could be modified slightly, after initial reactions were reviewed, to a set that would be admissible. Notice that mealy-mouthed language is already being used: reasonable -- admissible; not correct or precise. If the load were applied in the +X,+Y,+Z directions, one would expect the foot to move over to contact the bolts on the -X sides of the bores, the -Y sides of the bores, and to engage the bolt head rather than the bolt nut for both bolts. It was these rigid body notions that were dashed by the elastic reality of the case. Actions at one bore were different than actions at the other. Loads were offset from the foot and the loading surface was canted to the plane of the foot. These produced moments that were reacted at the bolts. Rigid body calculations were made for each load to help decide on the initial boundary assignments in the first trial of each run. This approach has logical appeal, but it often was considerably off the mark.

In order to improve the first trial, a small pilot model with a coarse mesh was assembled from plate elements and had each bore represented by a point. Readings from the bore points and boundary edge points helped to improve the initial SPC assignments in the solid model.

This analysis used solid elements entirely for the whole model which contributed to a complication in satisfying moments. Pairs of points are needed to create couples when using solid elements, while if plate bending elements were used instead, any bending requirements could be met at a single point rather than over a pair of points. The tendencies of pairs of points to form couples proved troublesome at boundaries. To explain this it will be helpful to redefine some terms.

First of all "boundary" is defined to be that set of points wherein a subset of whose components are constrained to zero displacement. This is a particularly severe condition in view of the inevitible redundancy of constraints. An admissible boundary is one that pushes only and does not pull on the mating boundary strucuture. This restriction makes an ideal argument for using unidirectional nonlinear boundary springs. The nonlinear supports will allow nonzero displacements and still produce a push force. Exploring such a case would be an attractive venture, but this paper concentrates only on the linear trial method. The measure used to discriminate for admissibility of boundary candidates was the sign of the SPCForces at the boundaries. If any boundary components were found to pull, it necessitated redefining the boundary constraints to avoid this pulling condition. Quite often it was not enough to just eliminate the offending component, because the pulling behavior often moved to the neighboring retained point. Another suprise occurred at the bolt heads. It seemed representative for bolt head constraints to be modeled as an annulus of a double circle of points. As it turned out, pairs of inner and outer radial points acted as couples with opposite signs which is inadmissible, because opposite signs means one is pulling while the other is pushing. Consequently, bolt head and bolt nut reactions were modeled as a single circle of points. Even restricting bolt constraints to single circles was most often not sufficiently curtailed to eliminate all pulling. Trial with only arcs of a circle in various positions and different spans were made before sometimes, an admissible head or nut representation was found.

At times during this analysis, I wanted to say, "What does it matter if there is some pulling?" Severe high stresses occurred in regions where high constraint forces of opposite signs were present. Good answer.

The canted, offset position of the loading produced a tendency for the foot to tilt with respect to the mounting surface in every loading case. A triplet of points on an edge transversely opposite a bore in one direction constituted the candidate boundary set at each of 4 locations. As trials were made it was found that sometimes the triplet had to be reduced to a pair or a single point before it became admissible. In the case of fore and aft edges, it was found that sometimes contact was made at the edge nearest the load but tilting towards the far end was taken up elastically before reaching the far end so that the far edge never became a boundary constraint. The distribution of constraints on the near edge was found to vary from the entire edge to a biased partial set.

Absence of pulling is not the only criterion for admissibility. Over-constraining must be guarded against when trying to trace critical stresses. It is possible to have excessive constraints even though they are all pushing. The requirement used for an admissible quantity of constraints is that the opposing equilibrating elastic constraints be of the same order of magnitude as the opposing forces for rigid body equilibrium. An average of six trial runs per load case were needed to find an admissible set of constraints. Results were considered to be on the

ORIGINAL PAGE IS OF POOR QUALITY

conservative side, because the contact area broadens as deformation takes place in the actual case. Broadening of the contact area was not taken into account in this analysis. As a result this analysis should show stresses slightly higher than actual.

The advantage for an analysis, such as this, is that it gives much more information than an experimental set-up using strain gages, because the finite element mesh has a smaller gage length and has several orders of magnitude more measurements. The load path becomes well traced and the peaking and releasing of stresses which leads to cracks and fatigue is well defined.

APPLICATION

To illustrate how this method worked in practice, this paper will trace the steps taken in homing in on an admissible set of constraints for a single loading condition.

SUBCASE 3412; XYZ loads at the cradle are -283/-559/-422

It might be easier to describe the evolution of reactions if positions are oriented with respect to the bracket parts. For instance, the place where loads go in is the cradle and the triangular shaped ligament connecting the cradle to the base is the brace. Opposite the brace the side is named "open". Positions in the other direction are distinguished by the terms "distant" from the loaded cradle and "near" the load. The bores are not of equal size. The bore nearest the cradle is the larger so the terms large bore (LB) and small bore (SB) help to keep the reaction straight. Finally, the vertical direction can be designated by the bolt head side on top and the bolt nut side on the bottom. See the sketch with labels per this scheme.

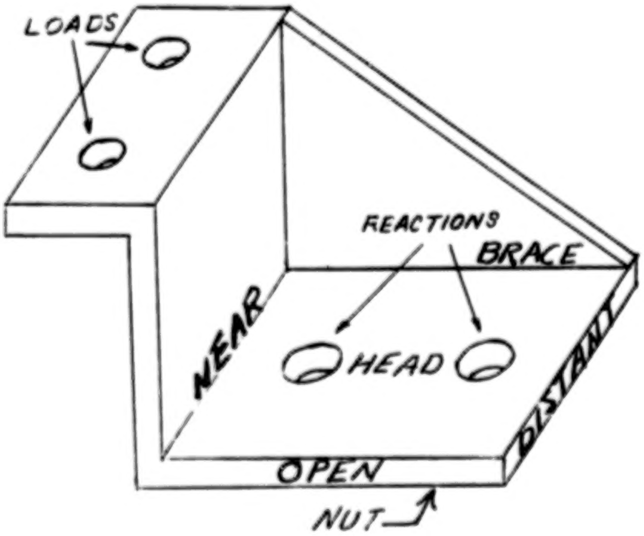

The initial SPC set was assigned in an attempt to balance the loads with pushing forces only. To oppose the -X load, a set of SPC's was put in place at the LB(large bore) on the cardinal point towards the open side. The couple created by the X load and the LB X reaction can be balanced by putting a constraint on the cardinal point at the SB(small bore) towards the brace side.

To oppose the -Y load an SPC set was put on the nut side of LB causing a moment which could be opposed by an SPC on the head side of SB.

To oppose the -Z load the cardinal points toward the near side of both bores, constraints were put on the near side of both LB and SB. To oppose the moment in Z forces about the X-axis, a constraint was applied at the distant edge.

In particular, the initial combination of SPC sets consisted of:
(a) a full array of 3 pairs of points (nut surface, mean surface, and head surface) on the SB brace location for X reaction.
(b) a full column of 3 points (nut, mean, and head) on the LB open location for X reaction.
(c) a 270 degree arc of points from "near" around "brace" to "distant" on the head surface around SB for Y reaction.
(d) a 270 degree arc of points from "near" around "open" side to "distant" on the nut surface around LB for Y reaction.
(e) a line of points on the "distant" edge beyond SB for Mx reaction.
(f) a full array of 3 pairs of points on the SB near side for Z reaction.
(g) a full column of 3 points on the LB near side for Z reaction.

The results showed a number of places that were pulling, but the one giving the greatest offense was the line of points on the distant edge.

The first modification tried to temper the effect of the distant edge by introducing an additional constraint on the brace egde opposite SB, while keeping all else unchanged. The results showed no relief in the pulling of the distant edge and only slight correction around the bores.

The second modification abandoned the distant edge line. The arc on the nut surface of LB was shifted from 270 degrees on the open side to 180 degrees on the brace side.

The arc on the head surface of SB was reduced to 180 degrees on the brace side.
The triplet of points on the brace edge of SB was reduced to a pair.
The results were considerably improved, but some pulling in Z persisted.

The third modification reduced 3 pairs in the SB near side to the upper 2 pairs.
The column of constraints in LB near side were removed.
The triplet on the open side of LB was reduced to the upper pair.
The results showed there was still pulling in Y, and the Z pushing magnitudes on SB were high.

The fourth modification reduced the 180 degree arc on the nut surface of LB to a 45 degree arc on the brace side.
The triplet on the near side of LB was resoted to moderate those in SB.
The results were close but there was some pulling on the brace side of SB and on the near side of LB.

The fifth modification reduced the 3 pairs to the lower 2 pairs on the brace side of SB.
The triplet on the near side of LB was reduced to the lower pair.
The results were admissible!

In summary, the net overall change entailed:
reducing a full 3 pairs of SB brace side to the lower 2 pairs;
reducing a full triplet of LB open side to the upper pair;
eliminating the distant edge line and enabling a pair of points on the brace edge of SB;
moving the LB 270 degree arc on the open side of the nut surface to a 45 degree arc on the brace side of the nut surface;
reducing a full 3 pairs of SB near side to the upper 2 pairs;
reducing a full triplet of LB near side to the lower pair.

This cut and try method was applied to every loading case in order to achieve admissibility. What kept one going was the optimistic certainty that just one more try would bring the constraints into line. And just like Charlie Brown's baseball team something unexpected turned up each time to frustrate the success of the next try. The next three illustrations show the surfaces only of the solid element modelling used for the bracket as viewed from 3 different positions.

ORIGINAL PAGE IS
OF POOR QUALITY

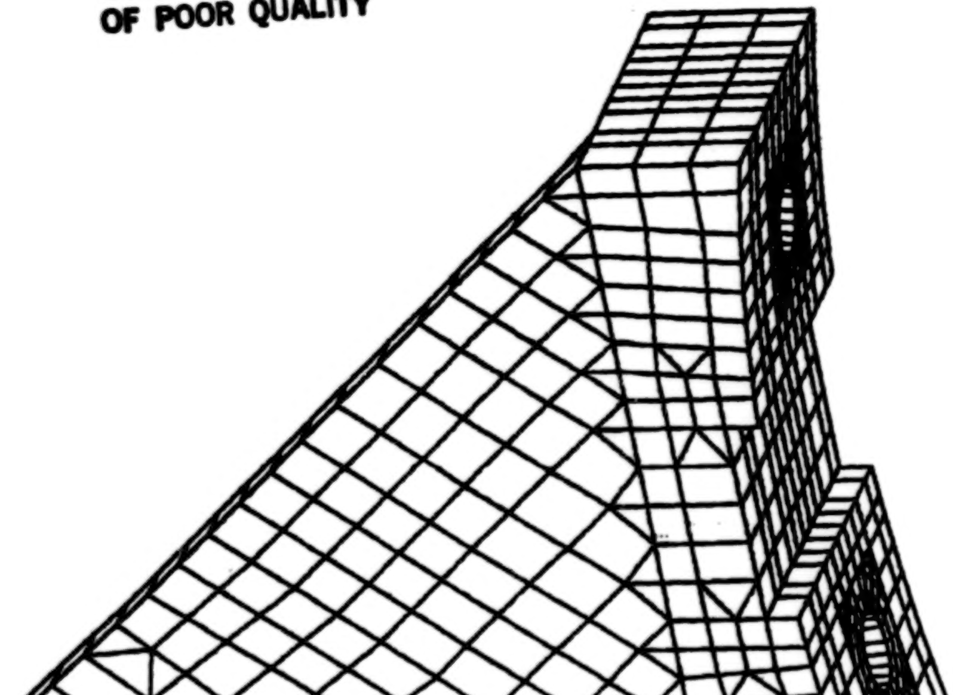

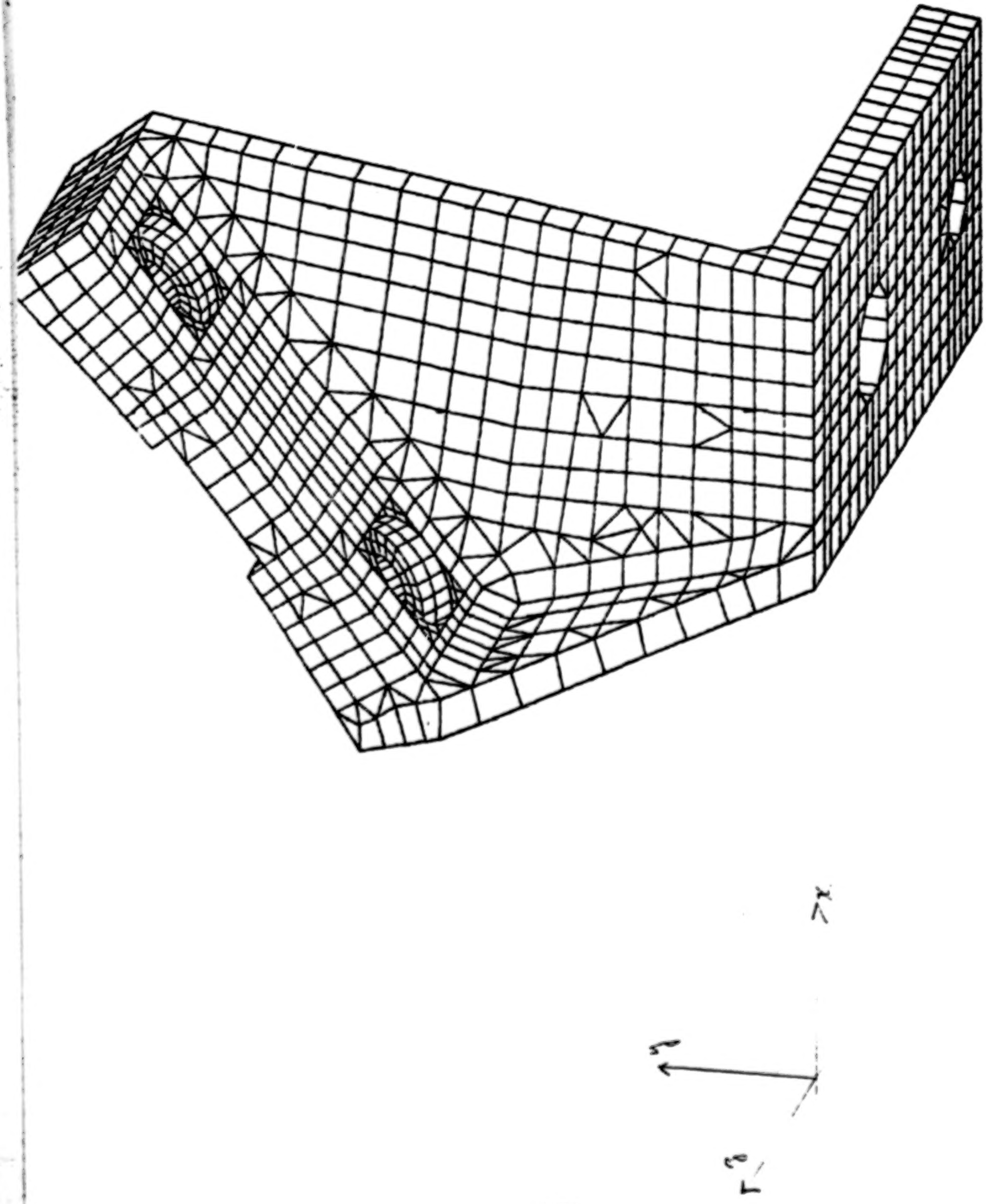
x
y
z

ORIGINAL PAGE IS
OF POOR QUALITY

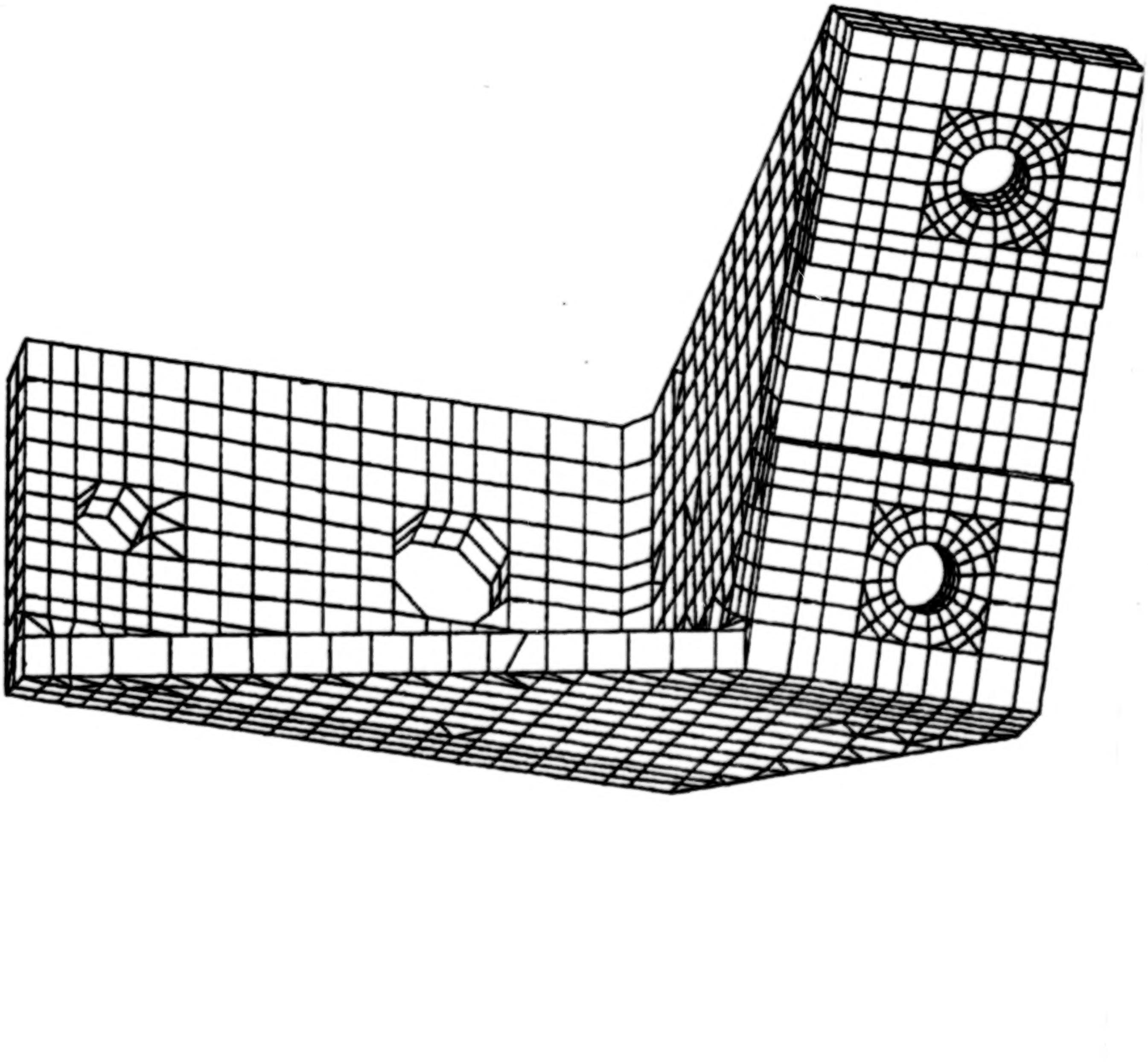

ORIGINAL PAGE IS
OF POOR QUALITY

RESULTS

The following illustration shows color contours of stresses from a single loading case.

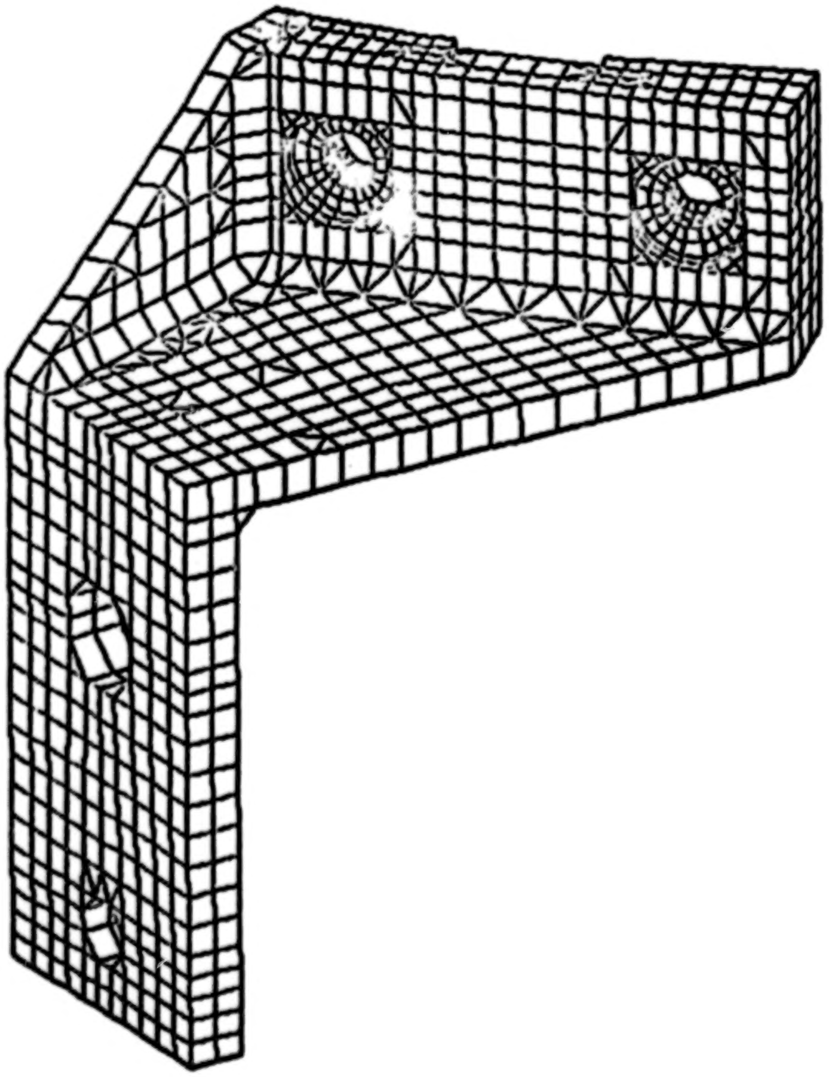

CONCLUSIONS

In conclusion it is fair to say that the method works and gives reliable results slightly on the conservative side. It still leaves an element of uncertainty as to whether the honed set of constraints is unique, since a reduced set of working locations was used. Some shifting say to intercardinal points might cause some change in the stresses. In spite of this nagging doubt, it claims to be a reasonably good method. It can be tested further by running a set of unidirectional nonlinear springs to obtain a measure of its approximations.

Some comment might be made as to the efficiency of the computing techniques, e.g. Brute Force as was done here which devoted a complete run for every trial. 2. Condensation of all points except boundary candidates with restart of only the modified A-set. 3. Substructuring with a unit substructure assigned to each cluster of boundary points and the bulk to the parent structure. 4. A true nonlinear investigation to recover the magnitudes of the boundary forces for each load case with a companion run of the linear case which would then apply these boundary forces for a lengthy stress recovery phase.

The reason that the Brute Force method was used is that the storage required to implement the other routes taxed the limited resources of the VAX.

The maxim that fits this story is: that whenever the mesh of a model is so fine that a bore can't be represented as a point, one must be prepared for a considerable amount of extra care if the stresses in the region of the boundary are important. In the words of the Great CPU:

HE WHO MESHES FINE,

FINDS A MESH.

☆U.S. GOVERNMENT PRINTING OFFICE1983 639 -008/39 REGION NO. 4

END

DATE

FILMED

MAR 13 1984